University of Massachusetts Medical School

eScholarship@UMMS

Deconstructing bioluminescence: from molecular detail to in vivo imaging.

Spencer T. Adams Jr.
University of Massachusetts Medical School

Let us know how access to this document benefits you.

Follow this and additional works at: https://escholarship.umassmed.edu/gsbs_diss

Part of the Biochemistry Commons, Evolution Commons, Molecular Biology Commons, Other Biochemistry, Biophysics, and Structural Biology Commons, and the Structural Biology Commons

Deconstructing bioluminescence: from molecular detail to in vivo imaging.

Spencer T. Adams Jr.

University of Massachusetts Medical School

DECONSTRUCTING BIOLUMINESCENCE:

FROM MOLECULAR DETAIL TO *IN VIVO* IMAGING

A Dissertation Presented

By

Spencer Todd Adams Jr.

Submitted to the Faculty of the

University of Massahusetts Graduate School of Biomedical Sciences, Worcester

In partial fulfillment of the requirements for the degree of

DOCTOR OF PHILOSOPHY

January 29, 2020

Biochemistry and Molecular Pharmacology

DECONSTRUCTING BIOLUMINESCENCE:
FROM MOLECULAR DETAIL TO *IN VIVO* IMAGING

A Dissertation Presented
By
Spencer Todd Adams Jr.

The signatures of the Dissertation Defense Committee signify
Completion and approval as to style and content of the Dissertation

_____

Stephen C. Miller, Ph.D., Thesis Advisor

_____

Brian A. Kelch, Ph.D., Member of Committee

_____

Miguel S. Esteves, Ph.D., Member of Committee

_____

William R. Kobertz, Ph.D., Member of Committee

_____

Jing-Ke Weng, Ph.D., Member of Committee

The signature of the Chair of the Committee signifies that the written dissertation
meets the requirements of the Dissertation Committee

_____

William E. Royer, Jr., Ph.D., Chair of Committee

The signature of the Dean of the Graduate School of Biomedical Sciences
signifies that the student has met all graduation requirements of the school.

_____

Mary Ellen Lane, Ph.D.,
Dean of the Graduate School of Biomedical Sciences

Program in Biochemistry and Molecular Pharmacology
January 29, 2020

DEDICATION

I dedicate this thesis to the following people:

To my beautiful wife, Lex: Thank you for your love and support for all of these years. You brighten my day even when my bioluminescent experiments fail to illuminate.

To my grandmother, Shirley: You took me in as a mother would and provided for me the tools for success.

To my aunt, Pam: You were a mother figure for me while growing up. It means a lot to me that you were there for me as I grew up.

To my dad, Spencer: Thanks for pushing me to be the best version of myself.

And to two very influential professors during my undergraduate studies, Mary Ann D'Aloia and Robin Cook-Hill: Thanks for the many hours you two spent with me during during office hours in my early years as a scientist discovering my passion for biology.

ACKNOWLEDGEMENTS

First, I would like to acknowledge my thesis advisor, Stephen Miller. I am grateful for you taking me into your lab and nurturing my development as a young scientist. Your guidance and encouragement in times when I thought I was not capable have been paramount to my success in pursuit of the Ph.D. I have immensely enjoyed these years in your lab.

Next, thank you to my committee members: Bill Royer, Brian Kelch, and Miguel Esteves. Each of you have been invaluable to my development and pursuit of maturing as a scientist. I am also graeful to Jeng-Ke Weng for serving as my outside committee member. Thank you for taking the time to participate in my Ph.D studies.

Thank you also to all of my lab mates and collaborators, both past and present: David Mofford, Steven Pauff, Adam Choi, Markus Bohn, Rhandeer Reddy, Kiran Reddy, Kate Liebmann, Deepak Sharma, Innus Mohammad, Xincai Ji, Ganapathy Sankaran, Elliot Wilion, and Jonathan Lloyd. Working along with all of you made grad school a great experience.

And finally, thank you to my wife, Lex. Your support during this experience has been immeasurable. I love you!

ABSTRACT

Bioluminescence is the chemical production of light that results when a luciferase enzyme catalyzes the luminogenic oxidation of a small-molecule luciferin substrate. The numerous luciferases and luciferins nature has evolved can be used to illuminate biological processes, from *in vitro* assays to imaging processes in live animals. However, we can improve the utility of bioluminescence through modification of these enzymes and substrates. My thesis work focuses on developing reporters that expand the bioluminescent toolkit and improving our understanding of how bioluminescence works on a molecular level.

The first part of my thesis focuses on characterizing luciferases and luciferins that improve bioluminescence imaging in vivo. Some of our luciferins can outperform the natural D-luciferin substrate in live mouse imaging, while others are selectively utilized by mutant luciferases in live mouse brain. We also engineered luciferins that can selectively report on endogenous enzymatic activity in live mice.

The second part of my thesis focuses on determining the molecular details of how enzymes related to firefly luciferase, long-chain fatty acyl-CoA synthetases (ACSLs), can function as latent luciferases. I have determined the structure for one of these enzymes and improved its bioluminescent activity with

synthetic luciferins enough to image in live mouse brain. I also characterized the

selectivity in chimerized enzymes that combine firefly luciferase and ACSLs. In

summary, my work improves the utility of bioluminescence for *in vivo* use and

informs us about how evolutionarily-related enzymes function as luciferases on a

molecular level.

TABLE OF CONTENTS

LIST OF TABLES

LIST OF SCHEMES

LIST OF FIGURES

LISTS OF SYMBOLS AND ABBREVIATIONS

α	alpha
Å	angstrom
AAV	adeno-associated virus
ACS	acyl-CoA synthetase
ACSL	long-chain fatty acyl-CoA synthetase
ACSM	medium-chain fatty acyl-CoA synthetase
ACSS	short-chain fatty acyl-CoA synthetase
ACSVL	very long-chain fatty acyl-CoA synthetase
AMP	adenosine monophosphate
ATP	adenosine triphosphate
BBB	blood brain barrier
BLI	bioluminescence imaging
Boc	*t*-butoxycarbonyl
BRET	bioluminescence resonance energy transfer
BSA	bovine serum albumin
Cd^{2+}	cadmium cation
CCD	charged-coupled device
CHO	Chinese hamster ovary
CH_3CN	acetonitrile

CMV	cytomegalovirus
CoA	coenzyme A
CoASH	coenzyme A with a free sulfhydryl group
CO_2	carbon dioxide
Δ	delta
°	degree
DMEM	Dulbecco's modified eagle's medium
DMSO	dimethyl sulfoxide
DLSA	5'-O-[N-(dehydroluciferyl)-sulfamoyl]adenosine
DNA	deoxyribonucleic acid
DTT	dithiothreitol
ε	molar extinction coefficient
EDTA	ethylenediaminetetraacetic acid
FAAH	fatty acid amide hydrolase
FBS	fetal bovine serum
Fluc	firefly luciferase
g	gram
GST	glutathione-S-transferase
HBSS	Hank's balanced salt solution
hFAAH	human fatty acid amide hydrolase
HRMS-ESI	high resolution mass spectrometry, electrospray ionization
hr	hour

hv	light
H_2O	water
IC_{50}	The half maximal inhibitory concentration: the inhibitor concentration that is required to decrease the maximal rate by half
IP	intraperitoneal
IPTG	isopropyl ß-D-1-thiogalactopyranoside
IR	infrared
Ki	The inhibitory constant: the dissociation constant for the enzyme/inhibitor complex
K_m	The Michaelis-Menten constant: the substrate concentration at which the reaction rate is half of V_{max}
L	liter
L	dehydroluciferin
Λ_{max}	wavelength maxima
LH_2	D-luciferin
LRE	luciferin-regenerating enzyme
LST	luciferin sulfotransferase
µ	micro
m	milli
M	molar (mol/L)
MAGL	monoacylglycerol lipase
Mg	magnesium
min	minute
$MgSO_4$	magnesium sulfate

mol	mole
MW	molecular weight
n	nano
NaCl	sodium chloride
NADPH	reduced form of nicotinamide adenine dinucleotide phosphate
NMR	nuclear magnetic resonance
PAP	3'-phosphoadenosine-5'-monophosphate
PAPS	3'-phosphoadenosine-5'-phosphosulfate
PCR	polymerase chain reaction
PET	positron emission tomography
p/s	photons per second
p/s/cm^2/sr	photons per second per square centimeter per steradian
PBS	phosphate buffered saline
PDB	protein databank
PMSF	phenylmethylsulfonyl fluoride
PMT	photomultiplier tube
Π	pi
PPase	pyrophosphatase
PPi	inorganic pyrophosphate
PTS	peroxisomal targeting sequence
rFAAH	rat fatty acid amide hydrolase
RLU	relative light unit

ROI	region of interest
RP-HPLC	reverse-phase high pressure liquid chromatography
RPM	rotations per minute
RT	room temperature
S	second
SD	standard deviation
SDS-PAGE	sodium dodecyl sulfate polyacrylamide gel electrophoresis
SEM	standard error of the mean
SET	single-electron transfer
S2	schneider 2
TCEP	*tris*(2-carboxyethyl)phosphine
TFA	trifluoroacetic acid
U	unit
UV	ultraviolet
V_{max}	The maximum velocity or rate of a reaction catalyzed by an enzyme when all enzyme active sites are saturated with substrate.
WT	wild-type
x g	times gravity
Zn^{2+}	zinc cation

PREFACE

Publications derived from work contained within this thesis:

CHAPTER I: **Adams Jr., S.T.** and Miller, S.C. (2019). Enzymatic Promiscuity and the Evolution of Bioluminescence. FEBS J. Online Ahead of Print.

Also in CHAPTER I: **Adams Jr., S.T.** and Miller, S.C. (2014). Beyond D-luciferin: Expanding the Scope of Bioluminescence Imaging *in vivo.* Curr. Opin. Chem. Biol. 0, 112-120.

CHAPTER II: Evans, M.S., Chaurette, J.P., **Adams Jr., S.T.**, Reddy, G.R., Paley, M.A., Aronin, N., Prescher, J.A., and Miller, S.C. (2014). A Synthetic Luciferin Improves Bioluminescence Imaging in Live Mice. Nat. Methods. 11, 393-395.

CHAPTER III: Mofford, D.M., **Adams Jr., S.T.**, Reddy, G.S.K.K., Reddy, G.R., and Miller, S.C. (2015). Luciferin Amides Enable in vivo Bioluminescence Detection of Fatty Acid Amide Hydrolase Activity. J. Am. Chem. Soc. *137, 8684-8687.*

CHAPTER IV: **Adams Jr., S.T.**, Mofford, D.M., Reddy, G.S.K.K., and Miller, S.C. (2016). Firefly Luciferase Mutants Allow Substrate-Selective Bioluminescent Imaging in the Mouse Brain. Angew. Chem. Int. Ed. *55, 4943-4946.*

CHAPTER V: Sharma, D.K., **Adams Jr., S.T.**, Liebmann, K.L., and Miller, S.C. (2017). Rapid Access to a Broad Range of 6'-Substituted Firefly Luciferin Analogues Reveals surprising Emitters and Inhibitors. Org. Lett. *19, 5836-5839.*

CHAPTER VI: Sharma, D.K., **Adams Jr., S.T.**, Liebmann, K.L., Choi, A., and Miller, S.C. (2019). Sulfonamides are an Overlooked Class of Electron Donors in Luminogenic Luciferins and Fluorescent Dyes. Org. Lett. *21, 1641-1644.*

CHAPTER I:

Introduction

Bioluminescence

Luminous reporters are frequently used to visualize biology. From determining localization of a protein in a cell to measuring gene silencing in live animals, light-based reporters can provide a real-time view of biology that may be otherwise invisible. For imaging at magnifications necessary for individual cells, fluorescent reporters are generally used (Ettinger and Wittman., 2014.). Alternatively, for imaging deep tissues in live animals, bioluminescence holds multiple advantages over other luminous imaging modalities (Close et al., 2010.). Bioluminescence's usefulness for imaging in live animals has pushed numerous labs and companies to investigate how they can extend its utility. Elucidating the molecular details of how bioluminescence works lays the foundation to build a bioluminescent toolkit.

Bioluminescence is the chemical production of light that results when an ezyme known as a luciferase oxidizes a small-molecule luciferin. This presents two different approaches to extending the utility of bioluminescence, either modify/create luciferases or modify/create luciferins. Combining engineered luciferases with synthetic luciferins allows us to go beyond the confines that restricted bioluminesce's evolution in nature. We find that synthetic luciferins can emit more robust light emission in select animal tissues or report on endogenous enzymatic activity in live cells or animals (Paley et al., 2013.; Mofford et al.,

2015.). Orthogonal luciferase-luciferin pairs are also possible and allow us to measure more than one process in the same animal (Jones et al., 2017.).

Bioluminescence has evolved more than once. Understanding the evolutionary trajectory of firefly luciferase (Fluc) from an ancestral long-chain fatty acyl-CoA synthetase (ACSL) enzyme presents the opportunity to artificially evolve luciferases and luciferins starting with this class of related enzymes. The abundance of ACSLs in nature provides many starting points for engineered bioluminescent reporters. Since ACSLs process fatty acids and gave rise to Fluc, this also suggests that Fluc-based bioluminescence may be appropriated for measuring endogenous fatty-acid processing enzymes in live cells or animals, including enzymes with pharmacological value (Mofford et al., 2015.).

Firefly bioluminescence

To produce light, a luciferase enzyme oxidizes a luciferin substrate to access an excited state. This excited-state oxyluciferin releases a photon of light when it relaxes to the ground state. In contrast to fluorescence, which requires incident light to generate an excited-state emitter, bioluminescent organisms achieve light emission through purely chemical means. This makes bioluminescence particularly suited to dark environments such as the night sky and the depths of the ocean. Bioluminescence has evolved multiple times in nature, with distinct luciferases and luciferins that accomplish light emission using unique protein and chemical scaffolds (Fallon et al., 2018.; Petushkov et al., 2014.; Davis et al., 2016.; Kaskova et al., 2017.; Kaskova et al., 2016.).

For example, deep tissue imaging in live animals requires a favorable signal-to-noise ratio. Bioluminescence exhibits no background, leaving the robustness of light emission as the key obstacle to its utility. One notable exception to the lack of background signal with bioluminescence exists in coelenteramide luciferins, which are prone to auto-oxidation. However, their use *in vivo* is further confounded by their emission spectra, which is heavily absorbed by hemoglobin. These factors, in addition to the toxicity of coelenteramide luciferins, make them poor bioluminescent reporters for deep-tissue imaging. Beetle-based bioluminescent reporters do not possess this auto-oxidizing tendency, making them better suited to this application.

Fireflies belong to a family of bioluminescent beetles that have evolved multiple distinct luciferases that all use D-luciferin to emit light (Amaral et al., 2019.). Firefly luciferase (Fluc) and its substrate D-luciferin were characterized over half a century ago (White et al., 1963.; White et al., 1965.; McElroy et al., 1969.) and have been widely adopted for research use.

Mechanism of beetle bioluminescence

The mechanism of firefly luciferase proceeds in two general steps: first D-luciferin is adenylated, then the AMP ester reacts with oxygen to access an excited-state molecule of oxyluciferin (Figure 1.1a) (Fraga, 2008.). The finer details of the light-emitting reaction as currently understood are as follows (Figure 1.2a): 1) the D-luciferin carboxylate attacks the alpha phosphate group of ATP to yield pyrophosphate and D-luciferyl-AMP; 2) deprotonation of the C4

carbon generates an enolate-stabilized carbanion (Mofford et al., 2014.; Min et al., 2011.; and Branchini et al., 2015.); 3) the carbanion reduces molecular oxygen by single-electron transfer (SET) to generate superoxide and a C4 radical (Mofford et al., 2014.; Min et al., 2011.; Branchini et al., 2015.); 4) the radicals combine to form a peroxide attached to the C4 carbon (Mofford et al., 2014.; Min et al., 2011.; Branchini et al., 2015.); 5) internal nucleophilic attack of the peroxide on the electrophilic carbonyl group displaces AMP, resulting in formation of a transient high-energy dioxetanone ring; 6) the oxygen-oxygen bond in the dioxetanone ring breaks, resulting in the release of carbon dioxide and the generation of an electronically-excited oxyluciferin; 7) the oxyluciferin relaxes to the ground state, releasing a photon of light.
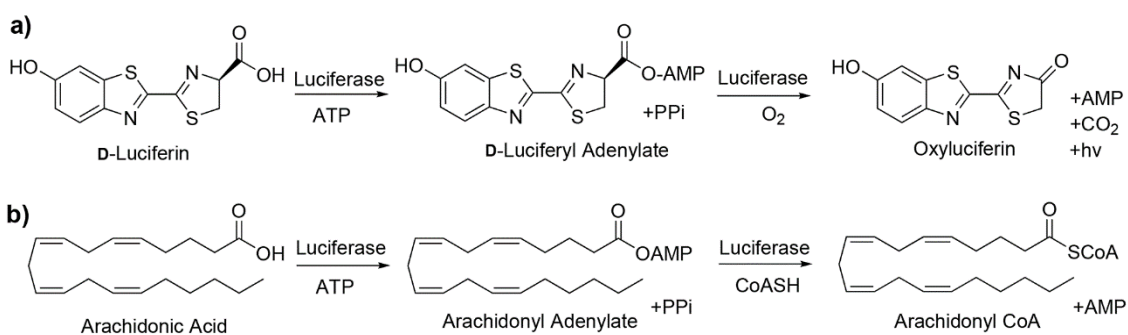
Figure 1.1. Fluc retains ancestral ACSL activity. A) Fluc catalyzes the adenylation and oxidation of D-luciferin to release a photon of light; B) Fluc can also ligate coenzyme A to fatty acids. Both reactions involve a key adenylated intermediate. (Adapted from Mofford et al., 2014).
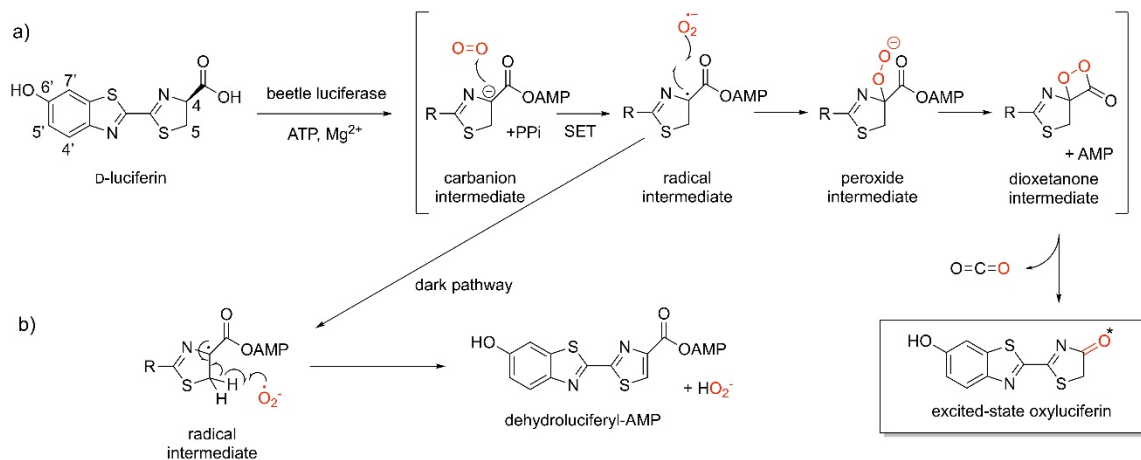
Figure 1.2. Mechanism of beetle bioluminescence. A) D-luciferin is adenylated, which makes the C4 carbon more acidic. The carbanion reduces molecular oxygen, forming a C4 radical and superoxide. Recombination of the radicals forms a peroxide that then attacks the AMP ester to form a strained dioxetanone ring. The oxygen-oxygen bond breaks, releasing carbon dioxide and forming an excited-state oxyluciferin, which radiatively relaxes to the ground state; B) In a "dark" reaction pathway, the C4 radical intermediate can instead form dehydroluciferyl-AMP, which is incapable of further oxidation and light emission.

The chemistry of light emission is inherent to the luciferin substrate, and oxygen plays a critical role. Notably, simply treating a luciferin ester in DMSO with base in the presence of oxygen will result in light emission, following the general mechanism described above (White et al., 1971.; Seliger and McElroy, 1962.). The energy needed to access an excited state is provided by breaking an oxygen-oxygen bond, a common feature of bioluminescent and chemiluminescent reactions. This suggests that enzymes capable of forming an AMP ester of luciferin should give rise to luciferase activity, where the subsequent light emission chemistry is largely directed by the luciferin ester.

It should be mentioned that a non-productive, "dark" reaction can also occur (Figure 1.2B). In step 4 of the luciferase mechanism outlined above, there is another possible outcome, in which superoxide does not form a C4-peroxide, but instead abstracts a hydrogen from the C5 carbon, forming dehydroluciferyl-AMP and a peroxide anion (Pirrung et al., 2017.). In this case, there is no formation of an excited-state oxyluciferin, and no light emission. Furthermore, dehydroluciferyl-AMP is a luciferase inhibitor that must be displaced for further catalysis to occur. For in vitro luciferase assays, the inclusion of coenzyme A is often used to help remove this unwanted inhibitory byproduct, presumably by forming the corresponding dehydroluciferyl-CoA.

Evolution of firefly bioluminescence

Bifunctionality of firefly luciferase

In addition to catalyzing light emission from D-luciferin, Firefly luciferase (Fluc) is also able to ligate coenzyme A to fatty acids (Figure 1.1) (Oba et al., 2003.). This makes Fluc a bifunctional enzyme; it can function as both a luciferase and a long-chain fatty acyl-CoA synthetase (ACSL). Enzymatic promiscuity to accommodate a range of substrates is a common theme in evolution, contributing to the rich diversity of chemistries that living organisms require (O'Brien and Herschlag, 1999.; Weng, J-K, 2014.). Fatty acyl-CoA synthetases (ACSs) are a diverse class of enzymes found in all kingdoms. These enzymes activate fatty acids with ATP, forming an acyl-AMP ester and pyrophosphate. In a second step, the AMP moiety is displaced with coenzyme A,

yielding a fatty acyl-CoA thioester. Since cells utilize various different lengths of

fatty acids, nature has evolved ACSs that are binned into four classes in the

scientific literature: short chain fatty acyl-CoA synthetases (ACSS) (which

process fatty acids of chain length 2-3 carbons long), medium chain fatty acyl-

CoA synthetases (ACSM) (which process fatty acids of chain length 4-12

carbons long), long chain fatty acyl-CoA synthetases (ACSL) (which process fatty

acids of chain length 12-22 carbons long), and very long chain fatty acyl-CoA

synthetases (ACSVL) (which process fatty acids of chain length greater than 22

carbons long) (Watkins, 2008.).

McElroy et al. noted similarities between the enzymatic activities of Fluc

and ACSLs as early as 1967, pointing out the shared need for adenylation to

activate fatty acid and D-luciferin substrates (McElroy et al., 1967.). Fluc shares

the greatest amino acid sequence identity with ACSL enzymes and even retains

its ancestral ACSL activity (Oba et al., 2003.). Fluc adenylates and ligates

coenzyme A to fatty acids of chain length greater than 12 carbons most

efficiently, which makes it a bifunctional enzyme: a luciferase and an ACSL,

depending on the substrate (Oba et al., 2003.). Despite the production of

different products, the overall chemistry of ACSLs and firefly luciferase are quite

similar in that both involve the formation of an activated AMP-ester intermediate

from a carboxylic acid. Significant differences occur in the subsequent reactions

of the adenylated intermediates. When a fatty acid is the substrate, the AMP

moiety is displaced by CoA to generate a fatty acyl-CoA (Oba et al., 2003.). L-

luciferin, the enantiomer of D-luciferin, will similarly form a CoA thioester (Fraga et al., 2005.; Nakamura et al., 2005.). It is only in the special case of D-luciferin that the substrate reacts with oxygen to form an excited-state oxyluciferin (Nakamura et al., 2005.).

Evolution from ancestral fatty acyl-CoA enzyme promiscuity

Fireflies are not the only bioluminescent beetles. Click beetles also evolved luciferases (Oba et al., 2010.). However, click beetle luciferases differ in sequence and enzymatic activity when compared to firefly luciferase (Oba et al., 2010.). Additionally, the location and morphology of the lantern organs differ between fireflies and click beetles. Both firefly and click beetle luciferases use the same substrate (D-luciferin), but they do not all emit light of the same color (Wood et al., 1989.). While most firefly species emit yellow-green light, some click beetles emit orange light (Stolz et al., 2003.). Since D-luciferin is the common light emitter in the bioluminescent reaction, this means there are differences in the environment of the oxyluciferin during its radiative relaxation to the ground state. Furthermore, Fluc retains ACSL activity, but click beetle luciferases such as the ventral and dorsal luciferases from *P. angustus* both lack ACSL activity (Oba et al., 2010.). These differences could reflect divergence of a common luciferase, or convergent evolution of two or more distinct ancestral enzymes to achieve light emission with D-luciferin. Complete genomes for different bioluminescent beetle species are now available, and analysis of these genomes adds credence to the latter theory: the luciferases for fireflies and click

beetles both arose from separate duplication events of ancestral ACSLs, which independently converged on luciferase activity with D-luciferin (Fallon et al., 2018.).

Sequence and structural conservation between firefly luciferase and fatty acyl-CoA synthetases

The structures of firefly luciferase and ACSLs share a common fold. In fact, homologous ACSLs were used to infer the unoccupied binding sites of luciferin and ATP within the first Fluc crystal structure (Conti et al., 1996.). These predictions in the apo-structure were largely confirmed when structures of Fluc co-crystallized with oxyluciferin and AMP were later published (Nakatsu et al., 2006.). Like ACSLs, firefly luciferase consists of a large ~440 amino acid N-terminal domain and a small ~110 amino acid C-terminal domain connected by a short hinge (Conti et al., 1996.). The interface between the two domains contains the active site, with the N-terminal domain contributing most of the residues responsible for binding the substrate, while the C-terminal domain introduces two lysine residues that participate in catalyzing the adenylation and oxidation reactions (Sundlov et al., 2012.). The two domains rotate independently of one another to mediate the two separate chemistries of adenylation and oxidation (Sundlov et al., 2012.). This rotation presents the two alternating lysine residues contained within the C-terminal domain (lysine 529 in the adenylation conformation and lysine 443 in the oxidation conformation) that mediate the adenylation and oxidation reactions and efficiently couples the reactions for

robust bioluminescence (Sundlov et al., 2012.). Lysine 529 likely activates ATP

toward attack by the carboxylate of luciferin, while lysine 443 helps to activate the

AMP ester of luciferin toward enolization (for the light emitting reaction) or attack

by CoASH (for the thioesterification reaction) (Sundlov et al., 2012.). These

lysine residues are conserved in ACS family enzymes and are critical for their

adenylation and CoA-ligation steps as well (Figure 1.3).
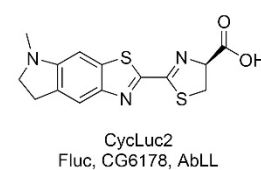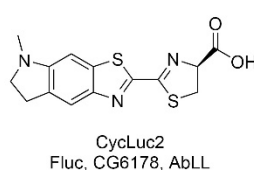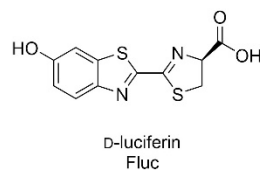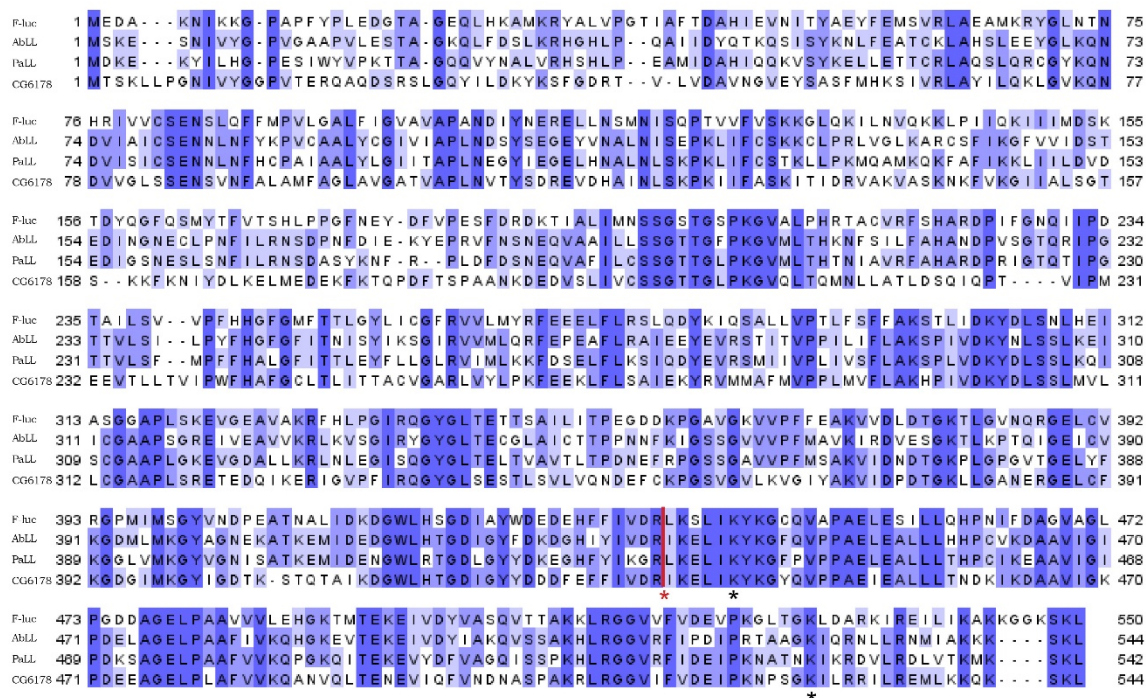
Figure 1.3. Alignment of firefly luciferase with homologous insect fatty acyl-CoA synthetases. *Photinus pyralis* firefly luciferase (Fluc), *Agrypnus binodulus* luciferase-like protein (AbLL), *Drosophila melanogaster* long-chain fatty acyl-CoA synthetase CG6178, and *Pyrophorus angustus* luciferase-like protein (PaLL) aligned using MUSCLE (Chojnacki et al., 2017.). Coloring indicates similarity in sequence, with darker shades of blue representing more similarity. Black asterisks under the lysine residues 443 and 529 (Fluc numbering) indicate catalytically important residues detailed in the text. The red vertical line and corresponding asterisk indicates where the N-terminal domains and C-terminal domains meet in the enzymes. Below the alignment are luciferin structures and the enzymes that can catalyze light emission from them.

Since Fluc shares sequence identity and enzymatic activity with insect

ACSLs, Oba et al. initially tested whether *D. melanogaster* CG6178, a

homologous ACSL from the fruit fly, could function as a luciferase and emit light with D-luciferin (Oba et al., 2004.). Unfortunately, CG6178 was incapable of functioning as a luciferase with the natural substrate. They next tested whether chimeras between Fluc and CG6178 are capable of luciferase activity (Oba et al., 2006.). The C-terminal domain of CG6178 (residues 436-544) was connected to the N-terminal domain of Fluc (residues 1-437) to make one of two chimeras. This chimera was found to be a functional luciferase. In a second chimera, CG6178's N-terminal domain (residues 1-435) was connected to the C-terminal domain of Fluc (residues 438-550). This latter chimera lacked luciferase activity, but retained ACSL activity.

These results illustrate that the N-terminal domain of Fluc is important for effective light emission with D-luciferin, but the C-terminal domain can be substituted with a corresponding domain from a related adenylating enzyme. In another compelling demonstration of the functional closeness of ACSLs to luciferase, Oba et al. functionally converted the *Agrypnus binodulus* luciferase-like protein AbLL into a luciferase capable of weakly emitting light with D-luciferin by mutation to restore a key residue in the binding site (serine 347 in Fluc) (Oba et al., 2009.). Interestingly, this serine makes a water-mediated hydrogen bond to the benzothiazole nitrogen that is important for the binding and orientation of the natural luciferase substrate D-luciferin, but is dispensable for synthetic luciferase substrates such as CycLuc2 (Harwood et al., 2011.). With the emerging number of ACSLs that bear homology to Fluc and can function as latent luciferases with

synthetic luciferins (Mofford et al., 2017.), it would be helpful to revisit the chimera experiments performed by Oba et al. in 2006 (Oba et al., 2006.), chimerizing domains from multiple ACSLs with Fluc to create luciferases with unique substrate preferences and activities.

Drosophila ACSL CG6178 is a latent luciferase with synthetic luciferins

Despite lacking luciferase activity with the natural substrate D-luciferin, Mofford et al demonstrated that the insect ACSL CG6178 is a latent luciferase when provided synthetic luciferins, specifically CycLuc2 (Mofford et al. 2014.). Additionally, CG6178 could catalyze light emission when provided D-luciferin that was pre-adenylated (Mofford et al., 2014.). This suggests that CG6178 can oxidize D-luciferin, but is prevented from performing the adenylation step that is initially required for bioluminescence. Determining the molecular basis for this substrate discrimination could thus hold the key to understanding CG6178's selectivity and enhancing its luciferase activity. Determining a structure for CG6178 could provide the detail needed to unlock the details of CG6178's latent luciferase activity. As a selective luciferase, CG6178 could be valuable for contributing to a growing palette of bioluminescent reporters usable for illuminating biology.

Using bioluminescence as a reporter

Firefly luciferase accepts modified luciferins

In nature, fireflies all use the natural substrate D-luciferin. However, the enzyme firefly luciferase can accept a wide range of synthetic luciferins (Kaskova et al., 2016.). This flexibility in luciferase's catalysis has been exploited by labs seeking improved reporters to augment the firefly bioluminescent system for research use (Figure 1.3B). Based on this willingness to catalyze light emission with such a wide range of luciferin analogs, it would be useful to explore more synthetic luciferins to identify compounds and develop a bioluminescent toolkit.

a)

Coelenterazine

Vargulin

Furimazine

b)

D-luciferin

Beetle
Luciferases

ATP, O₂

+AMP
+CO₂
+hν

1 R = OH   **3** R = NHMe
2 R = NH₂   **4** R = NMe₂

5 CycLuc1 (R = H)
6 CycLuc2 (R = Me)

7 aminoseleno-D-luciferin

8 BODIPY 650/665 X-AL

9 X = CH
10 X = N

11 X = S, Y = CH
12 X = NH, Y = N
13 X = O, Y = N

14 R = OH, n = 1   **15** R = NMe₂, n = 1
16 R = OH, n = 2   **17** R = NMe₂, n = 2
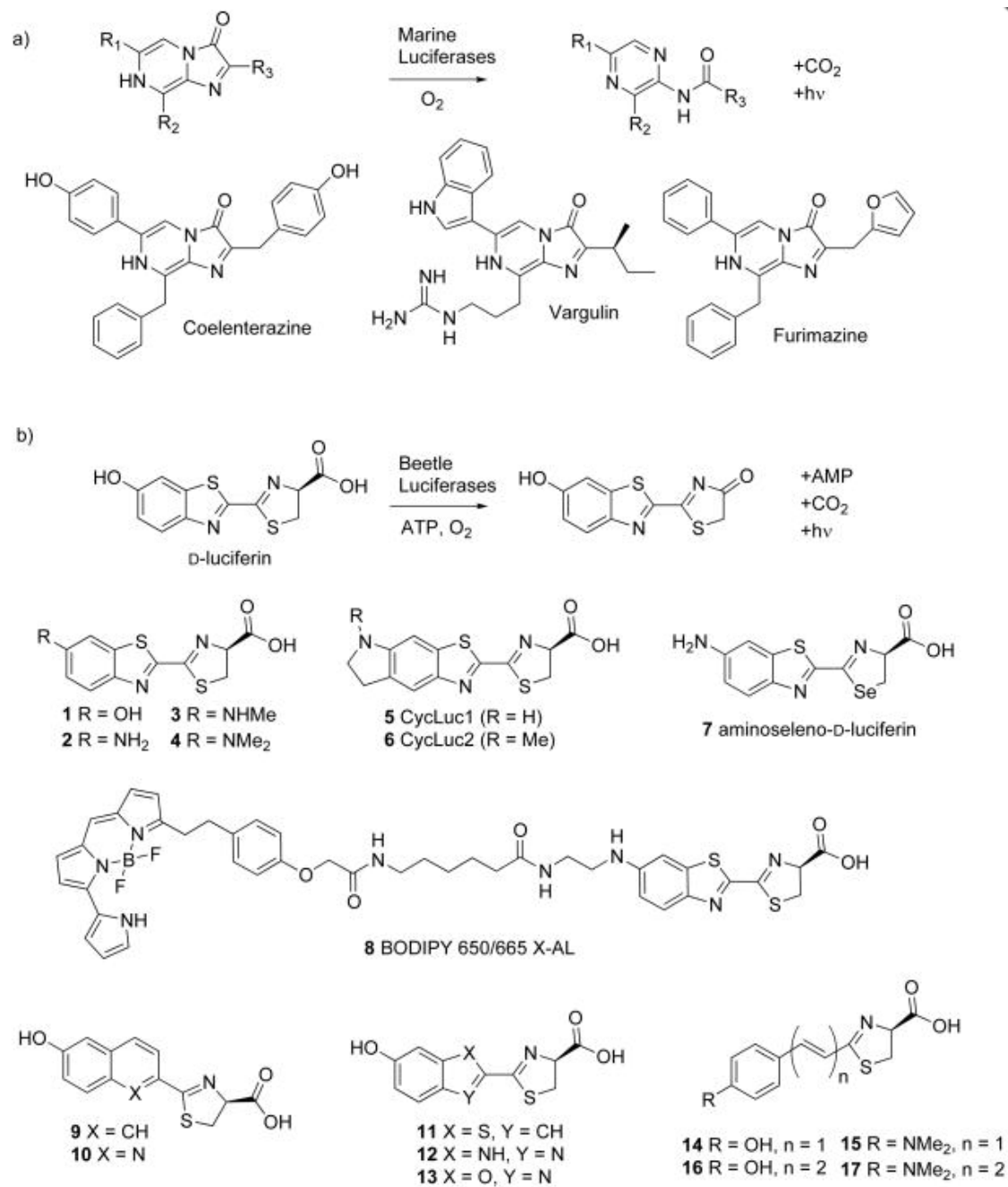
Figure 1.4. Natural and synthetic luciferins. Luciferases oxidize their luciferin substrates to access an excited-state molecule that emits light. A) Many luciferases utilize imidazopyrazinone luciferins, which are directly oxidized by their luciferase. Coelenterazine is the substrate for *Renilla, Gaussia,* and many other marine luciferases (Kaskova et al., 2016.). Vargulin is used by *Cypridina* and some fish (Kaskova et al., 2016.). Furimazine is the synthetic amidazopyrazinone substrate for NanoLuc (Hall, et al., 2012). B) Beetle luciferases all use the same substrate, D-luciferin, which must first be activated to an AMP ester before oxidation to the excited-state oxyluciferin (also shown in more detail in Figure 1.2). Consequently, D-luciferin is much more stable toward oxidation than imidazopyrazinones. Many synthetic modifications are tolerated by firefly luciferase.

In vivo use

Pioneering work by Contag and coworkers first established that bioluminescent bacteria could be imaged in live mice using a sensitive CCD camera, and then extended these results to other luciferases (Prescher and Contag, 2010). Many different luciferase-expressing cell lines, transgenic luciferase-expressing animals, and other bioluminescent reporters are now available for noninvasive imaging in live mice as has been extensively reviewed elsewhere (Prescher and Contag, 2010.; Dothager et al., 2009.).

The most common choices of luciferase and luciferin for *in vivo* bioluminescence imaging (BLI) are firefly luciferase and its substrate D-luciferin. Photon emission from this pair extends into tissue-penetrating red and near-infrared wavelengths (Zhao et al., 2005.), the substrate is nontoxic and stable in cells and live animals, and bioluminescence can be readily imaged several minutes after routine intraperitoneal (IP) injection of the substrate. Coelenterazine-utilizing enzymes such as *Renilla* and *Gaussia* are less commonly used due to the poor tissue penetration of the blue-green light emitted

by these marine luciferases (Haddock and Moline, 2010.) and the high cost and inherent instability of their imidazopyrazinone-based luciferin, which is prone to auto-oxidation (Otto-Duessel et al., 2006.). Typically, these luciferins must be prepared immediately prior to use, injected intravenously (IV), and rapidly imaged (Gil et al., 2012.; Stacer et al., 2013.; Mezzanotte et al., 2013.).

The most common method for BLI with D-luciferin is to inject 150 mg/kg intraperitoneally (IP), and to image the mice roughly 10 minutes later, when emission typically is at its peak. For the average mouse, this is 0.1 mL of a 100 mM D-luciferin solution. It is not clear how much luciferin actually reaches luciferase-expressing cells and tissues. The biodistribution of D-luciferin in the mouse is not homogenous, and access to some tissues (e.g., the brain) is relatively low (Berger et al., 2008.).

Synthetic luciferins, due to their chemical modification, are acknowledged to possibly influence tissue distribution in ways that differ from D-luciferin. Aminoluciferin (Figure 1.4: **2**) has been shown to emit 25% greater photon flux than D-luciferin from the ubiquitously-expressing transgenic luciferase mouse L2G85 when compared at a low IP injection dose of 0.1 mL of 1 mM substrate (Shinde et al., 2006.). Aminoseleno-D-luciferin (Figure 1.4: **7**) yields lower peak photon flux than aminoluciferin after IV injection of a 2.5 mM solution (0.1 mL) (Conley et al., 2012.). BODIPY 650/665 X-AL (Figure 1.4: **8**) was compared to aminoluciferin by injecting a mouse with a 0.1 mM solution (0.1 mL) into subcutaneous luciferase-expressing tumor cells (Kojima et al., 2013.). While the

light emission was red-shifted, the overall photon flux was lower than aminoluciferin and no comparison was made to D-luciferin or using standard IP or IV injection methods.

Shifting the color of bioluminescent light emission often comes at the cost of weaker overall signal

Because infrared light is less absorbed by hemoglobin (Weissleder and Ntziachristos, 2003.), much emphasis has been placed on finding ways to modulate luciferases to increase light emission in the red and near-IR. While the broad emission of firefly luciferase already contains a significant near-IR component over 650 nm, shifting the emission to even longer wavelengths would in theory enhance our ability to image deeply within living organisms. However, luciferase mutants and homologs with red-shifted spectra do not significantly increase the total emission of red light from D-luciferin compared to firefly luciferase (Viviani et al., 1999.; Branchini et al., 2010.; Liang et al., 2012.). As the peak emission is red-shifted, there is a concomitant reduction in light intensity, due in part to a lower quantum yield at the longer wavelength. Unfortunately, *in vivo* studies that control for luciferase expression levels have not shown improvements in sensitivity for red-shifted luciferases over the standard codon-optimized firefly luciferase luc2 (Mezzanotte et al., 2013.; Liang et al., 2012.).

Towards orthogonality

The noninvasive interrogation of multiple features in living animals can be achieved by combining luciferases that use D-luciferin with luciferases that use

coelenterazine or other imidazopyrazinones (Figure 1.4) (Stacer et al., 2013.; Mezzanotte, et al., 2013.; Maguire et al., 2013.). However, these approaches suffer the inherent shortcomings of imidazopyrazinones outlined above.

Alternatively, the complementary modification of luciferin substrates and mutation of luciferases could potentially allow the use of two (or more) selective beetle luciferin-luciferase pairs *in vivo*. Mutagenesis of firefly luciferase can improve the utilization and selectivity for synthetic aminoluciferins over D-luciferin *in vitro* and in live cells, suggesting that this approach is feasible (Harwood et al., 2011.).

Caged bioluminescent reporters

Geiger, Miska and coworkers pioneered the concept of bioluminogenic substrates that release D-luciferin or 6′-aminoluciferin upon the action of a hydrolytic enzyme (e.g., phosphatase, esterase, protease, β-galactosidase, or sulfatase) (Miska et al., 1987.; Miska et al., 1988.; Geiger et al., 1992.; Monsees et al., 1994.). Prior to enzyme activation, these molecules are not light-emitting substrates for luciferase. Enzymatic release of the luciferin substrate therefore reports the presence of this enzyme activity. Other workers have extended this "caged" or "pro-luciferin" concept to allow *in vivo* imaging of the enzymatic activity of β-galactosidase (Wehrman, et al., 2006.), proteases (Van de Bittner et al., 2013.; Godinat et al., 2013.), and cytochrome P450s (Roncoroni et al., 2012.) as well as the detection of reactive small molecules such as hydrogen peroxide (Van de Bittner et al., 2013.; Van de Bittner et al., 2010.). However, in employing

this strategy, care must be taken to ensure that the reporter is actually specific for the desired analyte and is generally bioavailable (Li et al., 2014.). Furthermore, caged luciferins that do not emit light with luciferase could still potentially be inhibitors (Miska et al., 1987.) or even non-luminogenic substrates, a possibility that has not been universally explored.

Caged luciferins are generally less soluble than their parent luciferin and cannot be supplied at the same high dose typically used for imaging with D-luciferin. Furthermore, signal is not detected immediately upon release of D-luciferin or 6′-aminoluciferin, but rather once the released luciferin contacts the luciferase enzyme. The construction of caged luciferins that release luciferin analogs possessing higher cell permeability, lower K_m values for luciferase and/or improved pharmacokinetic properties may therefore prove useful for increasing the sensitivity of these reporters.

Typically, caged luciferins have been used in transgenic mice that ubiquitously express luciferase (Cao et al., 2004.). In one interesting variant of this approach, BLI was used as a proximity reporter for two different cell types – an "activator" cell and a "reporter" cell (Sellmyer et al, 2013.). An activator cell expressing β-galactosidase converts the pro-luciferin Lugal into D-luciferin. Bioluminescence is only observed if the released D-luciferin diffuses out of the cell and into a reporter cell expressing firefly luciferase. Thus bioluminescence can be used to detect the proximity of the activator cells to luciferase-expressing reporter cells.

Caged luciferins could also potentially be used to improve delivery of the luciferin substrate. For example, esters of D-luciferin have been used in attempts to improve cellular delivery (Craig et al., 1991.). However, so far this approach has met with limited success, perhaps due to poor rates of esterase cleavage, low solubility, and/or the inhibition of luciferase by uncleaved esters. Luciferin esters are also inherently more reactive toward oxygen and prone to chemiluminescence than the parent luciferin. Developing caged luciferins that aid in access of luciferins to the site of luciferase expression would be useful to overcome the myriad of challenges that live animal imaging presents, especially in such environments as the brain, where D-luciferin is selectively pumped out of the blood brain barrier (Zhang et al., 2007.).

Scope of the thesis

Fireflies are a type of beetle that evolved the ability to emit light when their luciferase enzyme oxidizes their small molecule substrate, D-luciferin. Since bioluminescence uses chemistry to achieve light emission, luciferases and luciferins can be used as powerful tools to interrogate *in vivo* processes non-invasively. Our lab has developed many luciferin molecules, mutant luciferases, and enzymes homologous to firefly luciferase to improve the utility of bioluminescence while improving our understanding of how it works on a molecular level. My thesis work focuses on improving *in vivo* bioluminescence imaging and elucidating the molecular details of bioluminescence using homologous enzymes.

The first part of my thesis will focus on improvement of bioluminescent imaging *in vivo*. The natural D-luciferin substrate fireflies use to emit light is limited in its access to select mouse tissues. Some of our synthetic luciferin substrates outperform D-luciferin in live mouse brain, as shown in Chapter II (Evans et al., 2014.; Mofford et al., 2015.). In Chapter IV, I demonstrate how combining these luciferins with mutant luciferases can provide even greater improvements in light emission, while also exhibiting selectivity (Adams Jr. et al., 2016.). Additionally, in Chapter III we developed pro-luciferins, which require conversion to luciferin via a secondary enzymatic activity, that selectively report on endogenous fatty acid amide hydrolase activity (Mofford et al., 2015.). Therefore, my work uncovered improved bioluminescent reporters for *in vivo* use and an approach for longitudinally monitoring endogenous enzymatic activity in live animals.

The second part of my thesis will focus on elucidating the molecular requirements for bioluminescence. In Chapters V and VI, we explored the range of luciferin modifications tolerated by firefly luciferase and mutants. These synthetic luciferins allow us to probe the requirements of bioluminescence regarding the substrate. To interrogate the enzyme requirements for bioluminescence, we considered enzymes evolutionarily related to Fluc. Fireflies evolved their luciferase from an ancestral long-chain fatty acyl-CoA synthetase (ACSL) enzyme (Fallon et al., 2018.). Firefly luciferase still retains this ancestral activity and our lab revealed nascent luciferase activity in homologous ACSLs

(Oba et al., 2003.; Mofford et al., 2014.; Mofford et al., 2017.). We completed the first crystal structure for one of these ACSLs, the fruit fly enzyme CG6178, and improved its luciferase activity through mutagenesis following its comparison to structures of firefly luciferase in Chapter VII. In Chapter VIII, we also demonstrated that chimeric luciferase enzymes that combine one of the two domains from firefly luciferase and the other domain from one of the related ACSLs can all function as luciferases that exhibit *in vivo* selectivity for synthetic luciferins. The lessons learned from engineering luciferins, luciferases, and luciferase-like enzymes enhance our understanding of how bioluminescence works and provides numerous tools capable of illuminating biology.

Chapter II:

A Synthetic Luciferin Improves Bioluminescence Imaging in Live Mice

Melanie S. Evans, Joanna P. Chaurette, **Spencer T. Adams Jr.**, Gadarla, R. Reddy, Miranda A. Paley, Neil Aronin, Jennifer A. Prescher, and Stephen C. Miler. (2014) *Nat. Methods*. 11(4): 393-395.

Spencer T Adams Jr. performed striatal injections of AAV and performed live mouse imaging leading to creation of figures 2.9, 2.10, 2.11, and 2.13.

Summary

Firefly luciferase is the most widely used optical reporter for noninvasive bioluminescence imaging (BLI) in rodents. BLI relies on the ability of the injected luciferase substrate D-luciferin to access luciferase-expressing cells and tissues within the animal. Here we show that injection of mice with a synthetic luciferin, CycLuc1, improves BLI with existing luciferase reporters and enables imaging in the brain that could not be achieved with D-luciferin.

Introduction

Bioluminescence imaging (BLI) with firefly luciferase is a powerful and popular method to noninvasively visualize molecular and cellular features in live mice (Contag et al., 2002.; Dothager et al., 2009.; Prescher and Contag., 2010.).

Firefly luciferase chemically produces light from its small molecule substrate, D-luciferin. Introduction of these components into cells or whole animals produces light that can be captured by sensitive detectors. The inherent simplicity of this imaging method has led to its ubiquitous adoption for *in vivo* monitoring of numerous disease states and cellular functions (Contag et al., 2002.; Dothager et al., 2009.; Prescher and Contag., 2010.). Improvements to the sensitivity and dynamic range of BLI are therefore of immediate and general utility for a wide variety of applications.

Here, we show that BLI with an alternative luciferase substrate, CycLuc1 (Figure 2.1), greatly improves the sensitivity of this optical imaging technique. We find that CycLuc1 exhibits superior properties to D-luciferin *in vivo,* requiring less substrate for imaging and providing more intense and persistent light output. Moreover, this substrate enabled imaging of luciferase-expressing cells in the brains of live mice that could not be observed with D-luciferin. Thus, using CycLuc1 in place of D-luciferin expands the scope of bioluminescence imaging with existing luciferase-expressing reporters.
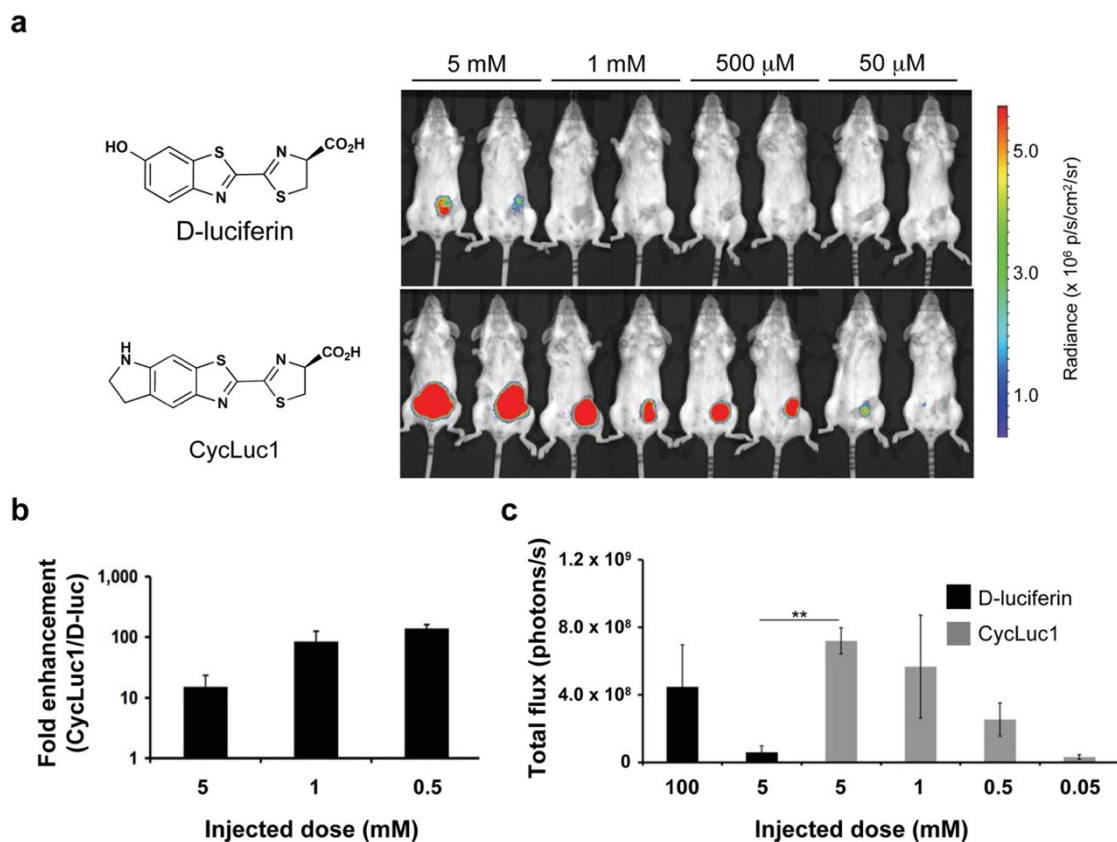
Figure 2.1. Comparative BLI of tumor xenografts with D-luciferin and CycLuc1. A) Photon flux from BALB/c mice harboring 4T1-luc2 tumors. Mice were injected i.p. with the indicated dose of D-luciferin or CycLuc1 and imaged 10 minutes post-injection. All images are plotted on the same scale. Photon intensities are shown in units of photons/s/cm^2/steradian and quantified in (B). C) Quantified light output from 4T1-luc2 cells in BALB/c mice (n = 3) injected i.p. with 100 µl of 100 mM D-luciferin (standard BLI conditions), 5 mM D-luciferin, or the indicated dose of CycLuc1. **P <0.01, (t-test).

Heretofore, efforts to improve the sensitivity of *in vivo* BLI have largely focused

on improving the expression levels of firefly luciferase or identifying mutations

that red-shift the emitted light to wavelengths that more readily penetrate through

tissues. Much less attention has been focused on modulating the properties of

the requisite small molecule luciferin, despite the importance of its cell

permeability and pharmacokinetic properties *in vivo.* In standard BLI, relatively

high concentrations of D-luciferin are required: 150 mg/kg is the typical dose for

routing i.p. injections, which equates to 0.1 mL of 100 mM D-luciferin for an

average 20 g. mouse. D-luciferin is also only modestly cell-permeable and

experiments with radiolabeled substrate have shown that its tissue distribution is

not homogenous and that uptake into some organs, such as the brain, is low.

Thus, while D-luciferin yields high light output *in vitro* and performs well *in vivo,* it

may not be the optimal substrate for imaging in the mouse.

No synthetic luciferin has yet shown improvement over the standard imaging

conditions with D-luciferin in live mice, which likely reflects issues of cell

permeability, poor biodistribution, reduced efficiency of light emission, and/or no

net increase in red light (tissue-penetrating) emission over D-luciferin. Recently,

a variety of new substrates for firefly luciferase have been reported, including

substrates with alkylated 6'-amino groups. All of these luciferin analogs yield

substantially lower levels of light emission than D-luciferin with the wild-type firefly luciferase *in vitro.* However, some substrates, such as the cyclic alkylaminoluciferin CycLuc1, exhibit improved light output in live cells relative to D-luciferin when compared at low substrate concentrations (e.g., <10 µM). Although D-luciferin yields superior photon flux from live cells when supplied at higher concentrations, we hypothesized that CycLuc1 could perform relatively well *in vivo* if the actual intracellular concentration of luciferin achieved in the mouse is limiting.

Results and Discussion

To evaluate CycLuc1 *in vivo*, we first tested its ability to image well-established mouse xenograft tumor models. We implanted 4T1-luc2 luciferase-expressing breast cancer cells into the right mammary fat pads of BALB/C mice, and imaged the mice eight days post-engraftment. Intraperitoneal injection of CycLuc1 yielded a >10-fold higher bioluminescent signal than could be obtained from D-luciferin injection at equivalent doses (Figures 2.1 and 2.2). Surprisingly, a 20-200 fold lower dose of CycLuc1 yielded the same peak photon flux as the standard imaging conditions of 150 mg/kg D-luciferin (Figure 2.1C and Figure 2.3). CycLuc1 doses up to 2000-fold lower than the standard D-luciferin imaging conditions could be imaged, while the equivalent concentrations of D-luciferin provided either weak or no signal (Figure 2.1). One hour after injection, the

relative light emission from CycLuc1 was even more pronounced, primarily due to a ten-fold drop in D-luciferin light emission over this period (Figure 2.2). The improved performance of CycLuc1 also translated across different cell types, mouse strains, and implantation sites. Photon flux from luciferase-expressing DB7 breast cancer cells (DB7-luc) implanted in the hind flanks of FVB mice was up to 40-fold higher with CycLuc1 versus D-luciferin administration at an equivalent dose (Figure 2.4). CycLuc1 also enabled detection of luciferase-expressing CMT-64 lung cancer cells implanted into the hind flank of C57BL/6 mice, one of the most widely used mouse strains, providing increased signal intensity at all doses examined (Figure 2.5).
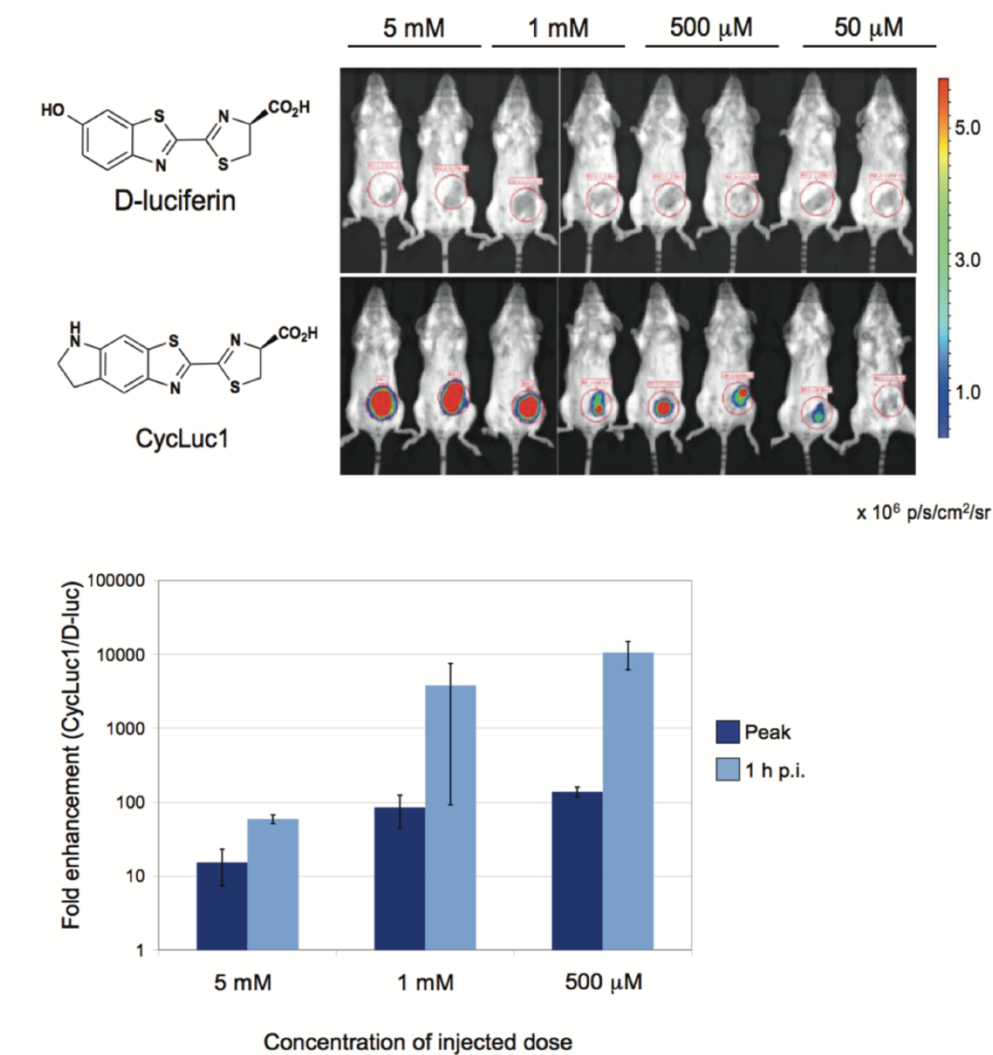
Figure 2.2. Comparative BLI of tumor xenografts with D-luciferin and CycLuc1 after 1 hour. BALB/c mice harboring 4T1-luc2 tumors were injected i.p. with the indicated dose of D-luciferin (top images) or CycLuc1 (bottom images) and imaged 1 h post injection. All images are plotted on the same scale. Red circles outline the regions of interest (ROIs) used to quantify photon flux (below). In the bar graphs, photon flux values were calculated for all ROIs, and the fold increase in bioluminescent signal achieved with CycLuc1 relative to D-luciferin (at varying concentrations) is plotted. Error bars represent the standard error of the mean.
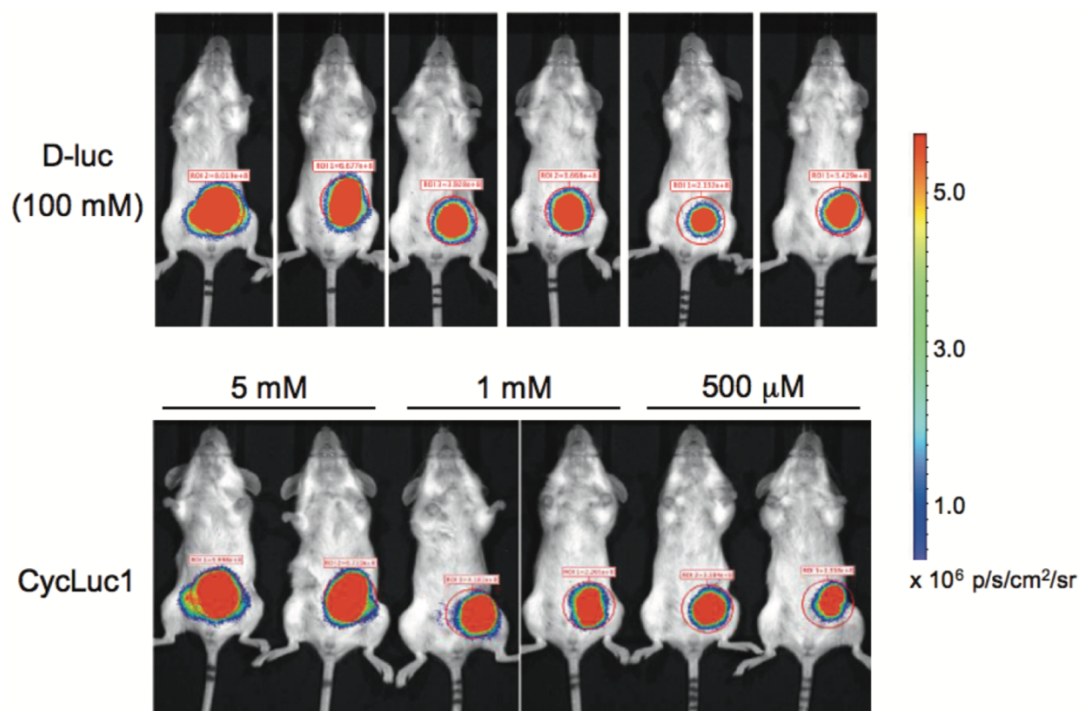
Figure 2.3. Bioluminescence images of 4T1-luc2 cells in BALB/c mice injected i.p. with 100 μl of 100 mM D-luciferin (standard BLI conditions) or the indicated dose of CycLuc1.
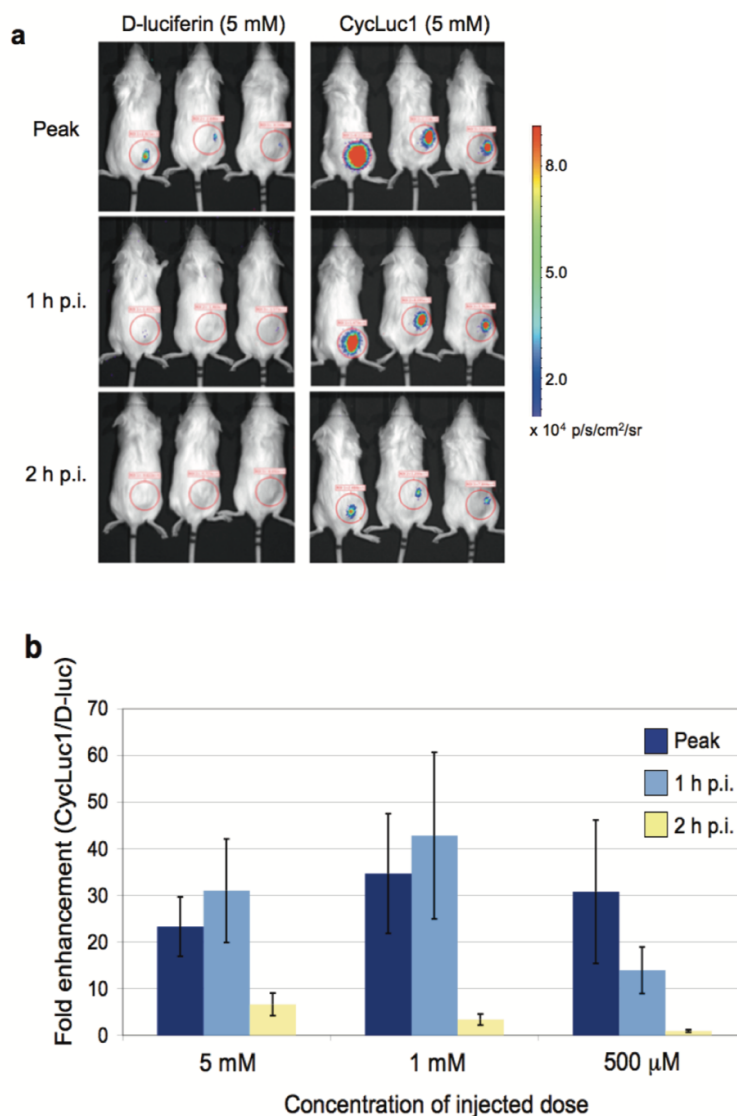
Figure 2.4. BLI of DB7-luc cells in FVB mice. DB7-luc cells were implanted into the right flanks of FVB mice prior to imaging with D-luciferin (5 mM-500 μM) or CycLuc1 (5 mM-500 μM). A) Representative images from mice treated with 5 mM solutions are shown at peak emission intensities (top panels), one hour post-injection (middle panels), and two hours post-injection (bottom panels). All images are plotted on the same relative scale, and the red circles outline the regions of interest (ROIs) used to quantify relative photon flux from the animals. B) The fold increase in bioluminescent signal achieved with CycLuc1 relative to D-luciferin (at various concentrations) is plotted. Error bars represent the standard error of the mean.
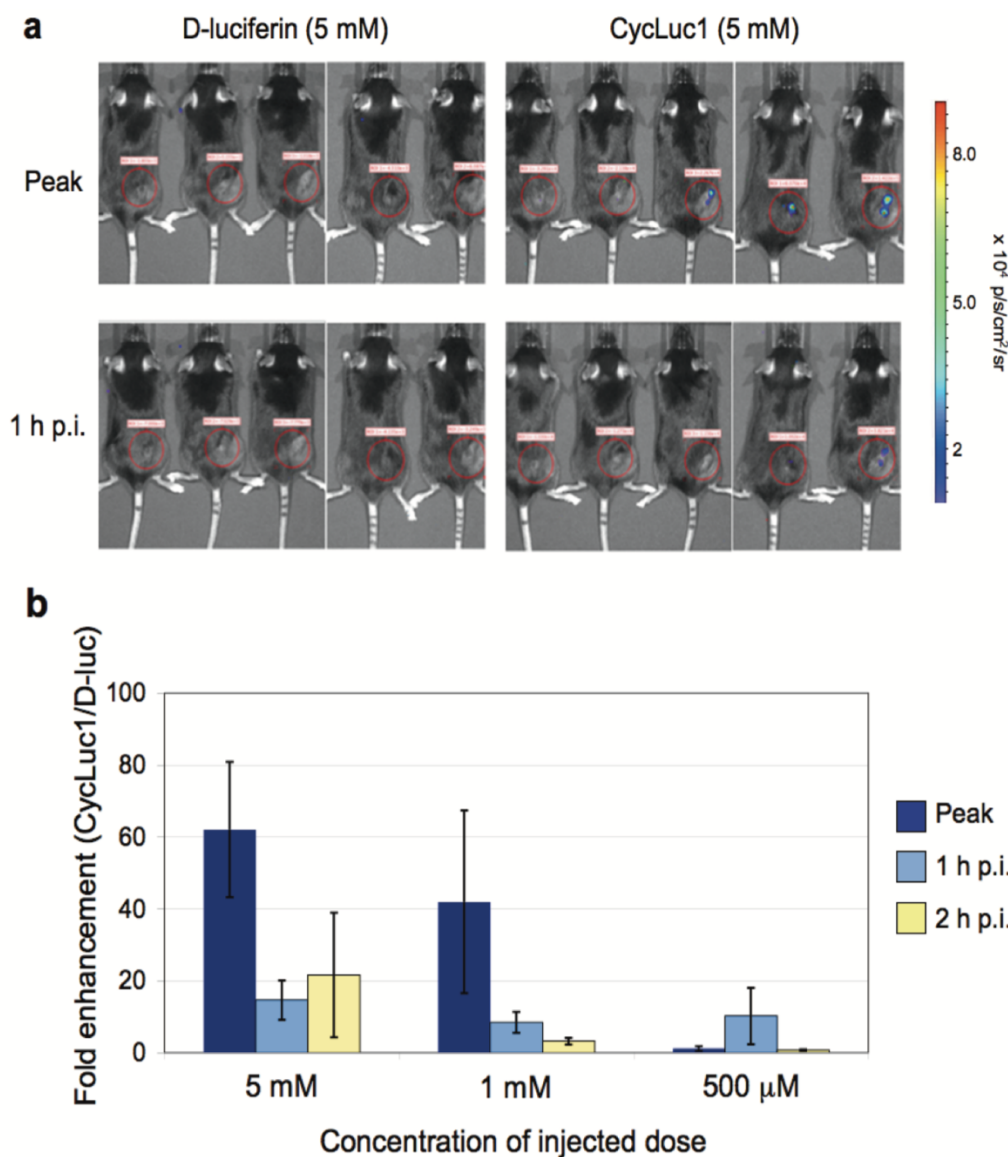
Figure 2.5. BLI of CMT-64-luc cells in C57BL/6 mice. CMT-64-luc cells were implanted into the right flanks of FVB mice prior to imaging with D-luciferin (5 mM-500 μM) or CycLuc1 (5 mM-500 μM). A) Representative images for mice treated with 5 mM solutions are shown at peak emission intensities (top panels), one hour post-injection (middle panels) and two hours post-injection (bottom panels). All images are plotted on the same relative scale, and the red circles outline the regions of interest (ROIs) used to quantify relative photon flux from the animals. B) The fold increase in bioluminescent signal achieved with CycLuc1 relative to D-luciferin (at various concentrations) is plotted. Error bars represent the standard error of the mean.

Next, to compare the distribution and trafficking of CycLuc1 and D-luciferin *in vivo,* we utilized a transgenic mouse that expresses luciferase in most tissues (L2G85-FVB). Consistent with previous studies, intraperitoneal injection of D-luciferin revealed access to tissues throughout the mouse, albeit with the highest photon flux confined to the abdominal cavity near the site of injection (Figure 2.6). In contrast, i.p. injection of CycLuc1 revealed a bioluminescent signal that was ten-fold higher in intensity and escaped from the abdominal cavity to give a broad distribution that was maintained for up to two hours (Figure 2.6). Comparison of intravenous injections was even more striking: CycLuc1 signal peaked at 4-5 min post-injection and then yielded a steady signal that was up to 100-fold greater than that of D-luciferin, and persisted for more than 60 min (Figures 2.7 and 2.8). By contrast, with D-luciferin the signal peaked immediately after injection, and dissipated over 20 min (Figures 2.7 and 2.8).
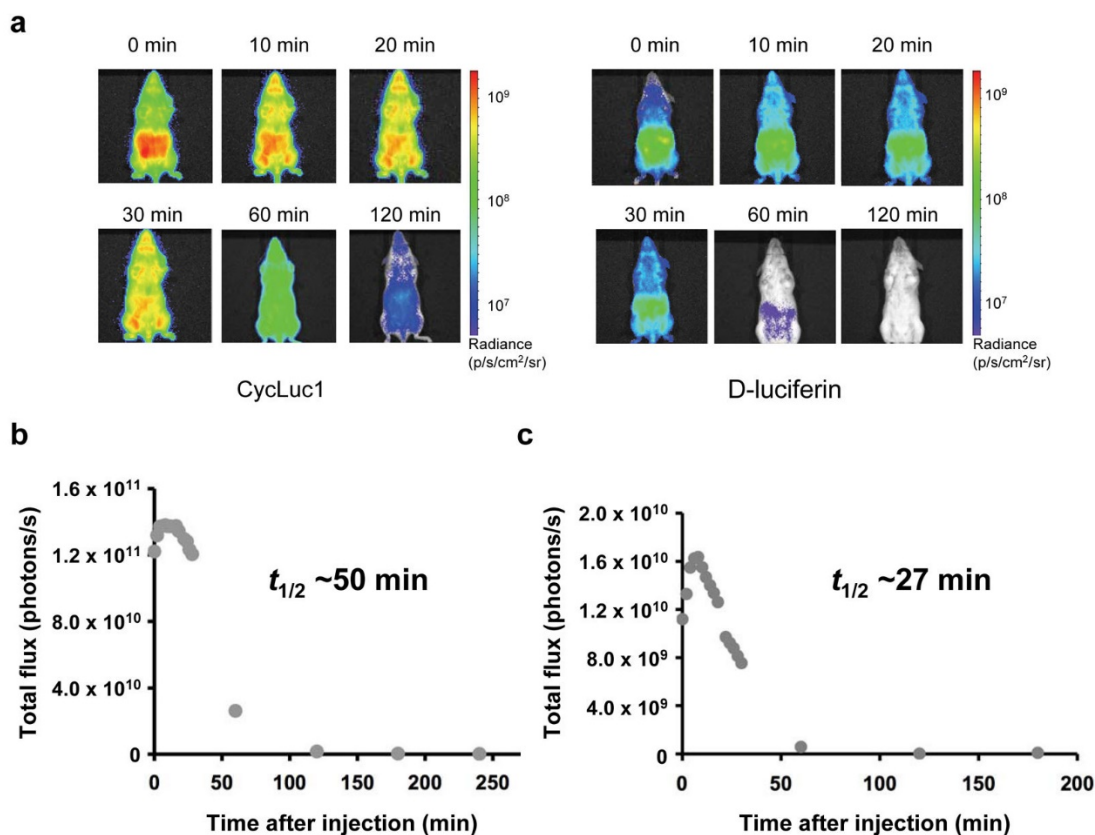
Figure 2.6. Comparison of intraperitoneally-injected D-luciferin and CycLuc1 in luciferase-expressing transgenic mice. A) Photon flux from L2G85-FVB mice injected i.p. with 100 µl of 5 mM CycLuc1 (left) or D-luciferin (right) and imaged over time. Photon intensities are shown in units of photons/s/cm^2/steradian and plotted on logarithmic scales. (B-C) Total photon output from L2G85-FVB luc mice treated with (B) CycLuc1 or (C) D-luciferin from above. The apparent bioluminescent half-lives are shown. Data are representative of three independent experiments.
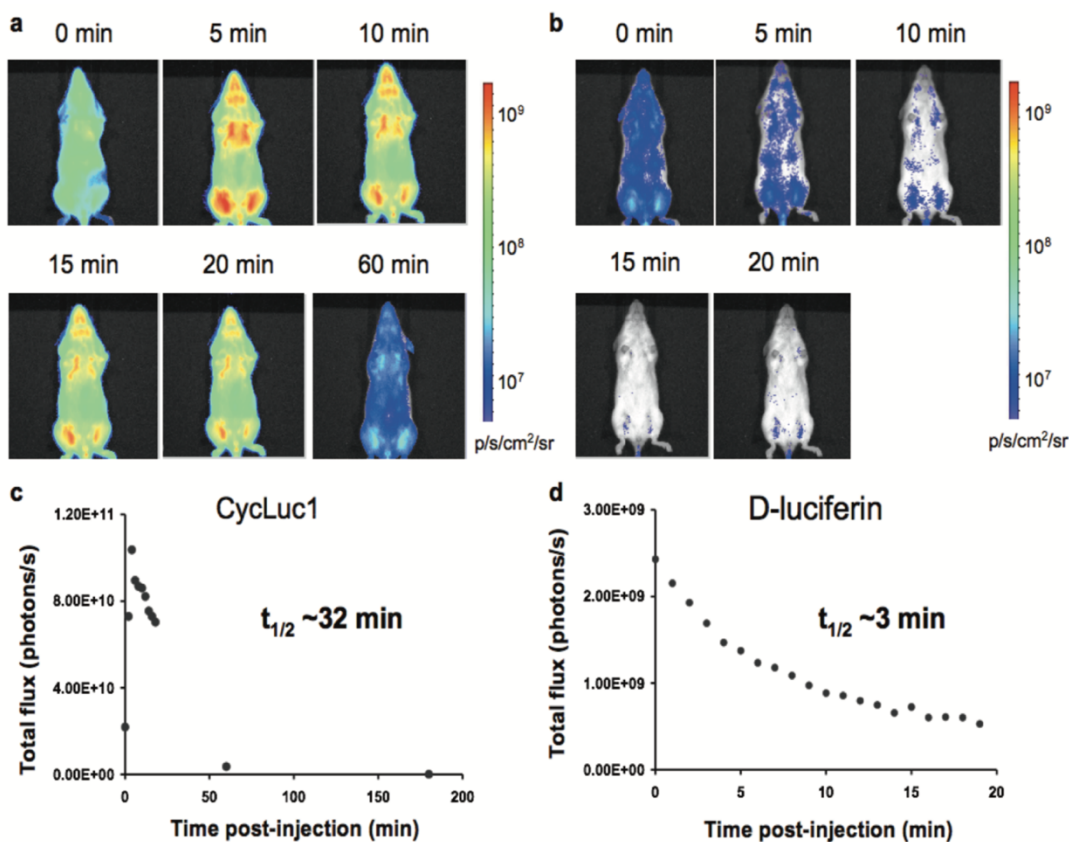
Figure 2.7. Comparison of tail vein-injected D-luciferin and CycLuc1 in luciferase-expressing transgenic mice. L2G85-FVB mice were injected i.v. with 100 µl of 5 mM (A) CycLuc1 or (B) D-luciferin. For (A-B), photon intensities are shown in units of photons/s/cm^2/steradian and plotted on logarithmic scales. C) Total photon output from L2G85-FVB luc mice treated with CycLuc1 (i.v.) or (D) D-luciferin (i.v.). The apparent half-life of bioluminescent signal ($t_{1/2}$) is shown. (Note: the animals were placed on the imaging bed immediately after injection and the start of signal acquisition.)
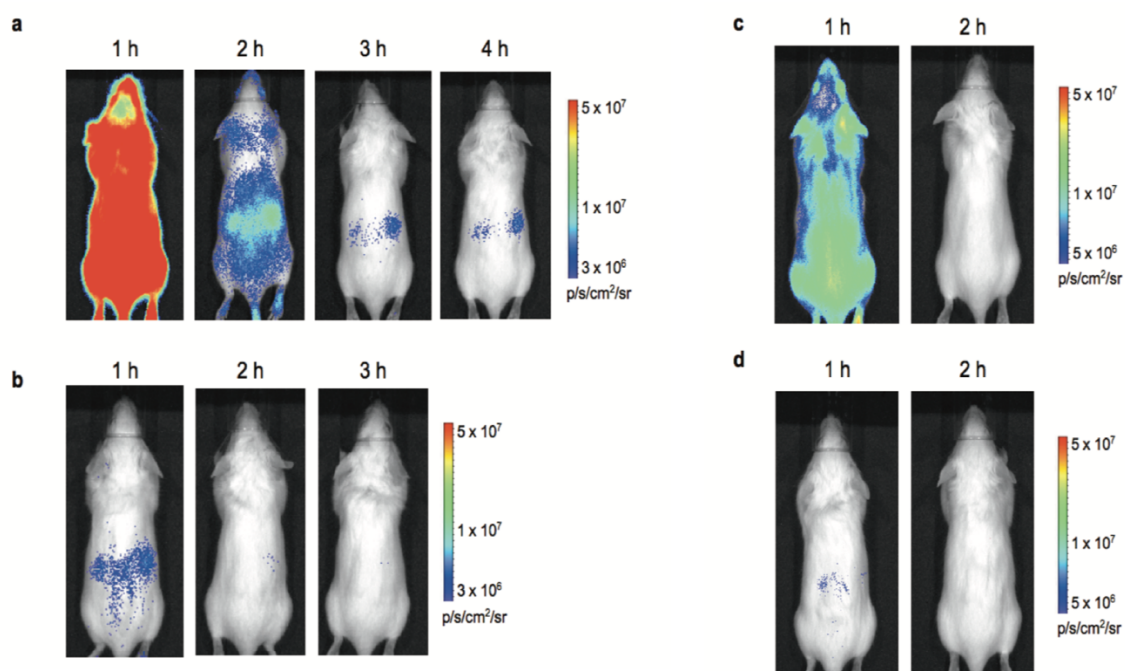
Figure 2.8. Biodistribution of D-luciferin and CycLuc1 in luciferase-expressing transgenic mice. Mice were injected with 100 µl of 5 mM (A) CycLuc1 or (B) D-luciferin and dorsal images were acquired until the bioluminescent signal returned to background levels (180 min for D-luciferin, 240 min for CycLuc1). Images were also acquired following intravenous (i.v.) injection of 100 µl of 5 mM (C) CycLuc1 or (D) D-luciferin. For (A-D), photon intensities are shown in units of photons/s/cm/steradian and plotted on logarithmic scales.

In light of these exciting results, we next asked whether CycLuc1 could improve bioluminescence signals in the brain. The blood-brain barrier limits the access of many small molecules to this tissue, and thus imaging in the brain is particularly challenging. To evaluate the ability of CycLuc1 to access brain tissue, we imaged mice that had been treated with adeno-associated virus 9 (AAV9) to express

codon optimized luc2 luciferase in the brain striatum. We found that i.p. injection of CycLuc1 provided an 8.1 ± 1.5 fold higher signal than the standard 150 mg/kg D-luciferin, despite a 20-fold lower imaging dose of CycLuc1 (Figures 2.9 and 2.10). Thus, CycLuc1 can readily cross the blood-brain barrier and access deep brain tissues. Next, we crossed Dat (also known as *Slc6a3*) Cre driver mice with *Rosa*26 floxed-stop luciferase reporter mice. *Dat-Cre* drives reporter expression at low levels from the endogenous *Rosa26* promoter in dopaminergic neurons, primarily in the substantia nigra, one of the deepest brain tissues. Injection of these mice with D-luciferin failed to yield any measurable brain signal *in vivo* (Figures 2.9 and 2.11). In sharp contrast, we found that CycLuc1 not only enabled imaging in these same mice but that homozygous mice with two copies of the *Rosa26-luc* allele could be readily distinguished from heterozygous mice by the 1.9 ± 0.2 fold higher photon flux (Figures 2.9 and 2.11).
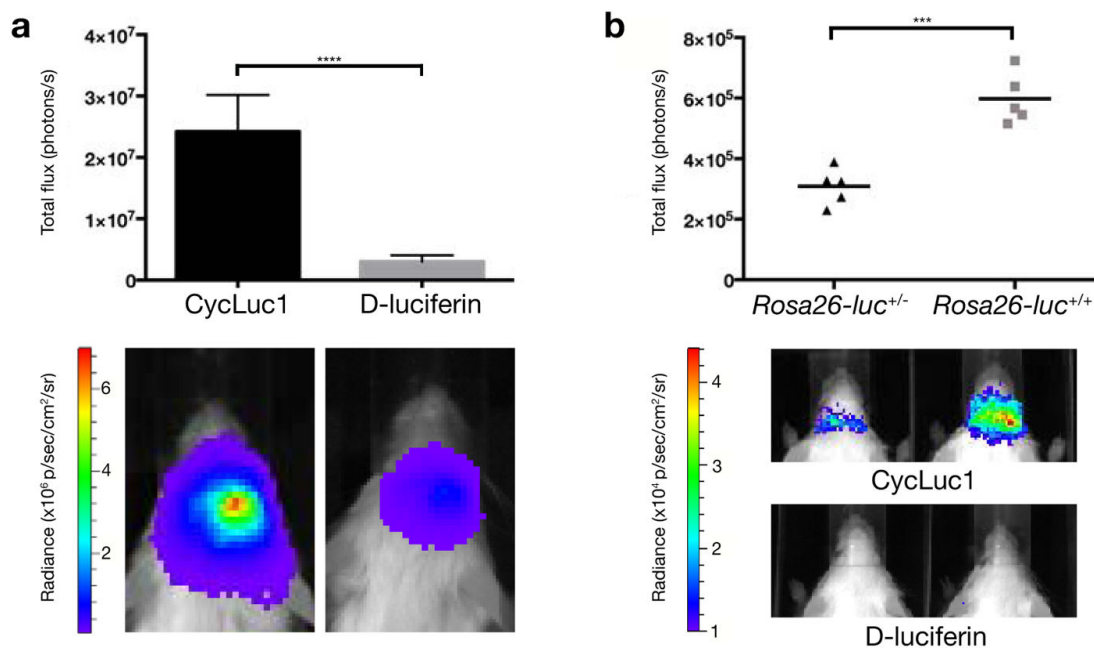
Figure 2.9. Comparison of D-luciferin and CycLuc1 in the brain. A) Photon flux from mice expressing AAV9-CMV-luc2 in the brain striatum ten minutes after i.p. injection with 100 µl of 5 mM CycLuc1 or 100 mM D-luciferin (n = 5). Error bars are S.E.M. ****P < 0.0001 (t-test). B) Photon flux from *Dat-Cre*$^{+/-}$*Rosa26-luc*$^{+/-}$ (n = 5) and *Dat-Cre*$^{+/-}$*Rosa26-luc*$^{+/+}$ (n = 5) mice after i.p. injection with 100 µl of 5 mM CycLuc1. *** P < 0.001 (t-test). No quantifiable photon flux was observed from the brain after i.p. injection with 100 µl of 100 mM D-luciferin.
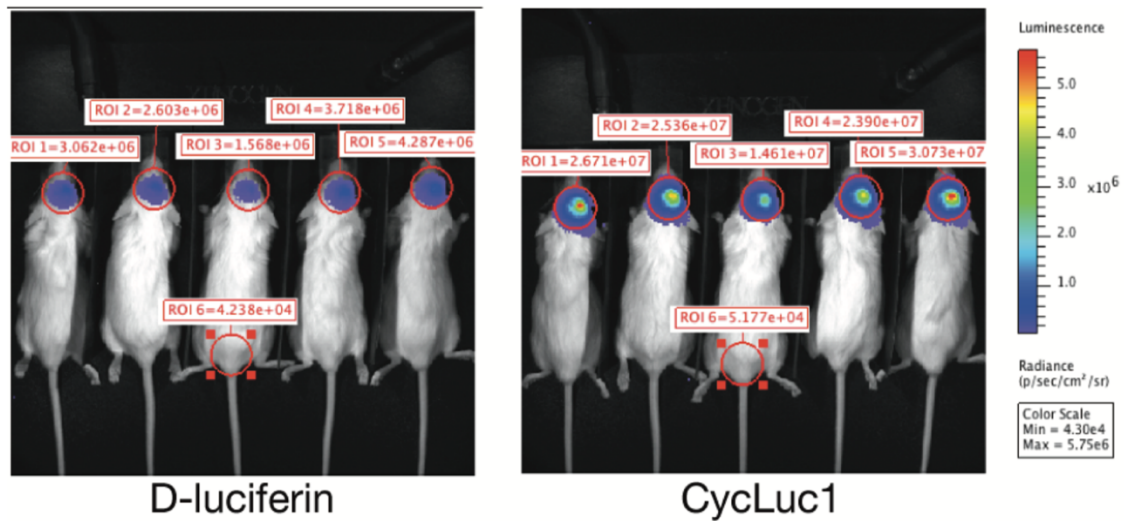
Figure 2.10. Comparison of photon flux from AAV9-luc2 mice. Five female FVB mice were treated with adeno-associated virus 9 (AAV9) as described in the Methods to express codon-optimized *luc2* luciferase in the brain striatum. Nine weeks after surgery, the mice were injected i.p. with the standard imaging dose of D-luciferin (0.1 ml of 100 mM) and imaged ten minutes post-injection. The next day, the same five mice were injected i.p. with 0.1 ml of 5 mM CycLuc1 and imaged ten minutes post-injection. Both images are plotted on the same scale, and the red circles outline the regions of interest (ROIs) used to quantify relative photon flux. ROI6 was used to measure background signal.
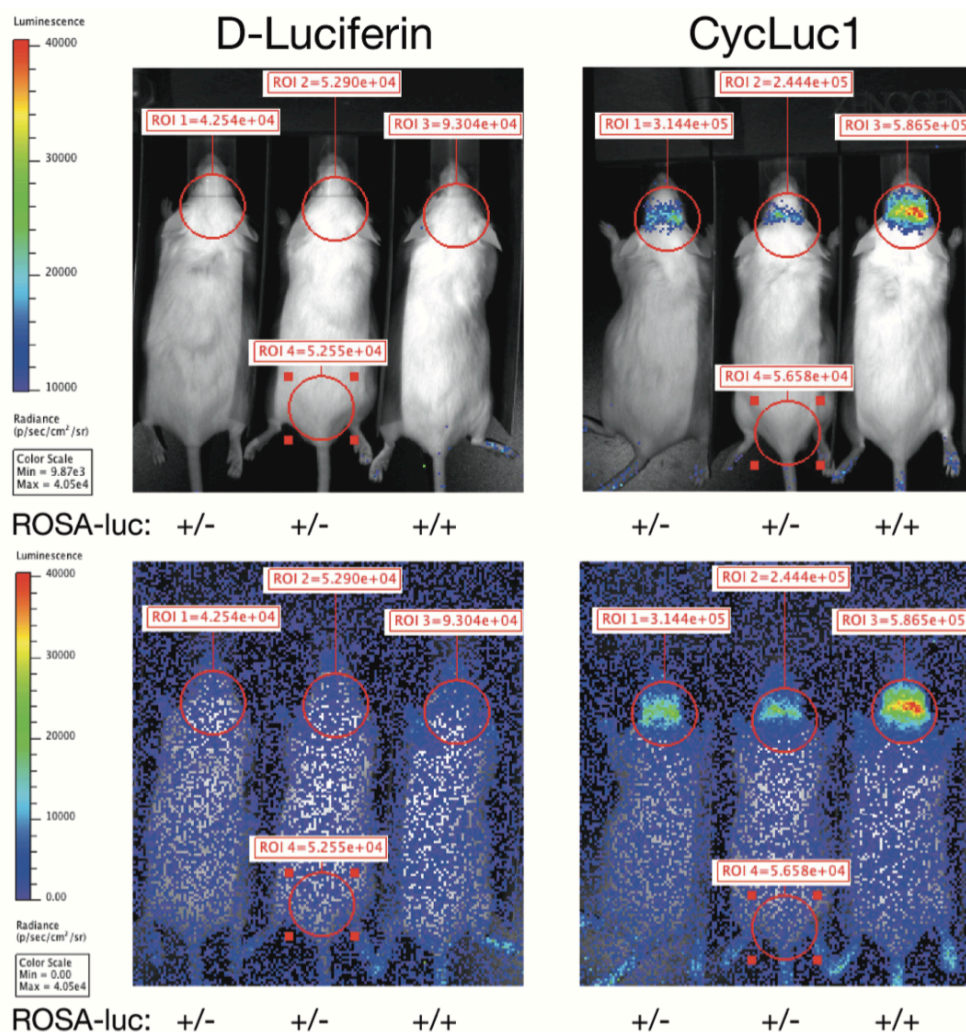
Figure 2.11. Comparison of photon flux from *Dat-luc* mice. *Dat-luc* mice were injected i.p. with the standard imaging dose of D-luciferin (0.1 ml of 100 mM) and imaged ten minutes post-injection. The next day, the same mice were injected i.p. with 0.1 ml of 5 mM CycLuc1 and imaged ten minutes post-injection. The first two mice are heterozygous for the *Rosa26-luc* allele, the third is homozygous. Both images are plotted on the same scale, and the red circles outline the regions of interest (ROIs) used to quantify relative photon flux. ROI4 was used to measure background signal. The top images were autoscaled by the Living Image software. In the bottom images, the same data is displayed with the minimum set to zero to show all signal, including camera noise.

The improved sensitivity of BLI with CycLuc1 has immediate ramifications for biological studies in mice. Simply replacing the obligatory injection of D-luciferin with CycLuc1 improves the sensitivity of bioluminescent detection, while retaining the use of existing luciferase reporters. CycLuc1 reduces the amount of substrate required for BLI and allows imaging at low doses where D-luciferin provides weak or no signal. Furthermore, CycLuc1 allows detection of low-level luciferase expression in deep brain tissues that cannot be detected with D-luciferin, and thus opens up new applications for noninvasive imaging in the brain. One potential contributor to the improved *in vivo* performance of CycLuc1 is a red-shift in the emitted photons to more tissue-penetrating wavelengths (Figure 2.12). However, the percentage of Cy5.5-filtered flux from the brains of live AAV-treated mice is actually slightly higher for D-luciferin than CycLuc1 (9.4% vs. 8.1%; Figure 2.13), perhaps reflecting the red-shift in luciferase emission previously reported at 37 °C *in vivo* (Zhao et al., 2005.). Moreover, a change in emission wavelength alone cannot explain the differences we observed in tissue distribution, signal persistence, or the ability to image at very low substrate concentrations where CycLuc1 is favored (Figure 2.13). *In vivo*, these same cells yield greater photon flux with CycLuc1, even in tumors that are located near the surface and/or proximal to the site of substrate injection. This suggests that the delivery of D-luciferin to luciferase-expressing cells *in vivo* is limiting, and that the cell permeability, lower K_m, and bioavailability of CycLuc1 play important roles in its superior *in vivo* performance.
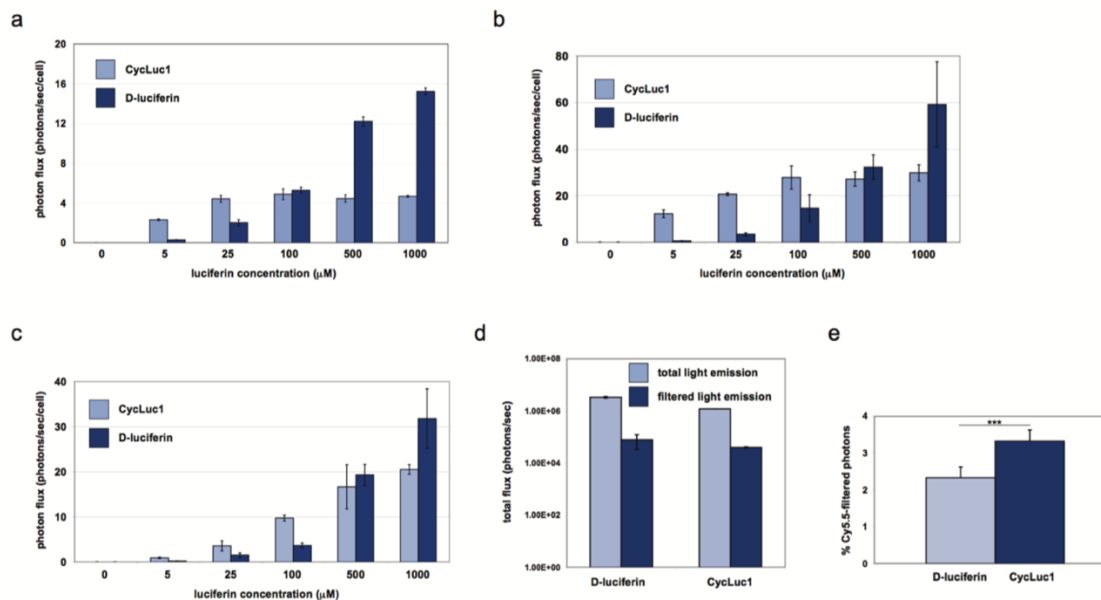
Figure 2.12. Live cell bioluminescence with CycLuc1 and D-luciferin through a Cy5.5 filter. Bioluminescence imaging of (A) DB7-luc, (B) 4T1-luc2, and (C) CMT-64-luc cells treated with the indicated concentration of CycLuc1 (light blue bars) or D-luciferin (dark blue bars). D) Light output from 50,000 4T1-luc cells treated with 1 mM D-luciferin or CycLuc1. Photons were collected either with an open filter (light blue bars) or after passage through a Cy5.5 filter (dark blue bars). The percent filtered light captured in each case is shown in (E), *** *P* < 0.001 (t-test). For (A-E), error bars represent the standard error of the mean for three independent experiments.
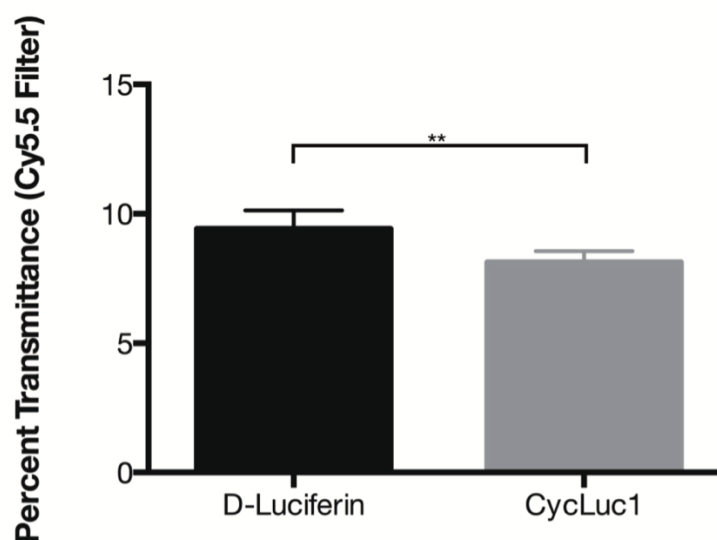
Figure 2.13. Photon flux from AAV9-luc2 mice through a Cy5.5 filter. Mice were imaged as described for Figure 10, with and without a Cy5.5 emission filter (695-770 nm bandpass). The ratio of Cy5.5-filtered photon flux to unfiltered photon flux is expressed as a percentage (D-luciferin: 9.4 ± 0.3 %; CycLuc1: 8.1 ± 0.2 %). Error bars are S.E.M. (n = 5 mice for each luciferin). ** $P < 0.01$ (t-test).

Conclusion

In conclusion, CycLuc1 improves *in vivo* BLI using existing luciferase reporters, yet requires much less substrate for imaging. Transgenic luciferase-expressing mice treated with CycLuc1 demonstrated that the analog has broad access to mouse tissues, and more persistent light emission than with D-luciferin by either i.p. or i.v. injection. In the brain, CycLuc1 provided stronger BLI signals than D-luciferin, and even enabled detection of luciferase expression that could not be imaged with D-luciferin. Based on these results, CycLuc1 can be recommended

for immediate use in BLI, while future adaptation of related synthetic luciferins and mutant luciferases is expected to allow even greater improvements in the sensitivity, selectivity, and scope of *in vivo* bioluminescence reporters.

Materials and Methods

Contributions

M.S.E. and J.A.P. imaged tumors and L2G85-FVB mice, G.R.R. synthesized CycLuc1, M.A.P. imaged cultured cells, J.P.C. bred *Dat* mice, S.T.A. and J.P.C. imaged AAV9 and *Dat* mice, N.A. contributed to the development of AAV9 and *Dat* mouse models and manuscript editing, S.C.M. designed CycLuc1, and S.C.M. and J.A.P. led the study and wrote the manuscript.

General

D-luciferin and CycLuc1 were synthesized as previously described. Luciferase expressing 4T1 cells, CMT-64 cells, and DB7 cells were provided by the Contag laboratory (Stanford University).

Mice

Pathogen-free BALB/c, FVB/N, C57BL/6, and luciferase-expressing transgenic mice (FVB-Tg(*CAG-luc, -GFP*)L2G85Chco/FathJ) were obtained from either Charles River or the Jackson Laboratory and housed in UC Irvine's AAALAC-accredited animal-care facility. All mice used were littermates or age-matched (6-

12 weeks of age) females, were provided access to food and water *ad libitum,*

and housed in the animal facilities at UC Irvine. All procedures with these mice

were approved by the Animal Care and Use Committee at UC Irvine (protocol

#2011-2987 to J.A.P.). FVB/NJ, B6.SJL-*Slc6a3$^{tm1.1(cre)Bkmn}$*/J("Dat-Cre"), and

FVB.129S6(B6)-*Gt* (*ROSA*)*26Sor$^{tm1(Luc)Kael}$*/J("*Rosa26-luc*") mice were purchased

from the Jackson Laboratory and were maintained and used according to the

guidelines of the Institutional Animal Care and Use Committee of the University

of Massachusetts Medical School (docket #A978-12 to N.A.). *Dat-Cre* mice were

mated with floxed-stop *Rosa26-luc* mice to generate white *Dat-cre$^{+/-}$Rosa26-luc$^{+/-}$*

and *Dat-Cre$^{+/-}$Rosa26-luc$^{+/+}$* mice. Offspring were genotyped by PCR.

Tumor cell inoculations

Mice were inoculated subcutaneously with 1 x 10^6 luciferase-expressing CMT-64

or DB7 cells in serum-free RPMI media. Tumors were allowed to establish for 1-2

weeks before imaging. To establish 4T1 tumors, aliquots of the cells were mixed

1:1 by volume with Matrigel (usually 5 x 10^5 cells in 50 µl serum-free DMEM

media plus 50 µl Matrigel per injection) and transplanted into the orthotopic

second or fourth mammary fat pads (left or right side) of mice. Eight days post-

engraftment, the mice were injected i.p. with 100 µl of either D-luciferin or

CycLuc1 (50 µM – 5 mM), and imaged ten minutes post-injection.

Bioluminescence imaging

To image tumor cells *in vivo*, mice were injected i.p. with 100 µl of luciferin stocks (in PBS). The animals were anesthetized with isoflurane (2% in 1 l/min oxygen), and bioluminescence images were acquired using the IVIS Lumina system (a Xenogen Product from Caliper Life Sciences, now Perkin-Elmer). Images were acquired every 2 min for 30 min (10 s exposure/image). The mice were also imaged 1 h post-injection and 2 h post-injection (10 s exposure/image). Images were analyzed using Living Image software. Regions of interest (ROIs) were drawn around each cell mass, and the total number of photons within each ROI were recorded. ROI size was held constant across all images. Prior to imaging with CycLuc1, the mice were stratified using standard BLI conditions (100 µl i.p. injection of 100 mM D-luciferin in PBS).

To analyze the biodistribution of D-luciferin and CycLuc1 *in vivo*, the compounds were injected (100 µl of 5 mM solutions in PBS) i.p. or i.v. into luciferase-expressing FVB transgenic mice. The mice were imaged over time as described above, and quantitative analyses of the light emission were performed using Living Image software as above.

Construction of AAV-CMV-luc2

Codon-optimized luc2 luciferase from pGL4 (Promega) was cloned into the EcoR1-Sal1 sites of a pAAV-CMV vector (gift of Guangping Gao). The plasmid

was packaged into AAV serotype 9 by the University of Massachusetts Medical School Viral Vector Core.

AAV9-CMV-luc2 vector striatal injections

FVB/NJ mice (5 females, 6 weeks old, Jackson Laboratory, Bar Harbor, ME) were anesthetized with 250 mg/kg tribromoethanol prior to surgery, placed on a stereotactic frame and injected with 0.25 µl 1e13 GC AAV9-CMV-Luc2 by micropump syringe (Nanofil, World Precision Instruments) at the lateral edge of the striatum/cortex border (anterior 1 mm, lateral 3 mm, and ventral 2 mm from bregma). Imaging was performed at least two weeks after AAV injection.

Brain imaging

Bioluminescence imaging luciferase-expressing mice was performed as described above in the University of Massachusetts Medical School Small Animal Imaging Core using an IVIS 100 imaging system and analyzed with Living Image software and Graphpad Prism 6.

Supplementary Material

Refer to Web version on PubMed Central for supplementary material.

Acknowledgements

Chapter III:

Luciferin Amides Enable *in vivo* Bioluminescence Detection of Endogenous Fatty Acid Amide Hydrolase Activity

David M. Mofford, **Spencer T. Adams Jr.**, G.S. Kiran Kumar Reddy, Gadarla Randheer Reddy, and Stephen C. Miller. (2015) *J. Am. Chem. Soc.*, 137(27): 8684-8687.

Spencer T. Adams Jr. performed striatal injections of AAV and tail vein injections of AAV, as well as mouse imaging and preparation of figures 3.10-3.18.

Summary

Firefly luciferase is homologous to fatty acyl-CoA synthetases. We hypothesized that the firefly luciferase substrate D-luciferin and its analogs are fatty acid mimics that are ideally suited to probe the chemistry of enzymes that release fatty acid products. Here, we synthesized luciferin amides and found that these molecules are hydrolyzed to substrates for firefly luciferase by the enzyme fatty acid amide hydrolase (FAAH). In the presence of luciferase, these molecules enable highly sensitive and selective bioluminescent detection of FAAH activity *in vitro*, in live cells, and *in vivo*. The potency and tissue distribution of FAAH inhibitors can be imaged in live mice, and luciferin amides serve as exemplary reagents for greatly improved bioluminescence imaging in FAAH-expressing tissues such as the brain.

Introduction

Firefly luciferase is best known for its light emission chemistry with D-luciferin, but it is also a long-chain fatty acyl-CoA synthetase (ACSL) that can bind fatty acid substrates such as arachidonic acid (Figure 3.1) (Oba et al., 2003.). Conversely, we have recently shown that an ACSL from the fruit fly *Drosophila melanogaster* is a latent luciferase that can emit light with a synthetic luciferin (Mofford et al., 2014). In both cases, adenylation of a carboxylic acid is the first step in catalysis. Furthermore, both enzymes can bind fatty acids ranging from octanoic acid to arachidonic acid, suggesting that D-luciferin and aminoluciferin analogs (Reddy et al., 2010.; Adams et al., 2014.;Mofford et al., 2014) are acting as fatty acid mimics. Based in part on this observation, we hypothesized that luciferins are ideally suited to probe the chemistry of enzymes that release fatty acid products.

Fatty acid amide hydrolase (FAAH) is a serine hydrolase that limits the lifetime and sphere of action of fatty acid amide second messengers by hydrolysis to their corresponding fatty acids (Figure 3.1) (Blankman and Cravatt, 2013.; Cravatt et al., 1996.). Most notably, arachidonoyl ethanolamine (anandamide) is a locally generated agonist for the cannabinoid receptor CB1. Inhibition of FAAH

prolongs the action of anandamide and is therefore an attractive drug target for the treatment of pain, anxiety, and cannabinoid dependence (Blankman and Cravatt, 2013.). Many FAAH inhibitors are being developed as potential therapeutics, and there is great interest in detecting FAAH activity *in vivo* (Shoup et al., 2015.). Current techniques to assay FAAH inhibitors in mice primarily require sacrificing the mouse, homogenizing the tissues, adding radioactive lipid substrates, and HPLC analysis of the products (Long et al., 2011.). This places large demands on time and quantities of mice required to evaluate inhibitors and furthermore cannot give longitudinal data from the same animal. Some inroads have been made with PET imaging probes for FAAH, but these are specialized and expensive tools with low throughput and signal-to-noise that lack the specificity for whole-body imaging (Shoup et al., 2015.).
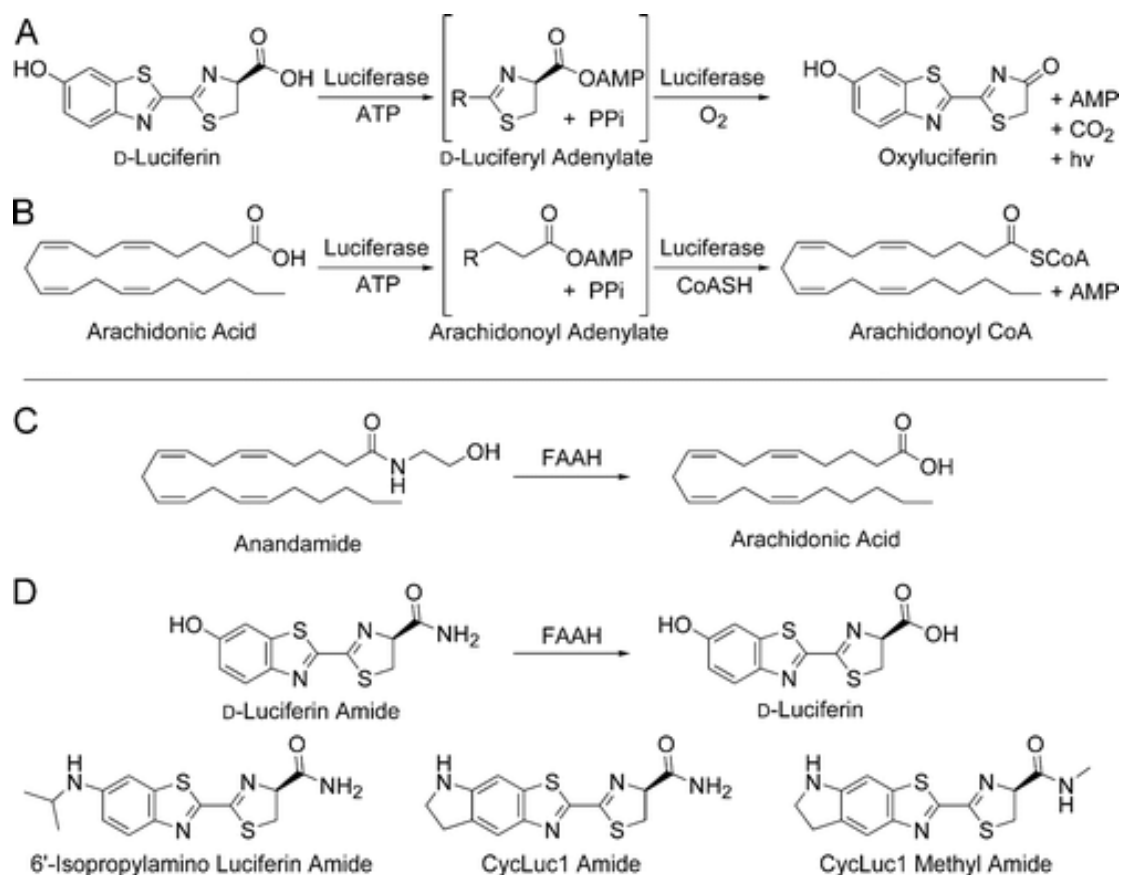
Figure 3.1. Enzyme mechanisms and luciferin structures. A) Firefly luciferase catalyzes light emission from D-luciferin. B) Firefly luciferase is also a fatty acyl-CoA synthetase. C) FAAH cleaves anandamide to arachidonic acid. D) Luciferin amides could allow bioluminescence imaging of FAAH activity.

FAAH readily accepts a wide range of saturated and unsaturated fatty acid amides in addition to anandamide (Cravatt et al., 1996.; Boger et al., 2000.) and has been shown to hydrolyze ethanolamides, primary amides, and methyl amides (Cravatt et al., 1996.; Boger et al., 2000.; Patricelli and Cravatt., 1999.). We therefore hypothesized that FAAH could hydrolyze luciferin amides to their respective carboxylates, resulting in the formation of a luminogenic

luciferase substrate (Figure 3.1). Here we show that luciferin amides allow exquisitely selective and sensitive imaging of endogenous FAAH activity in live cells and in live mice. FAAH is both necessary and sufficient for bioluminescence to occur and is the only enzyme activating these probes. The performance of FAAH inhibitors can be imaged in live mice, and inhibitors that cross the blood-brain barrier can be readily distinguished from those that cannot. Moreover, the amount of luciferin amide probe needed to perform this imaging is >1000-fold lower than typical D-luciferin imaging conditions but nonetheless improves overall signal from the brain. Thus, luciferin amides also excel at delivering luciferins into FAAH-expressing cells and tissues.

Results and discussion

To test our initial hypothesis, we synthesized four luciferin amides (Figure 3.1) by the condensation of electrophilic nitriles (Reddy et al., 2010.; Mofford et al., 2014.) with a D-cysteine amide. Without a free carboxylate, these luciferin analogs are not light-emitting substrates for purified firefly luciferase (Figures 3.2 and 3.3). Pretreatment of the luciferin amides with recombinant rat FAAH (Mofford et al., 2014) restores luminescent activity and could be specifically blocked by incubation with FAAH inhibitors such as PF3845 (Figures 3.2 and 3.3) (Ahn et al., 2009). The presence of FAAH or FAAH inhibitors has no effect on light emitted from the parent luciferins (Figures 3.2 and 3.3). Thus, luciferin amides can be used to detect FAAH activity and inhibition *in vitro*.
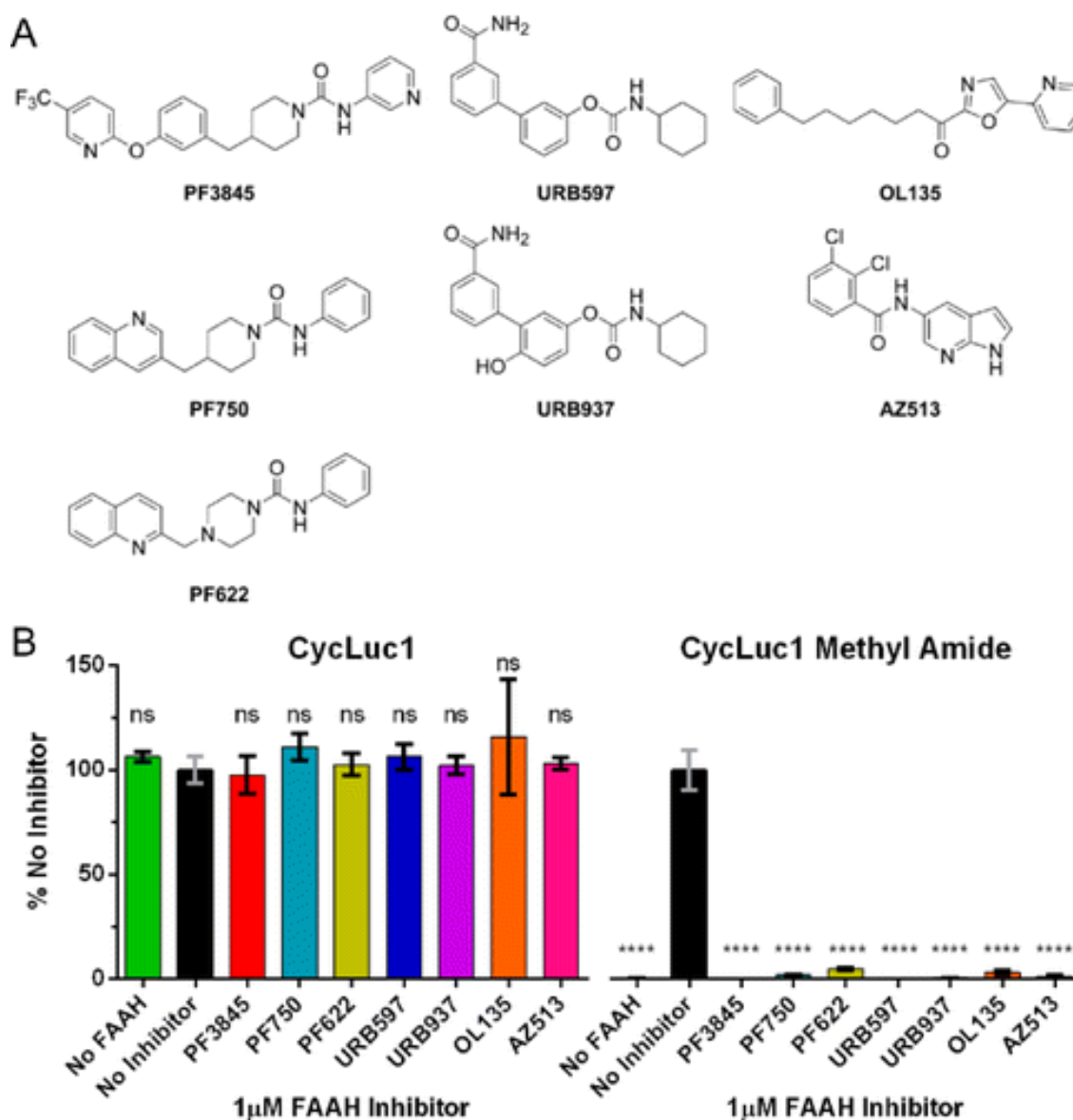
Figure 3.2. FAAH inhibitor structures and FAAH inhibitor screen. A) FAAH inhibitor structures. B) Photon flux from the indicated luciferin analog (10 µM) normalized to emission in the presence of FAAH with no FAAH inhibitor. The assay was performed in triplicate and is represented as the mean ± SEM.
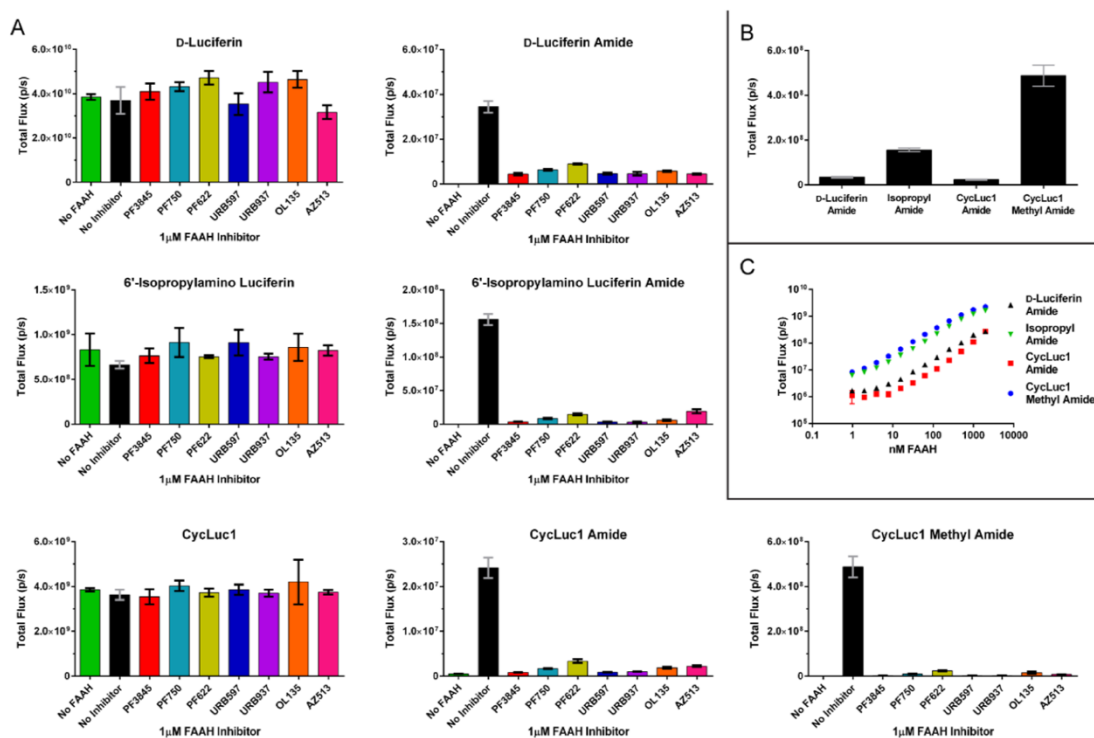
Figure 3.3. Luciferin amides report on rat FAAH activity *in vitro*. A) Photon flux from the indicated luciferin analog (10 µM) in the absence of FAAH or presence of FAAH with and without a FAAH inhibitor. B) Direct comparison of each luciferin amide after treatment with rFAAH without inhibitor from (A). C) Dependence of photon flux on the concentration of rFAAH (30-579) after 30 min. incubation with the indicated luciferin amide at pH 7.4., ambient temperature. All assays were performed in triplicate and are represented as the mean $\pm$ SEM.

We next sought to determine whether luciferin amides were specific to FAAH and sensitive enough to enable the detection of FAAH activity in live cells. Chinese hamster ovary (CHO) cells are known to express FAAH (Okamato et al., 2005.), an integral membrane protein (Blankman and Cravatt., 2013.), but at

levels insufficient to detect with fluorescence-based assays (Ramarao et al.,

2005.). In contrast, treatment of luciferase-expressing CHO cells with luciferin

amides resulted in robust bioluminescence (Figures 3.4A and 3.5). Potentially, in

the complex environment of the cell, luciferin amides could be cleaved by

proteases or other serine hydrolases. However, treatment with PF3845, which

specifically inhibits FAAH but no other serine hydrolases (Ahn et al.,

2009.), blocked emission from luciferin amides but had no effect on luciferase

activity in the presence of the parent luciferin (Figure 3.4A). Furthermore,

inhibitors of other serine hydrolases had no effect, and we evaluated the potency

of a wide range of FAAH inhibitors in the natural context of live cell membranes

(Figures 3.6 and 3.7). Lacking an ionized carboxylate, the luciferin amides also

served as excellent luciferin delivery vehicles in these FAAH-expressing cells,

yielding higher bioluminescence signals than their parent luciferins at

concentrations <100 μM (Figure 3.5). CycLuc1-methyl amide achieved higher

maximal photon flux than CycLuc1-amide, presumably because uncleaved

CycLuc1-amide can ultimately inhibit luciferase, while CycLuc1-methyl amide

cannot (Figures 3.5 and 3.8).
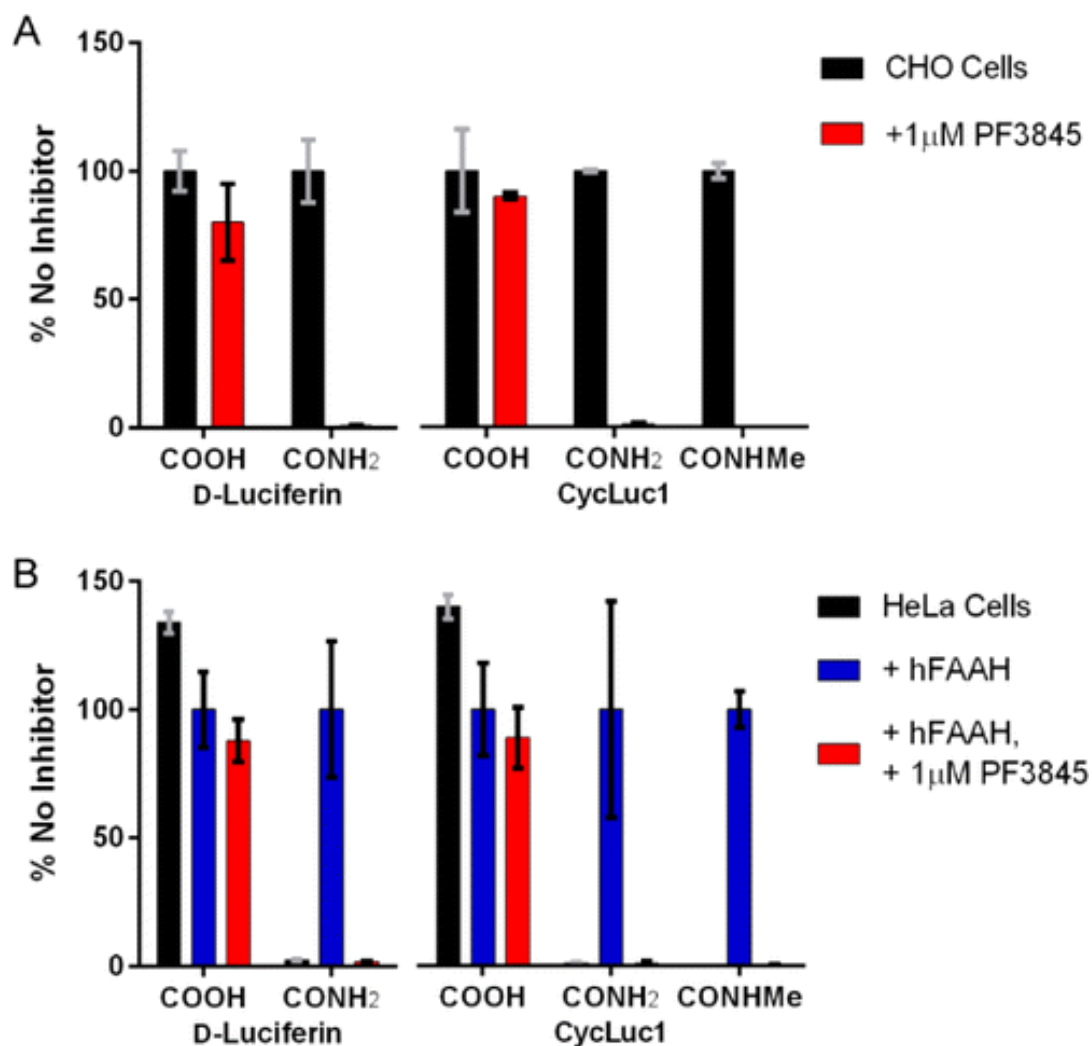
Figure 3.4. Luciferin amides report on FAAH activity in live mammalian cells. A) Relative photon flux from live luciferase-expressing CHO cells treated with the indicated luciferins and luciferin amides (125 µM) in the absence (black bars) or presence (red bars) of the FAAH inhibitor PF3845. The data are normalized to the uninhibited sample for each luciferin (black bars). B) Relative flux from live luciferase-expressing HeLa cells treated with the same set of substrates after transfection with empty pcDNA3.1 vector (black bars), pcDNA3.1-hFAAH (blue bars), or pcDNA3.1-hFAAH and treatment with the FAAH inhibitor PF3845 (red bars). The data are normalized to the uninhibited hFAAH-transfected sample for each luciferin (blue bars). All assays were performed in triplicate and are represented as the mean ± SEM.
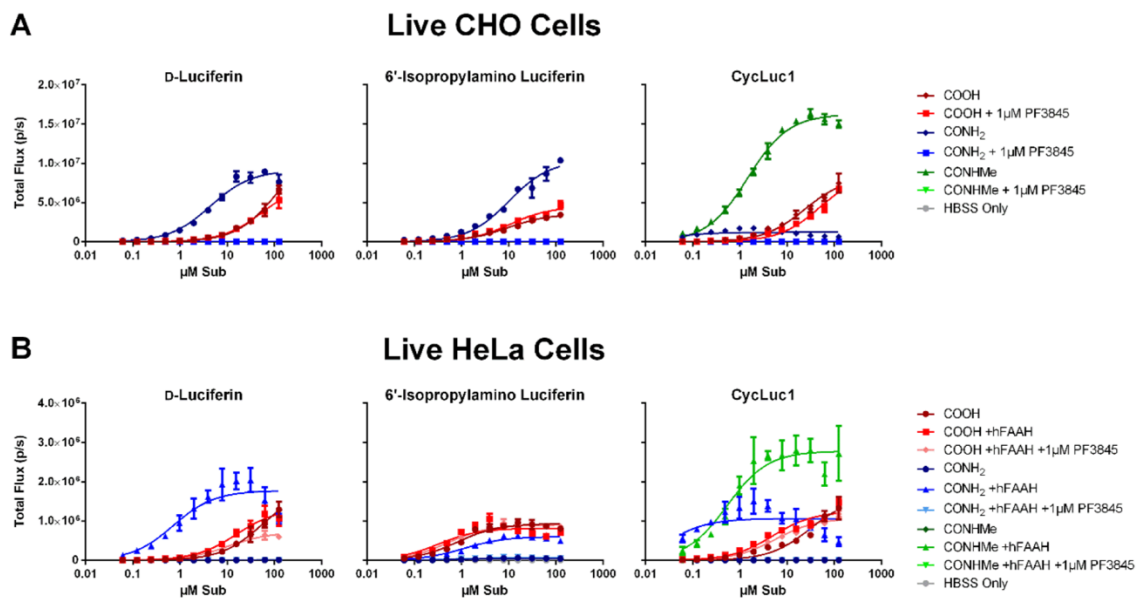
Figure 3.5. Luciferin amides report on FAAH activity in live cells and improve signal over parent luciferins. A) Live CHO cells transfected with luciferase were incubated with 1 µM PF3845 for five minutes and then imaged with varying concentrations of the indicated luciferin analog. B) Live HeLa cells co-transfected with either luciferase and human FAAH or luciferase and empty vector were incubated with 1 µM PF3845 for five minutes and then imaged with varying concentrations of the indicated luciferin analog. The assay was performed in triplicate and is represented as the mean ± SEM. Curves were fit to the Michaelis–Menten equation by nonlinear regression.
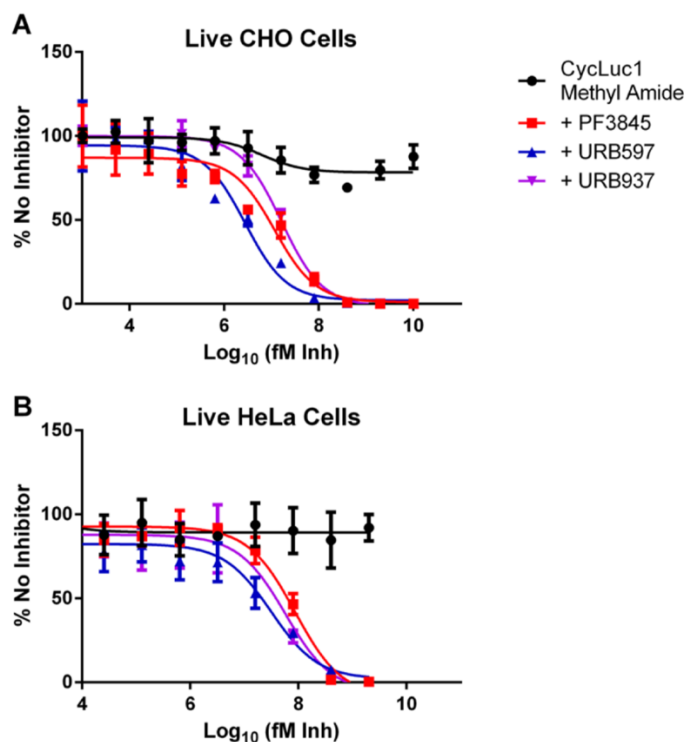
Figure 3.6. Luciferin amides report on inhibitor potency in live cells. A) Live CHO cells transfected with luciferase were incubated with varying concentrations of FAAH inhibitor for five minutes and then imaged with CycLuc1-methyl amide (10 µM). B) Live HeLa cells co- transfected with luciferase and human FAAH were incubated with varying concentrations of FAAH inhibitor for five minutes and then imaged with CycLuc1-methyl amide (10 µM). The assays were performed in triplicate and are represented as the mean ± SEM. Data was fit by nonlinear regression to log(inhibitor) vs. response (three parameters) to determine relative IC50 values. CHO cell IC50 values: PF3845, 12 nM; URB597, 2.7 nM; URB937, 16 nM. HeLa cell IC50 values: PF3845, 86 nM; URB597, 31 nM; URB937, 57 nM.
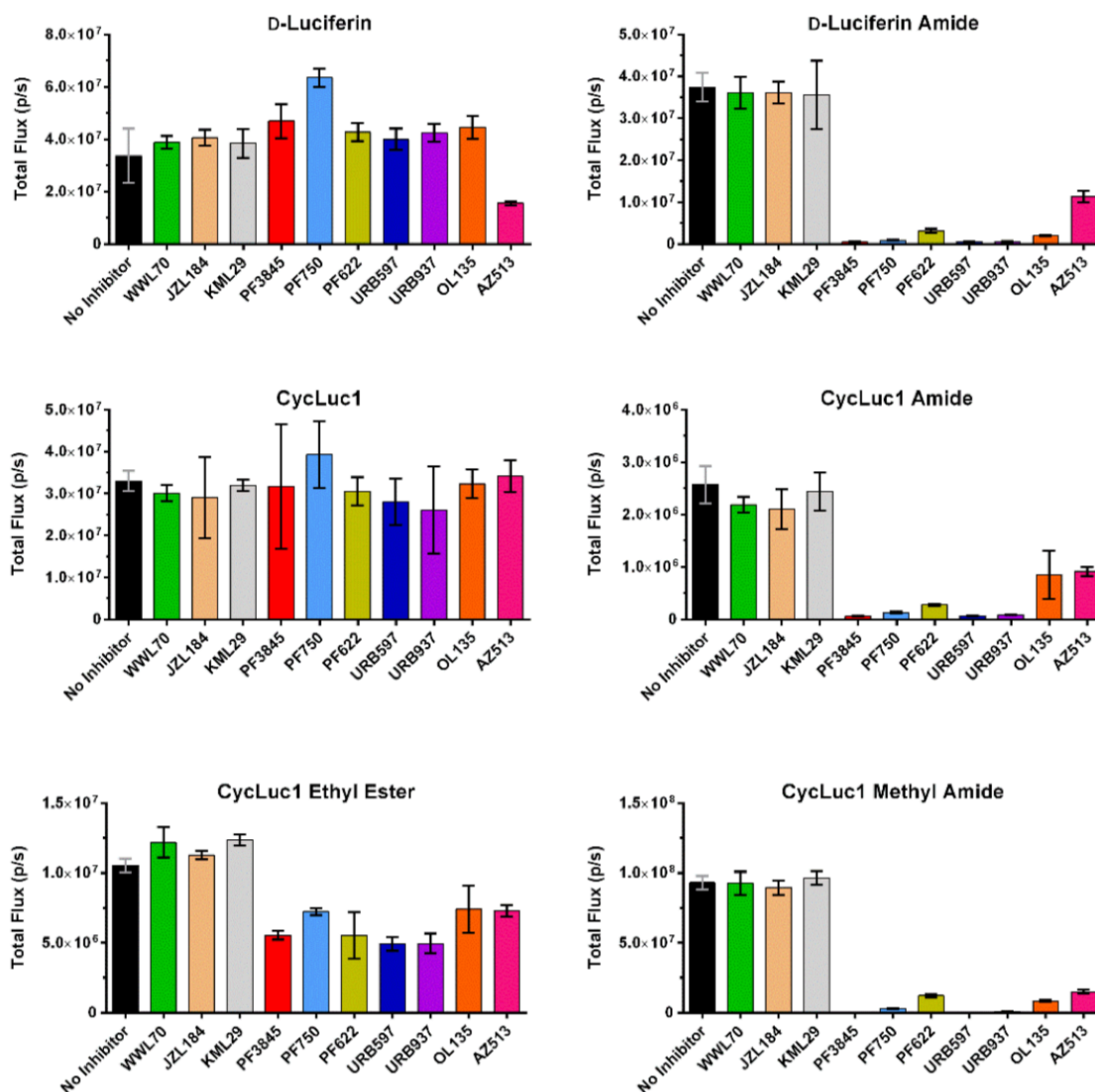
Figure 3.7. Luciferin amides report on FAAH activity in live CHO cells. Live CHO cells transfected with luciferase were incubated with 1 µM of the indicated serine hydrolase inhibitor for five minutes and then imaged with the indicated luciferin analog (10 µM). All assays were performed in triplicate and are represented as the mean ± SEM. FAAH inhibitors: PF3845, PF750, PF622, URB597, URB937, OL135, and AZ513; MAGL inhibitors: JZL184 and KML29; ABHD6 inhibitor: WWL70.
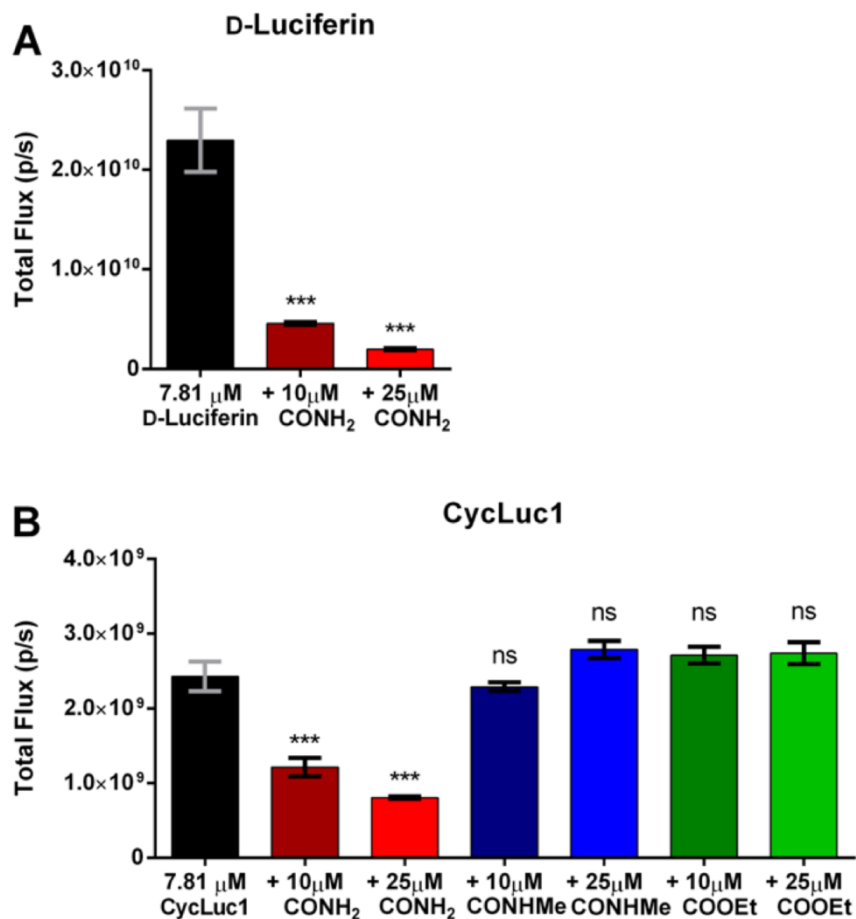
Figure 3.8. Luciferin primary amides can inhibit luciferase in vitro. A) Purified firefly luciferase treated with 7.81 µM D-luciferin alone or in the presence of 10 µM or 25 µM D-luciferin amide. B) Purified luciferase treated with 7.81 µM CycLuc1 alone or in the presence of 10 µM or 25 µM of CycLuc1-amide, CycLuc1-methyl amide, or CycLuc1–ethyl ester. The assay was performed in triplicate, is represented as the mean ± SEM. Each amide was compared to luciferin only by t- test. ns: not statistically significant; *** P <0.001.

HeLa cells do not express FAAH (Dickason-Chesterfield et al., 2006.; Day et al.,

2001.), and luciferin amides do not yield bioluminescence in luciferase-

expressing HeLa cells (Figure 3.4B). Transfection of HeLa cells with human

FAAH enabled bioluminescence with luciferin amides (Figures 3.4B and 3.5).

Specific inhibition of the transfected FAAH with PF3845 blocked bioluminescence

(Figure 3.4B) and the potency of FAAH inhibitors could be evaluated in these

FAAH-transfected live cells (Figure 3.6). FAAH has been shown to cleave some

fatty acid esters (Patricelli and Cravatt, 1999.), and we find that it indeed also

contributes to the cleavage of CycLuc1 ethyl ester (Figure 3.9). However, unlike

CycLuc1 amides, the ethyl ester of CycLuc1 is not exclusively cleaved by FAAH

and is hydrolyzed to CycLuc1 in both CHO and HeLa cells (Figure 3.9).
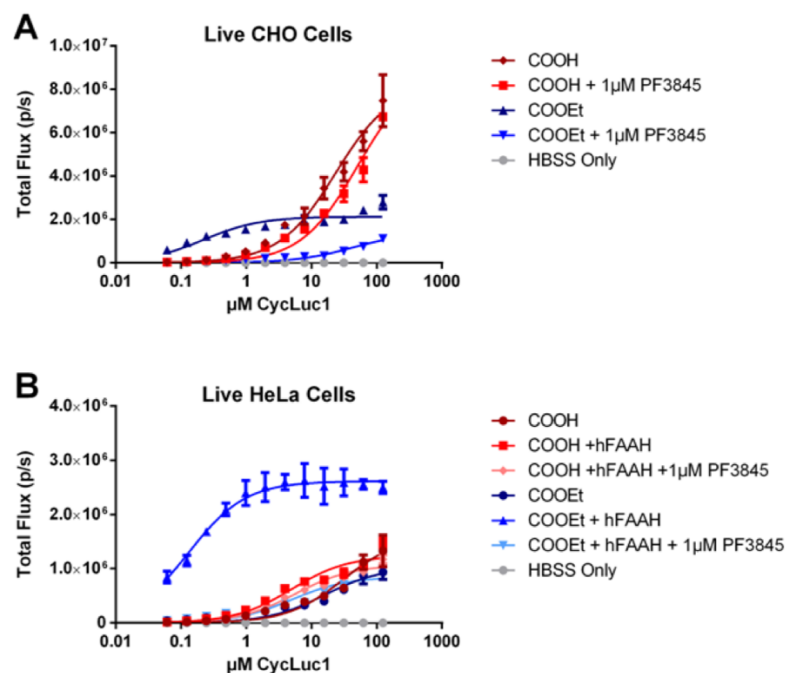
Figure 3.9. CycLuc1 ethyl ester supports bioluminescence from both live CHO and HeLa cells. A) Live CHO cells transfected with luciferase were incubated with 1 µM PF3845 for five minutes and then imaged with varying concentrations of either CycLuc1 or CycLuc1 ethyl ester. B) Live HeLa cells co-transfected with either luciferase and human FAAH or luciferase and empty vector were incubated with 1 µM PF3845 for five minutes and then imaged with varying concentrations of either CycLuc1 or CycLuc1 ethyl ester. The assay was performed in triplicate and is represented as the mean ± SEM. Curves were fit to the Michaelis–Menten equation by nonlinear regression.

In mice, FAAH is highly expressed in the brain (Long et al., 2011.). We thus

expected that luciferin amides would result in strong brain bioluminescence in

luciferase-expressing mice if able to access this tissue. We used adeno-

associated virus 9 (AAV9) to express luciferase only in the brain striatum (Evans

et al., 2014.). The amides are less water-soluble than the parent carboxylates,

necessitating a lower imaging dose. Nonetheless, CycLuc1-amide yielded

dramatically higher photon flux in these mice than the parent luciferin CycLuc1 or

the conventional substrate d-luciferin (Figure 3.10). A 400-fold lower dose of

CycLuc1-amide was markedly superior to the standard imaging dose of d-

luciferin (Figure 3.10). Even 1000-fold lower doses yielded higher brain

bioluminescence than d-luciferin (Figure 3.11).
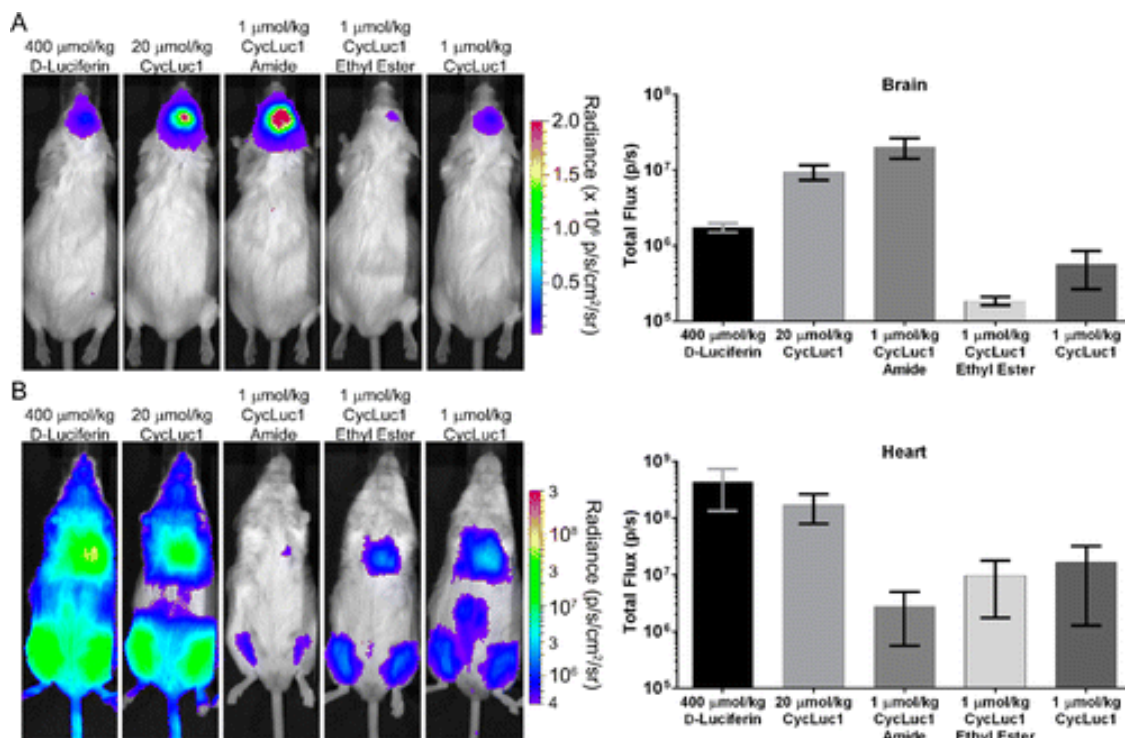
Figure 3.10. Bioluminescence from mice that express luciferase in specific tissues after treatment with luciferins and luciferin amides. CycLuc1-amide compared to d-Luciferin for bioluminescence imaging in live mice expressing luciferase in (A) the brain or (B) the heart and leg muscles. Quantification is represented as the mean ± SEM for n = 3 mice.
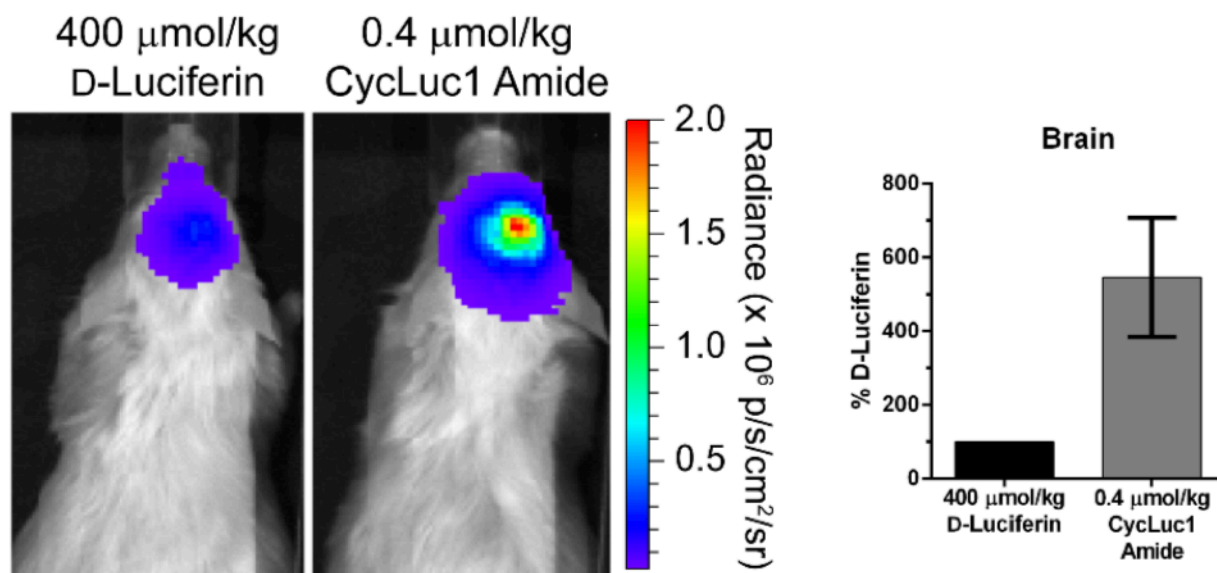
Figure 3.11. CycLuc1 amide increases total photon flux from the brain at 1000-fold lower dose than D-luciferin. Mice striatally injected with AAV9-CMV-luc2 were treated with 0.4 µmol/kg CycLuc1-amide or 400 µmol/kg D-luciferin. Quantification was normalized to D-luciferin signal for each mouse and is represented as the mean ± SEM for n=3 mice.

Pretreatment with PF3845 (Figure 3.2), which has been demonstrated to inhibit only FAAH in mice (Ahn et al., 2009.), completely blocked brain bioluminescence when using luciferin amides (Figure 3.12). Tail-vein injection of AAV9-CMV-luc2 primarily transduces heart (Inagaki et al., 2006.) and leg muscles (Figure 3.10), tissues where FAAH activity has been reported to be absent (Evans et al, 2014.). In these mice, luciferin amides yielded dramatically lower photon flux than could be achieved with their parent luciferins (Figure 3.10). By contrast, CycLuc1 ethyl ester was on par with equal doses of the parent luciferin in the heart and leg

muscles, but ineffective in the brain (Figure 3.10). These differences likely reflect the location of the liberating enzymatic activity and biodistribution of the more hydrophobic ester.

To visualize FAAH activity throughout the mouse, we next turned to transgenic mice that express luciferase in all tissues (Cao et al., 2004). When D-luciferin or CycLuc1 is introduced into these mice, the weakest light emission is from the head, and bioluminescence is dominated by superficial tissues (Figures 3.13 and 3.14). In marked contrast, injection of CycLuc1-amide revealed the strongest bioluminescence signals from the brain and kidneys (Figure 3.13), tissues known to have high FAAH activity (Long et al., 2011.). Ventral bioluminescence was less well-defined, which may reflect rapid transit of released luciferin out of FAAH-expressing tissues such as the liver (Figure 3.14). Pretreatment of mice with PF3845 completely blocked bioluminescence from luciferin amides in the brain and in all peripheral tissues (Figures 3.13, 3.15, and 3.16) but had no effect on bioluminescence from the parent luciferins (Figure 3.17). The aminoluciferin amides (Figure 3.1) readily sense FAAH activity *in vivo* (Figure 3.14), and can be imaged at extremely low doses (as low as 8 nmol/kg; Figure 3.18). Although D-luciferin amide senses FAAH activity *in vitro* and in live cells, it works poorly in live mice and cannot sense FAAH activity in the brain (Figure 3.14). This is consistent with our contention that the improved biodistribution properties of aminoluciferins and low K_m values render them superior for use as luminogenic sensors *in vivo* (Adams et al., 2014.). Interestingly, CycLuc1-methyl amide did

not exhibit an advantage over CycLuc1-amide in the mouse (Figure 3.14).

Presumably, inhibition of luciferase by uncleaved luciferin primary amides is not

an issue at the substrate concentrations achieved *in vivo*.
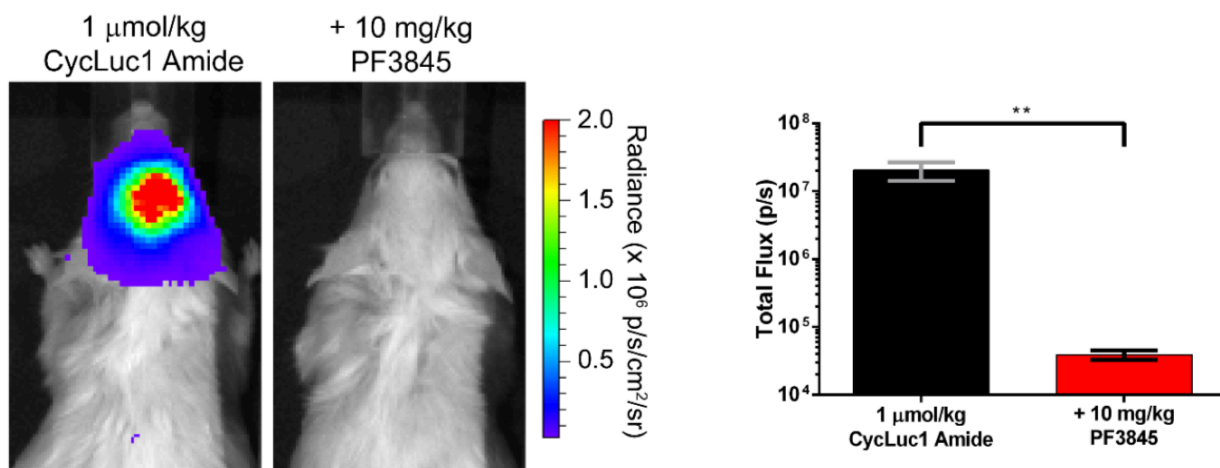
Figure 3.12. Inhibition of FAAH by PF3845 results in loss of signal from CycLuc1-amide in the brain. Mice striatally injected with AAV9-CMV-luc2 were imaged with CycLuc1-amide alone or after pre-treatment with 10 mg/kg PF3845. Quantification is represented as the mean ± SEM for n=3 mice and was compared by t test. ** P <0.01.
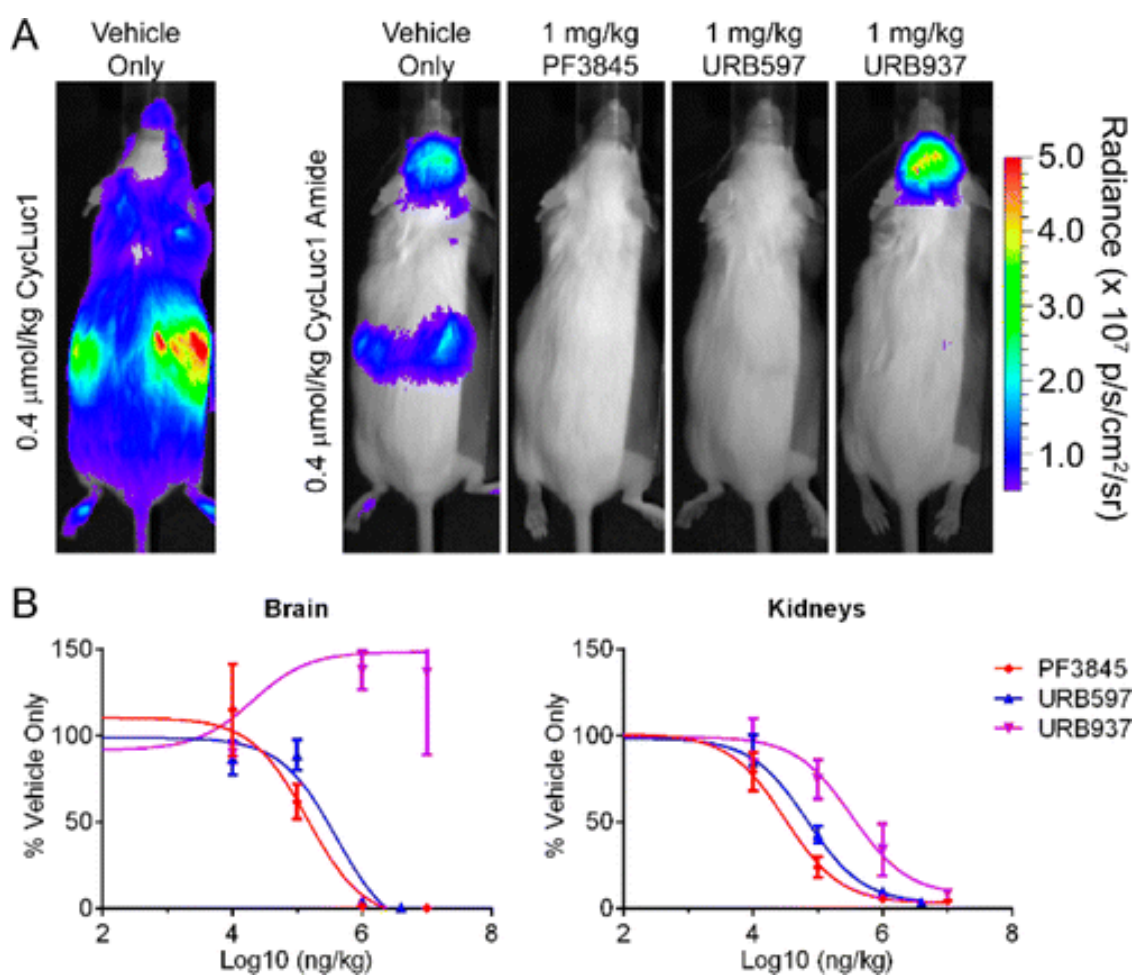
Figure 3.13. Luciferin amides report on FAAH activity in live mice that ubiquitously express luciferase. A) Bioluminescence imaging with CycLuc1 or CycLuc1-amide in ubiquitously expressing transgenic luciferase mice treated with vehicle only or the indicated FAAH inhibitor. B) Total flux from the brain and kidneys quantitated as a function of inhibitor concentration and normalized to the vehicle-only signal, represented as the mean ± SEM for n = 3 mice. Data were fit by nonlinear regression to determine relative IC_{50} values in the brain (PF3845, 0.14 mg/kg; URB597, 0.40 mg/kg; URB937, ND) and kidneys (PF3845, 0.03 mg/kg; URB597, 0.07 mg/kg; URB937, 0.33 mg/kg).
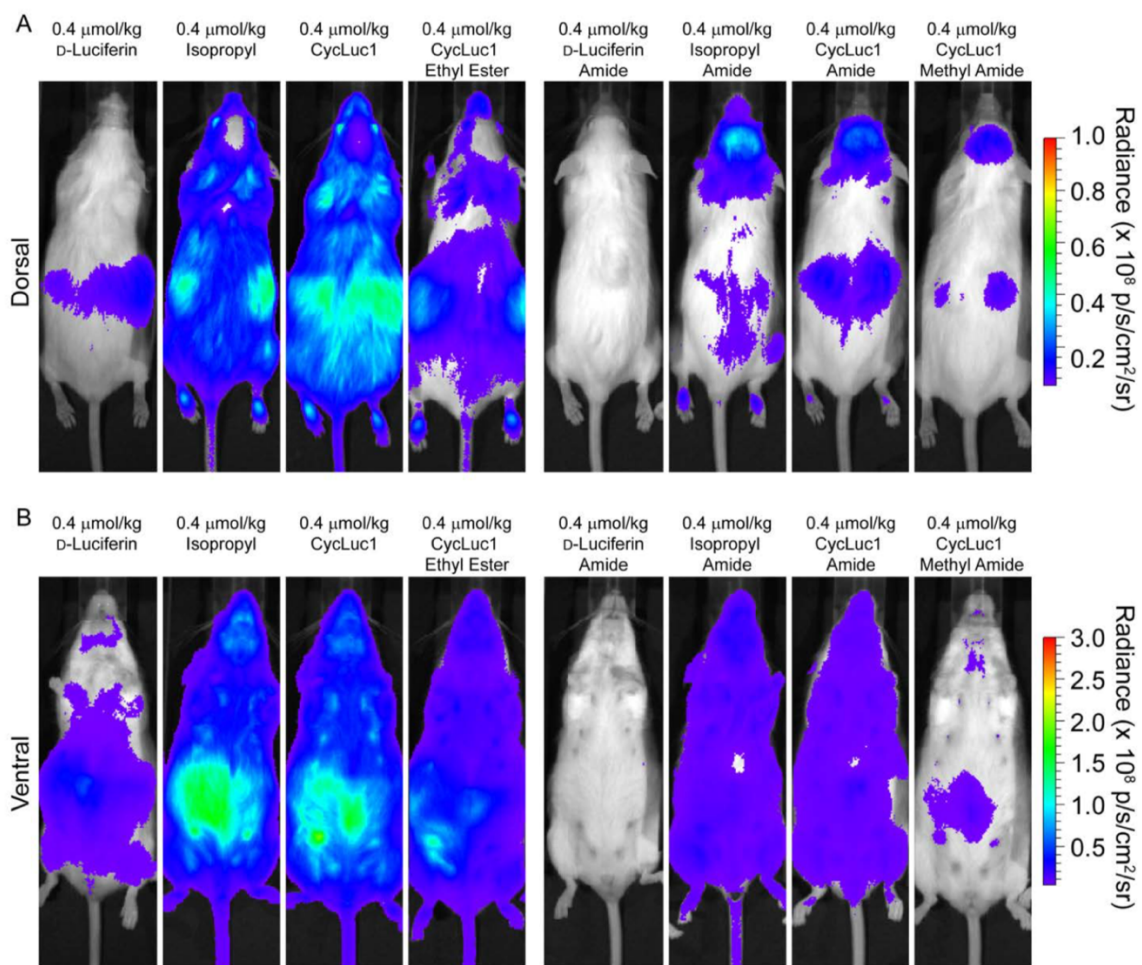
Figure 3.14. Bioluminescence from mice that ubiquitously express luciferase after treatment with luciferins and luciferin amides. A) Dorsal view of FVB-Tg(CAG-luc) mice injected with the indicated substrate. B) Ventral view of mice in A).
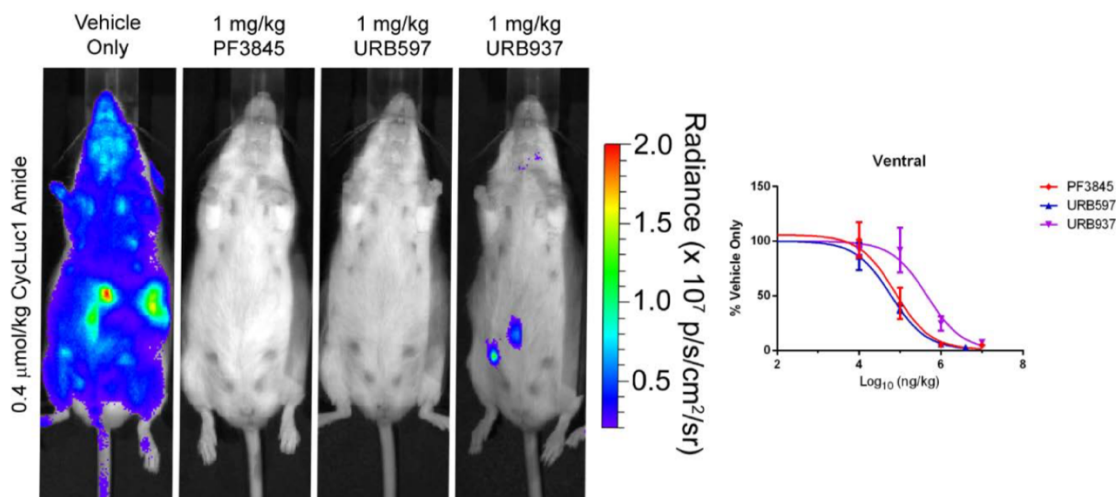
Figure 3.15. Ventral view of ubiquitously-expressing luciferase mice treated with CycLuc1 amide. Mice were pre-treated with vehicle only (18:1:1 PBS:Kolliphor:ethanol), or the indicated FAAH inhibitors. Quantification was normalized to the average vehicle-only signal and is represented as the mean ± SEM for n=3 mice. Data was fit by nonlinear regression to determine relative ventral IC50 values (PF3845: 0.08 mg/kg, URB597: 0.06 mg/kg, URB937: 0.46 mg/kg).
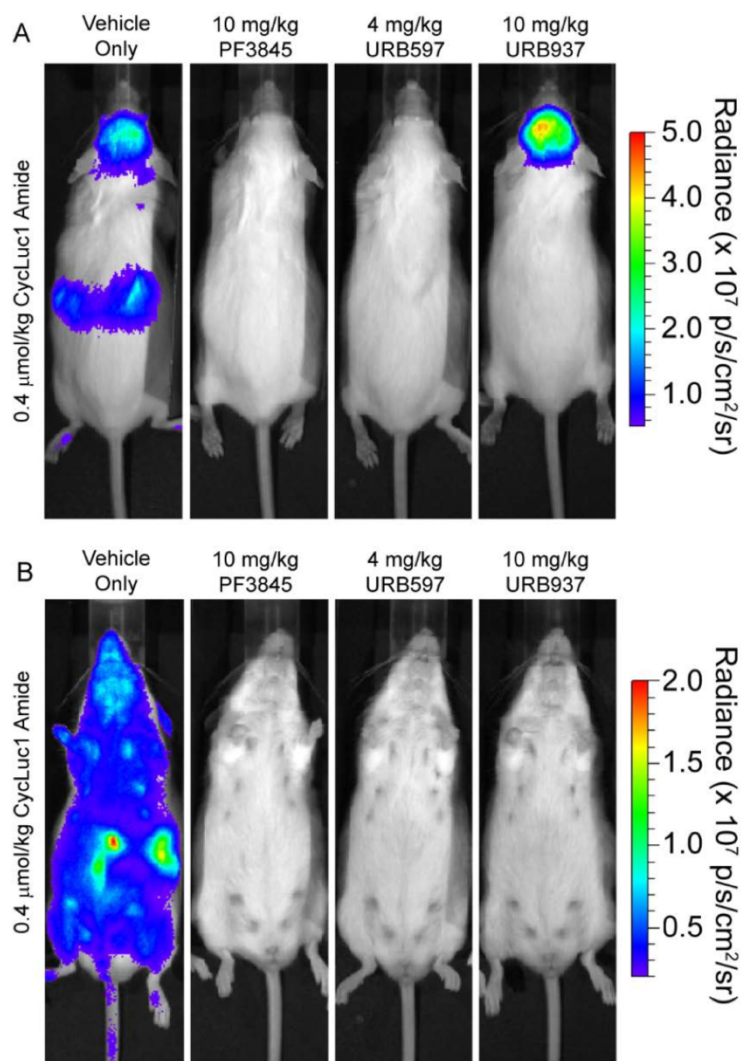
Figure 3.16. Mice ubiquitously-expressing luciferase treated with high inhibitor dose. Mice were pre-treated with vehicle only (18:1:1 PBS:Kolliphor:ethanol), or the indicated FAAH inhibitors and imaged with CycLuc1-amide.
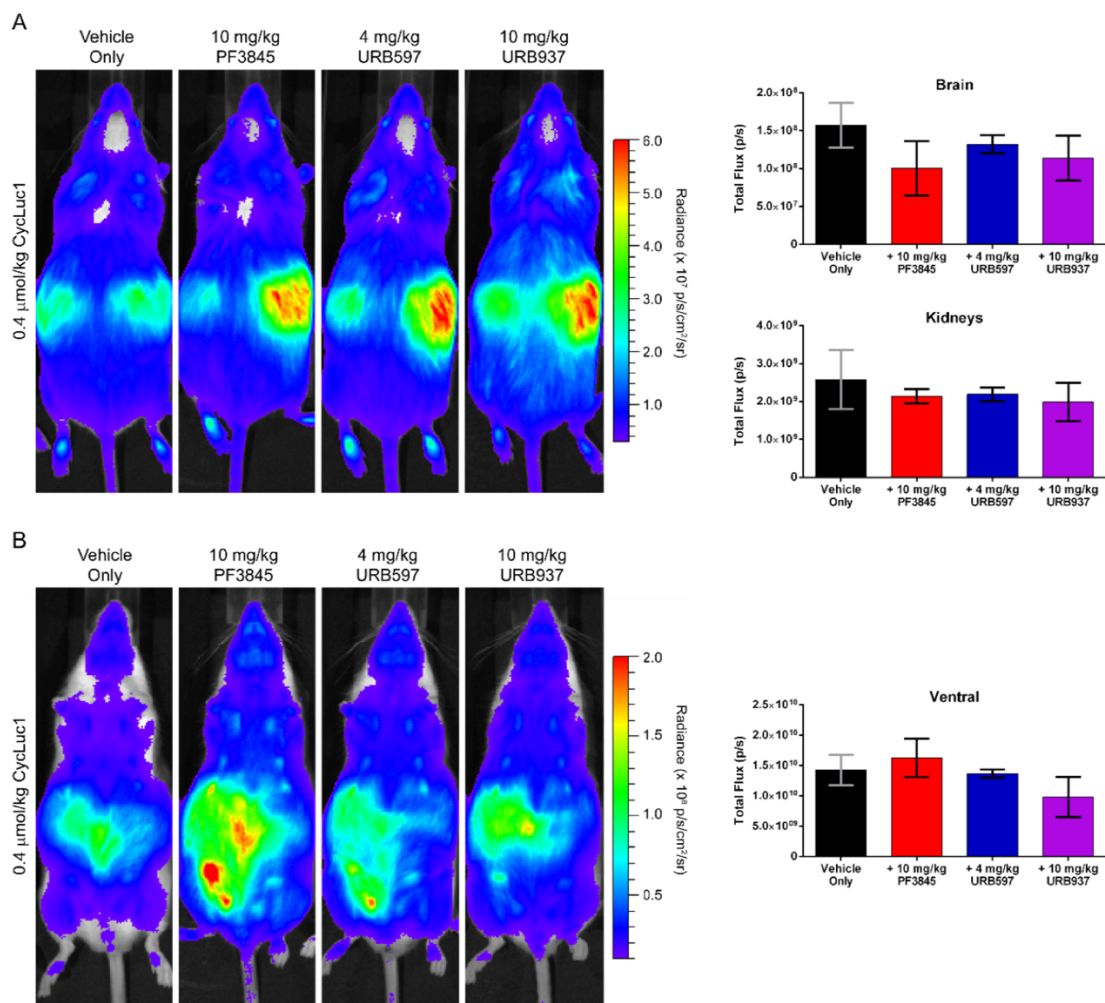
Figure 3.17. FAAH inhibitors do not affect parent luciferins. A) Dorsal view of live FVB- Tg(CAG-luc) mice, injected with the indicated inhibitor and treated with CycLuc1. B) Ventral view of mice in (A). Quantification is represented as the mean ± SEM for n=3 mice. Each inhibitor was compared to vehicle only by t-test. No statistically significant difference was found for any inhibitor.
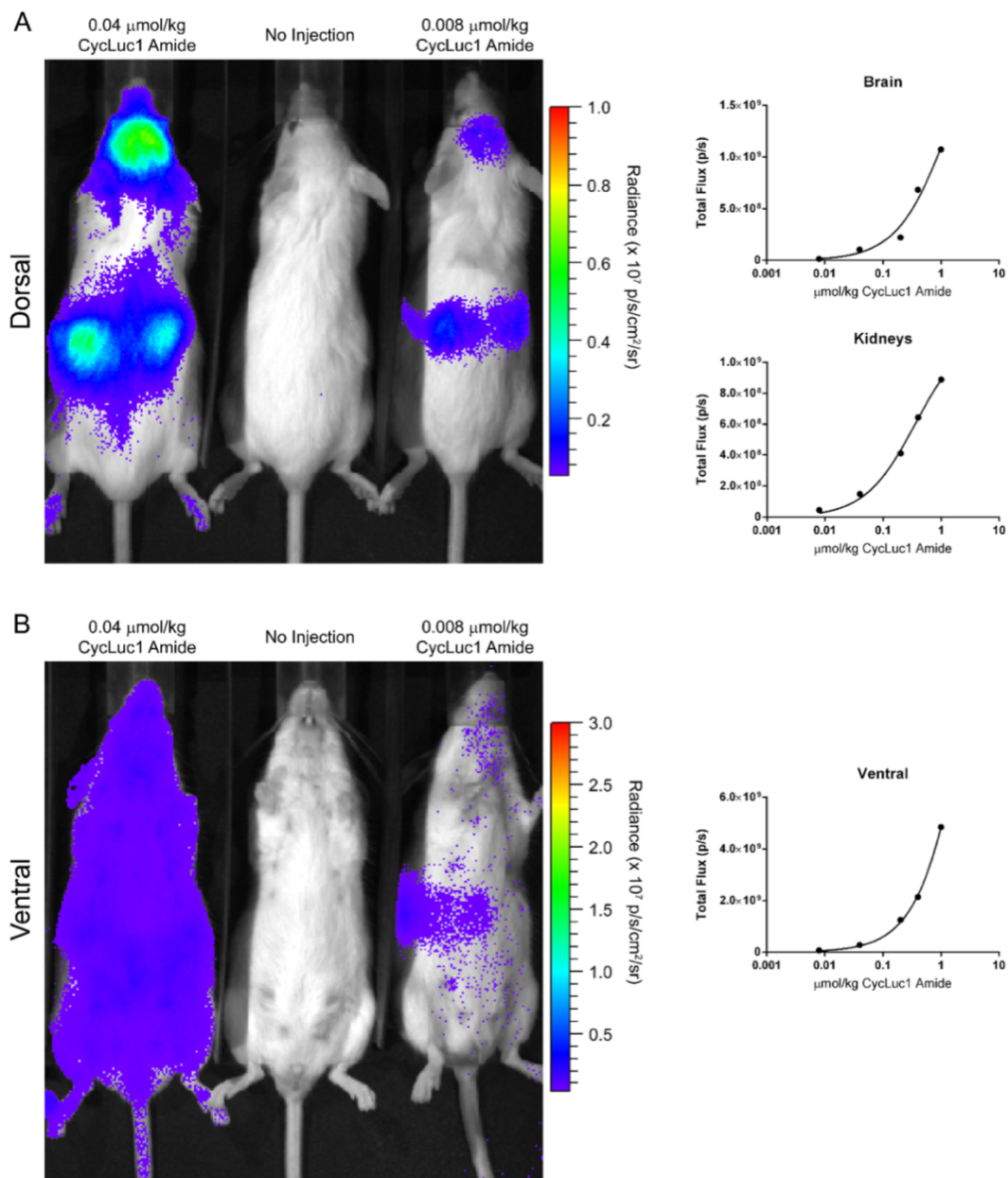
Figure 3.18. CycLuc1-amide can be imaged at doses as low as 8 nmol/kg and signal is not saturated at 1 µmol/kg. A) Dorsal view of FVB-Tg(CAG-luc) mice injected with the indicated concentration of CycLuc1 amide. B) Ventral view of mice in (*s*). Quantification is represented as n=1 mouse per substrate dose.

Finally, we sought to determine whether luciferin amides could be used to evaluate the tissue distribution of prospective FAAH inhibitors, which can have important effects on their efficacy (Clapper et al., 2010.). URB937 is a brain-impermeable FAAH inhibitor that differs from the global FAAH inhibitor URB597 by a single hydroxyl group (Figure 3.2) (Clapper et al., 2010.). Bioluminescence imaging with CycLuc1-amide confirmed that URB597 inhibits FAAH activity in both peripheral and brain tissues (Figures 3.13, 3.15 and 3.16), whereas no inhibition of FAAH activity is detected in the brains of URB937-treated mice (Figure 3.13).

Many bioluminescent sensors have been described based on "caged" pro-luciferins that can release a luciferin upon the action of an enzyme or reactive small molecule (Adams and Miller, 2014.; Van de Bittner et al., 2013.). The labile moiety is distinct from the luciferin and often separated by a self-immolative linker (Carl et al., 1981.). A limitation of this approach is that the luciferin itself is not contributing to specific recognition or selectivity; the best one can hope for is that its presence is innocuous. Our approach embraces the inherent fatty acid mimetic properties of luciferin analogs to create sensors for enzymes that release fatty acids. The power of this approach is borne out in the exquisite specificity and sensitivity of luciferin amides for FAAH even *in vivo*, simply by replacing an oxygen atom with nitrogen (Figure 3.1). Furthermore, we find that luminogenic sensors based on high-affinity, cell-permeable aminoluciferins perform better in mice than those based on d-luciferin. As the number of structurally distinct

luciferin analogs grows (Adams and Miller, 2014.; Mofford et al., 2014), we anticipate there will be additional opportunities to build sensors based on the inherent properties of the luciferin itself.

Conclusion

In summary, we have found that luciferin amides are highly sensitive and selective reporters of FAAH activity. These sensors readily translate from *in vitro* assays to live cells to *in vivo* imaging to report on the activity of a single enzyme in its natural context. The bioluminescence approach described herein reveals otherwise invisible endogenous enzymatic activity in live cells and mice and more broadly allows imaging of the biodistribution consequences of subtle modifications to a prospective therapeutic inhibitor *in vivo* (e.g., ability to cross the blood-brain barrier). Further refinement and modification of the structure of the luciferin (Adams and Miller, 2014.; Mofford et al., 2014) and the scissile bond could potentially allow extension of this bioluminescence detection approach to other enzymes (Long and Cravatt, 2011.; Bandiera et al., 2014.).Finally, luciferin amides are excellent reagents for increasing the sensitivity of bioluminescence imaging in FAAH-expressing cells and tissues, such as the brain, and allow orders of magnitude lower imaging doses than the natural luciferase substrate.

Materials and Methods

Contributions

D.M.M. devised experiments, performed in vitro assays, cell-based experiments, mouse imaging and analysis, and manuscript preparation. S.T.A. Jr. performed AAV deliveries via surgery, AAV deliveries via tail vein injection, and mouse imaging and analysis. G.S.K.K.R. and G.R.R. synthesized luciferins. S.C.M. devised experiments and helped with manuscript preparation.

General

Chemicals for synthesis were obtained from Aldrich unless otherwise noted. D-luciferin was obtained from Anaspec for *in vitro* work and from Gold Bio for mouse work. Serine hydrolase inhibitors were purchased from Cayman. CycLuc1 was synthesized as previously described (Reddy et al., 2010). Protein concentrations were determined using Coomassie Plus (Thermo Scientific). Immobilized glutathione (Thermo Scientific) was used for glutathione S-transferase (GST)-tagged protein purification. Kolliphor® EL was obtained from Sigma Life Sciences (Stock # C5135) Data were plotted and analyzed with GraphPad Prism 6.0. High resolution mass spectral data were recorded on a Waters QTOF Premier spectrometer (University of Massachusetts Medical School Proteomics and Mass Spectrometry Facility). Bioluminescence assays were performed on a Xenogen IVIS-100 system in the Small Animal Imaging facility. Data acquisition and analysis were performed with Living Image software. Data are reported as total flux (p/s) for each region of interest (ROI). For *in vitro*

and cellular assays, the ROIs correspond to each well of a 96-well plate. For in vivo assays, the ROIs correspond to the indicated region of a mouse.

Plasmid Constructs

Human and rat FAAH genes (hFAAH and rFAAH) were purchased from the Mammalian Gene Collection of Thermo Fisher Scientific (clone IDs: hFAAH 5728192, rFAAH 7370226). Residues 30-579 of the rFAAH gene were PCR-amplified and cloned into the EcoRI and NotI sites of pGEX6P-1, resulting in removal of the N-terminal transmembrane domain (Mileni et al., 2008.). Full length hFAAH was PCR-amplified and cloned into the KpnI and NotI sites of pcDNA3.1 to yield pcDNA3.1- hFAAH.

Protein Expression and Purification

Rat FAAH (30-579) and firefly luciferase were expressed as GST-fusion proteins using the pGEX6P-1 vector in the *E. coli* strain JM109. Cells were grown at 37°C until the OD_{600} reached 0.5-1, induced with 0.1 mM IPTG, and incubated at 20°C overnight. Cells were pelleted at 5000 rpm in a Sorvall 2C3C Plus centrifuge (H600A rotor) at 4°C for 15 min, then flash frozen in liquid nitrogen. *E. coli* pellets from 1 L of culture were thawed on ice, resuspended in 25 mL lysis buffer (50 mM Tris [pH 7.4], 500 mM NaCl, and 0.5% Tween 20) containing 1 mM phenylmethylsulfonyl fluoride, and disrupted by sonification (Branson Sonifier). Dithiothreitol (DTT) was added at 10 mM, and the resulting cell lysate

was clarified by centrifugation at 35,000 rpm in a Beckman 50.2 Ti rotor for 60 min at 4°C. The supernatant was batch-bound to immobilized glutathione for 1 hr at 4°C, and the beads were washed with lysis buffer containing 10 mM DTT, followed by wash buffer (50 mM Tris [pH 8.1], 250 mM NaCl, and 10 mM DTT) and storage buffer (50 mM Tris [pH 7.4], 0.1 mM EDTA, 150 mM NaCl, 1 mM TCEP). Twenty units of PreScission Protease (GE Healthcare) were added, and incubated overnight at 4°C to cleave the GST-fusion and elute the untagged protein into storage buffer.

Purified Protein rFAAH Activity Assays

FAAH inhibitors were prepared at 4 µM in substrate buffer (20 mM Tris [pH 7.4], 0.1 mM EDTA, 8 mM $MgSO_4$, and 4 mM ATP). Luciferins and luciferin amides were prepared at 40 µM in substrate buffer. Luciferase and rFAAH were prepared at 400 nM in enzyme buffer (20 mM Tris [pH 7.4], 0.1 mM EDTA, 1 mM TCEP, and 0.8 mg/mL BSA). In a black 96-well plate (Costar 3915), 25 µL FAAH inhibitor or substrate buffer was added to three wells each. rFAAH (25 µL) or enzyme buffer was added to the inhibitor and incubated at ambient temperature for 5 minutes. Luciferin or luciferin amide (25 µL) was then added to each well and incubated at ambient temperature for 20 minutes. Luminescence was then initiated by adding 25 µL of luciferase. Imaging was performed one minute after luciferase addition and integrated for 2-20s

at a final concentration of 1 µM FAAH inhibitor, 10 µM luciferin, 100 nM rFAAH, and 100 nM luciferase.

Purified rFAAH Dose-Response Assays

Purified rFAAH was prepared at concentrations ranging from 8 µM to 3.91 nM in enzyme buffer. Luciferin amides were prepared at 20 µM in substrate buffer. Luciferase was prepared at 400 nM in enzyme buffer. In a black 96-well plate (Costar 3915), 50 µL of each luciferin amide was added per well. rFAAH (25 µL) was then added to the amide and incubated at ambient temperature for 30 minutes. Luminescence was then initiated by adding 25 µL of luciferase. Imaging was performed one minute after luciferase addition for 2-20s at a final concentration of 2000 nM to 0.977 nM rFAAH, 10 µM luciferin amide, and 100 nM luciferase.

Luciferin Amide Inhibitor Assays with Purified Luciferase

Luciferin amides were prepared at 40 µM or 100 µM in substrate buffer. Luciferins were prepared at concentrations from 1000 µM to 0.488 µM in substrate buffer. Luciferase was prepared at 200 nM in enzyme buffer. In a black 96-well plate (Costar 3915), 25 µL luciferin amide or substrate buffer was added to three rows each. Luciferin (25 µL) was added to the luciferin amide. Luminescence was then initiated by adding 50 µL of luciferase. Imaging was performed one minute after luciferase addition for 2-20s at a final concentration

of 0 µM, 10 µM, or 25 µM luciferin amide, 250 µM to 0.122 µM luciferin, and 100 nM luciferase.

Cell Culture

Chinese hamster ovary (CHO) cells and HeLa cells were grown in a CO_2 incubator at 37°C with 5% CO_2 and were cultured in F-12K Nutrient Mixture (GIBCO) and Dulbecco's Modified Eagle's Medium (DMEM) (GIBCO) respectively. Both media were supplemented with 10% fetal bovine serum and 100 U/mL penicillin/streptomycin.

Transfections

CHO cells were transfected with codon-optimized firefly luciferase (luc2) as previously described (Mofford et al., 2014.). HeLa cells were transfected with pcDNA3.1-luc2 plasmid (Mofford et al., 2014.) and either pcDNA3.1- hFAAH or empty pcDNA3.1 vector. Transient transfections were performed at RT using Lipofectamine 2000 on cells plated at 60%–75% confluency in 96-well black tissue culture- treated plates (Costar 3916). For CHO cells, 0.075 µg DNA/well of pcDNA3.1-luc2 was transfected; for HeLa cells, 0.0375 µg DNA/well each of pcDNA3.1-luc2 and either pcDNA3.1- hFAAH or empty pcDNA3.1 was transfected. Assays were performed in triplicate 24 hrs after transfection.

Live Cell FAAH Activity Assays

Transfected cells were washed with HBSS. For substrate dose-response curves, the cells in 96- well plates were incubated with 50 µL of 2 µM FAAH inhibitor in HBSS or HBSS only at ambient temperature for 5 minutes. Then, 50 µL of 2x substrate was added to each well to achieve final substrate concentrations ranging from 125 µM to 0.061 µM. For inhibitor dose-response curves, the cells in 96-well plates were incubated with 50 µL of 2x FAAH inhibitor in HBSS at ambient temperature for 5 minutes (final inhibitor concentrations ranging from 10 µM to 0.21 pM). Then, 50 µL of 2x substrate was added to each well to a final luciferin concentration of 10 µM. Imaging was performed three minutes after addition of substrate.

Mice

All of the experiments involving mice were conducted in accordance with the Institutional Animal Care and Use Committee of The University of Massachusetts Medical School (docket #A-2474- 14). Female FVB mice and luciferase-expressing transgenic mice (FVB-Tg(*CAG-luc,- GFP*)L2G85Chco/FathJ) were purchased from Jackson Laboratories (Bar Harbor, ME).

Striatal injection of AAV9-CMV-luc2 into FVB mice was performed as previously described (Evans et al., 2014.).

Tail-vein injection of AAV

FVB mice were injected in the lateral tail vein with 1×10^{11} particles of AAV9-CMV-luc2 luciferase (Evans et al., 2014.) suspended in sterile filtered PBS at a final volume of 200 µL. The mice were held under a heat lamp to warm the tail for better visualization of the lateral tail vein due to vasodilation and then placed into a Tailveiner (Braintree Scientific, Braintree, MA). The tails were cleaned with a 70% isopropyl alcohol wipe and injection was performed using a 27.5 gauge needle. Once the needle was withdrawn, the tail was compressed with sterile gauze to ensure complete homeostasis. The mice were monitored afterwards for recovery of normal behavior before returning to their colony. Imaging was performed weeks to months after AAV injection.

Substrate and FAAH Inhibitor Preparation for Mouse Injection

All FAAH inhibitors were prepared by direct dissolution into 18:1:1 PBS:Kolliphor:ethanol and sterile filtering through a 0.22 µm syringe filter. Each inhibitor was injected intraperitoneally (i.p.) at 5 µL/g mouse. Inhibitors were prepared at 2 mg/mL, 0.2 mg/mL, 0.02 mg/mL, and 0.002 mg/mL to achieve final concentrations of 10 mg/kg, 1 mg/kg, 0.1 mg/kg, and 0.01 mg/kg respectively. Due to limited solubility, URB597 was prepared at 0.4 mg/mL and injected at 10 µL/g to achieve a dose of 4 mg/kg.

D-luciferin (100 mM) and CycLuc1 (5 mM) were prepared by direct dissolution into PBS and were sterile filtered through a 0.22 µm syringe filter. All other

luciferins were prepared by diluting a 50 mM DMSO stock into PBS and sterile

filtering through a 0.22 μm syringe filter. CycLuc1 ethyl ester was not soluble in

PBS and was therefore prepared by diluting the 50 mM DMSO stock into 18:1:1

PBS:Kolliphor:ethanol. Each substrate was injected i.p. at 4 μL/g mouse.

Substrates were prepared at 100 mM (D-Luciferin), 5 mM (CycLuc1), 250 μM

(substrates for AAV mice), and 100 μM (substrates for FVB-Tg[CAG-luc] mice) to

achieve final concentrations of 400 μmol/kg, 20 μmol/kg, 1 μmol/kg, and 0.4

μmol/kg respectively.

Bioluminescence Imaging of Mice

Each mouse was weighed to determine substrate and/or FAAH inhibitor dosing

and anesthetized using 2.5% isoflurane in 1 L/min oxygen. FAAH inhibitors were

injected i.p. at 5 μL/g mouse 30 minutes prior to luciferin injection. Luciferin

substrate was injected i.p. at 4 μL/g mouse and mice were imaged dorsally at 10

minutes and ventrally at 13 minutes.

Synthetic Procedures and NMR Data

These can be found in the supporting info of the paper available at the

publisher's website.

Acknowledgement

Chapter IV:

Firefly Luciferase Mutants Allow Substrate-Selective Bioluminescence Imaging in the Mouse Brain

Summary

Bioluminescence imaging is a powerful approach to visualize specific events occurring inside live mice. Animals can be made to glow in response to the expression of a gene, the activity of an enzyme, or the growth of a tumor. But bioluminescence requires the interaction of a luciferase enzyme with a small molecule luciferin, and its scope has been limited by the mere handful of natural combinations. Here we show that mutants of firefly luciferase can discriminate between natural and synthetic substrates in the brains of live mice. Using adeno-associated viral (AAV) vectors to express luciferases in the brain, we find that mutant luciferases that are inactive or weakly active with D-luciferin can light up brightly when treated with the aminoluciferins CycLuc1 and CycLuc2 or their respective FAAH-sensitive luciferin amides. Further development of selective luciferases promises to expand the power of bioluminescence and allow multiple events to be imaged in the same animal.

Introduction

Mice do not ordinarily glow in the dark. But if you introduce the enzyme firefly luciferase and the small molecule D-luciferin, they will glow in much the same way as a firefly does. Detection of the light emitted from these animals can be used to spy on specific events that would otherwise be invisible, such as gene expression and enzyme activity (Prescher and Contag, 2010.; Adams and Miller, 2014.). One limitation of this powerful technique has been the paucity of distinguishable luciferins and luciferases, restricting our ability to visualize multiple events in the same live animal using bioluminescence.

Firefly luciferase is particularly well suited to *in vivo* imaging (Adams and Miller, 2014.). The wavelength of the emitted light extends well into the red and near-infrared wavelengths that pass most easily through living tissues. Furthermore, the luciferin substrate is stable, easily administered, and offers several strategies to create luminescent probes (Adams and Miller, 2014.; Takakura et al., 2015.; Mofford et al. 2015.; Porterfield et al. 2015.). In efforts to expand upon the bioluminescent palette of the firefly while retaining its inherent benefits, we have synthesized new luciferin analogs and mutated the luciferase enzyme (Reddy et al., 2010.; Harwood et al., 2011.; Mofford et al. 2014.). We found that mutant luciferases can discriminate between D-luciferin and aminoluciferin analogs *in vitro* and in live cells (Harwood et al., 2011.; Mofford et al. 2014.). However, part

of the basis for this discrimination is a loss of substrate affinity, and it has been unclear how this discrimination would manifest in the context of live animals (Evans et al., 2014).

Here we perform bioluminescence imaging in the brain, and show that in this challenging environment, firefly luciferase mutants can discriminate between the natural substrate D-luciferin and synthetic luciferin analogs. We find that a balance of substrate selectivity and substrate affinity must be achieved to maintain high photon flux *in vivo,* more restrictive conditions than exist *in vitro.* Nonetheless, simple point mutations of luciferase are capable of discriminating between substrates. This work will help guide the development of additional luciferase-luciferin pairs that can be used to shed light on the molecular basis of disease and drug action in live animals.

We recently reported that the combination of three active-site mutations (R218K, L286M, and S347A) yielded a luciferase with 10,000-fold selectivity for a synthetic aminoluciferin substrate over the natural substrate D-luciferin (Figure 4.1) (Mofford et al., 2014). However, this selectivity came at the cost of an increased apparent Km compared to the individual mutants and the wild-type luciferase. A higher Km is not an issue for bioluminescence assays performed *in vitro,* but it could pose a problem for *in vivo* imaging, where substrate access is limiting (Evans et al., 2014).
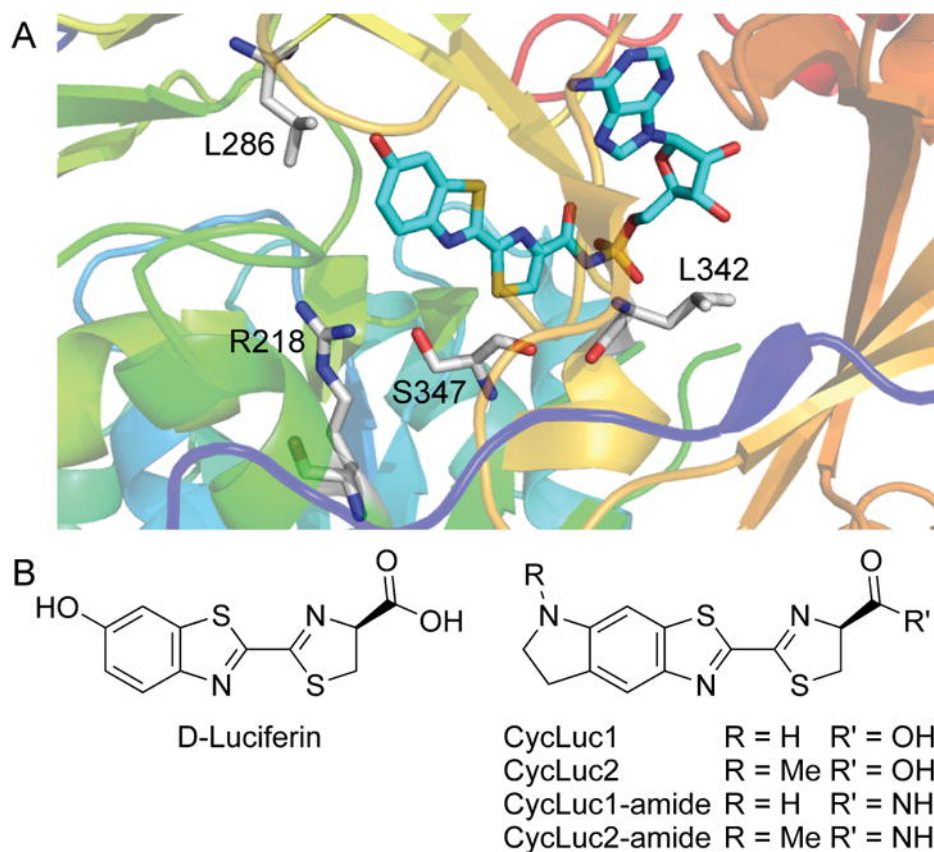
Figure 4.1. Location of mutated residues in firefly luciferase's active site and comparison of synthetic luciferins to D-luciferin. A) Crystal structure of firefly luciferase bound to a luciferyl-adenylate analog (PDB 4G36, rendered in PyMol). Mutations to R218, L286, and S347 in the luciferin binding pocket have allowed tuning of substrate specificity. L342 does not contact the core luciferin structure and is distal from the structural differences between D-luciferin, CycLuc1, and CycLuc2 (B).
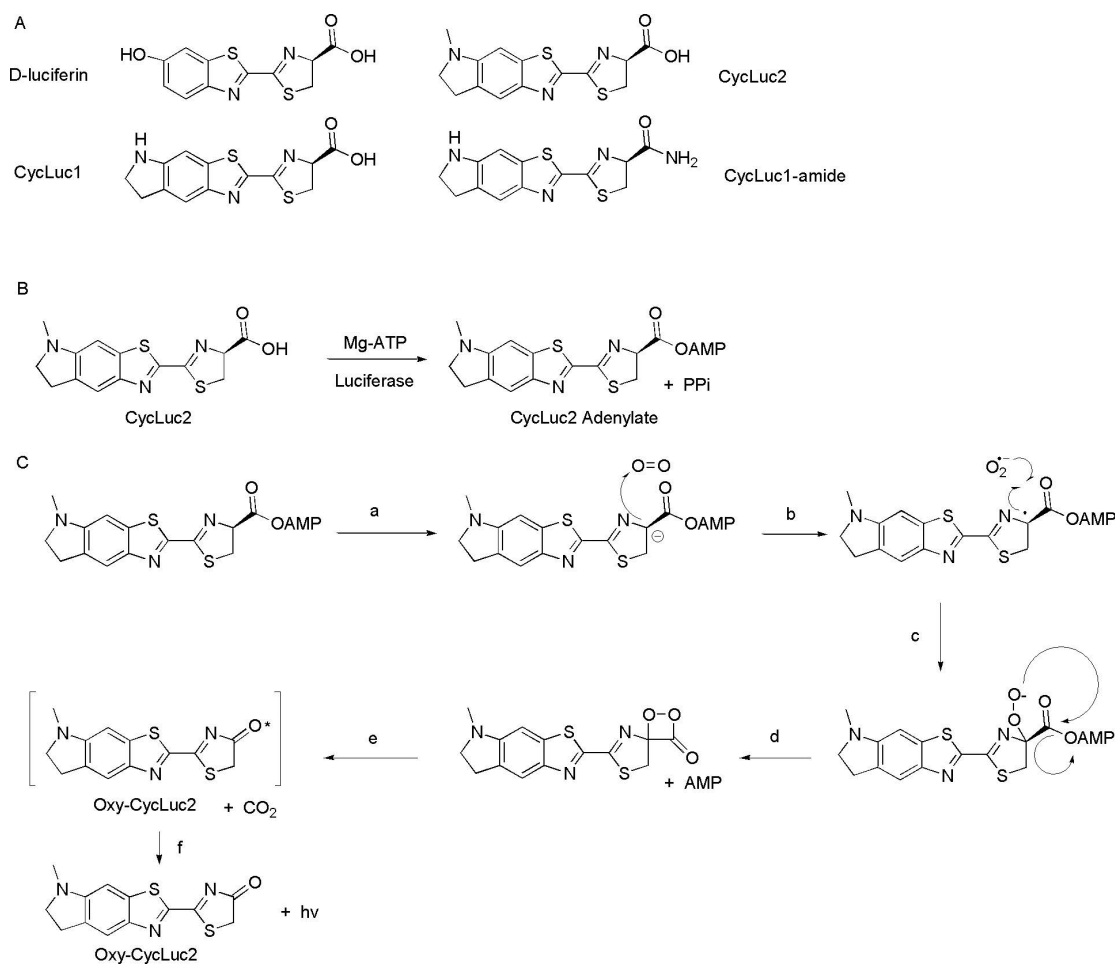
Figure 4.2. Substrate structures and mechanistic overview of firefly bioluminescent chemistry. Structures of D-luciferin, CycLuc1, CycLuc2, and CycLuc1-amide (A); Proposed mechanism of the luciferase reaction, shown with CycLuc2 in place of D-luciferin: B) Adenylation of the substrate is the key enzymatic chemistry required for bioluminescence. C) Subsequent light emission chemistry from the adenylate is largely driven by the chemistry accessible to this intermediate within the enzyme pocket: a) deprotonation of C4; b) single electron transfer to oxygen from the resonance-stabilized C4 anion; c) radical recombination with superoxide; d) displacement of AMP; e) decarboxylation of a dioxetanone; f) photon emission from an electronically-excited oxyluciferin.

Light emission from a luciferin substrate requires activation by ATP to form an

adenylated intermediate (Figure 4.1, Figure 4.2). Although residues in the ATP

binding site make no direct contact with the core luciferin scaffold, the ATP

binding site can influence (and be influenced by) luciferin binding. High ATP

concentration exacerbates the product inhibition that is observed with

aminoluciferins (Figure 4.3). The apparent Km value for ATP depends on the

luciferin substrate and is much lower for CycLuc1 and CycLuc2 compared to D-

luciferin (Table 4.1, Figure 4.3). Taking advantage of this behavior can thus

conceivably be used to distinguish between luciferins. Mutation of leucine 342,

part of the GYGLTE motif found in many adenylate-forming superfamily members

(Weimar et al., 2002.), can greatly increase the apparent Km values for both D-

luciferin and ATP yet retain high maximal luciferase activity (Branchini et al.,

2003.). We found that the L342A mutation confers substrate selectivity which

compares favorably to the previously reported R218K mutant (Figures 4.3, 4.4,

and 4.5). The change in apparent Km values for aminoluciferins is muted

compared to D-luciferin (Table 4.1). Combination of the two mutations into a

single luciferase results in further selectivity over D-luciferin (Table 4.1, Figure

4.4). Although not as selective as the R218K/L286M/S347A luciferase (Mofford

et al. 2014), the R218K/L342A double mutant yields the highest maximal

sustained photon flux with a synthetic luciferin to date, and no longer suffers

product inhibition (Figures 4.3, 4.4, and 4.5).
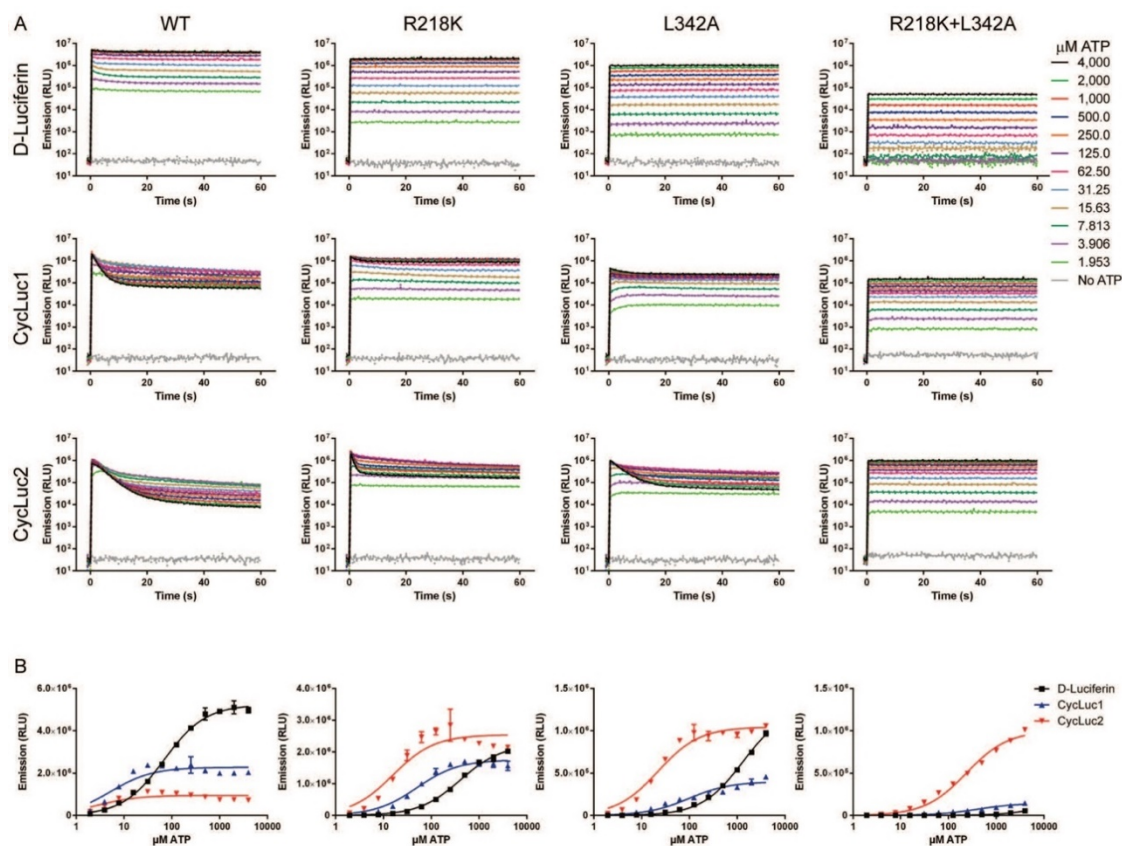
Figure 4.3. Substrate selectivity of the mutant luciferases: role of [ATP]. A) Burst kinetic data for WT and mutant luciferases with D-luciferin, CycLuc1, and CycLuc2 and varying [ATP], measured after rapid injection as described in the Experimental Methods. B) Sigmoidal dose-response fit to peak photon emission (0.5s post-injection) for each luciferase/luciferin as a function of [ATP].

$K_{m(app)}$ (µM)	D-Luciferin		CycLuc1		CycLuc2	
	Luciferin	ATP	Luciferin	ATP	Luciferin	ATP
WT[a]	6.2 ± 0.18	68 ± 3.0	NA	NA	0.69 ± 0.08	NA
R218K[a]	157 ± 7.7	408 ± 19	2.0 ± 0.22	50 ± 5.3	NA	16 ± 3.0
L342A[a]	232 ± 13	1320 ± 52	4.2 ± 0.39	96 ± 15	0.81 ± 0.06	22 ± 2.3
R218K+L342A[b]	>250	>4000	1000 ± 4.1	398 ± 51	40 ± 2.1	238 ± 17

[a] ATP titrations were performed at 100 µM D-luciferin, 10 µM CycLuc1/2; or
[b] 1 mM D-luciferin, 100 µM CycLuc1/2.

Table 4.1. Apparent Km values for luciferins and ATP with wild-type and mutant luciferases. NA = poor fit of data to a sigmoidal dose-response curve.
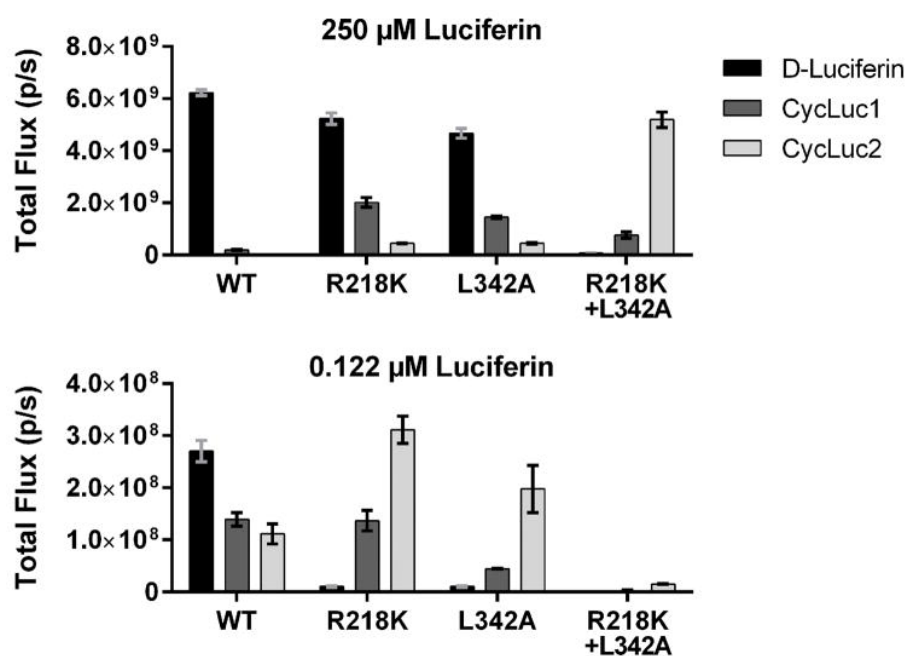
Figure 4.4. Photon flux from purified wild-type (WT) and mutant luciferases treated with high and low concentration of luciferin substrate (imaged as described in the Methods)**.**
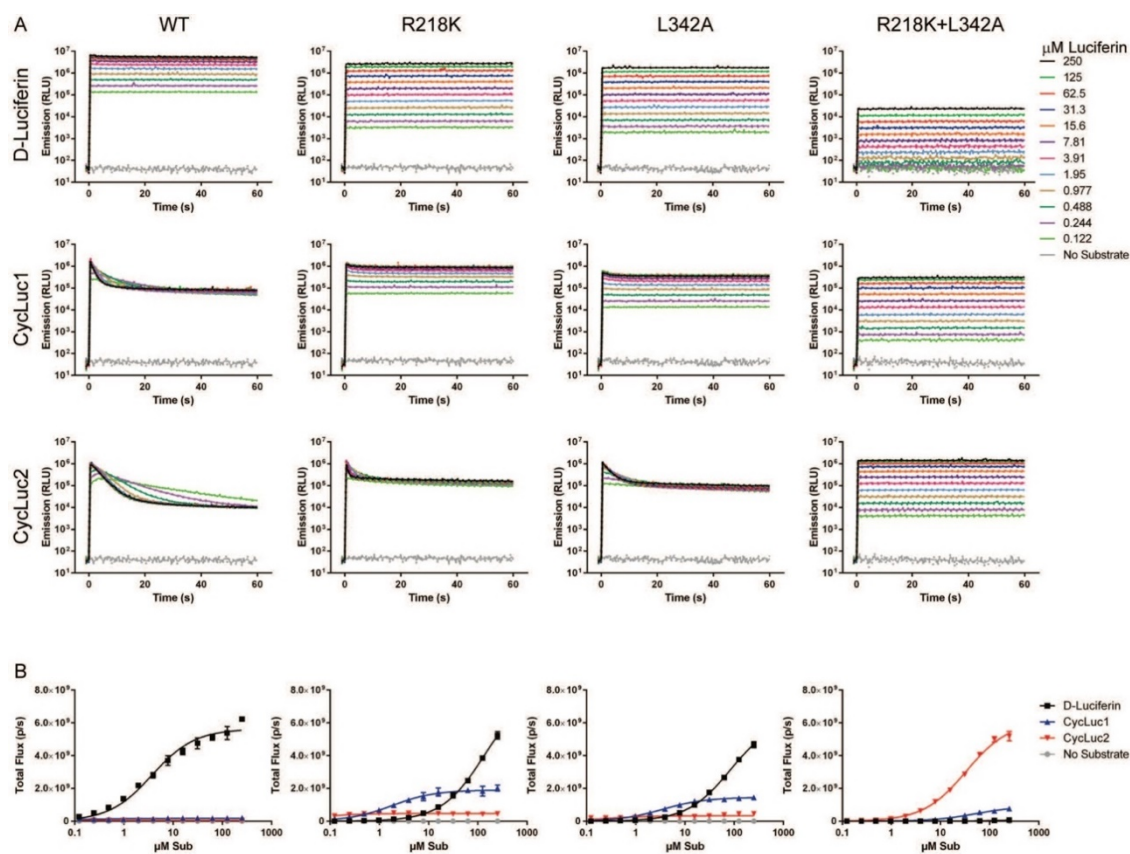
Figure 4.5. Substrate selectivity of the mutant luciferases: role of [luciferin].
A) Burst kinetic data for WT and mutant luciferases with varying concentration of D-luciferin, CycLuc1, and CycLuc2 measured after rapid injection as described in the Experimental Methods. B) Sustained photon emission for each luciferase and luciferin as a function of [luciferin], measured on the IVIS as described in the Experimental Methods.

To evaluate the performance of these three luciferase mutants *in vivo,* each

codon-optimized mutant was cloned into an adeno-associated viral (AAV)

plasmid under the control of a CMV promoter (Evans et al. 2014.), and packaged

into AAV9 vectors (Gao et al., 2004.; Clearley and Wolfe, 2006.). The AAV9-

luciferase viruses were then used to transduce FVB mice in the brain striatum

(Evans et al., 2014.). Unlike the use of luciferase-expressing tumor cells, this viral gene delivery method allows luciferase expression in endogenous mouse cells, for the life of the mouse (well over a year). As we have previously described for AAV9 transduction with the WT luciferase, each luciferase-expressing mouse was imaged after i.p. injection with a phosphate-buffered saline (PBS) solution of each luciferin (Mofford et al., 2015.; Evans et al., 2014.). These experiments were performed in the exact same set of mice, imaged with each substrate on sequential days.

Results and discussion

For all of the mutant luciferases, brain bioluminescence was dramatically reduced when using D-luciferin compared to CycLuc1 and CycLuc2 (Figure 4.6). With the L342A luciferase, D-luciferin gave no signal, while both aminoluciferins gave signal that was >50-fold over background. For the R218K luciferase, D-luciferin signal was 3-fold over background, but CycLuc1 and CycLuc2 were 40-50 fold brighter still. However, combining the R218K and L342A mutations did not yield synergism *in vivo.*

Although no photon flux above background was observed with D-luciferin for the double-mutant, the photon flux was also substantially lower for CycLuc1 and CycLuc2 than for the individual point mutants (Figure 4.7). Thus, at least in the

brain, the double mutant was less useful as a selective luciferase for these

substrates compared to L342A or R218K alone.
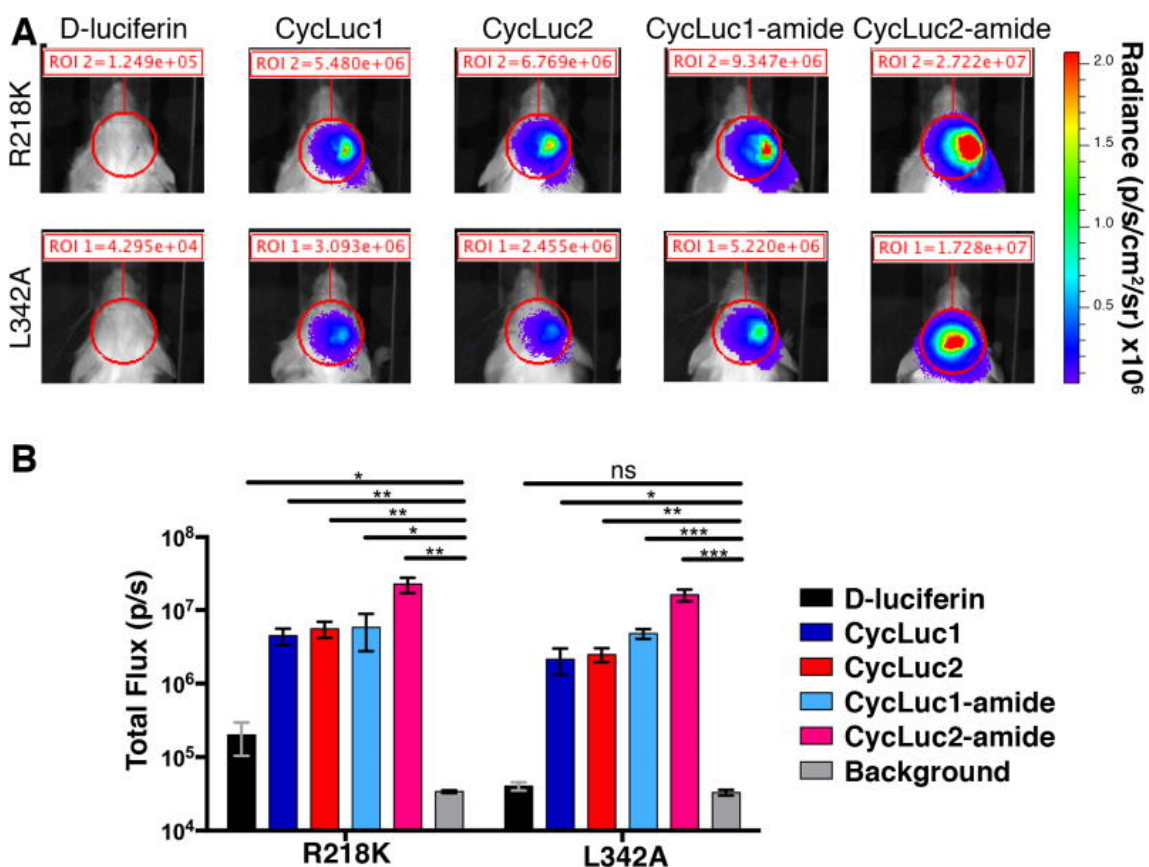
Figure 4.6. Mutant luciferase performance in the brains of live mice. A) Photon flux from a single AAV-transduced mouse compared after imaging with the indicated luciferase and luciferin (D-luciferin, 400 µmol/kg; CycLuc1, 20 µmol/kg; CycLuc2, 10 µmol/kg; CycLuc1-amide, 1 µmol/kg; CycLuc2-amide, 0.4 µmol/kg); B) Photon flux from the region of interest (ROI), n = 3 mice for each mutant luciferase. * p <0.05; ** p < 0.01; ns = not significant by t-test.
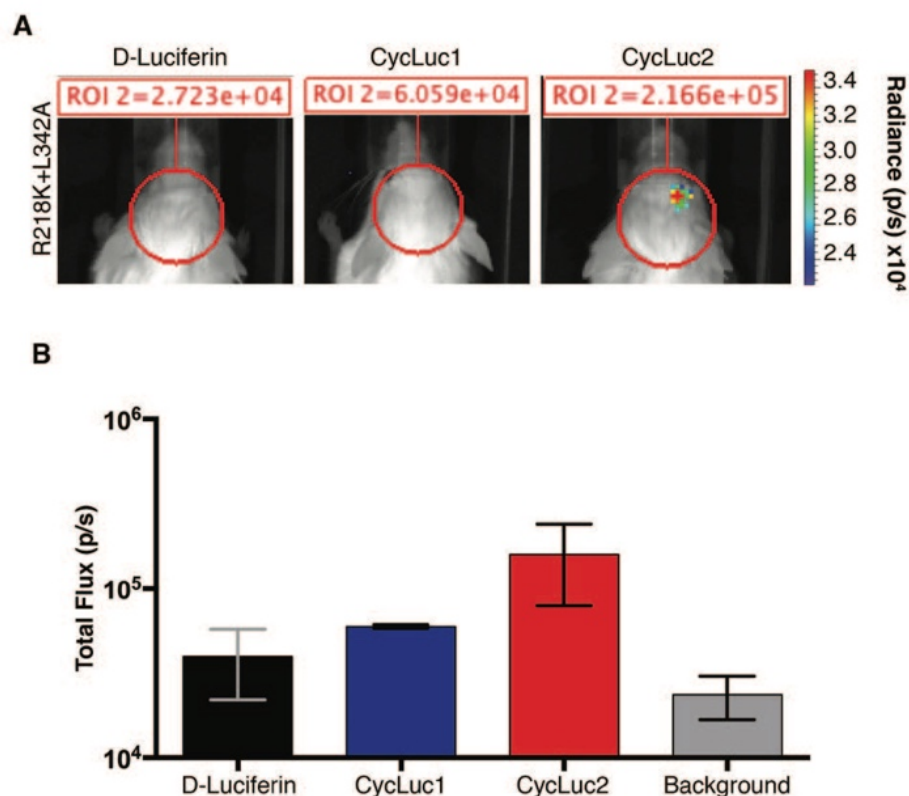
Figure 4.7. Mouse imaging with R218K/L342A luciferase. A) Photon flux from a single mouse transduced in the brain striatum with AAV9-CMV-luc2(R218K/L342A) after i.p. injection with the indicated luciferin (D-luciferin, 400 μmol/kg; CycLuc1, 20 μmol/kg; and CycLuc2, 10 μmol/kg); B) Photon flux from n = 2 mice.

Luciferin amides, sensors for the enzyme fatty acid amide hydrolase (FAAH), potentially offer a way to deliver luciferins into the brain more effectively (Mofford et al, 2015.; Mofford and Miller., 2015.). Because of high FAAH activity in the brain, the amides are converted into their respective luciferins, and imaging can be performed with very low doses of the luciferin amide (Mofford et al., 2015.). We therefore tested whether the amides of CycLuc1 and CycLuc2 (Figure 4.1)

could be used to detect AAV transduction in the brain with the mutant luciferases (Figure 4.3). Remarkably, i.p. injection of just 0.4 µmol/kg CycLuc2-amide allowed imaging of L342A luciferase in the brain with a signal that was >400-fold over background, equivalent or better than its performance with WT luciferase (Figure 4.8). By contrast, 400 µmol/kg D-luciferin failed to yield any detectable signal (Figure 4.6). Luciferin comparison at low equimolar doses further revealed the relative potency of each analogue (Figure 4.9).
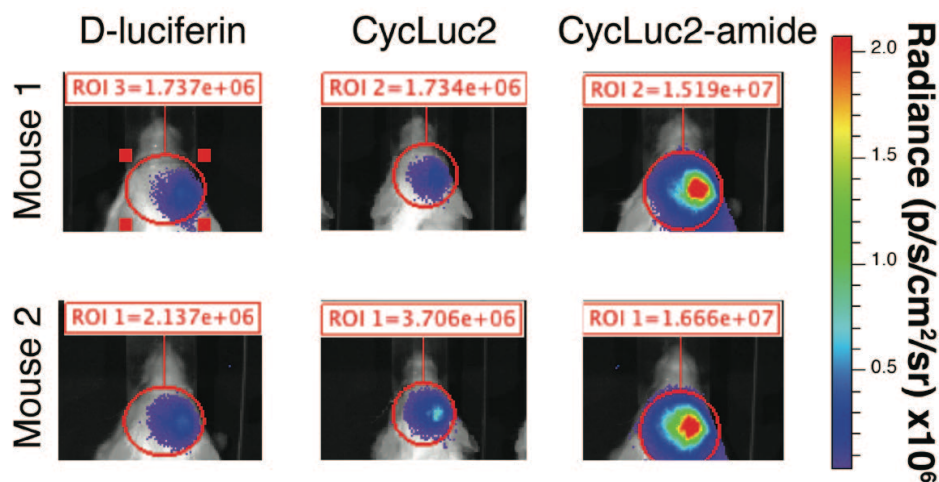
Figure 4.8. Mouse imaging with wild-type (WT) luciferase. Photon flux from mice transduced in the brain striatum with AAV9-CMV-luc2 after i.p. injection with the indicated luciferin (D-luciferin, 400 µmol/kg; CycLuc1, 20 µmol/kg; and CycLuc2, 10 µmol/kg). Each mouse was separately imaged, on sequential days, with all three luciferins.
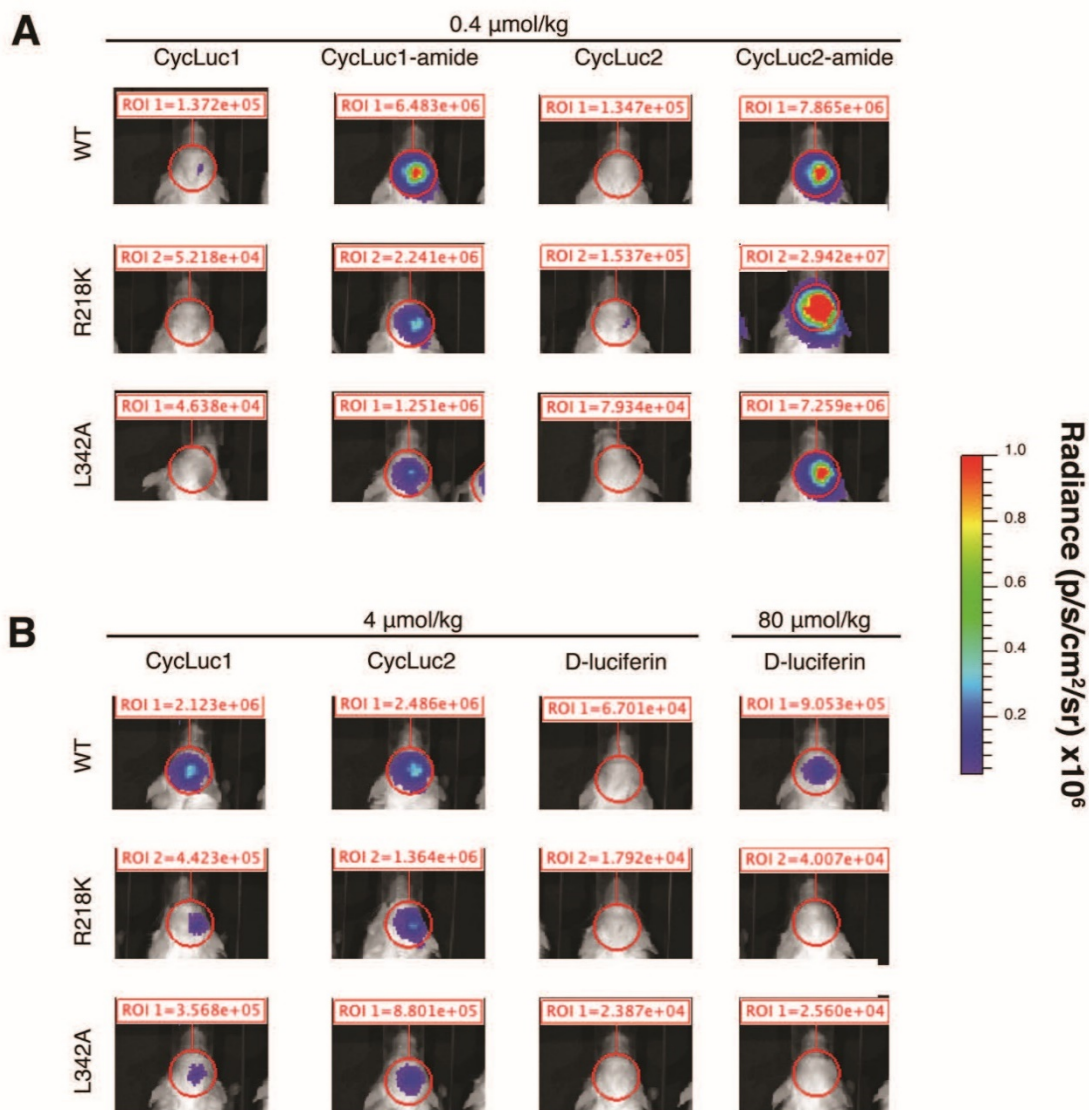
Figure 4.9. Comparison of luciferin analogs at equimolar dose after i.p. injection with A) CycLuc1, CycLuc1-amide, CycLuc2, and CycLuc2-amide at 0.4 µmol/kg; and B) CycLuc1, CycLuc2, and D-luciferin at 4 µmol/kg. D-luciferin at 80 µmol/kg is also shown for reference. Radiance of all images is represented on the same scale bar to the right.

Firefly luciferase exhibits a great deal of structural plasticity, and accepts an

almost bewildering array of molecules as substrates (Adams and Miller., 2014.;

Mofford et al., 2014.). Although we demonstrate here that mutant luciferases can strongly discriminate against D-luciferin *in vivo,* the inherent promiscuity of firefly luciferase has posed a challenge for the construction of truly orthogonal luciferases. That is, we can identify mutated enzymes that will emit light with CycLuc2 but not D-luciferin, but as of yet the converse has not been achieved. For most of the selective luciferases described thus far, we do not believe that the changes to the luciferin and luciferase are mirroring the classic "bump-hole" approach used for engineering ligand-receptor interactions (Belshaw et al., 1995.; Shah et al. 1997.). Rather, the primary basis for substrate selectivity is likely a loss of affinity for the core features of D-luciferin. Because aminoluciferins bind with higher affinity, they remain viable substrates. Going forward, one approach to more selective luciferases is to take advantage of homologous enzymes that are inherently more selective than firefly luciferase, and may therefore offer guidance as to how more precise substrate selectivity can be achieved (Mofford et al., 2014.). Here we also show that the interplay between the luciferin and ATP binding sites can play a role in discriminating between luciferins. Although leucine 342 is located far from the 6'-hydroxyl of D-luciferin (i.e. the site of the CycLuc1 and CycLuc2 modifications), mutation of this residue allows substrate selectivity in the brain. Future mechanistic work *in vitro* will be aimed at establishing the molecular basis for this interplay and uncovering how ATP binding affects the product inhibition seen with many luciferin analogs

(Figure 4.3). Perhaps ATP can rebind luciferase prior to release of the oxyluciferin product, resulting in a trapped complex.

Conclusion

Using AAV-delivered reporters, we have a platform on which to evaluate luciferases, luciferins, and luciferin-based sensors in different animal models and tissues (Mofford et al., 2015; Limberis and Wilson, 2006.; Zincarelli et al., 2008.; Tarantal and Lee, 2010.; Orabi et al., 2015.). Despite the ability of the L342A luciferase to emit light given sufficient quantities of D-luciferin and ATP in vitro, in the context of the live mouse brain we do not detect a signal. On the other hand, strong brain bioluminescence is observed from the L342A luciferase when using the aminoluciferins, but not with the double mutant R218K/L342A, despite its higher peak performance *in vitro.* Based on these results, a prudent design consideration (and proxy) for *in vivo* use, it is also important to keep in mind the role substrate modification has on the ability of the molecule to access particular tissues in the live animal (Mofford et al., 2015.). Together, we expect that the judicious application of mutant luciferases and modified luciferins will greatly expand the repertoire of noninvasive optical imaging tools.

Materials and Methods

Contributions

S.T.A. Jr. devised experiments, performed AAV deliveries in mice, performed
mouse imaging and analysis, and prepared manuscript. D.M.M. devised
experiments, performed in vitro work, live cell assays, and helped with
manuscript preparation. G.S.K.K.R. designed and synthesized synthetic
luciferins. S.C.M. devised experiments and helped with manuscript preparation.

Compounds. D-luciferin was purchased from Gold Bio. CycLuc1, CycLuc2,
CycLuc1-amide, 1,and D-cysteine amide were synthesized as previously
described (Reddy et al., 2010.; Mofford et al., 2015.).

**CycLuc2-amide [(S)-4,5-dihydro-2-(6,7-dihydro-5-methyl-5H-thiazolo[4,5-
f]indol-2-yl)thiazole-4-carboxamide]:**
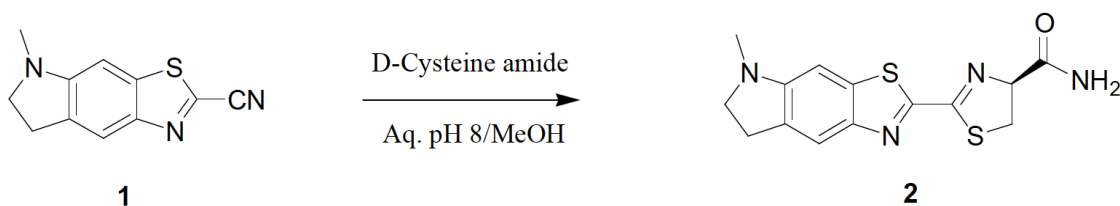
(S)-2-amino-3-mercaptopropanamide (D-cysteine amide, 7 mg, 0.0596 mmol)
was dissolved in 50 mM aqueous sodium phosphate buffer (pH 8, 2 mL) and

degassed using argon. This solution was added to 1 (10 mg, 0.049 mmol) in 2 ml

of degassed methanol. The reaction was stirred for 2 h, and then diluted with

sodium phosphate buffer and extracted with ethyl acetate (2 x 30 mL). The

combined organic layers were washed with water (3 x 30 mL) and dried

(Na_2SO_4), filtered and evaporated to afford CycLuc2-amide 2 as a yellow solid

(12 mg, 81%). 1H-NMR (400 MHz, $CDCl_3$): δ 7.71 (s, 1H), 6.72 (s, 1H and br s,

1H; overlapping), 5.68 (br s, 1H), 5.25 (t, 1H, J = 9.2 Hz), 3.75 (d, 2H, J = 10.0

Hz), 3.51 (t, 2H, J = 8.0 Hz), 3.10 (t, 2H, J = 8.0 Hz), 2.86 (s, 3H). 13C-NMR (100

MHz, $CDCl_3$): δ 173.5, 166.8, 153.7, 153.6, 146.5, 137.7, 132.9, 120.0, 96.1,

78.9, 55.8, 35.26, 35.18, 28.2. HRMS (ESI+) Calcd for $C_{14}H_{15}N_4OS_2$:

319.0687, Found: 319.0677.

Plasmid Constructs

Wild-type and R218K mutant luciferase genes were prepared as previously

described (Takakura et al., 2015.; Mofford et al., 2015.). The L342A and

R218K/L342A mutant luciferases were generated using the Q5 site-directed

mutagenesis kit (NEB) using the WT or R218K luciferase, respectively, as

template.

Enzyme Expression and Purification

Wild-type and mutant luciferases were expressed and purified as GST-fusion

proteins from the pGEX6P-1 vector as previously described.[3] Briefly, JM109

cells were grown at 37 °C until the OD600 reached 0.5-1, induced with 0.1 mM

IPTG, and incubated with shaking at 20 °C overnight. Cells were pelleted at 5000

rpm, then flash frozen in liquid nitrogen. The E. coli pellets from 1 L of culture

were thawed on ice, resuspended in 25 mL lysis buffer (50 mM Tris [pH 7.4], 500

mM NaCl, and 0.5% Tween 20) containing 1 mM phenylmethylsulfonyl fluoride,

and disrupted by sonification (Branson Sonifier). Dithiothreitol (DTT) was added

at 10 mM, and the resulting cell lysate was clarified by centrifugation at 35,000

rpm for 60 min at 4 °C. The supernatant was batch-bound to immobilized

glutathione (Thermo Scientific) for 1 hr at 4 °C, and the beads were washed with

lysis buffer containing 10 mM DTT, followed by wash buffer (50 mM Tris [pH 8.1],

250 mM NaCl, and 10 mM DTT) and storage buffer (50 mM Tris [pH 7.4], 0.1 mM

EDTA, 150 mM NaCl, 1 mM TCEP). Twenty units of PreScission Protease (GE

Healthcare) were added, and incubation continued overnight at 4 °C to cleave

the GST-fusion and elute the untagged enzyme. Protein concentrations were

determined using Coomassie Plus (Thermo Scientific).

Purified Protein Luminescence Assays - IVIS

Luminescence assays were performed as previously described (Mofford et al.,

2015.). Briefly, luminescence was initiated by adding 30 µL of purified luciferase

in enzyme buffer (20 mM Tris [pH 7.4], 0.1 mM EDTA, 1 mM DTT, and 0.8

mg/mL BSA) to 30 µL 2x substrate in substrate buffer (20 mM Tris [pH 7.4], 0.1

mM EDTA, 8 mM MgSO4, and 4 mM ATP) in a black 96-well plate (Costar 3915).

Imaging was performed one minute after enzyme addition using a Xenogen IVIS-

100 at a final enzyme concentration of 10 nM and final substrate concentrations

ranging from 0.122 to 250 μM. Data acquisition and analysis was performed with Living Image software. Data are reported as total flux (p/s) for each ROI corresponding to each well of the 96-well plate. The data were plotted using GraphPad Prism 6.0 and fit to a sigmoidal dose-response curve by non-linear regression. The cooled CCD in the IVIS has high quantum efficiency at the emission wavelengths of all substrates, and is the same detector used for in vivo imaging. However, these data do not reflect the initial rate and can be affected by product inhibition.

Luciferin Burst Kinetics Assays

Using a Promega GloMax-Multi Detection System, 50 μL of purified enzyme in enzyme buffer was rapidly injected into a white 96-well plate (Costar 3912) containing 50 μL of 2x substrate in substrate buffer to a final enzyme concentration of 0.2 nM and a final luciferin substrate concentration ranging from 0.122 to 250 μM. Measurements were taken every 0.5 s for 1 s pre-injection and 60 s post-injection. Data are reported as Relative Light Units (RLU) and were fitted to a sigmoidal dose-response curve by non-linear regression to determine apparent Km values (GraphPad Prism 6.0). Because the photomultiplier tube (PMT) in the GloMax has reduced sensitivity to red light, the photon emission of CycLuc1 and CycLuc2 are understated relative to D-luciferin. These data were not corrected for wavelength and were only used to determine apparent Km values.

ATP Burst Kinetics Assays

D-Luciferin was prepared at 400 µM in 20 mM Tris, [pH 7.4]. CycLuc1 and CycLuc2 were prepared at 40 µM in 20 mM Tris, pH 7.4. Separately, ATP was prepared in 20 mM Tris, pH 7.4 in two-fold serial dilutions from 16,000 µM down to 7.81 µM, with MgSO4 present in two-fold excess at concentrations from 32,000 µM to 15.63 µM. WT and mutant luciferases were prepared at 0.4 nM in enzyme buffer lacking EDTA. In a white 96-well plate (Costar 3912), 25 µL of the luciferin solution and 25 µL of the ATP-Mg solution were combined. Using a Promega GloMax-Multi Detection System, 50 µL of luciferase solution was rapidly injected to achieve a final luciferase concentration of 0.2 nM, a final luciferin concentration of 100 µM for D-luciferin and 10 µM for CycLuc1 and CycLuc2 (for WT, R218K, and L342A luciferases), and a final ATP concentration ranging from 4,000 µM to 1.95 µM, with Mg in two-fold excess. For the R218K/L342A mutant, which has higher apparent Km values for the luciferins, final concentrations of 1 mM D-luciferin and 100 µM CycLuc1 and CycLuc2 were used. Measurements were taken every 0.5 s for 1 s pre-injection and 60 s post-injection. Data are reported as Relative Light Units (RLU). Dose-response curves were plotted with data at the peak of the burst (0.5 s post injection) using GraphPad Prism 6.0 and fit to a sigmoidal curve by nonlinear regression to calculate the Km(app) for ATP with each luciferase/luciferin pair. Because the photomultiplier tube (PMT) in the GloMax has reduced sensitivity to red light, the photon emission of CycLuc1 and CycLuc2 are understated relative to D-luciferin.

These data were not corrected for wavelength and were only used to determine apparent Km values.

Mice

FVB/N mice were purchased from the Jackson Laboratory. All procedures involving these mice were approved by the Institutional Animal Care and Use Committee (IACUC) at the University of Massachusetts Medical School (protocol A-2714).

Construction of AAV-CMV-luc2

Mammalian codon-optimized luc2 luciferase from pGL4.1 (Promega) was mutated using a Quickchange mutagenesis kit (Agilent), and then cloned into the EcoRI-SalI sites of a pAAV-CMV plasmid. The AAV-CMV-luc2 mutant plasmids were packaged into AAV serotype 9 by the University of Massachusetts Medical School Viral Vector Core.

AAV9-CMV-luc2 vector striatal injections

Three female FVB/NJ mice per luciferase mutant were purchased from the Jackson Laboratory. Striatal injections were performed at 6 weeks of age. A chemical hand warmer under a gel pad wrapped in paper towel was placed onto a stereotactic frame. Each mouse was anesthetized with 90 mg/kg ketamine and 4.5 mg/kg xylazine (ketamine/xylazine mix) before surgery. Once anesthetized, they were placed on a stereotactic frame and had the hair on their scalp removed

by an application of super glue, followed by pulling the hair off as a single

section. Three alternate betadine and 70% ethanol washes of the denuded area

were performed with a new cotton-tipped applicator for each application.

Sterilized forceps were used to raise the skin on the scalp, then sterilized surgical

scissors were used to make a 1 cm incision anterior to posterior within the

denuded area covering the bregma suture. The site of injection was acquired at

the lateral edge of the striatum/cortex border (stereotactic coordinates: anterior 1

mm, lateral 3 mm and ventral 2 mm from bregma). The needle was left in place

for one minute, then the mutant luciferase containing AAV vector (1 µL of 2.5e12

GC/ml AAV9-CMV-Luc2 in PBS) was injected into the mouse at a rate of 125

nl/min using a micropump-controlled syringe (NanoFil, World Precision

Instruments). After injection, the needle was left in place for one minute before

withdrawing. The incision was sutured using 3 simple interrupted stitches of

dissolving suture material. The mouse was then treated with 0.05 mg/kg

buprenorphine i.p. before returning to its cage, and again every 6 hours for 48

hours post-surgery. The cages remained on a heat pad at 37 degrees Celsius

until mice regained righting reflex. Bioluminescence imaging was performed at

least 2 weeks after AAV delivery.

Preparation of luciferins for brain imaging

D-luciferin (100 mM), CycLuc1 (5 mM), and CycLuc2 (2.5 mM) were all prepared by dissolving dry compound directly into PBS. The respective amides were prepared by first dissolving dry compound into DMSO to a concentration of 50 mM, followed by dilution in PBS to a final concentration of 250 µM (CycLuc1-amide) or 100 µM (CycLuc2-amide). Once dissolved, all substrate stocks were filtered through a 0.2 µm filter (Millipore) prior to injection into mice.

Brain imaging

Mice were imaged in the University of Massachusetts Medical School Small Animal Imaging Core using an IVIS 100 imaging system. The animals were anesthetized with isoflurane (2% in 1 L/min oxygen), then injected i.p. with 4 µl of luciferin stock in PBS per gram of body mass. Images were acquired as 60 second exposures at 15 minutes after i.p. injection and analyzed using Living Image software. Regions of interest (ROIs) were drawn around the region covering the brain, and the total flux within each ROI was recorded. ROI sizes were identical across all images. Graphs and statistics were generated using GraphPad Prism 6.

Chapter V:

Rapid Access to a Broad Range of 6'-Substituted Firefly Luciferin

Analogues Reveals Surprising Emitters and Inhibitors

Deepak K. Sharma, **Spencer T. Adams Jr.**, Kate L. Liebmann, and Stephen C.

Miller. (2017) *Org. Lett.*, 19(21): 5836-5839.

Spencer T. Adams Jr. performed *in vitro* experiments and prepared figures 5.2,

5.3, 5.4, 6.6 and Table 5.1.

Summary

Light-emitting firefly luciferin analogues contain electron-donating groups in the

6'-position, but the scope of known 6'-substitution remains narrow. A two-step

route to a broad range of 6'-substituted luciferin analogues was developed to fill

this void and enable a more extensive study of the 6'-functionality.This chemistry

allowed direct access to "caged" amide and bright azetidine analogues, but also

revealed thioether inhibitors and unexpectedly luminogenic aryl amine

derivatives.

Introduction

The natural substrate for firefly luciferase, d-luciferin, contains an electron-

donating hydroxyl group in the 6′-position that is crucial for bioluminescence

(Figure 5.1) (Adams and Miller, 2014.). Synthetic analogues containing amine or

alkylamine donors are also luminogenic and can offer advantages for in vivo imaging (Evans et al., 2014.; Kuchimaru et al., 2016.). However, to date most firefly luciferin substrates and "caged" sensors have been synthesized from 6-amino or 6-hydroxy benzothiazoles, placing inherent restrictions on the nature of the electron-donating 6′-functionality (Adams and Miller, 2014.; Woodroofe et al., 2008.; Reddy et al., 2010.; Jathoul et al., 2014.; Takakura et al., 2015.; Mofford et al., 2015.; Heffern et al., 2016.; Steinhardt et al., 2017.). As such, only a relatively narrow range of 6′-substituted luciferin analogues are known, limiting our understanding of the chemistry of bioluminescence and ability to take full advantage of this imaging modality. In order to further investigate the role of this vital component, we explored the derivatization of 6-fluoro and 6-bromo-2-cyano-benzothiazoles via nucleophilic aromatic substitution and Buchwald–Hartwig amination, respectively. We found that this chemistry allowed access to new classes of luciferase substrates, inhibitors, and their precursors, with immediate applications for biocompatible chemistry and bioluminescence imaging.
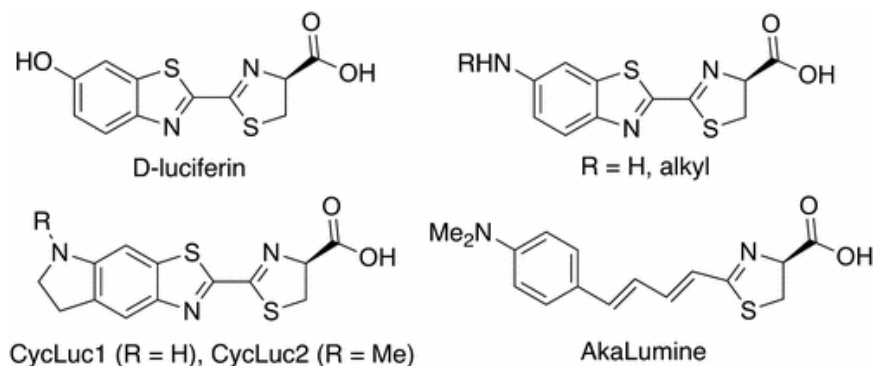
Figure 5.1. Firefly luciferase substrates all have hydroxy, amino, or alkylamino electron donors. Examples include d-luciferin, 6′-aminoluciferin, CycLuc1, and AkaLumine.

We envisioned that 6-halo-2-cyanobenzothiazoles could be modified at the 6-position by nucleophilic aromatic substitution or palladium catalysis (Grimm and Lavis, 2011.). One concern was that the activated nitrile is prone to react with nucleophiles. Indeed, fear of this possibility initially dissuaded us from exploring this route, in favor of reductive alkylation and other synthetic strategies (Reddy et al., 2010.; Mofford et al., 2014.). Nonetheless, this chemistry could offer access to a wide variety of analogues not readily accessible by other approaches.

Results and discussion

We first synthesized 6-fluoro-2-cyanobenzothiazole **3** (Scheme 5.1) and performed $S_N Ar$ reactions with a variety of cyclic secondary amines that could be challenging or tedious to synthesize by the conventional N-alkylation approach (Scheme 5.2). Of particular interest, azetidine-substituted fluorophores have

been reported to have higher quantum yields than those of analogous dyes (Grimm et al., 2015.). Although the desired 6-substituted-2-cyano-benzothiazoles **4**–**9** could be isolated in most cases, the yields from the S_NAr route were low (<20%; Scheme 5.2). The reaction with azetidine was particularly problematic (2% yield). Primary amines and weakly nucleophilic amines such as thiomorpholine dioxide failed to give any desired product. However, displacement with methanethiol was successful (48% yield), giving access to a new class of analogue that was expected to be fluorescent (Barr and Holewinski, 2002.; Granzhan et al., 2007.). The corresponding sulfoxide and sulfone could be prepared by oxidation with Oxone and mCPBA, respectively (Scheme 5.2). The thiophenol analogue could also be prepared, albeit in low yield (13%).

We next turned to Buchwald–Hartwig amination of **14**, synthesized from 6-bromo-2-chlorobenzothiazole by heating with KCN in DMSO, or alternatively in higher yield at room temperature using DABCO as a catalyst (Scheme 5.3) (Hauser et al., 2016.). Palladium-catalyzed amination using xantphos as a ligand (Kranenburg et al., 1995.; Yin and Buchwald, 2002.) allowed synthesis of the morpholine analogue in 71% yield vs 12% for the S_NAr reaction (Scheme 5.4). Additionally, the thiomorpholine dioxide analogue was obtained in 74% yield, and the azetidine, in 33% yield (low, but vastly improved over 2%). Boc-piperazine was similarly accessed, where the Boc group could be retained or later removed with TFA.
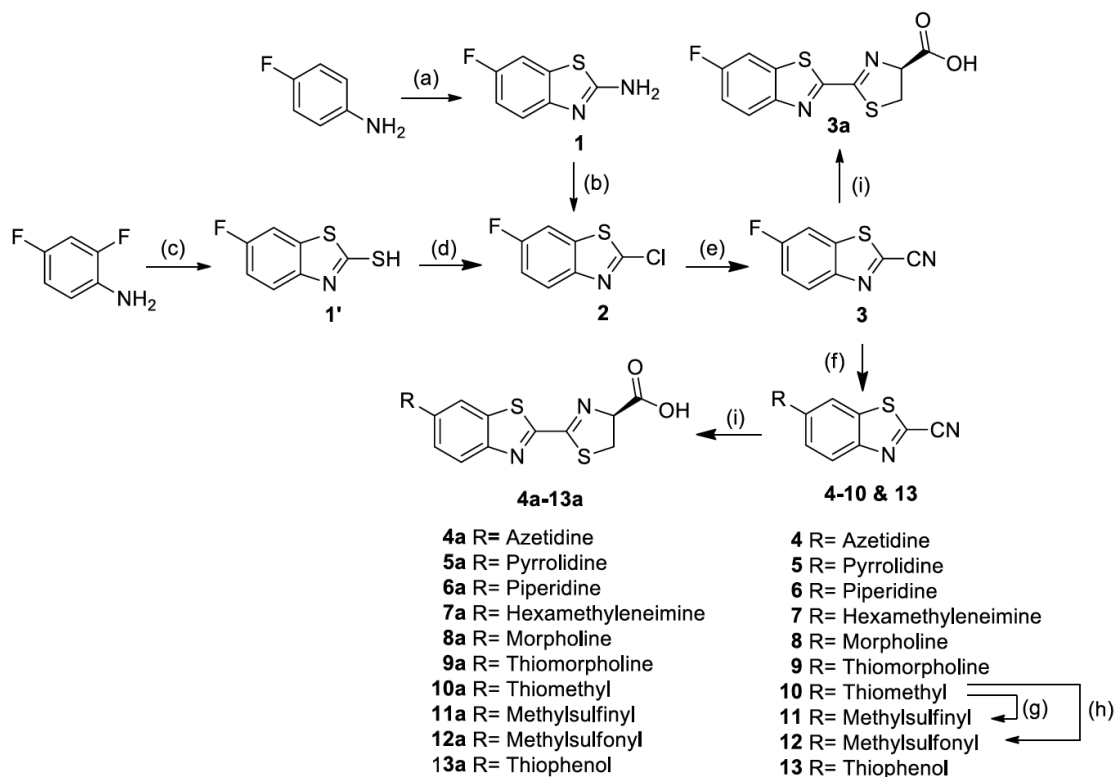
Scheme 5.1. (a) Bromine, potassium thiocyanate, acetic acid, rt, 21h then adjusted to pH 8 using NH₄OH; (b) t-butyl nitrite, CuCl₂, CH₃CN, rt, 2h, then 65°C for 1h; (c) potassium ethyl xanthogenate, DMF, 100°C, 4h; (d) SO₂Cl₂, rt, 2h; (e) Method A: KCN, DMSO, 90°C, 8h or Method B: KCN, DABCO, DMSO:H₂O (9:1), rt, overnight; (f) Nucleophile, K₂CO₃, DMF, 60°C, 4h; (g) mCPBA, DCM, rt, 12h; (h) Oxone, ethanol, 60°C, 8h; (i) D-cysteine, aq. MeOH.
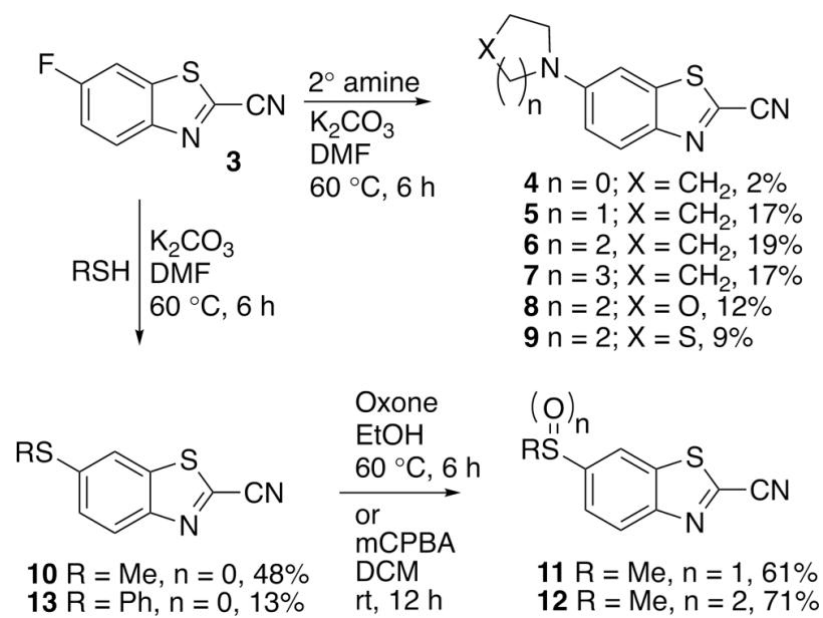
Scheme 5.2. Nucleophilic aromatic substitution of 6-fluoro-2-cyanobenzothiazole with secondary amines and thiols.
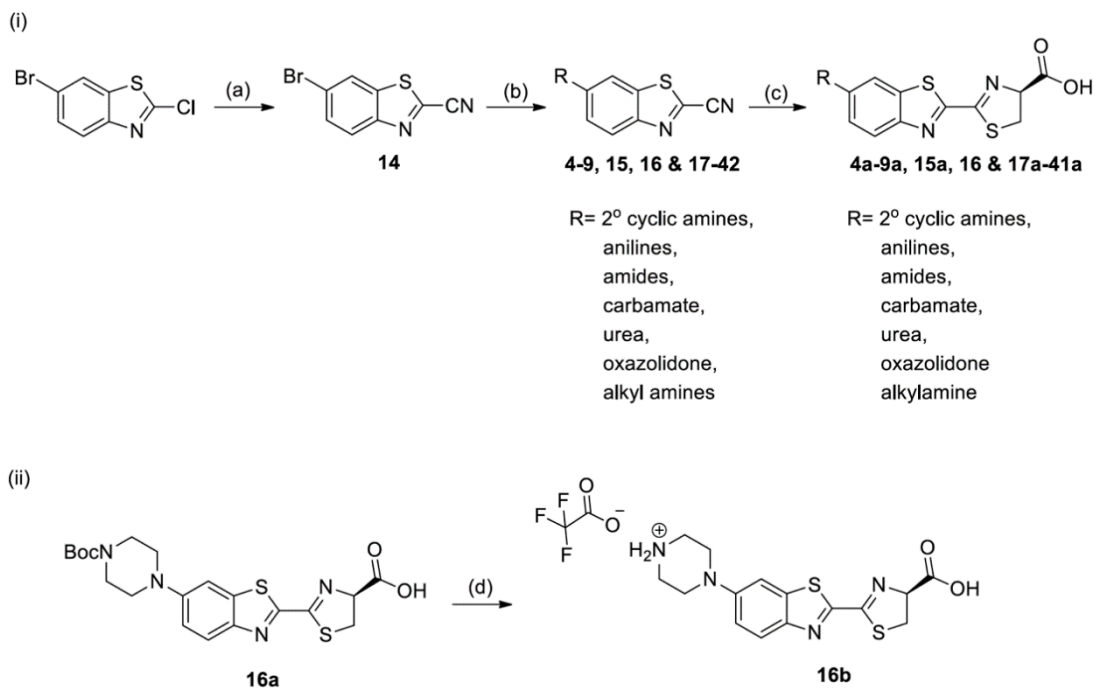
Scheme 5.3. Synthesis of piperazine luciferins. (i) (a) Method A: KCN, DMSO, 90°C, 8h; Method B: KCN, DABCO, DMSO: H_2O (9:1), rt, overnight. (b) nucleophile, Pd_2dba_3, xantphos, Cs_2CO_3, dioxane, 95-100°C. (c) D-cysteine, pH 8 buffer. (ii) (d) dichloromethane: trifluoroacetic acid (3:1), rt, 2h.

coupling partner
5 mol % Pd$_2$dba$_3$
10 mol % xantphos

Cs$_2$CO$_3$, dioxane
100 °C, 6 h

14

4 n = 0, X = CH$_2$, 33%
8 n = 2, X = O, 71%
9 n = 2, X = S, 55%
15 n = 2, X = SO$_2$, 74%
16 n = 2, X = BocN, 75%

17 all R = H, X = CH, 66%
18 R$_2$ = Et, 75%
19 R$_3$ = Et, 64%
20 R$_2$ = R$_6$ = Me, 50%
21 R$_3$ = R$_5$ = Me, 67%
22 R$_4$ = F, 57%
23 R$_4$ = OMe, 69%
24 R$_1$ = Me, 59%
25 R$_1$ = Me, R$_4$ = NHMe, 63%
26 R$_4$ = NMe$_2$, 54%
27 R$_4$ = OH, 73%
28 X = N, 69%

29 n = 1, 62%
30 n = 2, 87%

31 R$_1$ = Ph, R$_2$ = H, 62%
32 R$_1$ = H, R$_2$ = H, 58%
33 R$_1$ = H, R$_2$ = Me, 77%
34 R$_1$ = Me, R$_2$ = H, 82%
35 R$_1$ = Me, R$_2$ = Me, 62%

36 R$_1$ = BnO, R$_2$ = H, 38%

37 R$_1$ = NMe$_2$, R$_2$ = H, 45%
38 R$_1$ = NMe$_2$, R$_2$ = Me, 36%

39 73%

13 48%

40 R = CH$_2$CH=CH$_2$, 40%
41 R = CH$_2$CF$_3$, 19%
42 R = CH$_2$CH$_2$CH$_2$OH, 49%

Scheme 5.4. Buchwald-Hartwig substitution of 6-bromo-2-cyanobenzothiazole with a wide variety of partners.

Buoyed by the success of this approach, we then sought access to entire classes

of 6′-modifications heretofore unknown in luciferin analogues, in order to more

broadly explore the range of electron-donating groups (EDGs) that could be

accommodated in luciferin substrates or caged sensors. For example, no 6′-arylamino luciferin analogues have been reported. Excitingly, Buchwald-Hartwig amination with xantphos allowed ready access to a wide variety of 6-arylamino derivatives (Scheme 5.4, **17–30**). Furthermore, secondary and tertiary "caged" 6-amide analogs could also be synthesized directly in good yields under these conditions (**31–35**) (Yin and Buchwald, 2002.). Although simple 6′-amidoluciferins are all potential sensors for amidases, only the 6′-acetamide has been previously described (White et al., 1966.). We extended this chemistry to carbamates and ureas such as 2-oxazolidone **39**, benzyl carbamate **36**, dimethylurea **37**, and trimethylurea **38**. The thiophenol derivative **13** could be prepared in improved yield. Primary amines could also be coupled (**40–42**), enabling the direct synthesis of derivatives that previously required functional group protection (**42**).

The new 6-substituted nitriles were all readily converted into their respective luciferin analogues **3a-41a** by reaction with D-cysteine (Schemes 5.1 and 5.3). However, it should be noted that these nitriles are also of direct interest for their mild biocompatible condensation with N-terminal cysteines and related aminothiols (Ren et al., 2009.; Van de Bittner et al., 2013.; Godinat et al., 2013.; Ramil et al., 2016.).

A set of 36 new luciferin analogues was then evaluated in burst bioluminescence assays with purified firefly luciferase (Figures 5.2-4; Table 5.1) (Mofford et al., 2014.; Harwood et al., 2011.). This assay was used to determine whether the new analogues have the capacity for light emission. Unsurprisingly, monoalkyl

amine **40a** was the brightest, while azetidine **4a** led the new cyclic secondary

amines (Figures 5.2 and 5.5). Although disparate structures such as azepane **7a**

(Kakiuchi et al., 2017.), thiomorpholine **9a**, piperazine **16b** and

trifluoroethylamine **41a**were all good emitters, the thiomorpholine dioxide

analogue **15a**was unexpectedly only weakly luminescent (Figures 5.2A; 5.3-4),

despite its fluorescence (Table 5.2). Potentially, accommodation of the bulky

sulfone group requires twisting of the amine within the enzyme pocket, lowering

the quantum yield. Such differences could be exploited for the development of

orthogonal luciferase substrates (Harwood et al., 2011.; Mofford et al., 2014b.;

Adams et al., 2016.; Jones et al., 2017.) and for the creation and modulation of

selective luminogenic reporters (Mofford et al., 2015.).
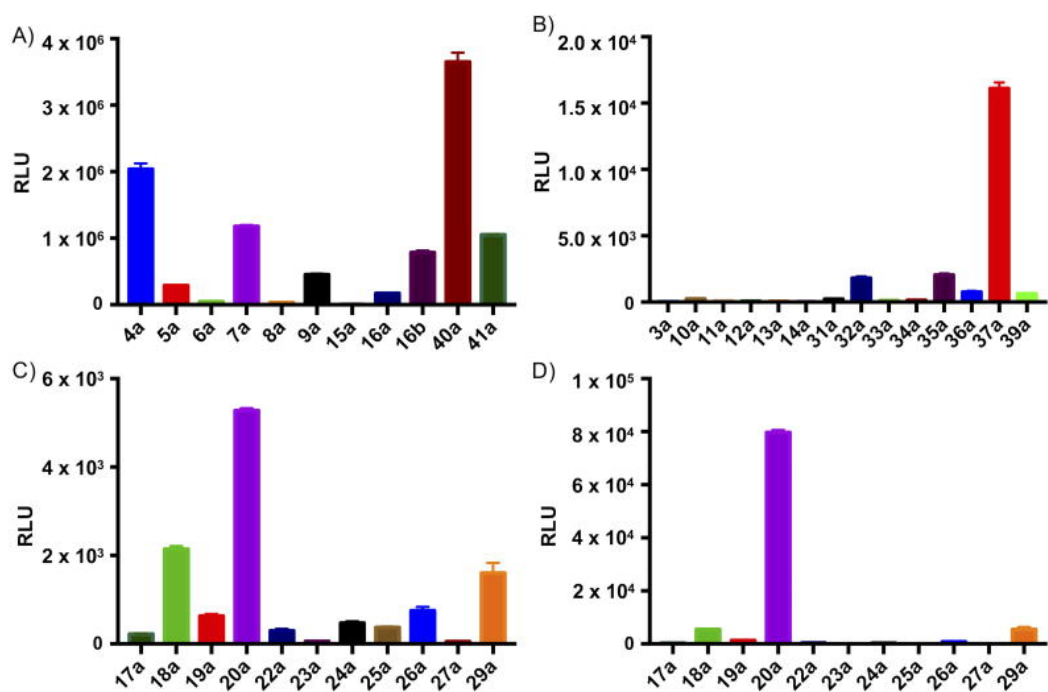
Figure 5.2. Bioluminescence emission from WT luciferase with luciferin analogs. A) alkylamino luciferins; B) putative "caged" luciferins; C) arylamino luciferins; D) arylamino luciferins incubated with R218K mutant luciferase. Note differences in scale between panels.

A)

B)
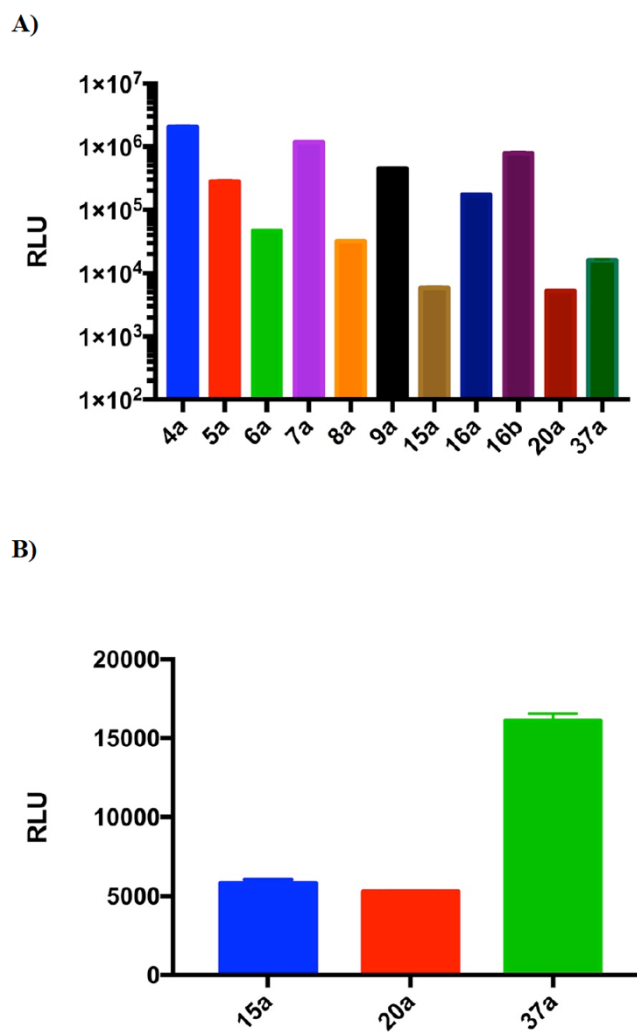
Figure 5.3. Burst bioluminescence emission from WT firefly luciferase with luciferin analogues. A) Log scale shows dramatically lower emission from thiomorpholine dioxide **15a** compared to other cyclic amines. B) Non-canonical luciferin analogues **20a** and **37a** compared to **15a** on a linear scale.

A)
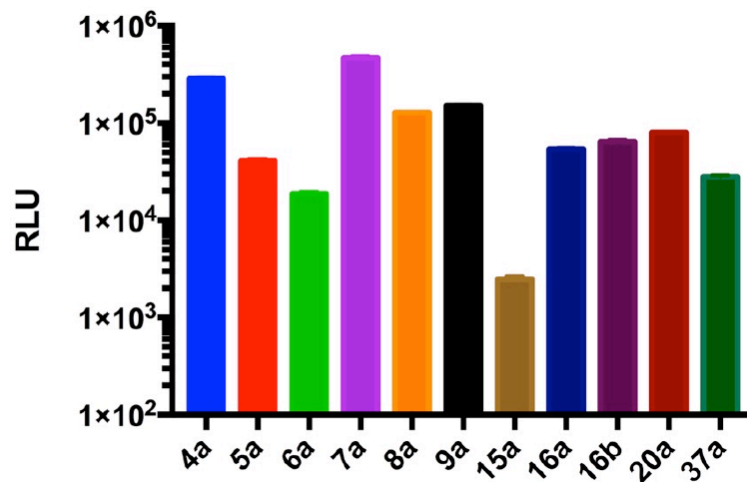
B)
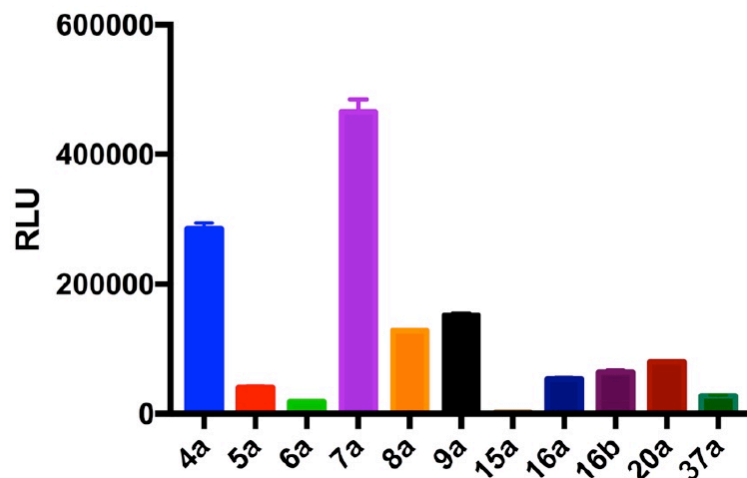
Figure 5.4. Burst bioluminescence emission from R218K mutant firefly luciferase with luciferin analogues on A) log scale and B) linear scale. The mutant enzyme improved emission from **8a** and non-canonical luciferin analogues **20a** and **37a**.
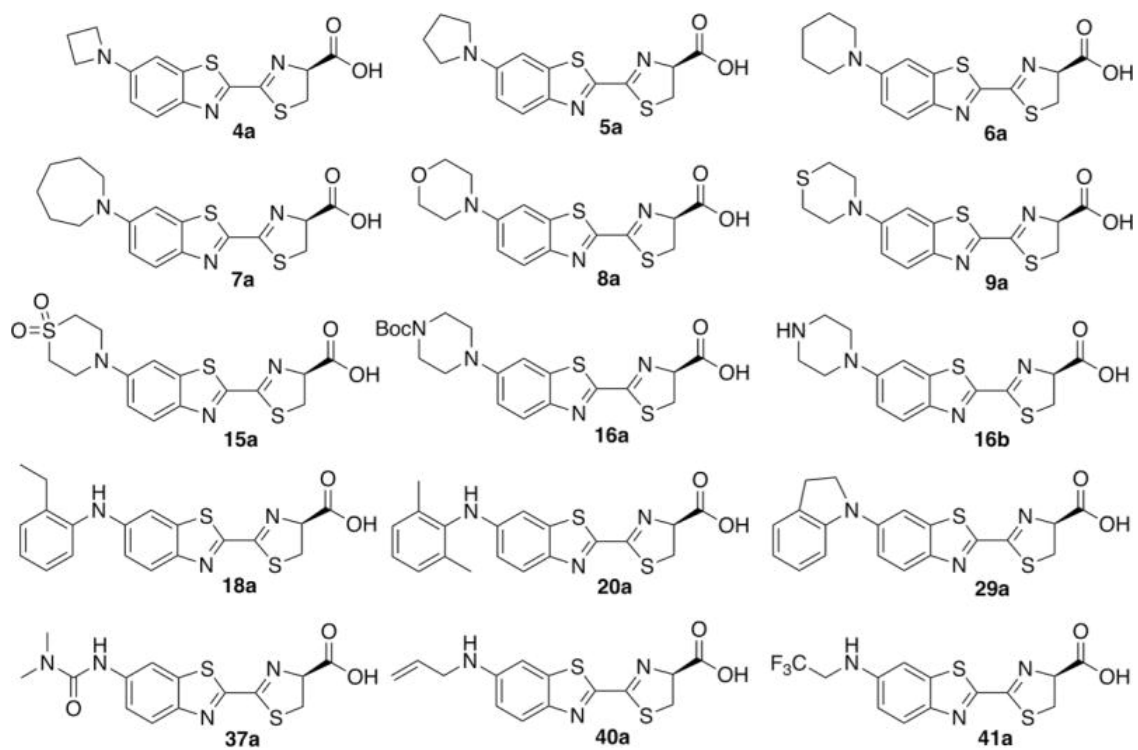
Figure 5.5. Newly-synthesized luminogenic substrates.

Substrate	Peak Wavelength (nm)	
	WT Firefly Luciferase	R218K Firefly Luciferase
D-luciferin	551	560
Azetidine (**4a**)	612	626
Pyrolidine (**5a**)	604	624
Piperidine (**6a**)	612	634
Azepane (**7a**)	607	ND
Morpholine (**8a**)	604	ND
Thiomorpholine (**9a**)	ND	614
TMPDO (**15a**)	557	ND
Boc-PIPE (**16a**)	547	587
Piperazine (**16b**)	554	596
2,6 DMAN (**20a**)	575	590
1,1 DMU (**37a**)	594	ND
ALL (**40a**)	602	606
TRIFET (**41a**)	559	572

Table 5.1. Peak bioluminescence emission wavelengths for selected luciferins.

Measurements were performed as previously described (Harwood et al., 2011.; Mofford et al., 2014.). ND = not determined.

In contrast to alkylamines, the presence of arylamine EDGs in dyes is generally associated with negligible fluorescence (Grimm and Lavis, 2011.; Granzhan et al., 2007.; Kitamura et al., 2007.; Peng et al., 2016.). However, fluorescence can be observed in rigid, viscous, or nonpolar environments (Table 5.2) (Granzhan et al., 2007.; Chen et al., 2003.; Kosower, 1982.; Ren et al., 2016.). We suspected that the luciferase active site might serve as a suitably rigid environment for luminescence. Although most of the aniline analogues were essentially non-luminescent, the subset of *ortho*-substituted anilines, expected to experience

hindered rotation, was indeed emissive: 2,6-dimethylaniline **20a**,

indoline **29a** and 2-ethylaniline **18a** (Figures 5.5.2C and 5). Furthermore, a

substantial increase in luminescence for **20a** was observed with a mutant

luciferase that is known to better accommodate many synthetic luciferins

(Figures 5.2D and 5.4), suggesting that further enhancement of 6′-arylamine

luminescence is possible by alteration of the substrate pocket.

Interestingly, not all "caged" analogs are completely dark (Figures 5.2B, 5.3, and

5.4). In particular, the dimethylurea derivative **37a** was luminescent and brighter

than **15a** (Figures 5.5.3 and 4). Several carboxamide analogues also had weak

emission (>1,000-fold weaker than D-luciferin, but still >10-fold over

background). In contrast, all of the new thio analogues are dark, despite the

fluorescence of the S-methyl analogue **10a** (Table 5.2) (Barr and Holewinski,

2002.; Granzhan et al., 2007.). Indeed, thioethers **10a** and **13a** are potent

luciferase inhibitors, as are the non-emissive aryl amines (Figure 5.6). On the

other hand, the thiomethyl sulfoxide **11a** and sulfone **12a** are only weakly

inhibitory, suggesting a potential strategy for constructing bioluminescent sensors

of S-oxidation based on relief of luciferase inhibition.

Compound	PBS			Methanol			Dioxane		
	Abs. (nm)	Em. (nm)	RQY	Abs. (nm)	Em. (nm)	RQY	Abs. (nm)	Em. (nm)	RQY
4a	369	554	0.40	380	516	0.78	383	464	1.24
7a *a*	414	550	0.13	402	517	0.76			
8a	346	546	0.22	363	518	0.73			
9a	354	533	0.47	366	512	0.75			
10a	344	494	0.29	342	465	0.33	340	405	0.82
11a	300	-	0	299	-	0			
12a	291	-	0	286	-	0			
15a	359	515	1.02	358	488	1.00	364	445	1.14
17a	384	-	0	389	-	0	384	469	1.12
6'-amino-luciferin	351	517	1	360	487	1	362	441	1

Table 5.2. Fluorescence properties of selected luciferin analogues.

Excitation wavelength was 351 nm in PBS and dioxane, 359 nm in methanol. An observed lack of fluorescence is indicated by a QY of 0 and "-" for emission wavelength. Grayed out boxes indicate no measurements were carried out.

[a]Excitation wavelength was 384 nm in PBS and methanol.
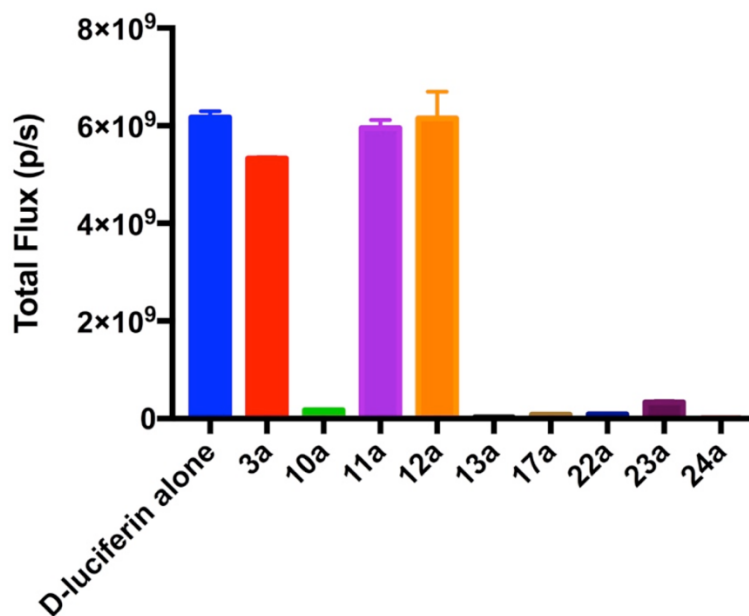
Figure 5.6. Inhibition of firefly luciferase by luciferin analogs. Purified firefly luciferase (10 nM) was treated with D-luciferin (250 μM) in the presence of the indicated luciferin analogue (10 μM). Thioethers and anilines were strongly inhibitory.

Finally, we evaluated the new panel of luciferin analogues (Figure 5.5) as

substrates for luciferase in live Chinese hamster ovary (CHO) cells (Figure

5.7, Figure 5.8). Unlike the in vitro assay, this requires the luciferin analogue to

cross the cell membrane. The brightest of the new substrates in this context was

the allylamine **40a** (Figure 5.9). None of the new dialkylamines was brighter than

CycLuc2, but the azetidine, azepane, and thiomorpholine analogues **4a**, **7a**,

and **9a** yielded higher photon flux than D-luciferin or the 6′-dimethylamino

analogue (Reddy et al., 2010.). The polar morpholine and piperazine

analogues **8a** and **16b** are substantially weaker emitters in cells, perhaps

reflective of their relatively poor permeability across the cell membrane, and in

the case of piperazine, a higher Km than the more lipophilic aminoluciferins

(Table 5.3). In cells expressing the R218K luciferase, bioluminescence emission

from D-luciferin could be exceeded by many of the alkyl aminoluciferins.

Impressively, this includes the unconventional 2,6-dimethylaniline derivative **20a**,

even though it is a relatively weak emitter.
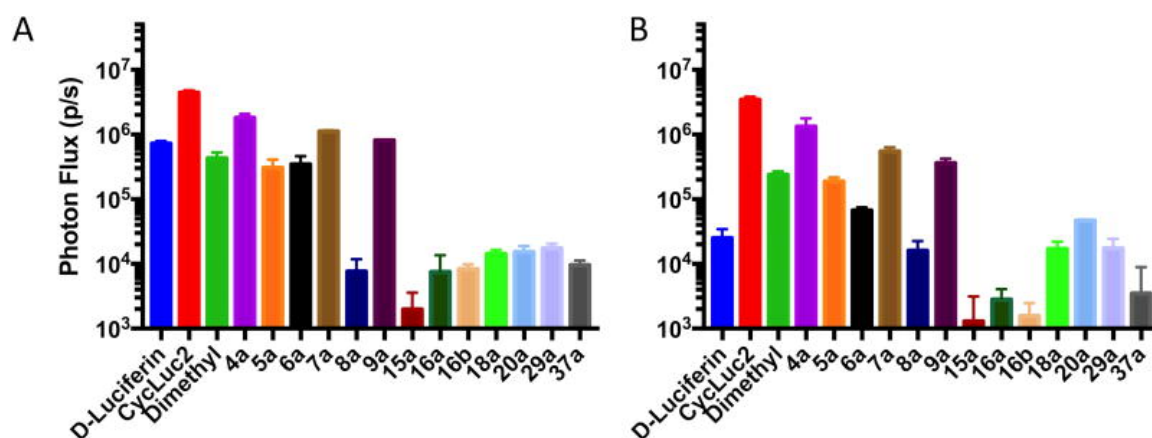
Figure 5.7. Comparison of bioluminescence from selected luciferin analogues in live CHO cells (10 µM). Live CHO cells expressing (A) wild-type firefly luciferase or (B) R218K mutant luciferase. Note log scale.
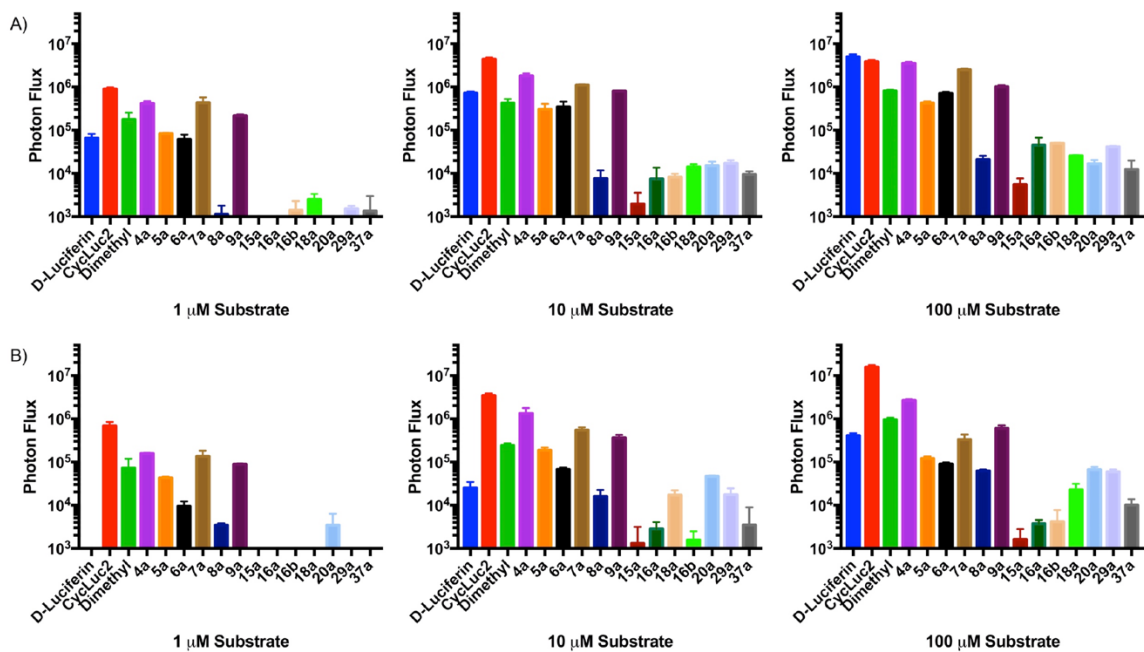
Figure 5.8. Comparison of bioluminescence from selected luciferin analogues in live CHO cells at multiple concentrations. Live CHO cells expressing A) wild-type firefly luciferase or B) R218K mutant luciferase were incubated with 1, 10, or 100 μM of the indicated substrate.
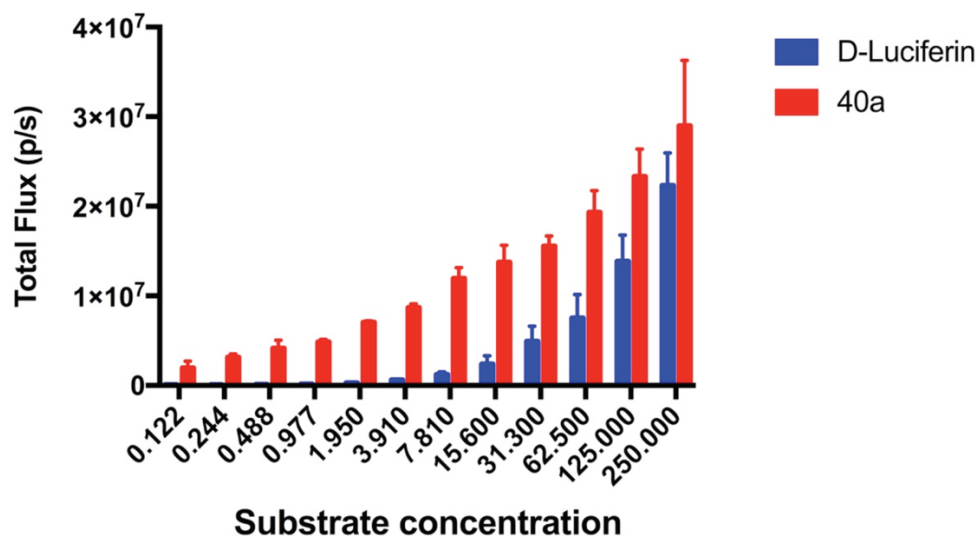
Figure 5.9. Dose-response of D-luciferin versus 40a with WT firefly luciferase in CHO cells. Live CHO cells expressing WT firefly luciferase treated with D-luciferin or allyl amine **40a**. Substrate concentration ranging from 0.122-250 µM.

Substrate	Wild Type Luciferase		R218K Luciferase	
	Apparent Km	R-squared	Apparent Km	R-squared
D-luciferin	7.5±0.86	0.9679	120±4.9	0.9978
Azetidine (4a)	0.534±0.079	0.8971	0.15±0.053	0.4778
Thiomorpholine (9a)	0.52±0.081	0.876	0.30±0.069	0.7413
Azepane (7a)	1.7±0.29	0.8861	9.0±0.97	0.9671
Morpholine (8a)	0.93±0.093	0.9587	1.6±0.18	0.9584
Piperazine (16b)	19±1.9	0.9787	53±2.2	0.9969
Boc-PIPE (16a)	7.9±0.73	0.9788	48±2.4	0.9955
TMPDO (15a)	3.5±0.61	0.9176	12±1.2	0.9785
Piperidine (6a)	1.3±0.21	0.9155	0.67±0.13	0.8532
Pyrrolidine (5a)	3.7±0.79	0.8756	1.3±0.23	0.8882
2ETHAN (18a)	nd	nd	0.36±0.095	0.6604
IND (29a)	nd	nd	4.2±0.42	0.9691
1,1 DMU (37a)	0.95±0.37	0.6294	9.1±1.2	0.9617
2,6 DMAN (20a)	nd	nd	1.9±0.23	0.9491
ALL (40a)	0.56±0.076	0.9099	0.53±0.083	0.8865
TRIFET (41a)	0.89±0.086	0.9698	1.1±0.10	0.9631

Table 5.3. Apparent Km values for selected luciferin analogues.

Conclusion

In summary, we have developed a two-step synthesis of luciferin analogues from a common intermediate. The essential 6′-donating group can be easily modified, enabling investigation of its role and supporting the development of many new substrates, inhibitors, and potential probes. Novel 6′-aniline analogues can be inhibitors or luminescent substrates, depending on the nature of the aryl substituent, and also hold potential as sensors of oxidative species (Takakura et al., 2015.; Peng et al., 2016.). Furthermore, numerous other "caged" luciferins can be directly accessed, and importantly not all are dark. This work thus pushes

the boundaries of what can be considered a luciferin and suggests new avenues to exploit this light-emitting chemistry for detecting and imaging chemical reactivity and biological processes.

Methods and Procedures

Contributions

D.K.S. designed and synthesized luciferins, characterized their photophysical qualities and prepared the manuscript. S.T.A. Jr. performed purified enzyme assays, determined wavelengths of bioluminescent light emission with luciferins, and helped with manuscript preparation. K.L.L. performed live cell experiments and helped with manuscript preparation. S.C.M. devised experiments and helped with manuscript preparation.

General

All reactions were performed in well-dried round bottom flasks with rubber septa under argon atmosphere, unless otherwise noted. D-luciferin was purchased from Gold Bio. Chemical reagents and solvents were purchased from Aldrich, Frontier Scientific, Matrix, Oakwood, Synthonix, Toronto Chemical Research, Chem-Impex, or TCI and used as received. Flash column chromatography was carried out on a CombiFlash RF automated chromatography system using RediSep RF Gold silica columns. Thin-layer chromatography (TLC) was performed using silica gel (60 F-254) coated aluminum plates (EMD Millipore), and spots were visualized by exposure to ultraviolet light (UV). NMR spectra

were acquired on Varian Mercury 400 MHz or Bruker Avance III HD 500 MHz NMR instruments. High-resolution mass spectra (HRMS) were recorded on a Thermo Scientific Orbitrap Velos Pro mass spectrometer coupled with a Thermo Scientific Accela 1250 UPLC and an autosampler using electrospray ionization (ESI) in the positive mode. UV absorbance was measured on a Varian Cary 50 Bio UV-Visible Spectrophotometer. Fluorescence data were recorded on a Horiba Scientific FluoroMax-4 using FluorEssence software. Solvents used for fluorescence spectra: PBS, 1X (Corning Cellgro), Methanol ≥ 99.9% pure (Sigma Aldrich), Dioxane 99+% pure (Acros Organic). Bioluminescence imaging assays were performed on a GloMax luminometer (Promega) or IVIS-100 (Xenogen, now Perkin-Elmer). GraphPad Prism ver. 7.0a (GraphPad Software, Inc.) was used to analyze data and generate graphs.

Luciferin Burst-Kinetics Assays

Wild-type and R218K mutant firefly luciferase were expressed and purified as previously described.[1,2] Using a GloMax Luminometer (Promega), 50 µl of enzyme buffer [20 mM Tris (pH 7.4), 0.1 mM EDTA, 0.8 mg/mL BSA, and 1 mM TCEP] containing firefly luciferase (2 nM) was rapidly injected into each well of a white 96-well plate (Costar 3912) containing luciferin analogue (500 µM) in substrate buffer [20 mM Tris (pH 7.4), 0.1 mM EDTA, 8 mM $MgSO_4$, and 4 mM ATP (AP Bio)], to a final enzyme concentration of 1 nM and luciferin analogue concentration of 250 µM. The peak emission occurring 0.5 s after injection was reported in Relative Light Units (RLU) and not corrected for the wavelength

sensitivity of the photomultiplier tube. To determine apparent Km values for emissive analogues, a two-fold dilution series of each substrate was prepared (final substrate concentrations ranging from 250 µM down to 0.122 µM). Peak emission occurring 0.5 s after injection of luciferase (0.1 nM final concentration) was fitted to a sigmoidal dose-response curve by non-linear regression in GraphPad Prism 7. All assays were performed in triplicate.

Luciferase Inhibition Assay

Fifty microliters of enzyme buffer [20 mM Tris (pH 7.4), 0.1 mM EDTA, 0.8 mg/mL BSA, and 1 mM TCEP] containing firefly luciferase (20 nM) was pipetted into each well of a 96-well plate containing 250 µM D-luciferin and 10 µM luciferin analogue in substrate buffer [20 mM Tris (pH 7.4), 0.1 mM EDTA, 8 mM MgSO4, and 4 mM ATP (AP Bio)]. Luminescence measurements were taken one minute after substrate addition in an IVIS-100, in triplicate. The data was analyzed with Living Image Software ver. 4.3.1 and reported as total flux (p/s).

Cell Assays

Chinese hamster ovary (CHO) cells were maintained at 37°C and 5% CO2 in F-12K medium (Gibco) containing 10% fetal bovine serum and 100 units/ml penicillin/streptomycin. Cells were seeded in black 96-well plates (Costar 3916) at 15,000 cells/ml. Twenty-four hours post-seeding, the cells were transiently transfected with pcDNA3.1 WT luc2 or R218K luc2, as previously reported, at 0.075 µg DNA/well using Lipofectamine 2000 (Invitrogen).2 Assays were

performed in triplicate 48 hours after transfection. Luciferin substrates were

diluted in Hank's balanced salt solution (HBSS) to 100 µM, 10 µM, and 1 µM.

Transfected CHO cells were washed with HBSS and incubated with 60 µl/well of

100, 10, or 1 µM substrate. Imaging was performed one minute after substrate

addition in an IVIS-100. Data acquisition and analysis were performed with Living

Image® software. Data are reported as total flux (p/s) for each ROI

corresponding to each well of the 96-well plate, and plotted and analyzed with

GraphPad Prism 7.0.

Relative Quantum Yield Measurement

Absorbance spectra were recorded at five different concentrations with

absorbance between 0.01-0.10 for each sample. Fluorescence spectra were

recorded on a Horiba Scientific FluoroMax-4. Relative quantum yields were

calculated from plots of absorbance vs. integrated fluorescence and were

referenced to that of 6'-aminoluciferin measured under the same conditions.

Acknowledgements

Chapter VI:

Sulfonamides are an Overlooked Class of Electron Donors in Luminogenic Luciferins and Fluorescent Dyes

Deepak K. Sharma, **Spencer T. Adams Jr.**, Kate L. Liebmann, Adam Choi, and Stephen C. Miller. (2019) *Org. Lett.*, 21(6): 1641-1644.

Spencer T. Adams Jr. performed *in vitro* experiments and prepared figures 6.2 (the bioluminescence curves in the top half) and 6.3-6.5.

Summary

Many fluorophores, and all bright light-emitting substrates for firefly luciferase, contain hydroxyl or amine electron donors. Sulfonamides were found to be capable of serving as replacements for these canonical groups. Unlike "caged" carboxamides, sulfonamide donors enable bioluminescence, and sulfonamidyl luciferins, coumarins, rhodols, and rhodamines are fluorescent in water.

Introduction

There is only one natural substrate for firefly luciferase: D-luciferin. The light-emitting chemistry of this molecule is not unique, as a broad range of synthetic substrates have now been shown capable of supporting bioluminescence (Miller

et al., 2018.; Zhang et al. 2018.; Hall et al., 2018.). However, most luminogenic examples are push−pull chromophores that contain hydroxyl, amine, or alkylamine electron donors (Figure 6.1). Here, we show that a new class of sulfonamidyl luciferin analogues are fluorescent molecules that are luminogenic substrates for firefly luciferase. Furthermore, we find that sulfonamidyl analogues of coumarin and xanthene dyes are also bright fluorophores. Sulfonamides are thus an overlooked class of electron donors that can be incorporated into both fluorescent and bioluminescent probes.
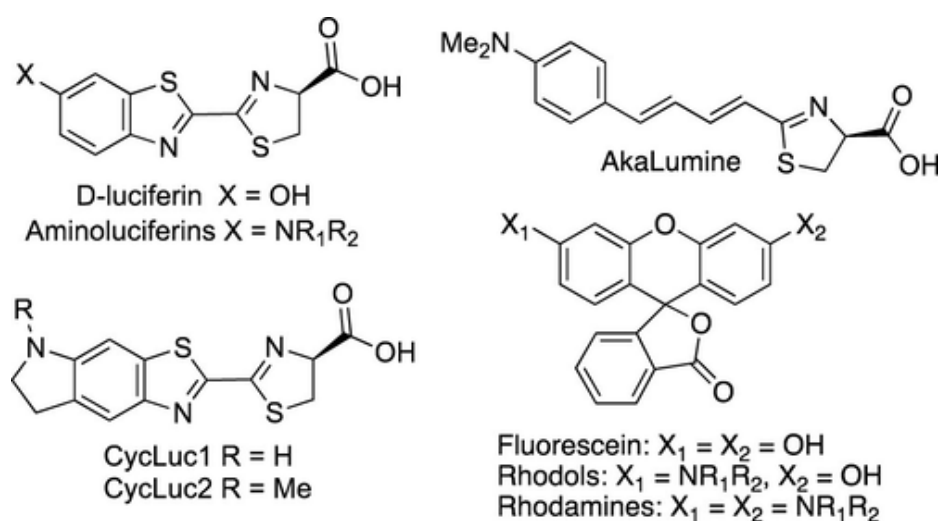
Figure 6.1. Examples of luciferins and xanthenes.

Results and discussion

In recent work to explore and expand the range of accessible luciferin analogues, we found that Buchwald−Hartwig amination of 6-bromo-2-

cyanobenzothiazole **1** with Xantphos and Cs_2CO_3 allowed ready access to a

wide variety of 6-substituted luciferin precursors (Sharma et al., 2017.). When

these reaction conditions were applied to methanesulfonamide, attack at the

electrophilic nitrile occurred instead, resulting in the imide **2** (Scheme 6.1).

Fortunately, simply replacing the ligand and base with tBuXPhos(**5**) and

K_3PO_4 allowed the synthesis of **3** to proceed in 67% yield. Condensation with D-

cysteine yielded the 6′-methanesulfonamide (mesyl) luciferin analogue **3a**.
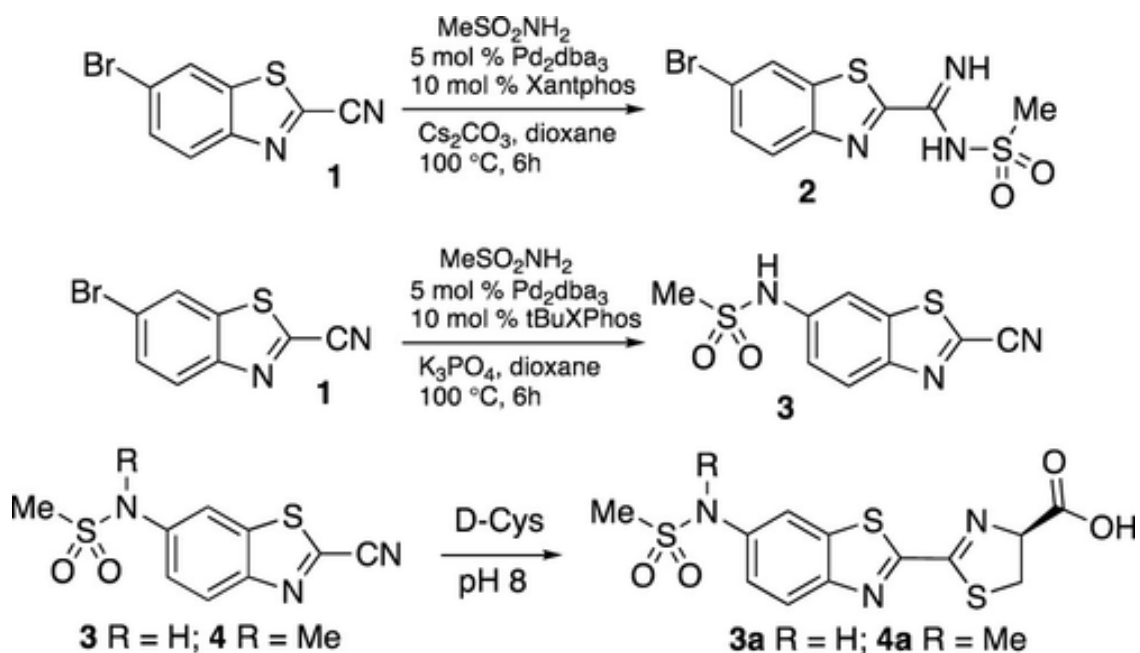
Scheme 6.1. Synthesis of Sulfonamidyl Luciferins.

In sharp contrast to 6′-acylamino luciferin analogues which are "caged" derivatives with little to no bioluminescent emission (Sharma et al., 2017.) we found that **3a** is luminogenic (Figure 6.2). This marked difference could be due in part to the lower pK_a of sulfonamides. Consistent with this hypothesis, **3a** exhibits pH- dependent fluorescence (pK_a of 7.8), suggesting that light emission occurs from the sulfonamide anion. Furthermore, the N-methylated sulfonamide analogue **4a** exhibits negligible bioluminescence, and its weakened fluorescence is blue-shifted by ~80 nm and lacks pH dependence (Figure 6.2 and Table 6.1).
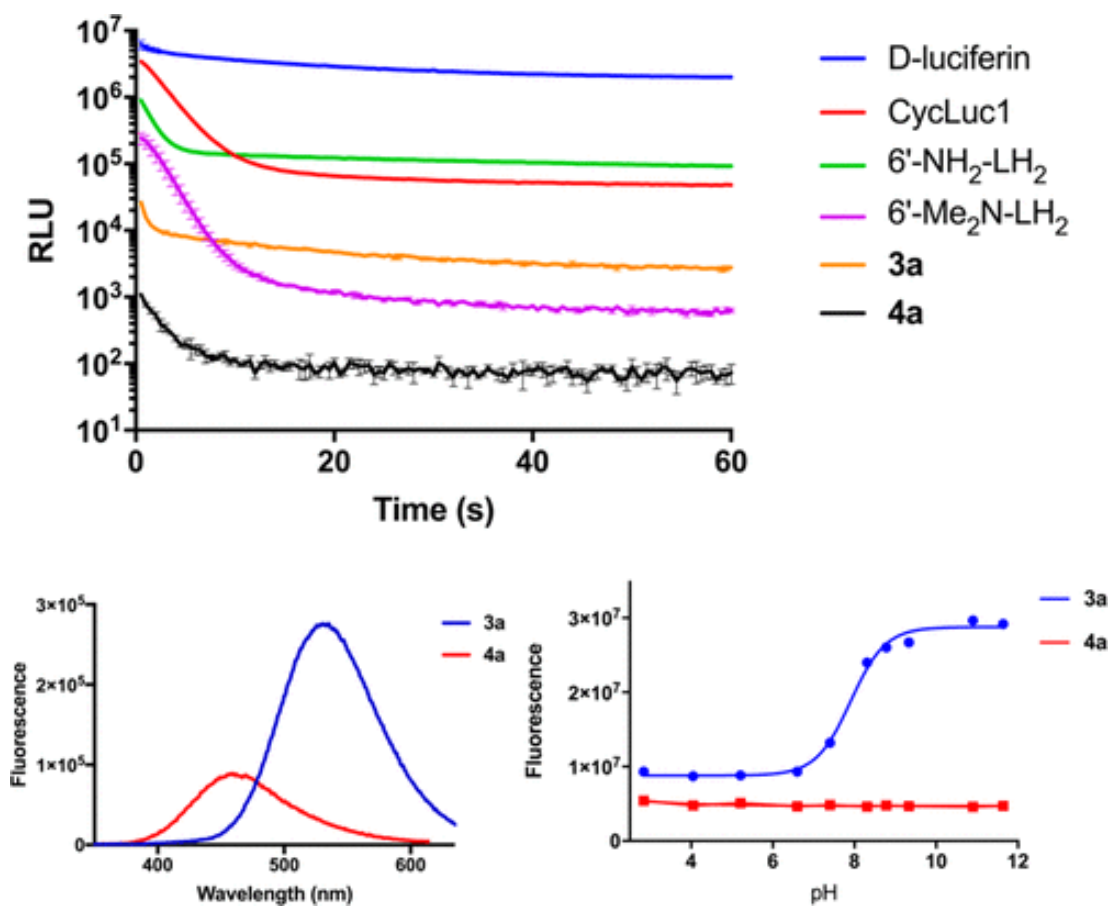
Figure 6.2. Bioluminescence and fluorescence of 3a-4a. Top: Rapid injection of 0.5 nM luciferase onto 250 µM luciferin. Bottom: Fluorescence properties of **3a** and **4a**.

Compound		pH 7.4 (PBS)[a]			pH 8.54 (PBS)[a]		pKa	Ethanol[b]		
	Absorption (nm)	Emission (nm)	RQY	Emission (nm)	RQY			Absorption (nm)	Emission (nm)	RQY
3a	321	537	0.26	536	0.85	7.76	321	433	0.07
4a	304	455	0.20	455	0.23	ND	302	435	0.24
9a	322	542	0.26	539	0.62	8.63	322	425	0.02
12a	324	541	0.29	540	0.57	8.71	324	428	0.10
25a	328	537	0.35	534	0.83	8.23	326	434	0.18
27a	327	534	0.51	535	1.28	7.40	324	430	0.16
28a	310	455	0.20	455	0.28	ND	310	426	0.12
32a	328	543	0.27	538	0.53	8.55	328	437	0.02
34a	322	547	0.26	539	0.60	8.97	324	429	0.14
41a	332	534	0.50	532	0.86	7.42	330	431	0.02
42a	302	450	0.06	450	0.08	ND	301	429	0.05
43a	332	510	0.26	504	0.63	4.54	331	507	0.57
6'-aminoluciferin	351	518	1	518	1	ND	352	477	1

Table 6.1. Fluorescence properties for selected sulfonamidyl luciferins.

[a]Excitation wavelength used for RQY study was 335 nm.

[b]Excitation wavelength used for RQY study was 325 nm.

ND = Not determined.

To further probe the scope of sulfonamide luminescence behavior, we synthesized a large panel of ~40 sulfonamidyl luciferin analogues (Schemes 6.2-6.6). Because firefly luciferase also has fatty acyl-CoA synthetase activity (Oba et al., 2003.; Mofford et al., 2014.; Mofford et al., 2017.), sulfonamides with aliphatic chains were expected to extend into the elongated binding pocket (**3a−15a**).

Bulky analogues were synthesized to probe the steric scope of accepted substrates (**16a−34a**), and electronic modifications were made to further probe the importance of the sulfonamide pK_a on its emissive properties (**35a−44a**).
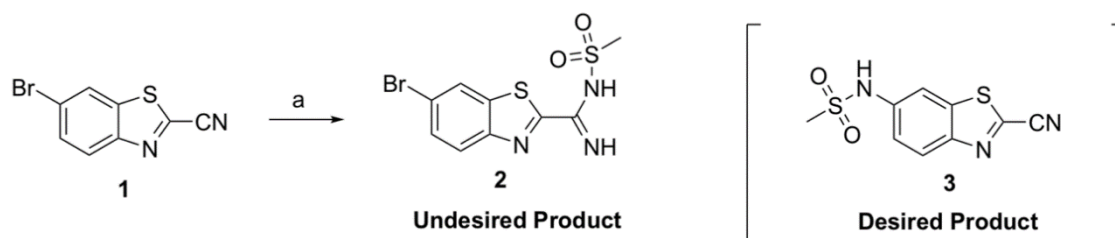
Scheme 6.2. Synthesis of sulfonamidyl luciferin nitrile precursor. a) Methane sulfonamide, Pd_2dba_3, xantphos, Cs_2CO_3, dioxane, 95-100°C.
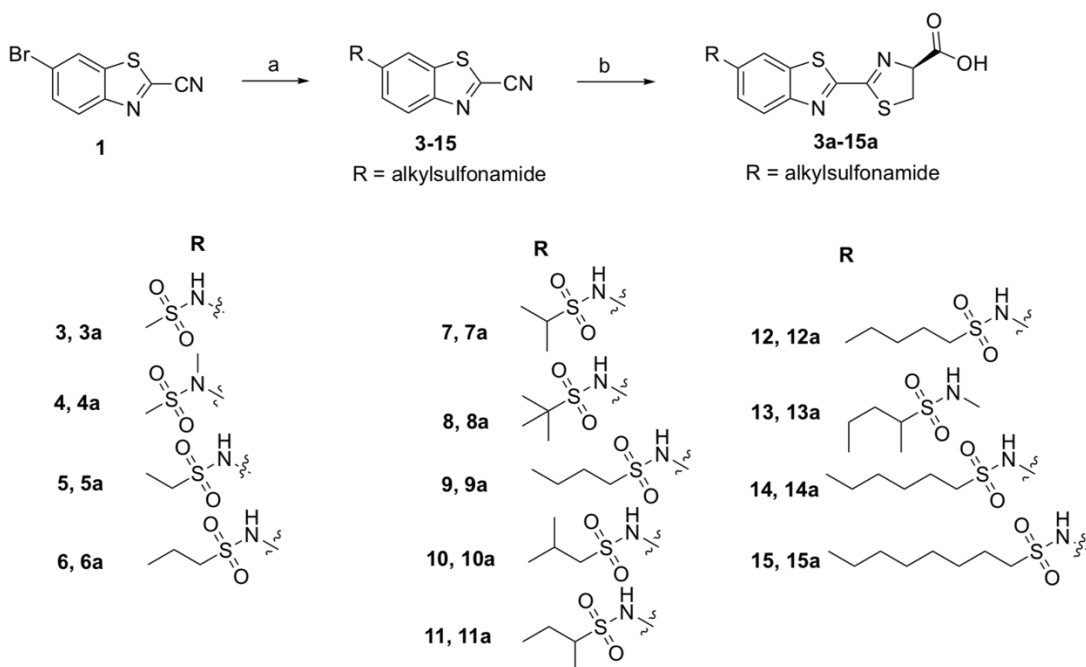
Scheme 6.3. Synthesis of sulfonamidyl luciferins 3-15. a) Alkyl sulfonamide, Pd_2dba_3, tBuXPhos, K_3PO_4, dioxane, 95-100°C; b) D-cysteine, pH 8 buffer.
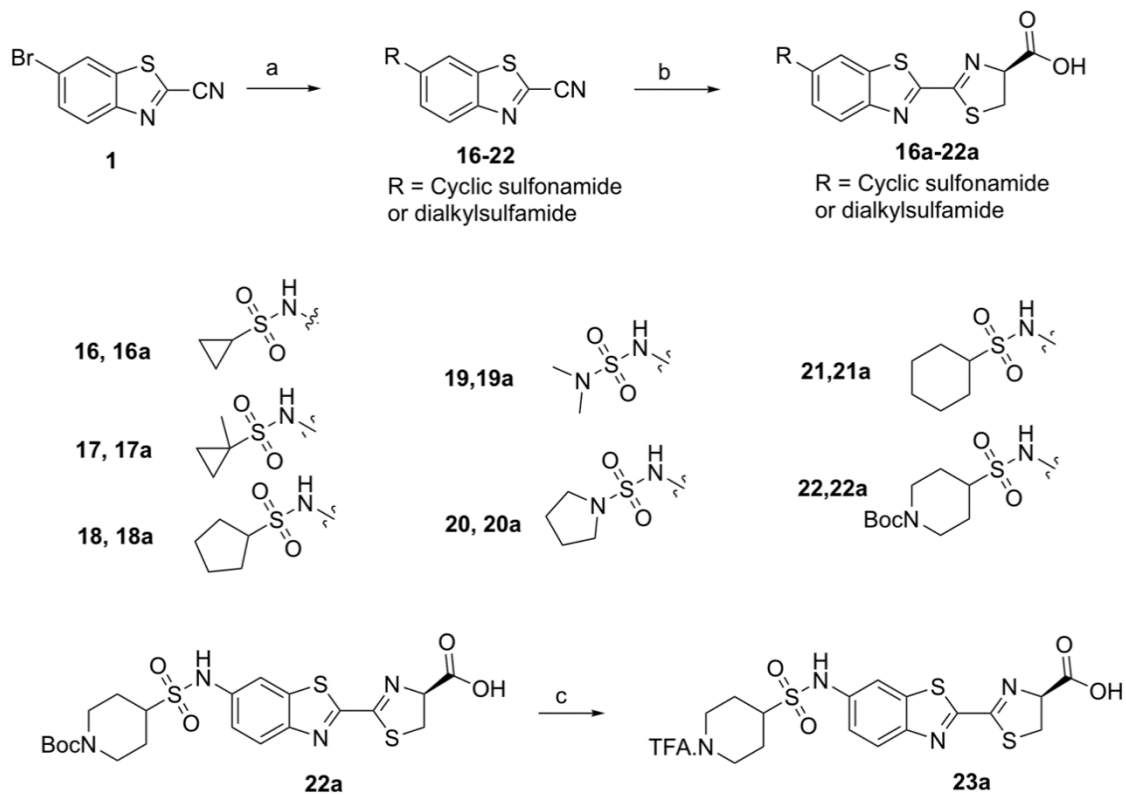
Scheme 6.4. Synthesis of sulfonamidyl luciferins 16-23. a) Cyclic alkylsulfonamide or dialkylsulfamide, Pd_2dba_3, tBuXPhos, K_3PO_4, dioxane, 95-100°C; b) D-cysteine, pH 8 buffer; c) DCM:TFA (3:1), 2 h, rt.
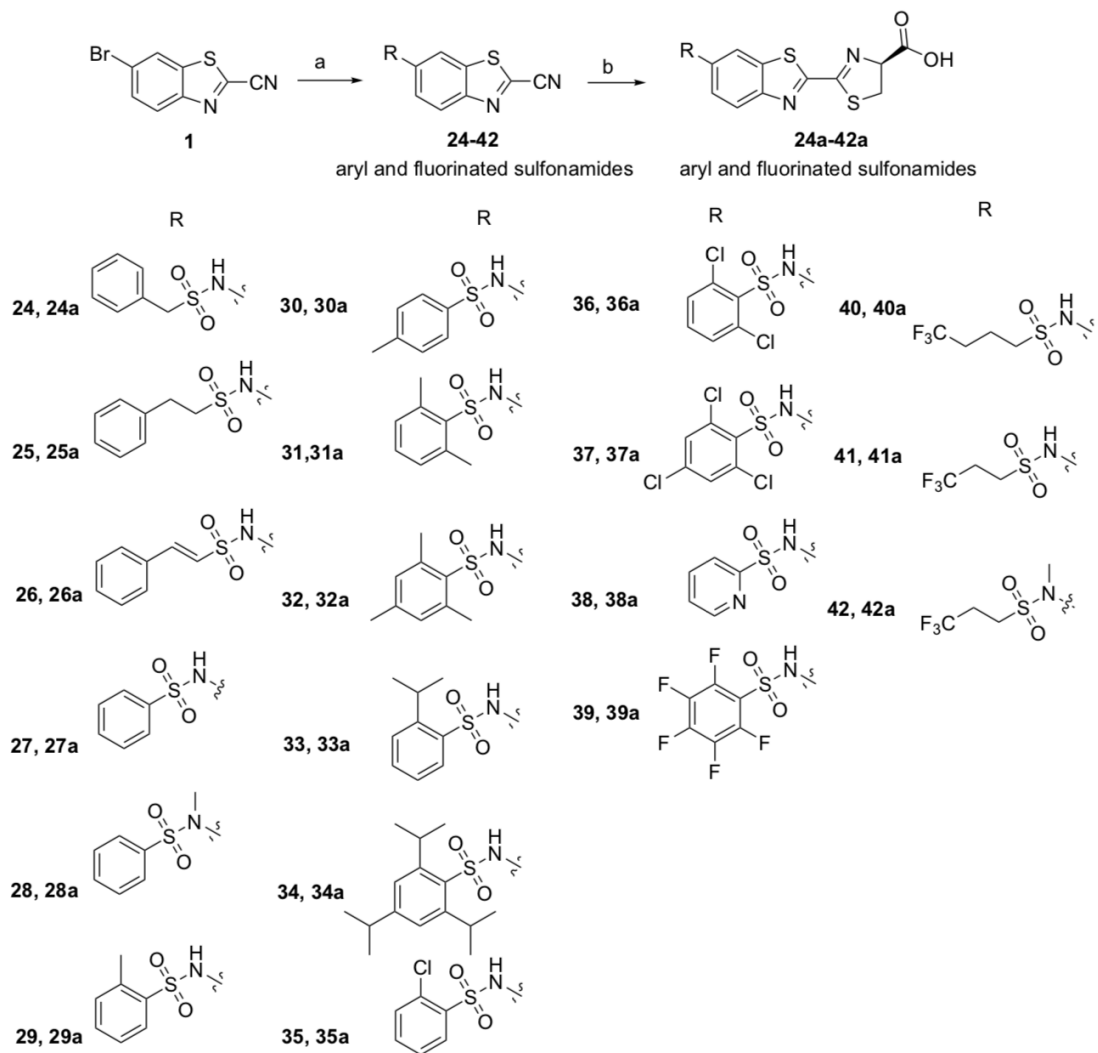
Scheme 6.5. Synthesis of sulfonamidyl luciferins 24-42. a) Aryl or fluorinated sulfonamide, Pd$_2$dba$_3$, tBuXPhos, K$_3$PO$_4$, dioxane, 95-100°C; b) D-cysteine, pH 8 buffer.
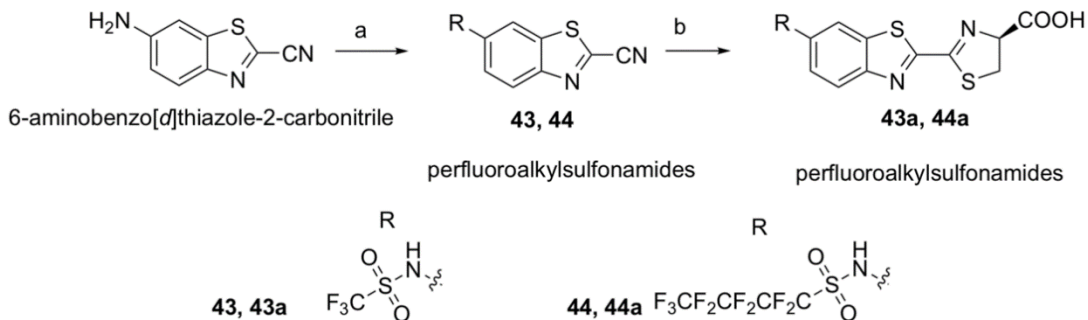
Scheme 6.6. Synthesis of sulfonamidyl luciferins 43 and 44. a) Fluorosulfonic anhydride, triethylamine, 0°C to rt, 3 h; b) D-cysteine, pH 8 buffer.

The modest light emission of **3a** could be greatly improved upon (Figure 6.3).

Generally, more lipophilic derivatives performed better as luminogenic

substrates, but interestingly, there is a substantial drop off in luminescent activity

for the hexylsulfonamide **14a** compared to that of the butyl, pentyl, and octyl

analogues (**9a**, **12a**, **15a**). Bulky phenethyl, 2,6- dimethylphenyl, and mesityl

analogues (**25a**, **31a**, **32a**) are also bright emitters. Intriguingly, the maximal

emission from **31a** is ~10% of that achieved with D-luciferin (Figure 6.4).

Furthermore, the decay in luminescence from the sulfonamides 1 min after

substrate injection is only ~3-fold from the initial rate, similar to D-luciferin, rather

than ~10−100-fold as observed for many aminoluciferin analogues (Figures 6.2

and 6.4) (Mofford et al., 2014.; Reddy et al., 2010.). Surprised by the brightness

of many sulfonamides, we performed LC/MS to verify that there is no

contaminating D-luciferin or aminoluciferin (Supporting Information).

9a R = CH$_3$, n = 2
12a R = CH$_3$, n = 3
14a R = CH$_3$, n = 4
15a R = CH$_3$, n = 6
40a R = CF$_3$, n = 2
41a R = CF$_3$, n = 1

25a

27a R$_1$ = R$_2$ = R$_3$ = H
29a R$_1$ = Me; R$_2$ = R$_3$ = H
31a R$_1$ = R$_2$ = Me; R$_3$ = H
32a R$_1$ = R$_2$ = R$_3$ = Me
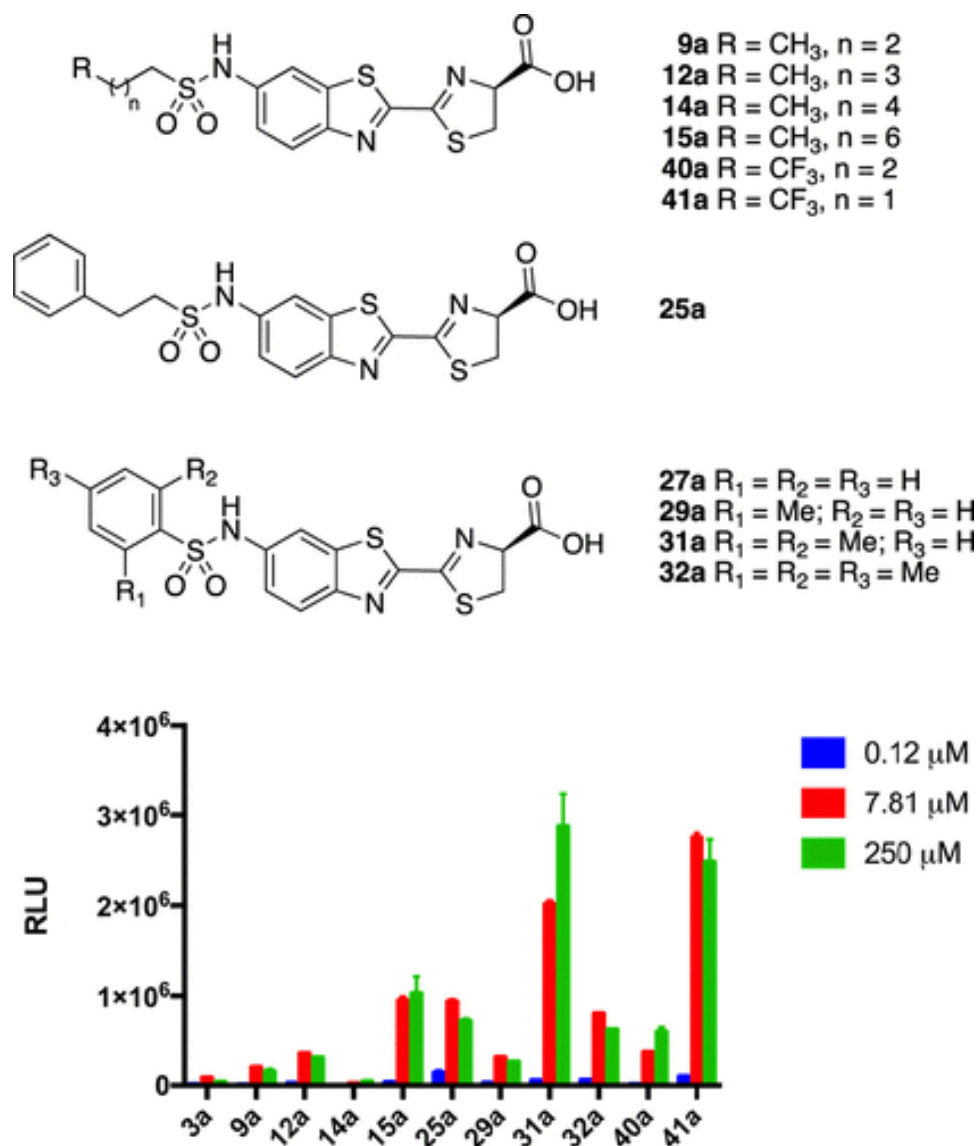
Figure 6.3. Sulfonamidyl luciferins (top) **and their relative light emission after rapid injection into 0.5 nM purified firefly luciferase** (bottom).
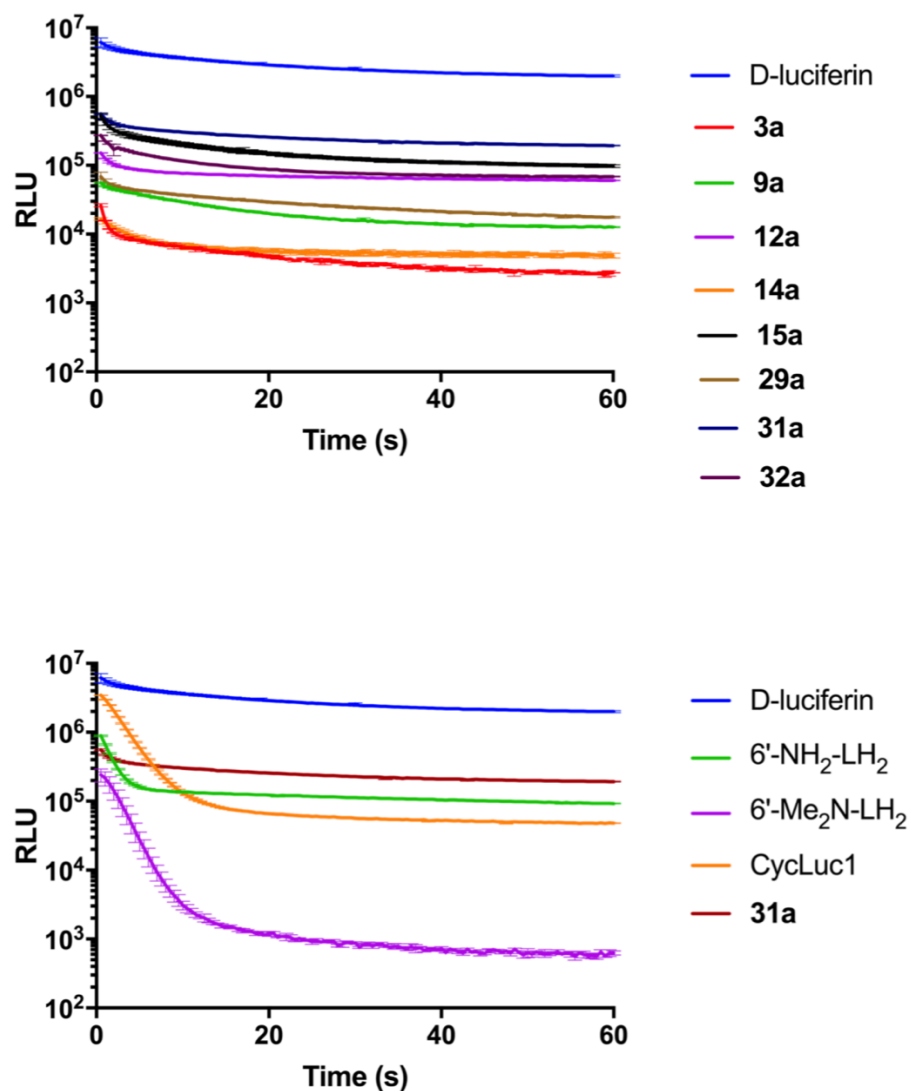
Figure 6.4. Burst luciferase assays. A solution containing 0.5 nM firefly luciferase was rapidly injected into 250 μM substrate as described in the methods. Top: D-luciferin compared to a range of sulfonamidyl luciferins (from brightest **31a** to weakest **3a** and **14a**). Bottom: Sulfonamidyl luciferin **31a** compared to D-luciferin, aminoluciferin, monoalkylated aminoluciferin CycLuc1, and dimethylaminoluciferin.

We measured the pH sensitivity of fluorescence for a subset of these new analogues (Table 6.1). Compared to 3a, the pK_a values for benzenesulfonamide **27a** and trifluoropropyl (TFP) sulfonamide **41a** are decreased from 7.8 to 7.4, and these analogues exhibited the highest quantum yields. On the other hand, the pK_a values for **9a**, **25a**, and **32a** were increased to 8.6, 8.2, and 8.6, respectively, yet they remain good luminogenic luciferase substrates. This suggests that deprotonation can occur within the active site for all of these analogues. For reference, the pK_a of D-luciferin is 8.7 (Morton et al., 1969.).

Bioluminescence from most of the sulfonamides occurred at a wavelength similar to that of D-luciferin (547−555 nm). However, **3a** and **9a** emit at 636 and 642 nm, respectively (Figure 6.5). This difference appears to derive from a subtle orientation and/or protonation effect within the enzyme pocket and not the pK_a value per se, as this red-shift is not observed for similar analogues **12a** and **15a**. Furthermore, some of the sulfonamides, such as **29a** and **41a**, give bimodal emission. D-Luciferin is known to exhibit similarly environmentally sensitive emission, including examples of bimodal emission (Harwood et al., 2011.; Branchini et al., 2003.).
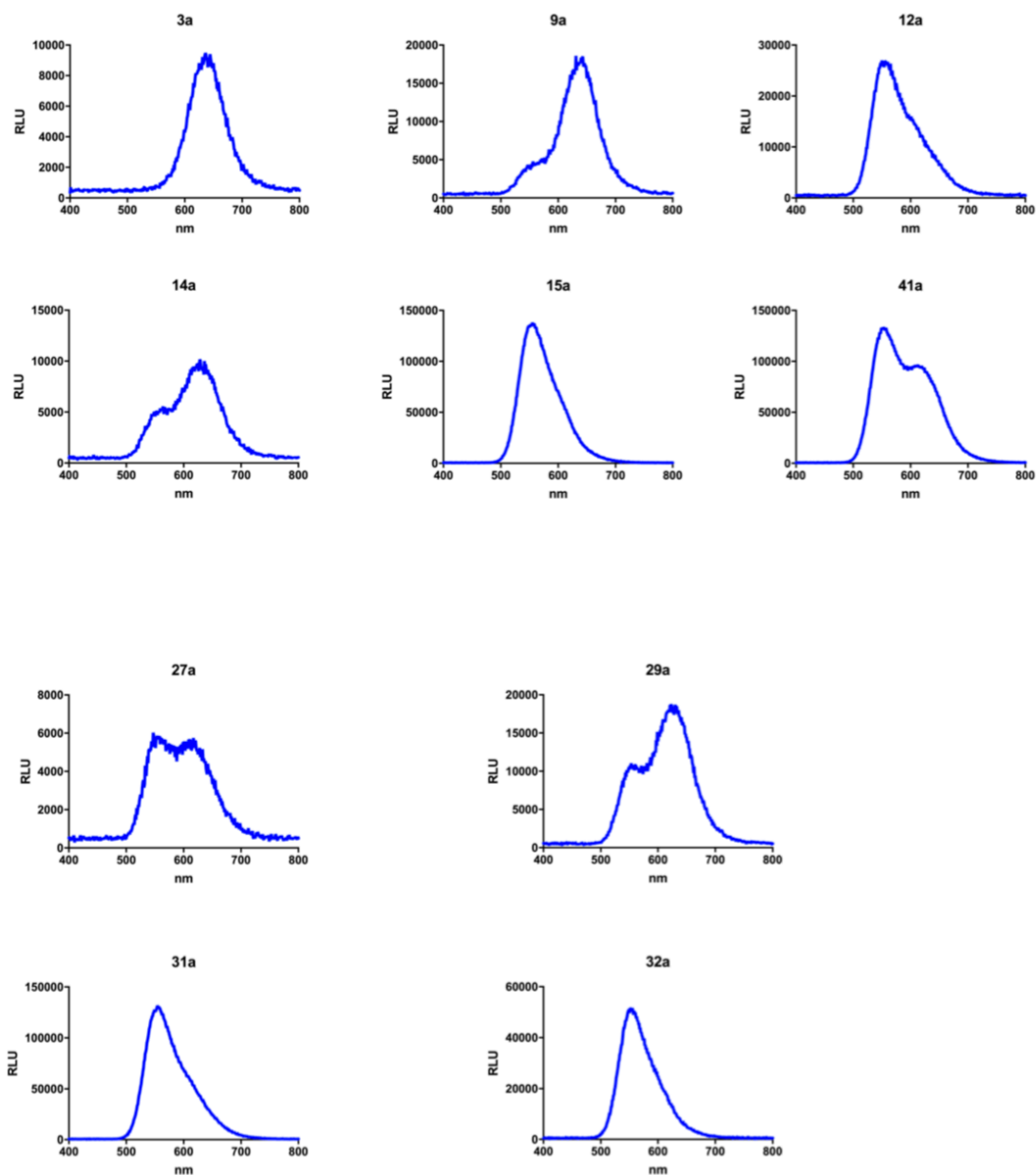
Figure 6.5. Bioluminescence emission spectra from selected sulfonamidyl luciferins (collected as described in the methods)**.** Several substrates give bimodal emission or have apparent shoulder peaks. Peak emission wavelengths are 636 nm (**3a**); 642 nm (**9a**); 555 nm (**12a**); 628 nm (**14a**); 555 nm (**15a**); 553 nm (**41a**); 547 nm (**27a**); 623 nm (**29a**), 554 nm (**31a**); 555 nm (**32a**).

In live cells, the brightest substrates include the mesityl and n-butyl sulfonamides

32a and **9a** (Figures 6.6 and 6.7). Surprisingly, n-octyl sulfonamide **15a** gave

weaker than expected emission based on the in vitro results (Figure 6.3),

suggesting that its ability to access the intracellular luciferase is restricted,

perhaps through sequestration in cell membranes and/or engagement with other

cellular targets. In cell lysates, the relative performance of **15a** was substantially

improved. Notably, sulfonamidyl luciferin analogues do not suffer from the

product inhibition normally associated with alkylated aminoluciferins in cell

lysates (Figure 6.6) (Harwood et al., 2011.), consistent with their behavior using

the purified luciferase (Figures 6.2 and 6.4).
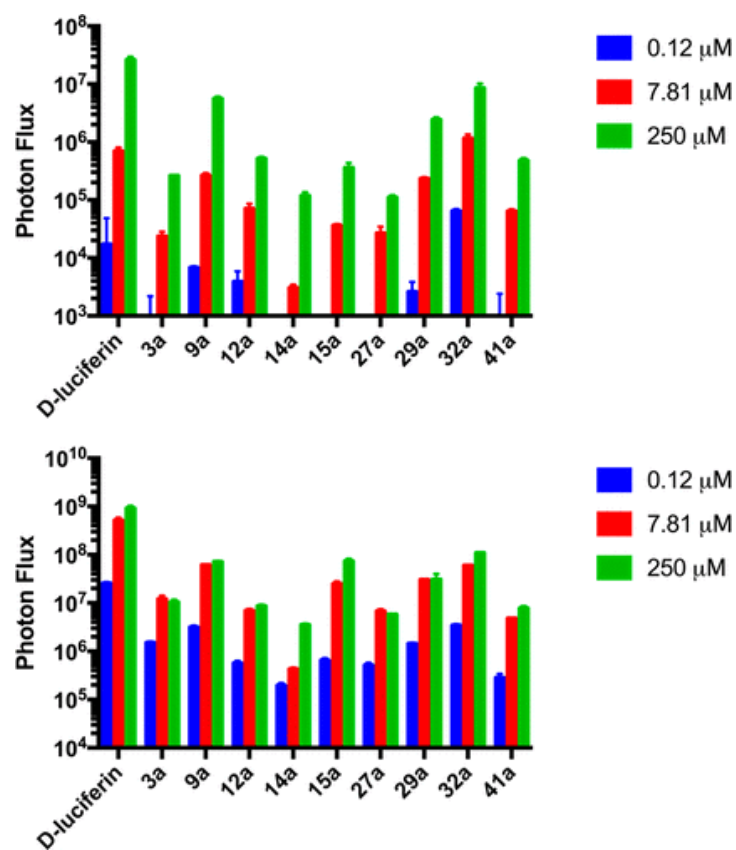
Figure 6.6. Bioluminescence of sulfonamidyl luciferins in live (top) **and lysed mammalian cells** (bottom)**.**
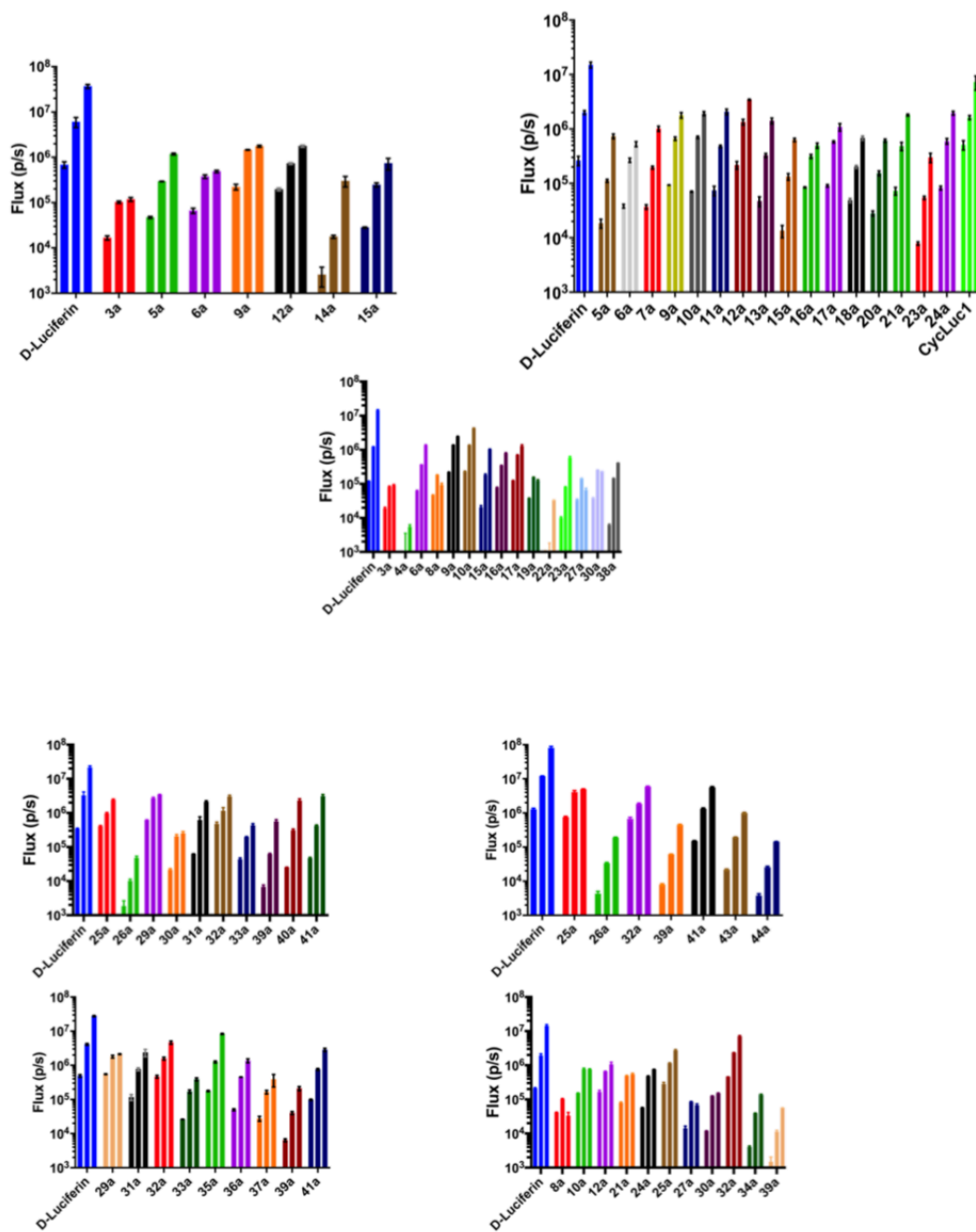
Figure 6.7. Live cell bioluminescence imaging of sulfonamidyl luciferins in CHO cells. Each substrate was used at 1, 10, and 100 micromolar, respectively, in triplicate, as described in the methods. Each panel represents a different experiment, performed on a different day.

Because all of the sulfonamidyl luciferins are fluorescent, it was surprising to find

few documented examples of fluorophores with sulfonamide donors. Shibata et

al. have reported two rhodamines containing 2,4-dinitrobenzenesulfonamide

donors, designed as "caged" sensors for thiols, neither of which exhibited

appreciable fluorescence (Shibata et al, 2008.). Nitrobenzenesulfonamide

coumarin and cresyl violet dyes are similarly nonfluorescent, presumably due to

electron-transfer quenching (Zhang et al., 2011.). Toluenesulfonamide-

substituted coumarin, cresyl violet, and rhodamine dyes have been reported, but

their fluorescence properties have scarcely been investigated (Zhang et al.,

2011.; Dakanali et al., 2005.; Grimm and Lavis, 2011.; Reddy et al., 1986.).

The lack of reported sulfonamidyl dyes may be due to the perception that they

will not be fluorescent, coupled with the need for deprotonation. To determine

whether sulfonamide donors can be utilized more broadly in fluorescent scaffolds

other than luciferin analogues, we synthesized TFP sulfonamidyl coumarin **45**,

which should have a low pK_a and no electron- transfer quenching (Figure 6.8). In

water at physiological pH, **45** is 89% as bright as the aminocoumarin, with a

similar extinction coefficient and emission that is red-shifted by 15 nm (Table

6.2). Next, we synthesized sulfonamidyl rhodol **46** and rhodamine **47**. The bis-

sulfonamide rhodamine **47** is colorless in ethanol, and the monosulfonamide

rhodol **46** nearly so, suggesting they exist predominantly as the spirolactone

(Figure 6.1). However, in water, we expected they would deprotonate to a ring-opened, anionic form. Indeed, the pK_a of rhodol **46** is 5.9, slightly lower than that of fluorescein (Figure 6.9). TFP-rhodol **46** has an extinction coefficient of 56400 M^{-1} cm^{-1} at 499 nm and fluoresces at 526 nm with a quantum yield of 0.78 (Table 6.3). Impressively, this is brighter than most rhodols with dialkylamine donors (Peng and Yang, 2010.; Grimm et al., 2015.). Moreover, the bis-TFP rhodamine **47** is also fluorescent, with a quantum yield of 0.40 and extinction coefficient of 51 000 M^{-1} cm^{-1}, suggesting that sulfonamides could also be incorporated into related red-shifted scaffolds such as oxazines (Pauff and Miller, 2011.) and azasilines (Choi and Miller, 2018.), as well as sulfone (Liu et al., 2016.), phosphorus (Chai et al., 2015.; Zhou et al., 2016.; Grzybowski et al., 2018.), and Si-substituted rhodamines (Grimm et al., 2017.) and rhodols (Jia et al., 2018.).
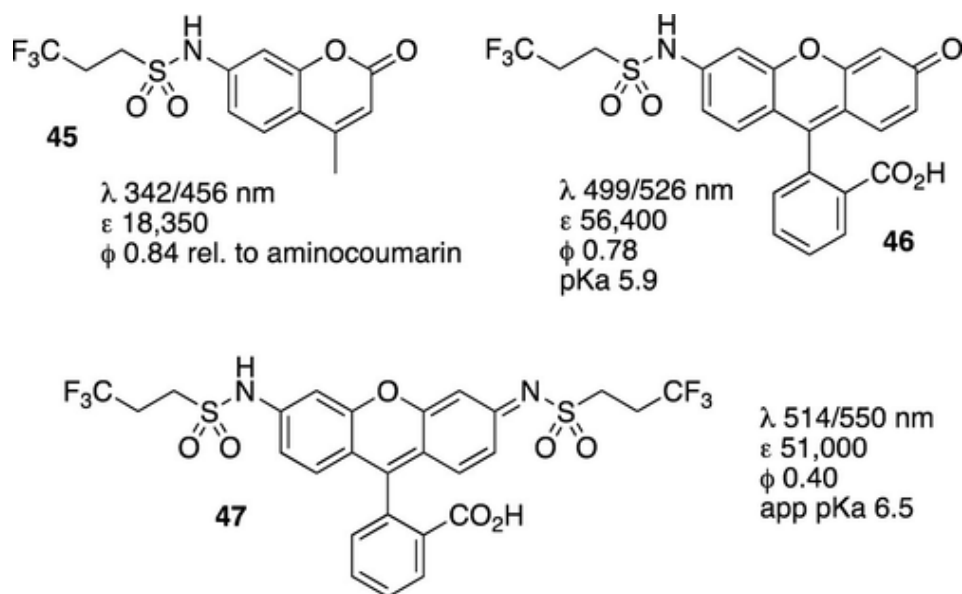
Figure 6.8. Properties of fluorophores with sulfonamide donors (depicted in ring-opened, protonated form).

Compound	pH 7.4 (PBS)				pH 8.54 (PBS)		
	Absorption (nm)	Emission (nm)	RQY	Molar extinction coefficient	Emission (nm)	RQY	Molar extinction coefficient
Aminocoumarin	342	441	1	17340 $M^{-1}cm^{-1}$	441	1	17920 $M^{-1}cm^{-1}$
45	342	456	0.84	18350 $M^{-1}cm^{-1}$	456	0.83	19910 $M^{-1}cm^{-1}$

Table 6.2. Fluorescence properties of TFP Coumarins 45.
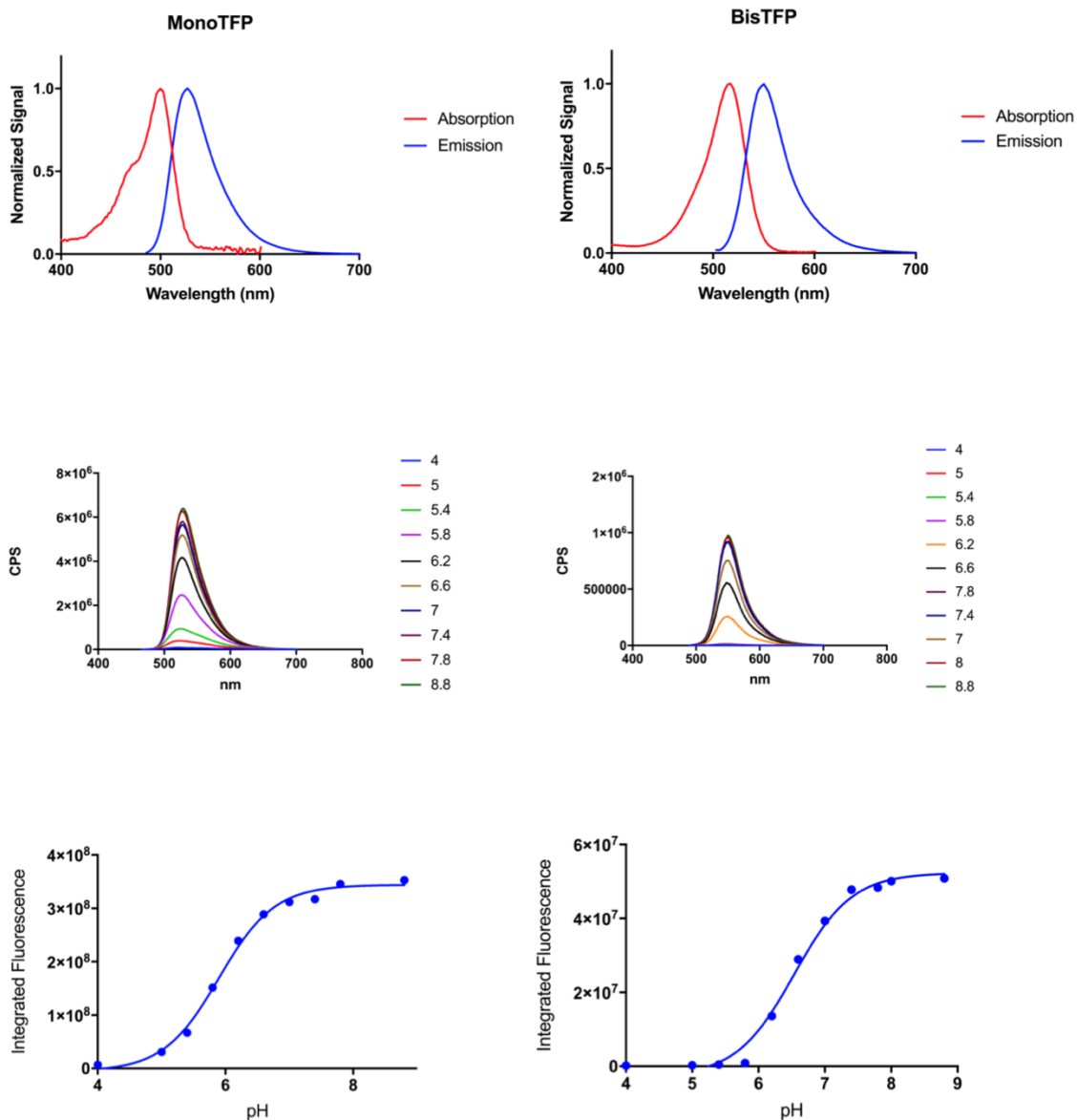
Figure 6.9. Fluorescence properties of trifluoropropyl (TFP) sulfonamidyl rhodol 46 (left panels) **and rhodamine 47** (right panels)**.** Top: excitation and emission spectra (summarized in Table 6.3). Middle: pH-dependence of fluorescence. Bottom: Curve fitting yields apparent pKa values of 5.9 for **46** and 6.5 for **47**.

Compound	Absorption (nm)	Emission (nm)	QY	Molar extinction coefficient
46	499	526	0.78	56,400 $M^{-1}cm^{-1}$
47	514	550	0.40	51,000 $M^{-1}cm^{-1}$

Table 6.3. Fluorescence properties of TFP Rhodol 46 and Rhodamine 47.

Conclusion

In summary, sulfonamide electron donors do not behave like "caged" carboxamides but instead expand the scope of luminogenic molecules beyond the canonical hydroxyl and amino-substituted analogues. The relative brightness of sulfonamide-substituted fluorophores suggests that further improvements in bioluminescence from sulfonamidyl luciferins can be achieved through mutation, and the ability to easily tune the molecular properties of sulfonamidyl luciferins can aid in the construction of selective new luciferin−luciferase pairs (Mofford et al., 2014.; Harwood et al., 2011.; Jones et al., 2017.) as well as specific bioluminescent sensors that can take advantage of this new functionality(Mofford et al., 2015.; Heffern et al., 2016.). Furthermore, sulfonamide donors have been previously overlooked for incorporation into fluorescent probes, opening up new possibilities in fluorophore design.

Protocols and Methods

Contributions

D.K.S. designed and synthesized luciferins, characterized their photophysical qualities and prepared the manuscript. S.T.A. Jr. performed purified enzyme assays, determined wavelengths of bioluminescent light emission with luciferins, and helped with manuscript preparation. K.L.L. performed live cell experiments and helped with manuscript preparation. A.C. designed and synthesized dyes and helped with manuscript preparation. S.C.M. devised experiments and helped with manuscript preparation.

General

All reactions were performed in well-dried round bottom flasks with rubber septa under an argon atmosphere, unless otherwise noted. Chemical reagents and solvents were purchased from Aldrich, Frontier Scientific, Matrix, Oakwood, Synthonix, Toronto Chemical Research, Chem- Impex, Enamine, 1ClickChemistry Inc., Synquest Laboratories, Santa Cruz Biotechnology or TCI and used as received. Fluorescein ditriflate (Grimm et al., 2011.) and 6-bromo-2-cyanobenzothiazole (Sharma et al., 2017.) (compound **1**) were synthesized as previously described. Flash column chromatography was carried out on a CombiFlash Rf automated chromatography system using RediSep Rf Gold silica columns. Thin- layer chromatography (TLC) was performed using silica gel (60 F-254) coated aluminum plates (EMD Millipore) and spots were visualized by exposure to ultraviolet light (UV). NMR spectra were acquired on a Bruker

Avance III HD 500 MHz NMR instrument. High-resolution mass spectra (HRMS) were recorded on a Thermo Scientific Orbitrap Velos Pro mass spectrometer coupled with a Thermo Scientific Accela 1250 UPLC and an auto sampler using electron spray ionization (ESI) in the positive mode. Absorbance was measured on a Varian Cary 50 Bio UV- Visible Spectrophotometer. Fluorescence data were recorded on a Horiba Scientific FluoroMax-4 using FluorEssence software. Solvents used for fluorescence spectra were ethanol (Decon), dioxane (Oakwood), and PBS (Corning Cellgro). LC-MS analyses were performed on an Agilent Technologies 6130 quadrupole LC/MS connected to an Agilent diode array detector using an Agilent ZORBAX SB-C18 Rapid Resolution HT 2.1 x 50 mm column, 1.8 micron particle size, with a mobile phase of water/acetonitrile including 0.1% formic acid. In vitro bioluminescence assays were performed on a Promega GloMax Discover luminometer. Cellular bioluminescence assays were performed on a Xenogen IVIS 100. GraphPad Prism 7.0a (Graph Pad Software, Inc.) was used to analyze data and generate graphs.

In Vitro Luciferase Assay

Luciferin analogues were prepared by dilution of 50 mM DMSO stocks into substrate buffer (20 mM Tris HCl pH 7.4, 0.1 mM EDTA, 8 mM $MgSO_4$, and 4 mM ATP). The final volume added into each well of a white 96-well plate (Costar 3912) was 60 µl. The plates were then loaded into a Promega GloMax Discover instrument, where each well was injected with 60 µl of 1 nM recombinant firefly

luciferase (Harwood et al., 2011.; Mofford et al., 2014.) in enzyme buffer (20 mM Tris HCl pH 7.4, 0.1 mM EDTA, 0.8 mg/mL BSA, and 1 mM TCEP), followed by measuring the bioluminescent light output at 0.5 second intervals for one minute. Note that once the luciferase is added, both the enzyme and substrate are at half their originally prepared concentrations.

Fluorescence and Relative Quantum Yield Measurement for Sulfonamidyl Luciferins

Absorbance spectra were recorded at five different concentrations with absorbance between 0.01-0.10 for each sample. Extinction coefficients were calculated from the slope of absorbance versus concentration. Relative quantum yields were calculated from plots of absorbance vs. integrated fluorescence and were referenced to that of 6'-aminoluciferin measured under the same conditions. Fluorescence spectra were recorded in PBS at different pH values, and pKa values were determined from plots of pH vs. integrated fluorescence.

Bioluminescence Emission Wavelength Measurement

Luciferin analogues were prepared at 20 µM by dilution from a 50 mM DMSO stock into substrate buffer (20 mM Tris HCl pH 7.4, 0.1 mM EDTA, 8 mM MgSO4, and 4 mM ATP). Recombinant firefly luciferase was prepared at 200 nM in enzyme buffer (20 mM Tris HCl pH 7.4, 0.1 mM EDTA, 0.8 mg/mL BSA, and 1 mM TCEP). A quartz cuvette containing 1.5 mL of the enzyme solution was

placed into a FluoroMax fluorometer. Into the quartz cuvette, 1.5 mL of the respective luciferin analogue in substrate solution was injected into the luciferase enzyme solution, and the resulting emission was scanned from 400-800 nm with a 10 nm emission slit and closed excitation slit.

CHO Cell Bioluminescence Assays

Chinese hamster ovary (CHO) cells were maintained at 37°C and 5% CO_2 in F-12K medium (Gibco) containing 10% fetal bovine serum and 100 units/mL penicillin/streptomycin as previously reported. CHO cells were grown to ~80% confluence, then trypsinized, seeded in black 96-well plates (Costar 3916) at 15,000 cells/mL, and returned to the incubator overnight. Twenty-four hours post-seeding, the cells were transiently transfected with pCDNA3.1-WTLuc2 at 0.075 µg DNA/well using Lipofectamine 2000 (Invitrogen), as previously reported. Assays were performed in triplicate 48 hours after transfection in a Xenogen IVIS-100. Substrates were diluted in Hank's balanced salt solution (HBSS) to 100 µM, 10 µM, and 1 µM. Each 96-well plate of transfected CHO cells was gently washed with HBSS and overlaid with 60 µl/well of 100, 10, or 1 µM substrate. Bioluminescence imaging was performed one minute after addition of substrate. Lysed cell assays were performed as previously described (Harwood et al., 2011.; Mofford et al., 2014.). Data acquisition and analysis were performed with Living Image software, and reported as total flux (p/s) for each ROI

corresponding to each well of the 96-well plate. Data were plotted and analyzed with GraphPad Prism 7.0.

Photophysical Properties of TFP Rhodol (46) and Rhodamine (47)

Compounds were diluted from a 10 mM DMSO stock into 0.1 M NaOH. The diluted solution was allowed to equilibrate in the dark at room temperature for 15 minutes before a second dilution was made. The second dilution was allowed to equilibrate in the dark at room temperature for another 15 minutes before the absorption or fluorescence signal was read. Absorbance spectra were recorded at five different concentrations with absorbance between 0.01-0.10 for each sample. Extinction coefficients were calculated from the slope of absorbance versus concentration. Quantum yields were determined from plots of absorbance versus integrated fluorescence, using fluorescein and Rhodamine 6G as reference standards. To determine pKa values, dyes **46** and **47** were diluted from a 10 mM DMSO stock into the appropriate buffers (pH 4 – 5.4, 0.2 M citrate; pH 5.8 – 7.8, 0.1 M phosphate; pH 8.4 – 8.6, 0.1 M Bicine/Tris) to a final concentration of 5 µM and allowed to equilibrate in the dark for 15 minutes. Integration of fluorescence and curve fitting was performed using GraphPad 7.

CHAPTER VII:

FruitFire: a Luciferase Based on a Fruit Fly Metabolic Enzyme

Spencer T. Adams, Jr., Markus F. Bohn, Celia A. Schiffer, and Stephen C. Miller. *Currently preparing for submission.*

Summary

The fruit fly enzyme CG6178 shares high sequence identity with firefly luciferase, but is incapable of catalyzing bioluminescence with firefly luciferin. Recently, we found that it has weak luciferase activity when supplied with synthetic luciferin analogues such as CycLuc2. To better understand the basis for this substrate discrimination and to engineer the enzyme to be a more robust luciferase, we determined the structure of CG6178 using x-ray crystallography. We then mutated select residues in the active site to create FruitFire, which exhibits a lowered Km for CycLuc2, 20-fold improved activity, and even some weak light emission with D-luciferin. When expressed in mice, FruitFire enabled bioluminescence imaging in the brain using the pro-luciferin CycLuc2-amide. The conversion of a fruit fly fatty acyl-CoA synthetase into a luciferase capable of in vivo imaging underscores the potential for similar success with a range of other adenylating enzymes.

Introduction

Fruit flies, like the majority of insects, do not glow in the dark. But why not? Fireflies and other bioluminescent beetles use luciferase enzymes to oxidize the small-molecule substrate D-luciferin for light emission. The fruit fly *Drosophila melanogaster* expresses a long-chain fatty acyl-CoA synthetase (ACSL), CG6178, which is 41% identical to firefly luciferase (Fluc) (Oba et al., 2004.). We previously demonstrated that this enzyme harbors latent luciferase activity when supplied a suitable synthetic luciferin, such as CycLuc2 (Figure 7.1) (Mofford et al., 2014.). Although this latent luciferase activity is relatively weak, it suggests that fatty acyl-CoA synthetases (ACSs) can inform us about the molecular details of what makes beetle luciferases different from their ancestral enzymes. Further, enzymes like CG6178 may be mutated to yield novel and selective luciferases.
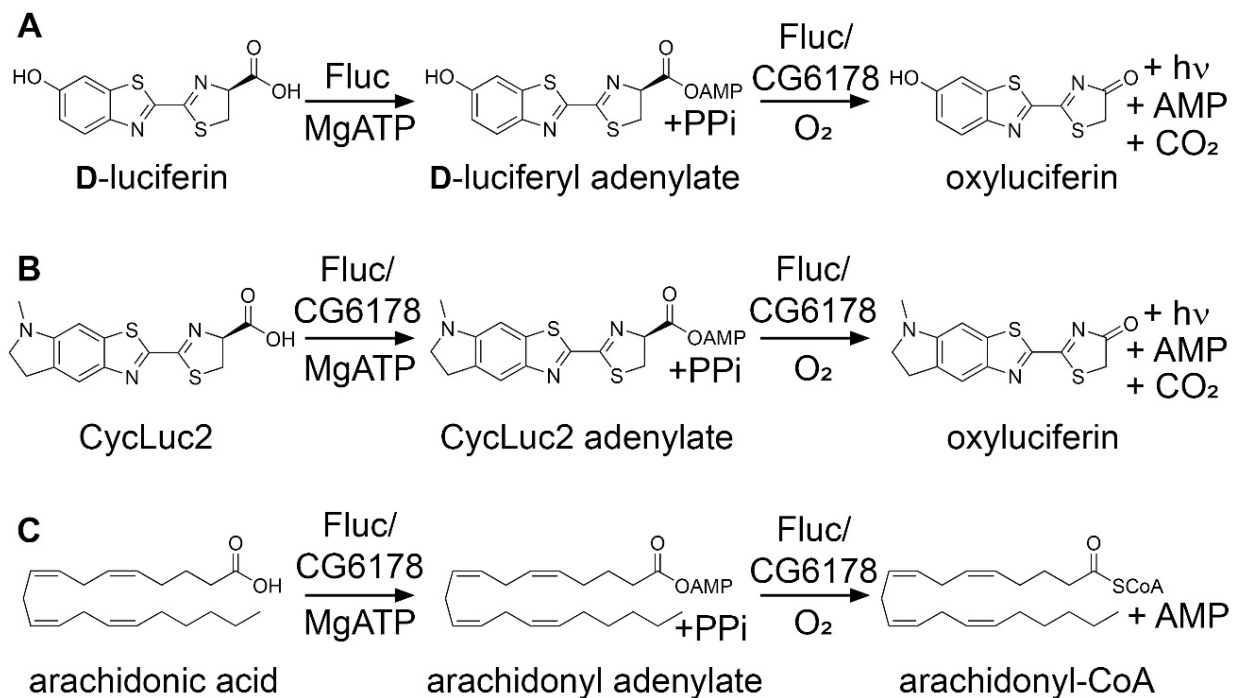
Figure 7.1. Firefly luciferase and CG6178 are bifunctional. Firefly luciferase (Fluc) is a luciferase that catalyzes light emission from D-luciferin (A) and CycLuc2 (B). Fluc is also a long-chain fatty acyl-CoA synthetase, ligating coenzyme A to long-chain fatty acids (C). CG6178 catalyzes light emission from CycLuc2 (B), but not D-luciferin (A). CG6178 natively functions as an ACSL (C). Thus, both enzymes are bifunctional.

Fluc is a two-domain protein, with a substrate-binding channel that lies at the interface of its larger N-terminal domain and smaller C-terminal domain (Figure 7.2) (Conti et al., 1996.). Fluc is able to catalyze light emission from luciferins and attach coenzyme-A to fatty acids, making it a luciferase and an ACS, respectively (Oba et al., 2003.). In the bioluminescent reaction, D-luciferin is first adenylated, then this AMP ester reacts with oxygen to form an excited-state oxyluciferin (Figure 7.1A) (McElroy et al., 1996.; White et al., 1971.;

DeLuca, M., 1976.; Wood, K.V., 1995.). The oxyluciferin then relaxes to the

ground state, emitting a photon of light (McElroy et al., 1996.; White et al., 1971.;

DeLuca, M., 1976.; Wood, K.V., 1995.). Similarly, when Fluc binds fatty acids of

appropriate length, it adenylates them (Figure 7.1B) (Oba et al., 2003.). However,

once the fatty acid is adenylated, coenzyme A displaces AMP from the acyl

adenylate, forming a fatty acyl-CoA ester (Oba et al., 2003.). Although the N-

terminal domain is primarily responsible for substrate recognition, the C-terminal

domain is necessary for efficient bioluminescence (Oba et al., 2006.). The C-

terminal domain facilitates light emission by alternating between two alternating

conformations (rotating 140° relative to the N-terminal domain) to present two

different lysine residues that are important for efficiently coupling the adenylation

and subsequent oxidation/thioesterification steps (Sundlov et al., 2012.).
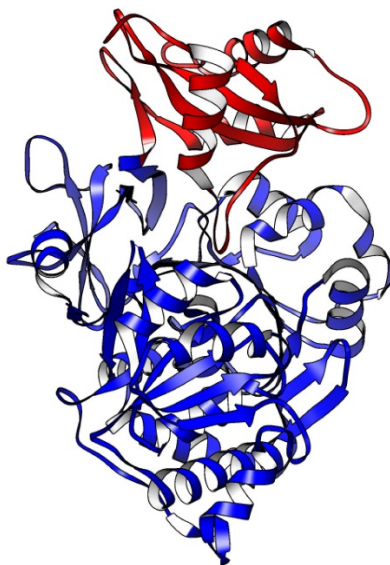
Figure 7.2. Firefly luciferase is a two-domain protein. Structure of Photinus pyralis luciferase (4G36; Sundlov et al., 2012.) shown with the N-terminal domain colored blue and the C-terminal domain colored red. A flexible hinge connects the two domains (not highlighted). Substrates bind at the interface of the two domains.

CG6178 is an insect ACSL that shares 42% identity with Fluc on the amino-acid level (Figure 7.3) (Oba et al., 2003.). Given the significant sequence homology and shared evolutionary history between Fluc and ACSLs, this fruit-fly enzyme has garnered attention from labs seeking to identify and characterize novel luciferase enzymes. Characterization of CG6178 revealed that the enzyme is a luciferase capable of catalyzing light emission from synthetic luciferins, but not the natural substrate D-luciferin (Oba et al., 2003.; Mofford et al., 2014.). To understand the molecular basis for CG6178's latent luciferase activity and substrate discrimination, we determined the structure of the enzyme.
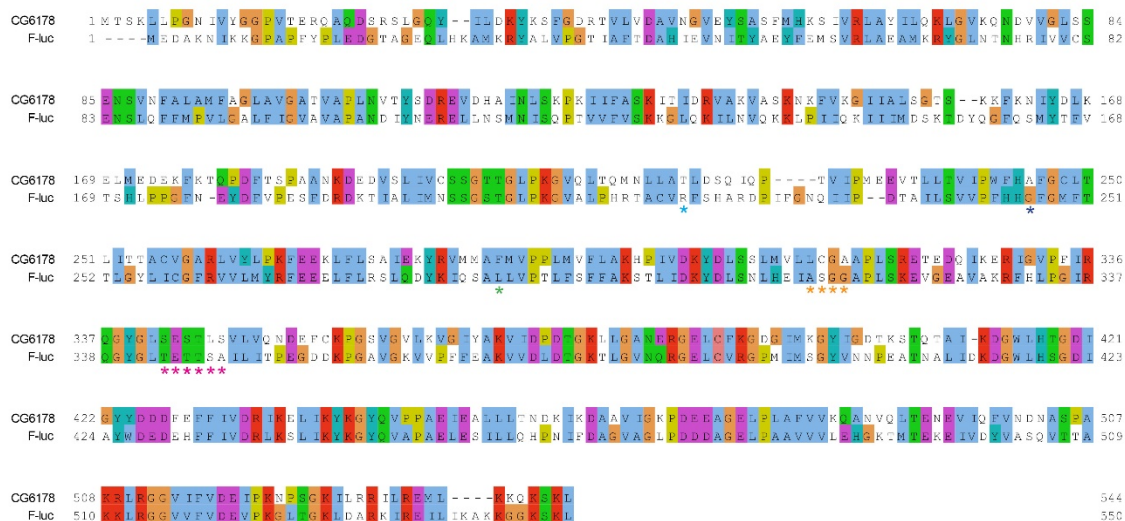
Figure 7.3. CG6178 shares 42% amino-acid identity with firefly luciferase.
Firefly luciferase sequence (UniProt accession number: Q27758) aligned with CG6178 sequence (UniProt accession number: Q97CC6) using Clustal under MUSCLE settings (Edgar, R.C., 2004.). Asterisks indicated residues later targeted for mutagenesis. Asterisk color corresponds to residue coloring in Figure 7.5.

Here we report the crystal structure of CG6178, which shares the same overall fold as firefly luciferase, but has a steric protrusion constricting the substrate binding site. Through the introduction of point mutations to residues that comprise this bump, we improved the luciferase activity in this fruit fly enzyme. The mutated CG6178, which we now dub "FruitFire," has increased bioluminescent activity with CG6178's preferred substrate (CycLuc2), catalyzes light output with the synthetic luciferin CycLuc2-amide robust enough for bioluminescence imaging in the brains of live mice, and can also emit light with D-luciferin.

Results and discussion

X-ray data was collected at the APS 23-ID beamline and the initial solution was generated using Fluc (PDB 4G36) as a search model (Sundlov et al., 2012.). Our structure was determined at 2.48 Angstrom resolution with a crystallographic R-value of 0.19 and an R-free value of 0.24 (Table 7.1). The structure contains 534 out of 544 residues. The first residue and the last 6 residues are all exposed on the surface of the protein and we were not able to satisfactorily model them into density.

Parameter	
Data collection	
Wavelength, Å	1.033
Resolution range, Å	29.03-2.499 (2.588-2.499)
Space group	$P2_12_12_1$
Unit cell a, b, c	55.85 77.7778 113.315
Unit cell α, β, γ	90 90 90
Total reflections	99870
Unique reflections	17684 (1713)
Multiplicity	5.6
Completeness, %	99.72 (98.67)
Mean I/σ(I)	17.46 (2.95)
Wilson B-factor	36.33
R-merge	0.104 (0.671)
Refinement	
R-work	0.1996 (0.2361)
R-free	0.2469 (0.2752)
No. of nonhydrogen atoms	4113
Macromolecules	3998
Ligands	31
Water	84
Protein residues	534
rms, bonds	0.003
rms, angles	0.8
Ramachandran favored, %	95.66
Ramachandran outliers, %	3.96
Clash score	5.5
Average B-factor	39.21
Macromolecules	39.12
Solvent	37.07

Table 7.1. Crystallographic Statistics for CG6178 Structure.

As expected, the CG6178 structure shares the same overall fold with

firefly luciferase (Figure 7.4). As calculated with PyMol, our CG6178 structure

exhibits an RMSD of 1.45 Å with Fluc (PDB ID: 4G36) (Sundlov et al, 2012).

Efforts to co-crystallize CG6178 with either CycLuc2 or D-luciferin were

unsuccessfull. However, ATP dramatically improved crystallizability. Within our

structure, we see density for an adenylated moiety. However, the identity of the

ligand is ambiguous. In Figure 7.5, we show the electron density maps for either

an adenylated fatty acid or an adenylated polyethylene glycol molecule, both of

which fit equally well. Therefore, we modeled luciferin into CG6178's active site

by superimposing its structure onto a co-crystal structure of Fluc with a non-

hydrolyzable bisubstrate analog DLSA, then visualized CG6178's active-site

residues that surrounded this substrate's predicted binding location. CG6178's

active site residues differ from the ones in Fluc (Figure 7.6).
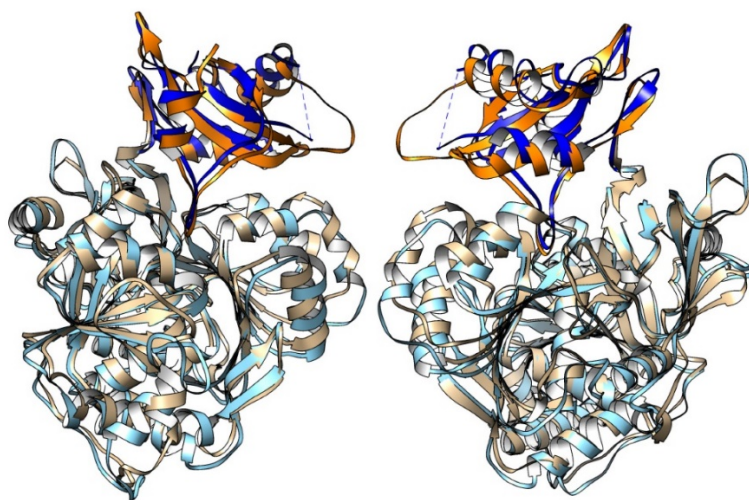
Figure 7.4. Firefly luciferase and CG6178 share an overall fold. Fluc (PDB ID: 4G36; Sundlov et al., 2012.) (N-terminal domain in light blue and C-terminal domain in dark blue) and CG6178 (N-terminal domain in beige and C-terminal domain in brown) were aligned using UCSF Chimera (Petterson et al., 2004) and are represented in two poses rotated approximately 180° about the vertical axis. The structures are well-conserved among the two proteins.
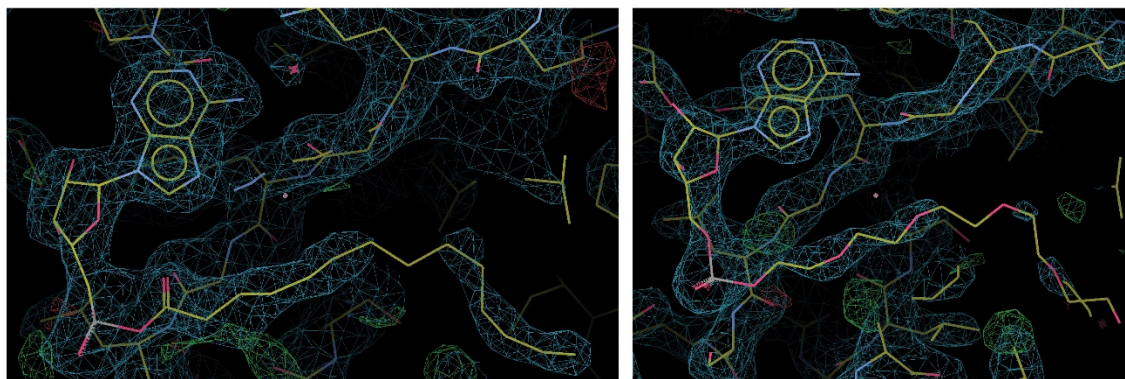
Figure 7.5. The identity of the ligand bound to the CG6178 structure is not clear. Though the density for CycLuc2 generated negative density (not shown), a long alkyl chain (left panel) or polyethylene glycol chain (right panel) extended from the AMP moiety are equally supported by our model. Sigma values set to RMSD= 1.0 in both panels.
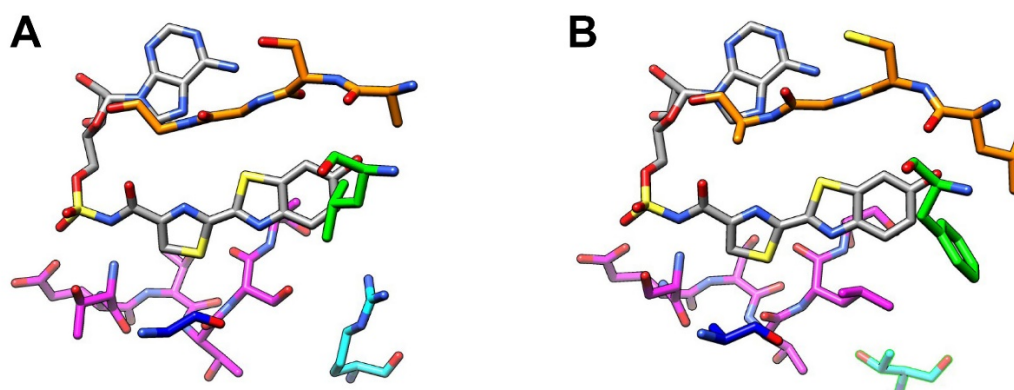
Figure 7.6. Active site residues selected for mutagenesis. CG6178's structure (panel B) was superimposed over Fluc co-crystallized with DLSA (panel A) to identify residues for mutagenesis. The alignment was used to show the predicted location of luciferin in CG6178's active site and the surrounding residues.The colors shown correspond with the residues' location in the sequence alignment in Figure 7.3. Figure prepared using UCSF Chimera (Petterson et al., 2004).

Based on these differences, we initially created 11 CG6178 mutants in an attempt to improve the enzymes luciferase activity (residues chosen for mutagenesis are asterisked in Figure 7.3 and the specific mutations and combinations of these residues are shown in Figure 7.7, panel C.). Once these mutants were created, they were tested for their performance in vitro compared to wild-type CG6178 with both CycLuc2 and D-luciferin. The best performing mutant among the 11 mutants involved the residues 342-S-E-S-T-L-S-347 mutated to mimic the sequence in Fluc to 342-T-E-T-T-S-A-347. Despite some of the other mutants improving the activity of CG6178 relative to wild-type, the

combination of mutating this region along with other active site residues did not

provide an additive benefit to the activity of CG6178.

Mutant #	ASGG	F → L	TTSA	LCGG	TETTSA	A → G	T → R
1	●	●					
2	●						
3	●		●				
4				●			
5					●	●	●
6					●	●	
7					●		
8	●	●			●	●	●
9	●	●			●	●	
10	●				●	●	●
11	●	●			●		●
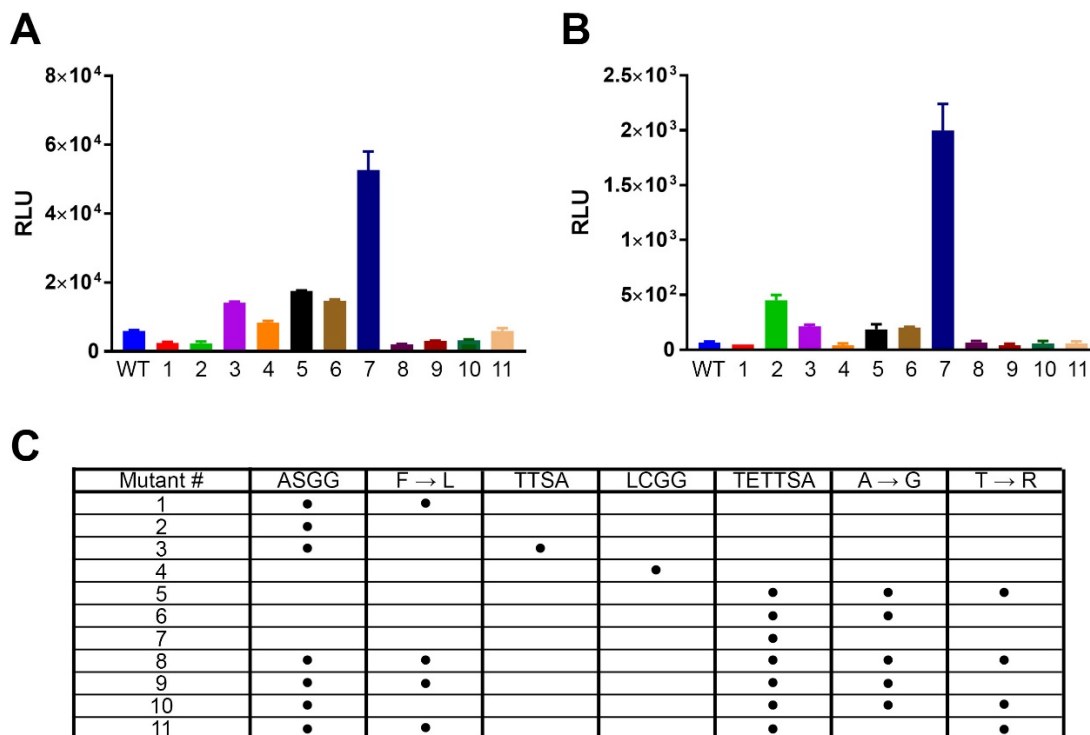
Figure 7.7. Activity of CG6178 active site mutants with CycLuc2 and D-luciferin. Residues asterisked in Figure 7.3 and shown in Figure 7.6 were mutated in various combinations and tested in vitro for their performance with CycLuc2 (panel A) or D-luciferin (panel B). The specific residues mutated in each mutant are indicated in the table in panel C.

Within the region that provided the greatest improvement in activity from

the initial mutant screen, CG6178 residues 344-347 create a protrusion that

constricts the active site relative to firefly luciferase (Figure 7.8). We hypothesize

that substrates with aliphatic fatty acid side-chains can readily traverse this

narrow constriction, but D-luciferin cannot, or at least not in a conformation

suitable for attack of its carboxylate on ATP during the adenylation step. This

discrimination is not an issue for CG6178 to perform its native ACSL activity. It is

not immediately clear why CycLuc2 would perform better than D-luciferin in this

respect. However, CycLuc2 is a more hydrophobic and rigid substrate that may

enable some deformation of the active site that is not possible with D-luciferin.

Removal of the constriction in CG6178's active site could therefore be beneficial

for the luciferase activity of CG6178 with both CycLuc2 and D-luciferin.
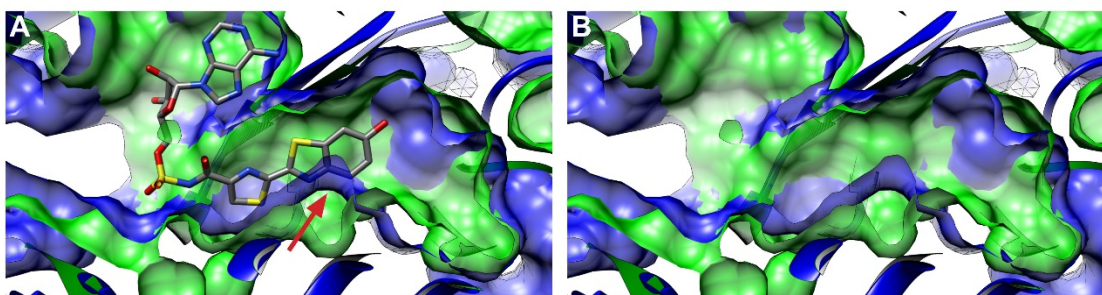
Figure 7.8. Comparison of firefly luciferase's and CG6178's active sites highlights differences. Fluc (PDB ID 4G36; Sundlov et al., 2012) (shown in green) and CG6178 (shown in blue) were aligned using UCSF Chimera (Petterson et al., 2004.) and surfaces shown to compare the substrate binding pocket: (A) with luciferase's co-crystallized bisubstrate analog of D-luciferin adenylate (DLSA) shown and (B) without the compound shown. The red arrow in (A) shows where CG6178 has a protrusion that impinges the active site in the region occupied for the substrate to access ATP during the adenylation step of catalysis.

Failure to adenylate D-luciferin precludes light emission with this

substrate, and indeed there is evidence that CG6178 is incapable of adenylating

D-luciferin. The sidechain of leucine 346 that creates CG6178's protrusion

(highlighted in Figure 7.9A) aligns with the sidechain of serine 347 in firefly

luciferase. Serine 347's side-chain hydroxyl group makes a hydrogen-bonding

interaction with the benzothiazole nitrogen via an intermediate water molecule in

firefly luciferase and is a key residue for efficient catalysis of bioluminescence

(Nakatsu et al., 2006.). However, previous work has shown that simply mutating

the leucine residue 347 in CG6178 to serine as suggested from the sequence

alignment was insufficient to enable CG6178 to efficiently emit light with D-

luciferin (Oba et al., 2009.). Furthermore, mutation of serine 347 in firefly

luciferase has a detrimental effect on bioluminescence from D-luciferin, but is

well tolerated by aminoluciferins (Harwood et al., 2011.). To test our hypothesis

that this bump limits the luciferase activity of CG6178, we generated four mutants

of CG6178 that contained mutations to the leucine and flanking residues and

tested their ability to improve the luciferase activity of CG6178 with its preferred

substrate CycLuc2 and with the natural D-luciferin substrate. A table in Figure 7.9

details the mutant sequences we selected (Alignment of relevant Fluc and

CG6178 sequences in Figure 7.9C and corresponding CG6178 mutant

sequences in Figure 7.9D). These sequences were chosen to reduce the size of

the bump in CG6178's active site using alanines and/or to restore a serine side

chain that functionally mimics the serine residue in firefly luciferase. Mutants 1-3

retain the same residues as wild-type CG6178 for residues 344 and 345, but

mutate 346 (the lysine primarily causing the bump) and residue 347 (serine in the

wild-type sequence). The fourth mutant mutates all residues to mimic the

sequence from wild-type firefly luciferase.
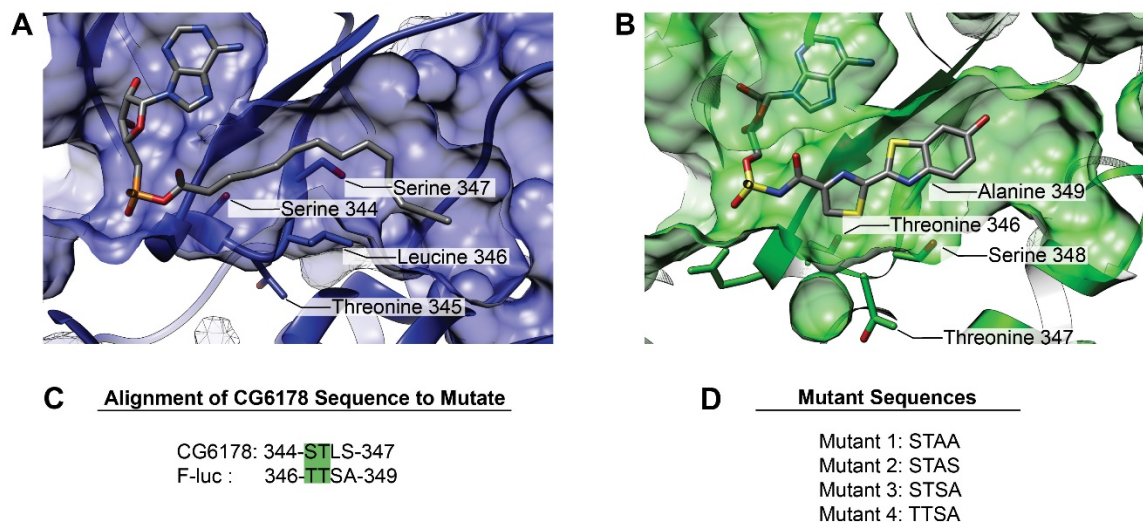
Figure 7.9. Mutant strategy for improving the luciferase activity of CG6178.
CG6178's (A) and Fluc's (B) (PDB 4G36; Nakatsu et al., 2012.) active site
surfaces modeled with UCSF Chimera (Petterson et al., 2004.). The residues
that contribute to CG6178's protrusion are highlighted in A and the corresponding
residues that align with them in Fluc are highlighted in B and in sequence form in
C. Mutant sequences for the bump residues are detailed in D.

To test the whether these CG6178 mutants had improved the enzyme's

bioluminescent activity, we initially assayed purified protein over a range of

concentrations with D-luciferin and CycLuc2 (Figure 7.10). We found that three of

the four CG6178 mutant enzymes improved the luciferase activity of CG6178

with CycLuc2, with the best performing mutant increasing light emission by 20-

fold at 250 μM substrate concentration (saturating luciferin concentration).

Further, the CG6178 mutants also lowered the Km for luciferin CycLuc2 from 15

µM for the wild-type enzyme to 2.13 µM for the "STSA" mutant (Table 7.2),

suggesting the mutants would be more useful in contexts where substrate access

is limiting, such as *in vivo.* Mutant 3 exhibited the best performance overall and

was renamed FruitFire.
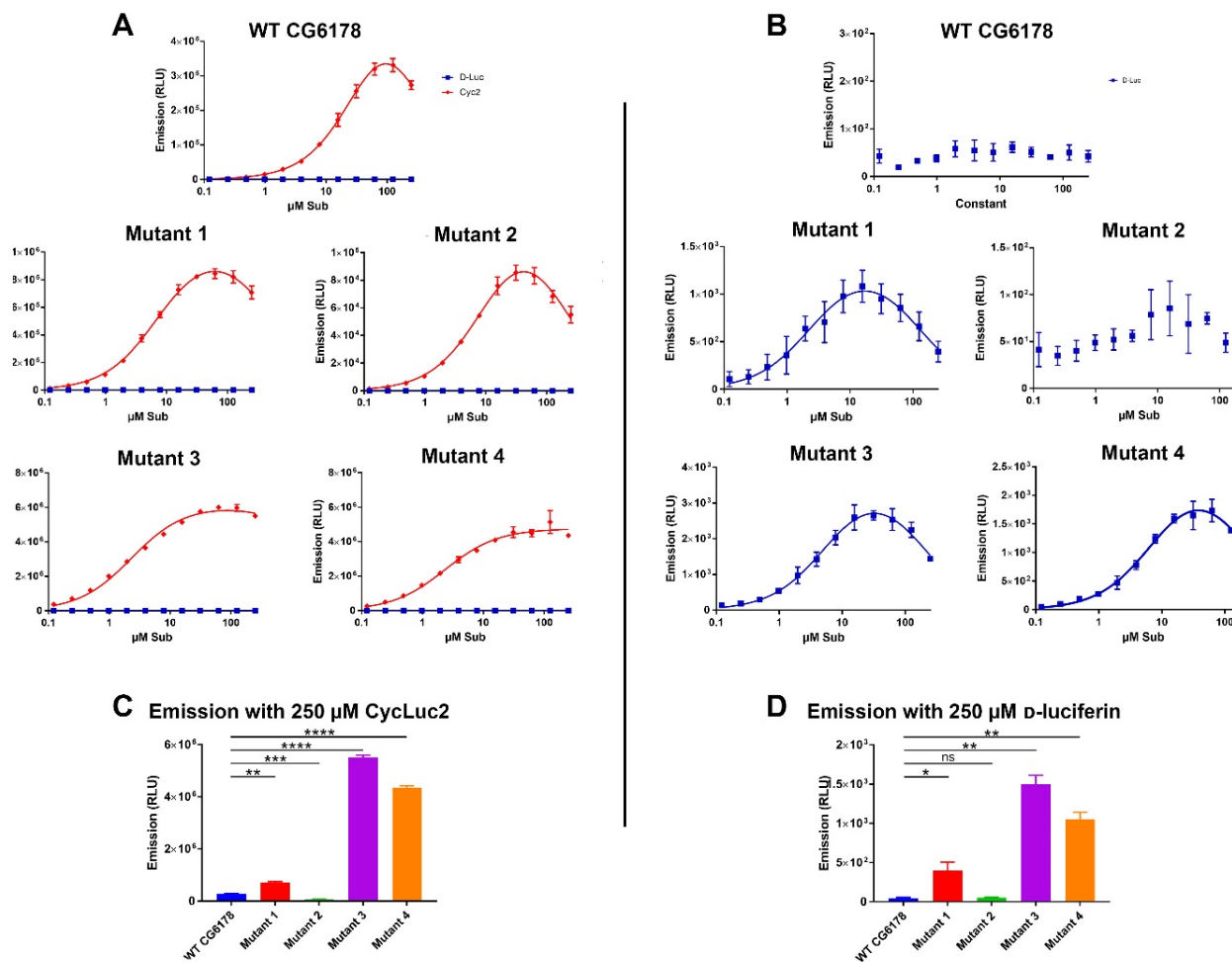
Figure 7.10. *In vitro* **performance of CG6178 mutants.** Wild type CG6178 and the 4 mutants detailed in Figure 6D were incubated with either D-luciferin or CycLuc2 over a range of concentrations from 0.122 µM to 250 µM. Panel A contains graphs of both substrates with each enzyme, while panel B only contains graphs for D-luciferin, showing the response of the dimmer substrate with a lower scale. Due to the different scales used for each dose-response, panels C and D show the relative performance of CycLuc2 and D-luciferin at saturating substrate concentration (250 µM) with each enzyme, respectively.

Enzyme	Km (µM)	
	D-luciferin	CycLuc2
WT CG6178	0.119	15
Mutant 1	0.844	4.57
Mutant 2	0.155	3.78
Mutant 3/Fruitfire	1.36	2.13
Mutant 4	1.48	2.35

Table 7.2. *In vitro* Km vales for wild type CG6178 and mutants. Data from figure 7 was analyzed using nonlinear regression to calculate Michaelis constants. Compared to wild type CG6178, Fruitfire (highlighted in red) has a lower Km.

We next tested whether these mutants would permit light emission with D-luciferin. Mutant 2, which exhibited poorer luciferase activity than wild-type CG6178 with CycLuc2, did not catalyze light emission from D-luciferin. However, mutants 1, 4, and FruitFire were each able to catalyze weak but measurable light emission with D-luciferin in a dose-dependent manner (7.10B and 7.10D). The relative emission with D-luciferin is approximately 3 orders of magnitude lower than CycLuc2, with FruitFire again exhibiting the highest activity.

Following the successful improvement of bioluminescent light intensity and lower Km for CycLuc2 in CG6178 through mutagenesis, we wanted to determine if the same results applied to live cells. We transfected Chinese hamster ovary (CHO) cells with either wild-type luc2, wild-type CG6178, or Fruitfire, then incubated them with serially diluted D-luciferin or CycLuc2 from 250 µM to 0.122 µM concentration with 96 well plates, imaged with the IVIS-100 imaging system to measure the dose-response of the enzyme-substrate pairs in cells. Compared

to wild-type CG6178, FruitFire exhibited a lower apparent Km with CycLuc2

(Figure 7.11).
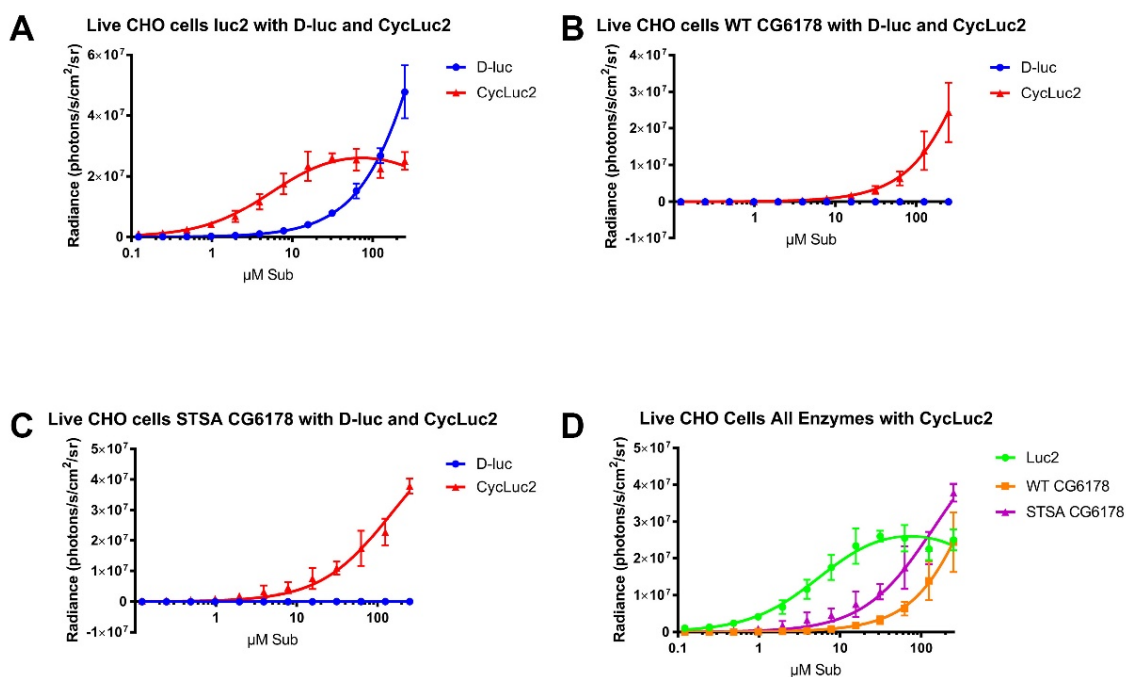
Figure 7.11. Improved performance of FruitFire over wild-type CG6178 in live cells. Wild-type luc2 luciferase (A), wild-type CG6178 (B), and FruitFire (C) were each used to transfect Chinese hamster ovary (CHO) cells, then were imaged over a concentration range from 0.122 µM to 250 µM with either D-luciferin or CycLuc2. Panel D shows the relative performance of all three enzymes with CycLuc2 on the same graph, which highlights the lower Km for FruitFire than wild type CG6178 in live cells.

The lower Km and greater luminescence activity of FruitFire luciferase

with CycLuc2 compared to wild type CG6178 suggests the former may be

suitable for *in vivo* use. To test this hypothesis, we delivered both enzymes into

live mouse brain via stereotactic delivery of adeno-associated viral (AAV)

vectors. Once the respective genes established expression in the mice's brains,

we injected them intraperitoneally with either D-luciferin, CycLuc2, or CycLuc2-

amide on separate imaging days to assess the enzymes' relative performance

with the substrates. CycLuc2-amide differs from the parent compound, CycLuc2,

by addition of an amide group (Figure 7.12) (Mofford et al., 2014.). Presence of

this amide group makes the compound a pro-luciferin which must be converted

to CycLuc2 by endogenous enzymes present in mouse brain (Mofford et al.,

2014.). CycLuc2, despite requiring unmasking by a secondary enzymatic activity,

greatly improves the access of the substrate to mouse brain following delivery

and results in greater light emission (Mofford et al., 2014.). Wild-type CG6178

expressed in mouse striatum was incapable of light emission when treated with

D-luciferin, CycLuc2, or CycLuc2-amide. However, FruitFire emits measurable

light when treated with CycLuc2-amide (Figure 7.12). FruitFire's two mutated

residues are sufficient to convert the fruit fly enzyme CG6178 to a luciferase

capable of measurable light emission in live mouse brain with the synthetic

luciferin CycLuc2-amide.
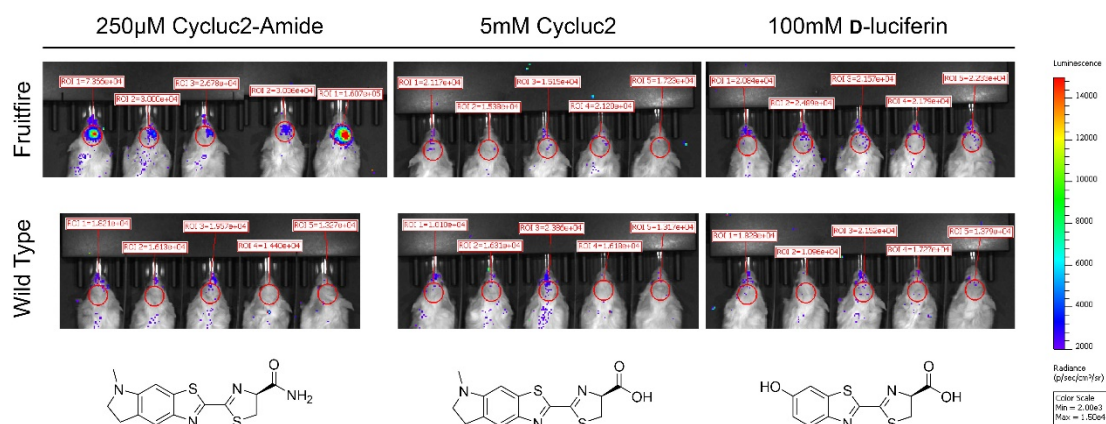
Figure 7.12. FruitFire emits measurable light in live mouse brain when imaged with CycLuc2-amide. Fruitfire or wild-type CG6178 were delivered into live mice's brains via stereotactic injection of viral vectors containing genes for the enzymes. Once expressing either of these enzymes, the mice were injected intraperitoneally with either D-luciferin, CycLuc2, or CycLuc2-amide on separate imaging days (compound structures for each substrate shown under the corresponding images) and imaged with an IVIS Spectrum imaging system. Measurable light emission was achieved with mice expressing Fruitfire following administration of CycLuc2-amide, but not with CycLuc2 or D-luciferin. Wild-type CG6178 did not catalyze measurable light emission with any of the substrates.

Conclusion

Fluc is a bifunctional enzyme, acting as both a luciferase and an ACSL. The chemistry is dependent on what substrate the enzyme binds; luciferins are oxidized for light emission and long-chain fatty acids are attached to coenzyme A. The reverse is also true in some cases, with some ACSLs exhibiting luciferase activity with luciferins. One such bifunctional ACSL is the fruit fly enzyme CG6178 (Mofford et al., 2014.). CG6178 is capable of emitting light with the

synthetic luciferin CycLuc2, but not the natural D-luciferin substrate (Mofford et al., 2014.). We wanted to elucidate the nature of CG6178's substrate discrimination and improve its luciferase activity. Once we determined the structure of CG6178, we generated mutants of multiple active-site residues and tested their relative performance. Of these mutants, changing one contiguous stretch of residues from 342-347 had the most impact. Taking a closer look at this region, we could see that residues 344-347 formed a loop that creates a unique protrusion via the sidechain of leucine 346. This leucine sidechain aligns with the sidechain of a serine residue responsible for binding the luciferin substrate via an intermediate hydrogen-bonded water molecule in Fluc (serine 347 in Fluc). Previously, efforts were made to functionally convert CG6178 to a functional luciferase by mutating leucine 346 to a serine residue based on sequence alignments alone (Oba et al., 2009.). However, this single point mutation was not sufficient to permit light emission with D-luciferin (Oba et al., 2009.). We mutated the leucine and surrounding residues that comprise the bump in CG6178 and found that mutating two residues was sufficient to improve light emission in CG6178 by 20-fold over the wild-type enzyme with CycLuc2, while also lowering the Km for CycLuc2 by approximately 7-fold. This same double-mutant also permits dose-dependent light emission *in vitro* with D-luciferin. We named this mutant enzyme FruitFire luciferase. Further experiments with FruitFire luciferase showed that it also exhibits a lower apparent Km in live CHO cells than the wild-type enzyme with CycLuc2 and is capable of producing

measurable light emission in live mouse brain with CycLuc2-amide. The robust improvement of CG6178's luciferase activity via structure-directed mutagenesis highlights the utility of enzymes homologous to Fluc to serve as alternative platforms for bioluminescent reporter engineering.

Materials and Methods

Contributions

S.T.A. Jr. devised experiments, performed purified enzyme assays, performed live cell assays, crystallized CG6178, analyzed x-ray data and built structural model, performed all mouse experiments, and prepared the manuscript. Markus F. Bohn (formerly of Celia Schiffer's lab in the department S.T.A. Jr. performed thesis research in) mentored S.T.A. Jr. for crystallography work leading to the structure. G.R.R. and G.S.K.K.R. designed and synthesized luciferins. S.C.M. helped devise experiments. Thanks to Celia Schiffer for providing a lab with immensely talented scientists to show me how to work with protein structures and for the Kelch lab for shooting my CG6178 crystal at the Synchotron.

Plasmid Constructs: Plasmids for bacterial expression were prepared by cloning the target gene into pGex-6P1 vector. For live cell assays, luc2 and CG6178 were cloned into pcDNA3.1. CG6178 mutants, including FruitFire, were ordered as complete plasmids in pGex-6P1 and pcDNA3.1 from Genscript.

Enzyme Expression and Purification: Enzymes were expressed as GST-fusion proteins from pGex6P-1 vectors. Liter cultures of BL21-DE3 cells

transformed to express the protein of interest were grown at 37 °C until the culture's OD600 reached between 0.5-1. The culture was cooled to room temperature, then induced with 0.1 mM IPTG, followed by incubation and shaking at 20 °C overnight. The following day, cells were pelleted at 5000 rpm and flash frozen with liquid nitrogen. The frozen pellets were kept on ice and resuspended in 25 mL lysis buffer (50 mM Tris [pH 7.4], 500mM NaCl, and 0.5% Tween 20) containing 1 mM phenymethylsulfonyl fluoride, and disrupted by sonication. Dithiothreitol (DTT) was added at 10 mM, followed by ultracentrifugation at 35k rpm for 1 hour at 4 °C. The supernatant was bound to immobilized glutathione beads (Thermo Scientific) in a Pierce column (Pierce Scientific) for 1 hour at 4 °C. The beads were washed with lysis buffer containing 10 mM DTT, followed by wash buffer (50mM Trish [pH 8.1], 250 mM NaCl, and 10 mM DTT) and storage buffer (50 mM Tris [pH 7.4], 0.1 mM EDTA, 150 mM NaCl, and 1 mM TCEP). Twenty units of PreScission Protease (GE Healthcare) were added, then the beads were incubated overnight at 4 °C on a Labquake tube rotator (Thermo Scientific) to cleave the GST-linkage, permitting elution of the untagged enzyme the following day. Protein concentrations were determined using the Nanodrop 100 (ThermoFisher) using the protein mass and molar extinction coefficient method (calculated using the Peptide Property Calculator at: biotools.nubic.northwestern.edu/proteincalc.html).

For crystallographic use, CG6178 was further purified using size-exclusion chromatography with a Superdex 75 column (GE Life Sciences), where the

protein collected eluted as a single band and was collected for concentration. CG6178 enzyme for crystallography was concentrated to 30 mg/mL using cellulose Millipore Amicon® Ultra – 4 Ultracel – 30K centrifugal filters (MilliporeSigma).

Crystallization of CG6178: To crystallize CG6178, a sitting drop method was used. Hampton Research Intelli-Plate 48-3 plates were used. After optimized hits following multiple screens, the following method reliably produced crystals within 24 hours: 200 µl of crystallization solution (0.1M Tris pH 7.5, 0.2M $(NH_4)_2SO_4$, 28% PEG 3350, and 10 mM ATP disodium salt) was deposited into the reservoir of each well. Then, 2 µl of the crystallization solution was mixed 1:1 with 2 µl of 30 mg/mL CG6178 in each of 3 sample drop drop wells within each well. Plates were immediately sealed with Hampton Research ClearSeal Film and stored at 25 °C.

Crystal Harvesting and Data Collection: Crystals were harvested from their drops with MiTeGen crystal mounts attached to goniometer bases using a MiTeGen wand and deposited immediately into liquid nitrogen. Cryopreserved crystals were transferred to magnetic cryovials and stored in at cryogenic temperatures for transport to the beamline. No cryoprotectant was used. Data was collected at the 23-IDB beamline at the Advanced Photon Source within the Argonne National Laboratory, Chicago, Illinois, U.S.A.

Data Processing: The crystal diffraction intensities were indexed, integrated, and scaled using HKL3000. Structures were solved using firefly luciferase (PDB 4G36) as a search model in molecular replacement calculation. Model building and refinement were performed using Coot and Phenix. Ligand models were generated using eLBOW to generate .cif files that could be placed using Phenix LigandFit.

Purified Protein Luminescence Assays – GloMax: 50 µL of purified luciferase in enzyme buffer (20 mM Tris [pH 7.4], 0.1 mM EDTA, 1 mM DTT, and 0.8 mg/mL BSA) were added to 50 µL 2X substrate in substrate buffer (20 mM Tris [pH 7.4], 0.1 mM EDTA, 8 mM $MgSO_4$, and 4 mM ATP) in a white 96-well plate (Costar 3912). Light was measured and integrated for each half second for 1 minute after enzyme addition using a Promega GloMax at a final enzyme concentration of 40 nM and final substrate concentrations ranging from 0.122 µM to 250 µM. Data was exported into Excel for formatting, then pasted into Graphpad Prism for graphing. Data are reported as emission (relative light units, RLU) for each well of the 96-well plate. The values at the final 1 minute time point were plotted for each concentration to generate dosage-response curves. Graphs were fit to a sigmoidal dose-response curve by non-linear regression.

Live Cell Assay: Chinese hamster ovary (CHO) cells were transduced with pcDNA3.1 vector backbone containing either luc2, wild type CG6178, or FruitFire. Cells were plated into 96-well black plates (Costar 3915) at 10k cells per well. After 24 hours, cells were transfected with 0.075 g DNA per well using

Lipofectamine 2000 (ThermoFisher). Prior to imaging the transfected cells, a master plate containing the substrates titrated from 250 μM to 0.122 μM over the 12 columns was prepared at sufficient volume to supply substrate to the plates for all three enzymes being assayed. At 24 hours post-transfection, cells were imaged by removing the media containing the Lipofectamine, washing each well with 60 μl Hank's Balanced Salt Solution (HBSS), aspirating the HBSS, then adding 60 μl per well of the appropriate substrate. After a 3 minute hold, the cells were imaged with the Perkin Elmer IVIS 100. Data collection and Regions of Interest (ROIs) were performed with Living Image Software, then data exported to Excel for formatting. The formatted data was plotted using Graphpad Prism as dosage response curves and analyzed using nonlinear regression models.

AAV Vector Construction: Luc2, wild-type CG6178, and CG6178 mutants were cloned into the EcoRI-SalI sites of a pAAV-CMV plasmid. AAV-luciferase, AAV-wild type CG6178, and AAV-FruitFire constructs were packaged into AAV9 serotype viral vectors by the Viral Vector Core at the University of Massachusetts Medical School.

Mice: FVB/N mice were purchased from the Jackson Laboratory. Mouse procedures were approved by the Institutional Animal Care and Use Committee (IACUC) at the University of Massachusetts Medical School (protocol A-2474).

Striatal Delivery of AAV Vectors: Striatal injections of FVB/NJ mice were performed at 6 weeks of age. Each mouse was induced with isoflurane

anesthesia, then restrained in a stereotactic frame, fitted with isoflurane nose cones to maintain anesthesia. Mice were kept on a chemical hand warmer wrapped in autoclaved paper towels to maintain body temperature. Hair from the mice's scalp was removed by applying superglue, followed by removing the glued hair with sterilized forceps. The denuded scalps were then washed three times alternately, using 70% ethanol and betadine, using a fresh sterile swab each time. Then, while holding up the scalp with sterilized forceps, a 1 cm anteroposterior incision was made in the middle of the scalp with sterile surgical scissors. The bregma suture was visualized and used as a reference for acquiring the injection site at the lateral edge of the striatum/cortex border (stereotactic coordinates: anterioposterior: +1 mm anterior, mediolateral: +3 mm right lateral, and dorsoventral: -2 mm ventral from bregma). A dental drill wrapped in sterile paper towel containing a sterilized bit was used to drill a hole through the skull at this site, then the needle lowered into the brain at the appropriate depth. After waiting 1 minute, the injection of 1 µl of 2.5e12 GC/ml AAV9 in PBS) was delivered at 125 nl/min using a micropump-controlled syringe (NanoFil, World Precision Instruments). After the injection completed, the needle was left in place for one minute before withdrawing. The scalp was sutured using 3 simple interrupted sutures of dissolvable suture. The mice each then received the following subcutaneously prior to returning them to their cages: 4 mg/kg meloxicam SR, 0.05 mg/kg buprenorphine and 200 µl PBS. The cages remained

on heat pads at 37 °C until mice regained their righting reflexes.

Bioluminescence imaging began at least 2 weeks after completing the surgeries.

Preparation of Luciferins for Brain Imaging: D-luciferin (100 mM) and

CycLuc2 (5 mM) were prepared by dissolving dry compound directly into PBS.

CycLuc2-amide was prepared by first dissolving dry compound into DMSO to a

concentration of 50 mM, followed by dilution in PBS to a final concentration of

250 μM. Once dissolved, each substrate stock was filtered through a 0.2 μm filter

(Millipore Millex GV) prior to injection in mice.

Brain Imaging: Mice were imaged using the University of Massachusetts

Medical School Small Animal Imaging Core using an IVIS Spectrum imaging

system. Mice were induced with isoflurane anesthesia (2% in 1 L/min oxygen),

then injected intraperitoneally with 4 μl of luciferin stock in PBS per gram of body

mass. Images were acquired as 2 minute exposures at 15 minutes after

intraperitoneal injection and analyzed using Living Image software. Regions of

interest (ROIs) were drawn around the region covering the brain, and the total

flux within each ROI was recorded. ROI sizes were identical across all images.

Graphs and statistics were generated using GraphPad Prism.

CHAPTER VIII:

Chimeras between Firefly Luciferase and Fatty Acyl-CoA Synthetases are Substrate-Selective Luciferases

Spencer T. Adams, Jr., et al. *Currently preparing for submission.*

Summary

To create their luminous display, fireflies oxidize the small-molecule D-luciferin with their enzyme firefly luciferase (Fluc). In addition to this bioluminescent activity, Fluc can attach coenzyme A to fatty acids, making it also a long-chain fatty acyl-CoA synthetase (ACSL). The latter activity hearkens to Fluc's evolutionary origins and, conversely, some ACSLs with homology to Fluc also emit light with synthetic luciferins. However, the relative intensity of light emission with these latent luciferases is much weaker than Fluc. To create luciferases with enhanced selectivity with synthetic luciferins and greater light emission, we created chimeras combining Fluc and ACSLs. These Fluc-ACSL chimeras were all capable of generating robust light output with synthetic luciferins, even when made with an ACSL that has no luciferase activity on its own. One of the chimeras generates greater light emission than Fluc in live cells and live mice. The chimeras detailed here highlight how ACSLs can augment bioluminescent reporter design for greater utility.

Introduction

Bioluminescence is the chemical production of light that results when a luciferase enzyme catalyzes the oxidation of a small-molecule luciferin to an excited-state product. This excited-state oxyluciferin next relaxes to the ground state, generating a photon. Bioluminescence's use of chemistry to accomplish light emission creates a reporter with a great signal-to-noise ratio (Weissleder and Ntziachristos, 2003.). Over half a century of inquiry has unraveled the identification of numerous unique luciferases and luciferins (White et al.,1963.; White et al., 1965.; McElroy et al., 1969.). Each luciferase and luciferin contributes to our growing knowledge of how bioluminescence works, while creating reporters useful for illuminating biology.

Fireflies are one of the best studied bioluminescent species. The broad emission spectra extending into red wavelengths and relative intensity of light emission make firefly bioluminescence an exceptional reporter for penetrating animal tissues (Zhao et al., 2005.). Elucidation of how firefly luciferase (Fluc) catalyzes light emission from the natural substrate D-luciferin thus becomes imperative to enhancing its utility through modifying the luciferase and luciferin. Fireflies emit light using a two-step reaction (Figure 8.1). D-luciferin is adenylated in the first step, then oxidized to the excited-state oxyluciferin product in the second step.
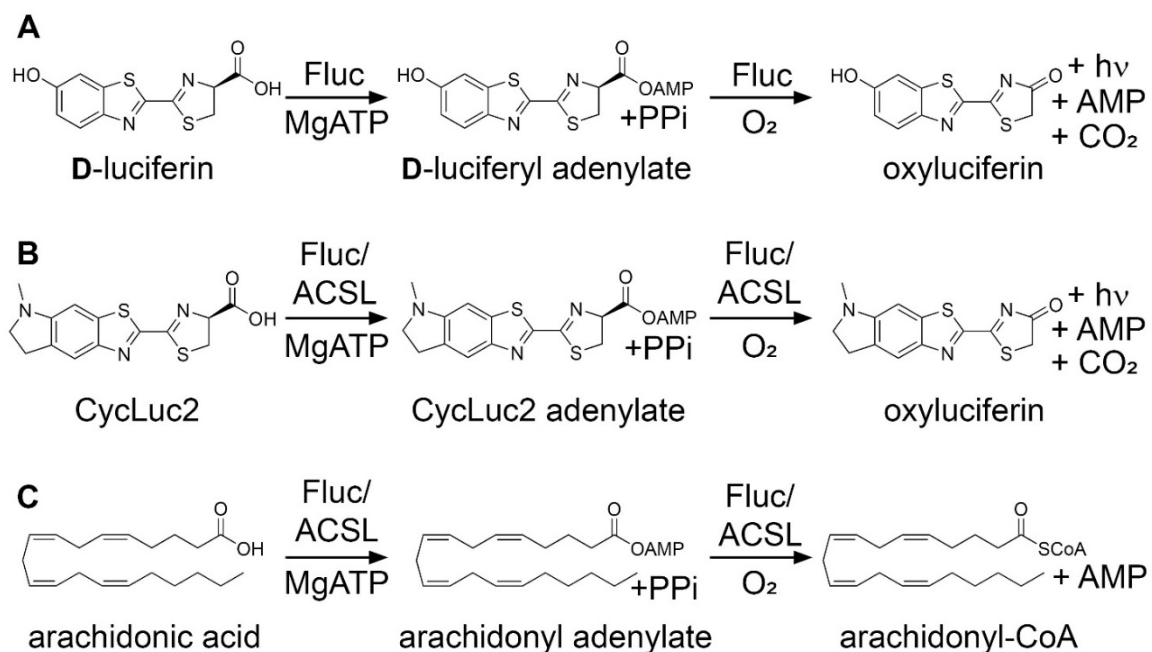
Figure 8.1. Firefly luciferase (Fluc) and some long-chain fatty acyl-CoA synthetases (ACSL) are bifunctional. A) Fluc catalyzes light emission with D-luciferin in a two-step reaction. D-luciferin is adenylated, then oxidized to make an excited-state oxyluciferin, which then relaxes to the ground-state to release a photon. B) Fluc and some homologous ACSLs catalyze light emission with synthetic luciferins, such as CycLuc2, following the same two-step reaction. C) Fluc and ACSLs catalyze the ligation of coenzyme A to fatty acids of appropriate length, such as arachidonic acid. The fatty acid is initially adenylated, then the AMP moiety is displaced to attach coenzyme A, yielding the fatty acyl-CoA product.

Interrogation of Fluc's enzymatic activity, coupled with the understanding of the enzyme's shared evolutionary history with insect long-chain fatty acyl-CoA synthetases (ACSLs), has opened a new area of inquiry about how bioluminescence works and how we might make novel reporters to expand the bioluminescent palette (Oba et al., 2004.; Oba et al. 2006.; Oba et al., 2009.;

Mofford et al., 2014., Mofford et al., 2017.). In addition to emitting light with luciferins, Fluc can also catalyze the ligation of coenzyme A to long-chain fatty acids (Oba et al., 2004.). This makes Fluc bifunctional, possessing both luciferase and ACSL activities. Some of these ACSLs bearing significant homology to Fluc are also latent luciferases, catalyzing light emission from synthetic luciferins (Mofford et al., 2017.). Such ACSLs with latent luciferase activity are found in *Drosophila menalogaster* (CG6178) and *Agrypnus binodulus* (*Agrypnus binodulus* luciferase like protein, AbLL), while an ACSL with similar homology to Fluc from *Pyrophorus angustus* (*Pyrophorus angustus* luciferase-like protein PaLL) exhibits no luciferase activity (Mofford et al., 2017.). The latent luciferase activity observed in CG6178 and AbLL are only revealed with synthetic luciferins, positioning them as candidates for creating orthogonal luciferases with suitable luciferins. However, their light output is poor compared to Fluc.

To create novel luciferases with unique substrate selectivity and improved brightness, we created chimeric luciferase-ACSL proteins. Fluc is a two-domain protein with a larger N-terminal domain and smaller C-terminal domain (Figure 8.2) (Conti, et al., 1996.). The N-terminal domain is primarily responsible for substrate binding, surrounding the substrate as seen in Figure 8.2. The C-terminal domain rotates relative to the N-terminal domain, presenting two catalytic lysine residues in each of two conformations: lysines 529 and 443 in Fluc's sequence, promoting adenylation and oxidation, respectively (Sundlov et al., 2012.).
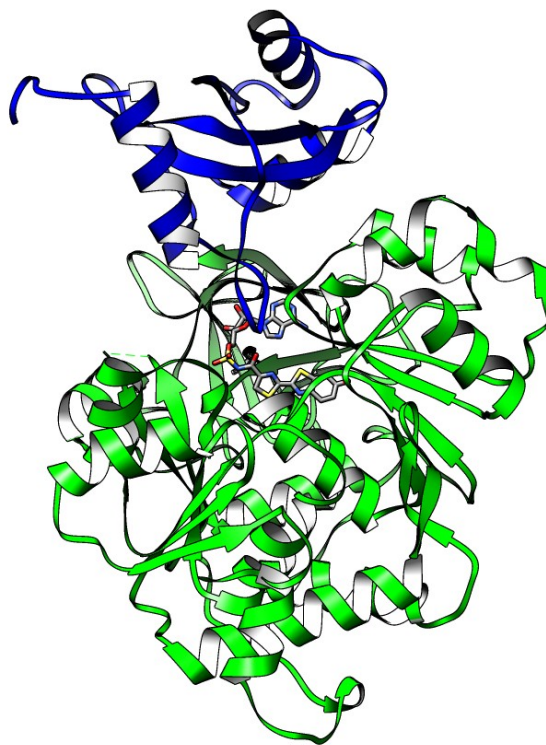
Figure 8.2. Firefly luciferase is a two domain protein. Firefly luciferase (PDB ID: 4G36 (Sundlov et al., 2012.) is shown with its N-terminal domain in green and C-terminal domain in blue. The non-hydrolyzable bisubstrate analog DLSA is shown at the interface of the two domains, where the luciferin is adenylated and oxidized to emit light. Figure prepared with UCSF Chimera (Petterson et al., 2004).

Previous attempts to create chimeras with Fluc and CG6178 had demonstrated

that modest luminescence with D-luciferin is achievable by splicing the C-

terminal domain of CG6178 to the N-terminal domain of Fluc at the linker region

(Arginine 437 in Fluc's sequence), while a chimera composed of CG6178's N-

terminal domain and Fluc's C-terminal domain was only able to function as an

ACSL (Oba et al., 2006.). We hypothesized that replacing Fluc's C-terminal

domain with the C-terminal domains from CG6178, AbLL, and PaLL would create unique luciferases selective for synthetic luciferins and with robust light emission.

Results and discussion

To gain a greater understanding of how the ACSLs homologous to Fluc might differ in their activity, we generated homology models of the enzymes to analyze how their active sites compare to Fluc (Figure 8.3) (Waterhouse et al., 2018.). Previous experiments had demonstrated that although AbLL shares greater homology with Fluc than CG6178, it has less luciferase activity when tested with a panel of synthetic luciferins (Figure 8.3) (Mofford et al., 2017.). PaLL also shares greater amino acid identity than CG6178 with Fluc but exhibits no luciferase activity with D-luciferin or synthetic luciferins (Table 8.1) (Mofford et al., 2017). The SWISS model we used to generate the homology models had great predictive power when we compared its results to our previously unpublished structure of CG6178 (Adams Jr. et al., *in preparation.*). CG6178's active site exhibits a unique protrusion that likely prevents proper alignment of D-luciferin relative to ATP for the adenylation step of bioluminescence chemistry (Adams Jr. et al., *in preparation.*). The SWISS model predicts this protrusion using only luciferase as a template to model CG6178's sequence (Figure 8.4). Interestingly, the homology models we created predict that the active site of PaLL would not permit luciferin to fit, while the model for AbLL shows a similar active site to Fluc

(Table 8.1). This correlates with our experimental observations. The Models also predict conservation of the lysine residues the C-terminal domain must contribute for its role in bioluminescence. The model of AbLL shows an active site further constricted beyond what we saw in CG6178, possibly explaining its poorer performance as a luciferase. Additionally, the model of PaLL predicts an active site that would not permit luciferin to interact with ATP for the adenylation step. It is not clear if PaLL can even bind luciferin based on our model. The model predicts a small tunnel that would permit a fatty acid chain to bind and attack ATP, consistent with its native activity.
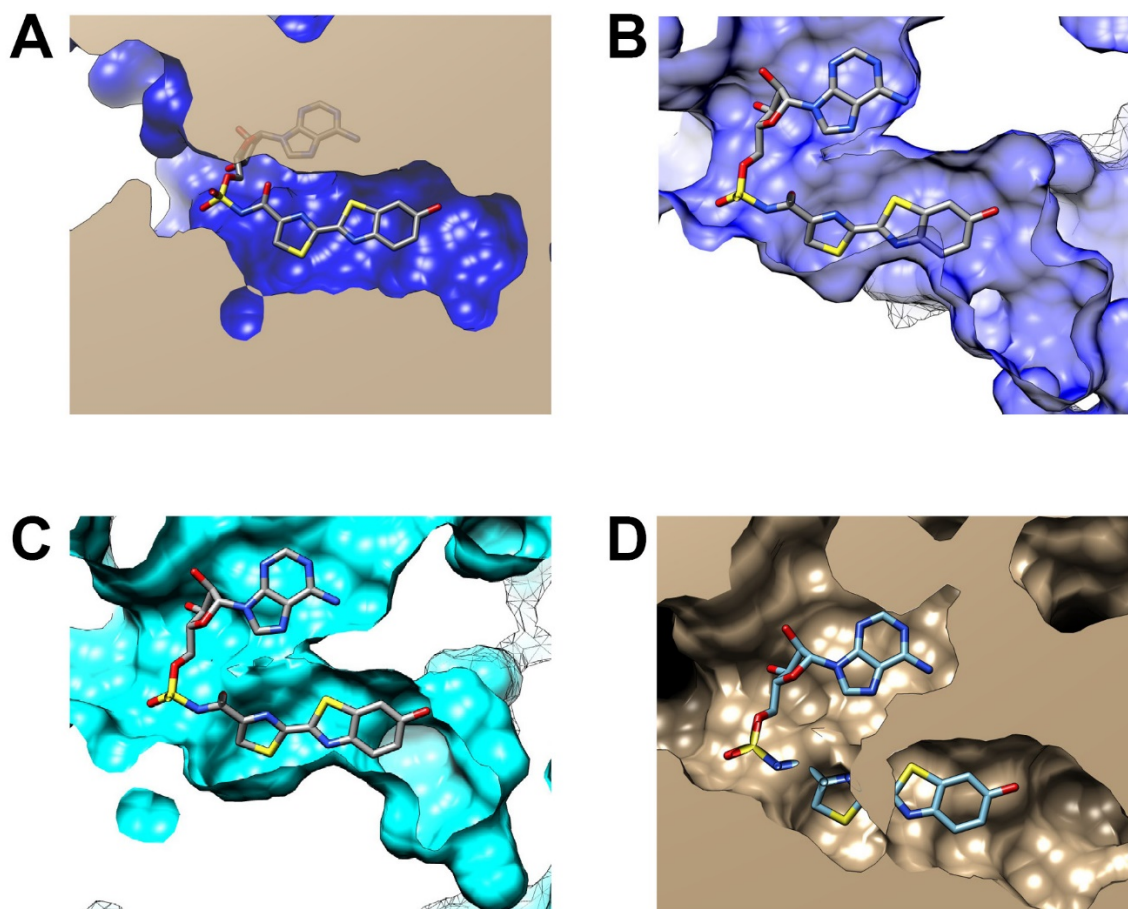
Figure 8.3. Comparison of homology models for AbLL and PaLL active sites with firefly luciferase and CG6178. The SWISS model was used to generate models of AbLL and PaLL for comparing their active sites with firefly luciferase and CG6178 (Waterhouse et al., 2018.). Firefly luciferase's active site (Panel A) is less constricted than CG6178's (panel B). AbLL's active site (panel C) is predicted to be smaller than CG6178's. PaLL's active site (panel D) is only predicted to have a small tunnel that would accommodate a fatty-acid chain, but would prevent luciferin binding and/or adenylation. Images were produced using UCSF Chimera (Petterson et al., 2004).

Percent Amino Acid Identity Between Proteins

	PaLL	CG6178	AbLL
Fluc	47	42	46
AbLL	61	44	
CG6178	46		

Table 8.1. Percent amino acid identity between firefly luciferase and the ACSLs used to make chimeras.
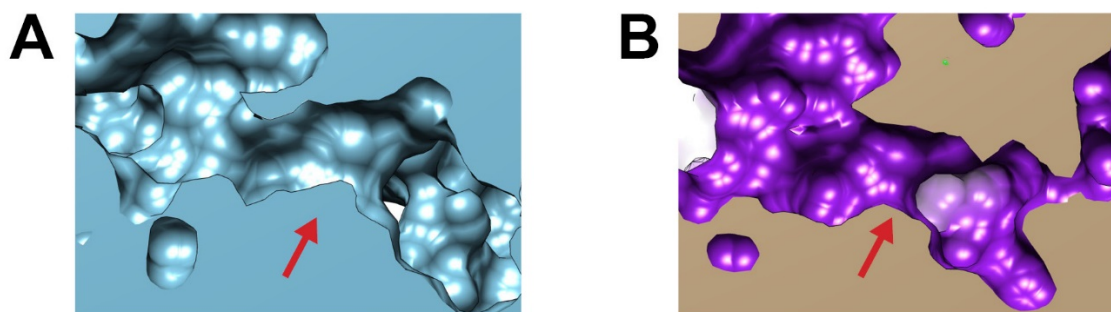
Figure 8.4 SWISS Model predicts the protrusion in CG6178 we observed experimentally. The left panel shows our CG6178 structure determined using x-ray crystallography (Adams et al. *in preparation.*). The right panel shows a homology model of CG6178 prepared using the SWISS model (Waterhouse et al., 2018.)with Fluc (PDB ID:4G36) as a template for CG6178's sequence. The red arrows show the location of a protrusion that we predict is responsible for CG6178's inability to emit light with D-luciferin. Images were produced using UCSF Chimera (Petterson et al., 2004).

We aligned the sequence of Fluc with the sequences of AbLL, CG6178, and

PaLL, then identified the residues forming the linker (Figure 8.5). The chimeric

luciferases were created by attaching the C-terminal domain from each of the

ACSLs with the N-terminal domain of Fluc. We used Gibson assembly to create

the chimeras following amplification of these domains (Figure 8.6). These

chimeras will be referred to as Fluc/AbLL, Fluc/CG6178, and Fluc/PaLL.
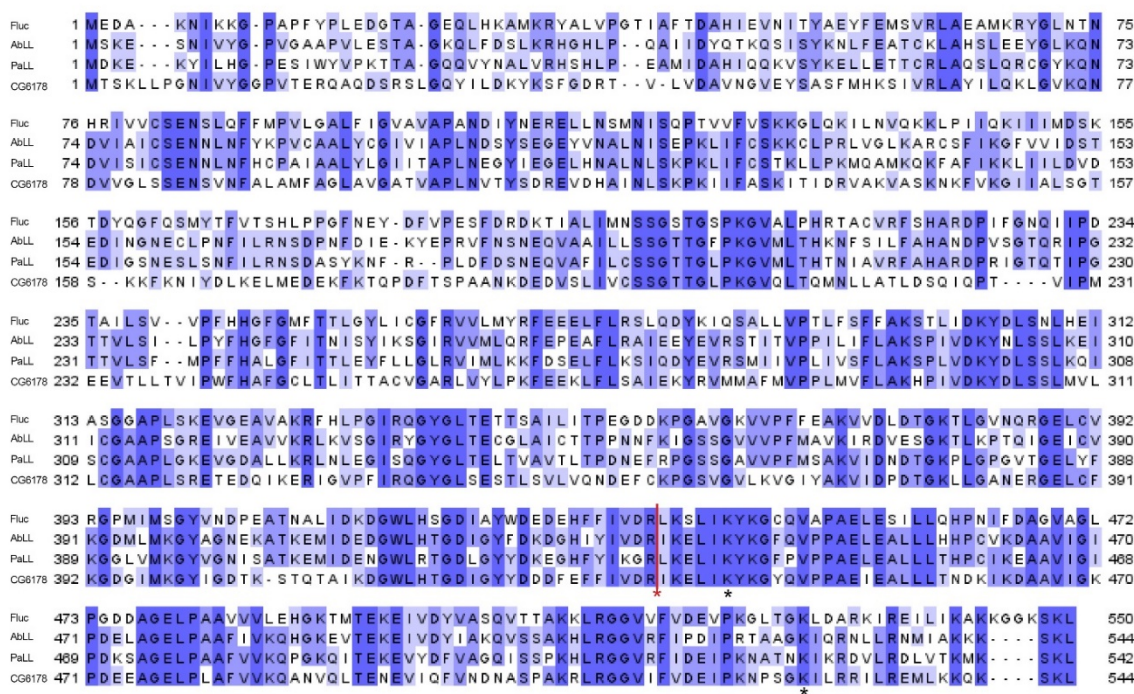
Figure 8.5. Luciferase shares homology with insect ACSLs. Sequences for *Photinus pyralis* luciferase, *Agrypnus binodulus* luciferase-like protein (AbLL), *Pyrophorus angustus* luciferase-like protein (PaLL), and *Drosophila melanogaster* long-chain fatty acyl-CoA synthetase CG6178 (CG6178) were aligned using MUSCLE. Darker shades of blue represent greater homology. The junction where the N-terminal domains and C-terminal domains are represented by a red vertical line and red asterisk. Black asterisks indicate locations of the two C-terminal catalytic lysines.
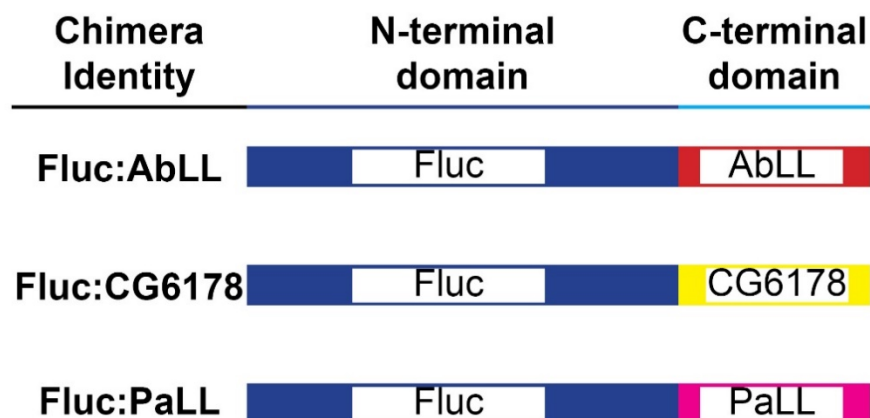
Figure 8.6. Chimera design strategy. The N-terminal domain of Fluc (residues 1-436) were joined to C-terminal domains of *Agrypnus binodulus* luciferase-like protein (AbLL), *Drosophila melanogaster* CG6178 (CG6178), and *Pyrophorus angustus* luciferase-like protein (PaLL), at the junction indicated for the linker residues in alignments from Figure 8.5.

Once the chimeras were made, we tested their *in vitro* activity. Purified enzyme was mixed with either D-luciferin or CycLuc1 (Figure 8.7) across a concentration range from 0.122 μM to 250 μM to measure the dose-response of luciferase activity with these substrates (Figure 8.8). The chimeras all emit measurable light in a dose-dependent manner with D-luciferin, albeit at lower intensity than Fluc. The best performing of these chimeras with D-luciferin was Fluc/CG6178, which emits 15-fold less light than WT luc2 at 250 μM substrate concentration. At this concentration of D-luciferin, Fluc/CG6178 emits about 5-fold greater flux than Fluc/AbLL, which emits slightly less than 3-fold greater flux than Fluc/PaLL. With 250 μM CycLuc1, WT luc2 and Fluc/AbLL perform comparably and both emit about 2-fold greater flux than both Fluc/CG6178 and Fluc/PaLL. However, none

of these enzymes obey Michaelis-Menten kinetics with CycLuc1, rather exhibiting

similar amounts of light emission at all concentrations measured.

D-luciferin   CycLuc1
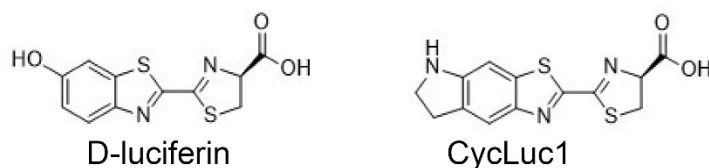
Figure 8.7. Luciferins used for experiments. D-luciferin and CycLuc1 were
used to test the selectivity and relative brightness of light emission among the
chimeras.
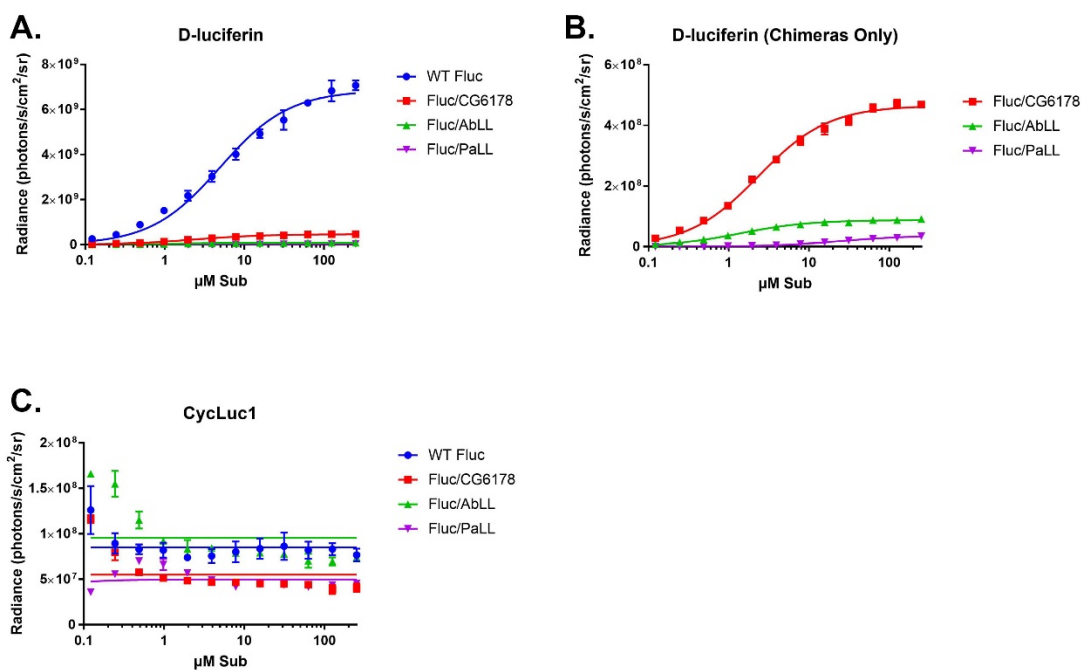
Figure 8.8. *In vitro* performance of luciferase-ACSL chimeras. Fluc and
chimeras were tested in vitro for light emission with D-luciferin and CycLuc1. A)
Dose-response of WT Fluc, Fluc/CG6178, Fluc/AbLL, and Fluc/PaLL with D-
luciferin. B) Same as A, but with WT Fluc removed for scale showing chimeras.
C) Dose-response of WT Fluc, Fluc/CG6178, Fluc/AbLL, and Fluc/PaLL with
CycLuc1.

Despite all of the C-terminal domains used to generate the chimeras contain the conserved catalytic lysines needed to promote adenylation and oxidation of luciferin, the chimeras vary in their activities with D-luciferin and CycLuc1. Though Figure 8.3 shows the differences in active sites for AbLL, CG6178, and PaLL, these models are for the whole protein. The luciferin is binding within the N-terminal domain (Figure 8.2), so we expect differences in activity would be the result of how the C-terminal domain promotes the adenylation and oxidation reactions. The structures of AbLL and PaLL would be helpful in analyzing their C-terminal domains. The differences in activity between the chimeras may be a result of changes in domain-domain interactions between the different C-terminal domains from each ACSL with the N-terminal domain of Fluc. Though we achieved activity with all the chimeras, the differences in the ACSL C-terminal domains relative to Fluc represent divergent paths in evolution to specialize in acting on distinct substrates.

Next, we tested the performance of the Fluc-ACSL chimeras in live cells (Figure 8.9). We transfected Chinese hamster ovary (CHO) cells with vectors containing either WT luc2 or one of the three chimeras. Once expressing these enzymes, we tested the enzymes' performance over a range of substrate concentrations by adding either D-luciferin or CycLuc1 from 0.122 µM to 250 µM and measuring light emission with an IVIS Spectrum instrument. D-luciferin generates greater radiance than CycLuc1 at saturating substrate concentration with WT luc2.

However, CycLuc1 yielded greater radiance at all measured concentrations with all three of the chimeras. Unexpectedly, Fluc/CG6178 generated greater radiance than WT luc2 with CycLuc1 at higher substrate concentrations. Additionally, the chimeras exhibit a lower apparent Km with CycLuc1 than with D-luciferin. Western blots were used to gauge the relative expression of the chimeras relative to Fluc within CHO cells and showed that Fluc/CG6178 was present in greater quantities than the other two chimeras, possibly explaining its exceptional performance (Figure 8.10).
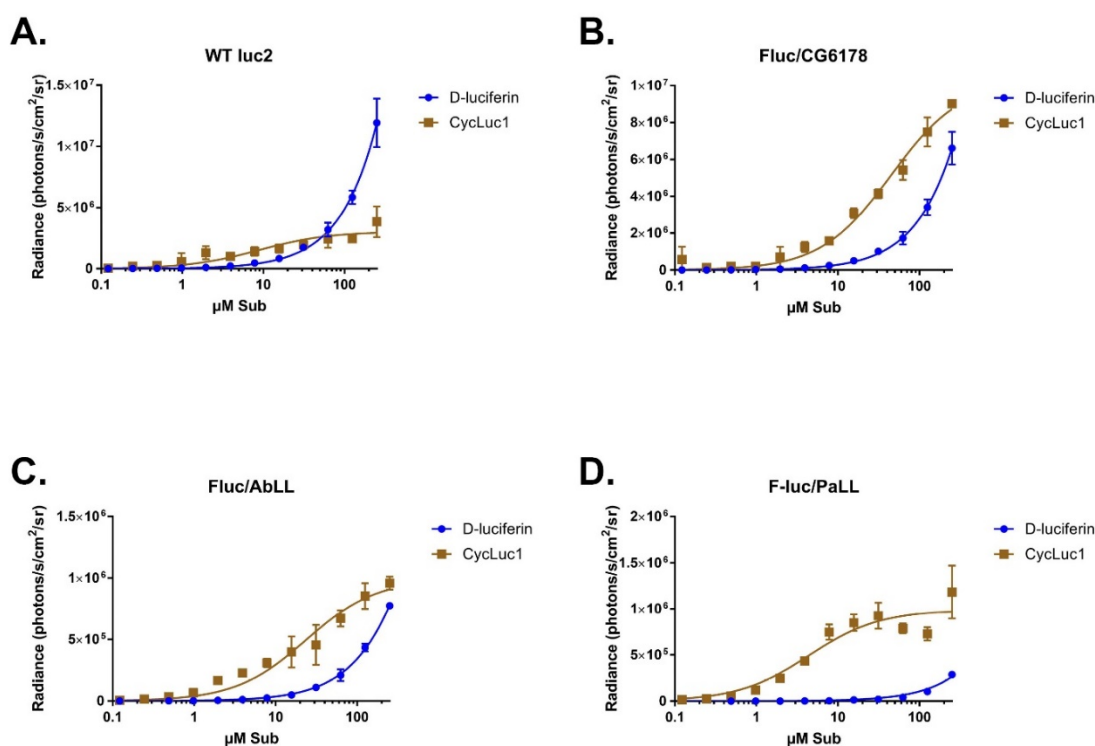
Figure 8.9. Live cell performance of luciferase-ACSL chimeras. Dose-response with D-luciferin and CycLuc1 in live CHO cells for: A) Luc2 (optimized version of Fluc) B) Fluc/CG6178 chimera C) Fluc/AbLL and D) Fluc/PaLL. Graphs are not on the same scale.
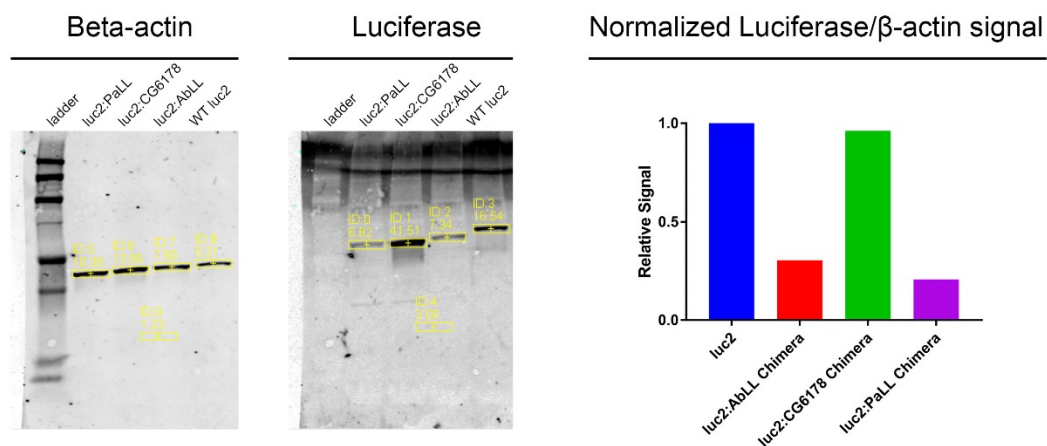
Figure 8.10. Western blots of CHO cell lysates show Fluc/CG6178 chimera is present in greater quantities than the other two chimeras. A Western blot of CHO cell lysates showed that, controlling for beta-actin levels, Fluc/CG6178 chimera was present in quantities similar to Fluc, while the Fluc/AbLL and Fluc/PaLL chimeras were present in approximately three to four-fold lower quantities.

Encouraged by the unexpected robust light emission with Fluc/CG6178 and the

other chimeras in live cells, we turned to using these enzymes for bioluminescent

imaging in live mice (Figure 8.11). We employed an intranasal instillation of

adeno-associated viral (AAV) vector containing either WT luc2 or one of the three

chimeras to establish expression of each enzyme. Once the mice were

expressing their respective enzymes, we administered either D-Luciferin or

CycLuc1 on separate imaging days and measured light emission using an IVIS

Spectrum instrument. Mice expressing WT luc2 produced more light with D-

Luciferin than with CycLuc1, which we would expect in peripheral tissues. Similar

to the preference for CycLuc1 in live cells, mice expressing the Fluc/AbLL chimera preferred CycLuc1 over D-Luciferin by about 2-fold. Mice expressing the Fluc/CG6178 chimera exhibited even more selectivity for CycLuc1 over D-Luciferin, emitting about 7-fold greater radiance with the synthetic luciferin. Further, the mice expressing the Fluc/CG6178 chimera emit more light with CycLuc1 than WT luc2 with D-Luciferin. Mice expressing the Fluc/PaLL chimera emit measurable light with CycLuc1, but little to no light with D-luciferin. The exceptional performance of the Fluc/CG6178 chimera may be explained by its greater expression and/or stability leading to greater quantities of the enzyme *in vivo*, as we had seen with our Western blot data. However, all of the chimeras are capable of bioluminescence imaging in live mice, even when composed of the C-terminal domain from PaLL, an enzyme with no luciferase activity as a complete enzyme.
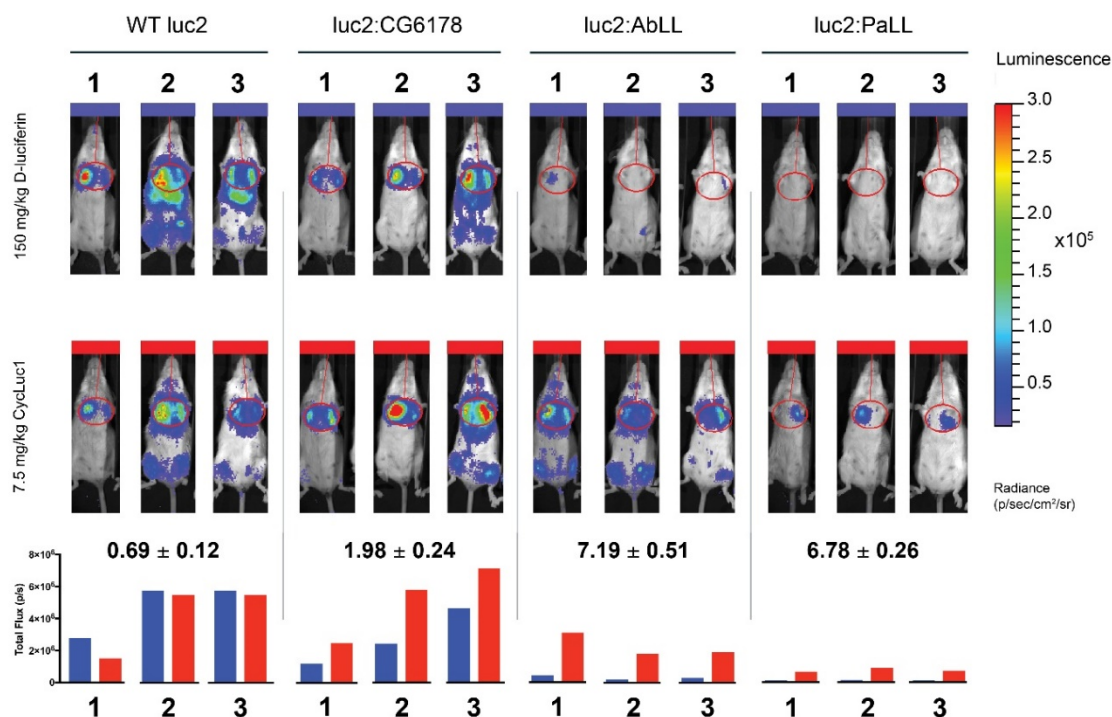
Figure 8.11. Luciferase-ACSL chimeras emit robust light in live mice with the synthetic luciferin CycLuc1. Codon-optimized wild-type firefly luciferase and the three chimeras were expressed in live mouse lung following intranasal instillation with adeno-associated viral vectors. Mice were then injected intraperitoneally with either D-luciferin (blue bars on graph) or CycLuc1 (red bars on graph) on separate days and imaged with an IVIS instrument to measure flux. All images are scaled the same. Flux was then compared mouse by mouse for each substrate to represent the relative performance with these two substrates between enzymes. Numbers indicate the CycLuc1/D-luciferin average ratio +/- standard deviation.

Conclusion

Bioluminescence is a powerful tool for illuminating biology. As we gain a greater understanding of how bioluminescence works on a molecular level, we simultaneously open avenues for improved reporters. One application where

bioluminescence excels is in live animals, where a robust signal and lack of background improve the sensitivity of measurement (Prescher et al., 2010). Unfortunately, due to animal tissues' light absorption properties, resolution of spectrally distinct signals is technically difficult (Weissleder and Ntziachristos, 2003.; Jones et al., 2017.) However, orthogonal luciferase-Luciferin combinations that retain robust light emission can be temporally resolved for measurement of separate processes within the same animal. The chimeras detailed in this manuscript are selective for synthetic luciferins while still achieving bright emission, even outperforming the commercially-available luc2 with D-Luciferin as in the case of the luc2:CG6178 chimera with CycLuc1 in live mouse lung. The relative performance of luc2:CG6178 to WT luc2 was unexpected, but underlines the potential for improved bioluminescent reporters based on the emerging group of latent luciferases that share homology with Fluc. Homology modeling predicts that the N-terminal domains are different between the ACSLs we used to derive the chimeras. Though the C-terminal domains are interchangeable to make functional luciferases, the N-terminal domains appear to have diverged more in the evolution of Fluc, permitting the relatively bulky luciferin substrate to occupy a tunnel previously evolved to accommodate fatty acids.

Protocols and Methods

Contributions

S.T.A. Jr. devised experiments, helped design chimeras, performed live cell experiments, performed all mouse experiments, and prepared the manuscript. D.M.M. devised experiments, designed chimeras, and performed purified enzyme experiments. G.R.R. and G.S.K.K.R. designed and synthesized luciferins. S.C.M. devised experiments.

General

Chemicals were purchased from Aldrich, Matrix Scientific, Oakwood, or TCI. ATP was purchased from both MP Biomedicals and Sigma. D-luciferin was obtained from Gold Bio. CycLuc1 was synthesized as previously described (Reddy et al., 2010). Data were plotted with GraphPad Prism. Plasmid constructs The DNA sequences for long-chain fatty acyl-CoA synthetases CG6178, AbLL, and PaLL were codon optimized for mammalian expression, synthesized by GenScript, and cloned into the BamHI–NotI sites of pGEX6P-1. WT luc2 luciferase was used in pGEX6P-1 as previously described (Mofford et al., 2014).

Plasmid constructs

The DNA sequences for long-chain fatty acyl-CoA synthetases CG6178 and AbLL were codon optimized for mammalian expression, synthesized by GenScript, and cloned into pGEX6P-1. WT luc2 luciferase was used as previously described (Mofford et al., 2014). Plasmid constructs containing the chimeric enzymes were generated using Gibson Assembly (NEB). Fragments of each cDNA corresponding to the desired region of each enzyme were PCR

amplified and purified via agarose gel purification. PCR primers were designed to give overlapping ends of complementary DNA with the adjacent fragment of DNA for that chimera, per Gibson Assembly instructions. Each DNA fragment and pGEX6P-1 plasmid digested with BamHI and NotI were incubated with Gibson Assembly master mix per the manufacturer's instructions to generate the final combined constructs.

Enzyme expression and purification

Luciferase and chimeras were expressed and purified as GST-fusion proteins from the pGEX6P-1 vector as previously described (Mofford et al., 2014). Briefly, JM109 cells were grown at 37 °C until the OD600 reached 0.5-1, induced with 0.1 mM IPTG, and incubated with shaking at 20 °C overnight. Cells were pelleted at 5000 RPM, then flash frozen in liquid nitrogen. The E. coli pellets from 1 L of culture were thawed on ice, resuspended in 25 mL lysis buffer (50 mM Tris [pH 7.4], 500 mM NaCl, and 0.5% Tween 20) containing 1 mM phenylmethylsulfonyl fluoride, and disrupted by sonification (Branson Sonifier). Dithiothreitol (DTT) was added at 10 mM, and the resulting cell lysate was clarified by centrifugation at 35,000 RPM for 60 min at 4 °C. The supernatant was batch-bound to immobilized glutathione (Thermo Scientific) for 1 hr at 4 °C, and the beads were washed with lysis buffer containing 10 mM DTT, followed by wash buffer (50 mM Tris [pH 8.1], 250 mM NaCl, and 10 mM DTT) and storage buffer (50 mM Tris [pH 7.4], 0.1 mM EDTA, 150 mM NaCl, 1 mM TCEP). Twenty units of PreScission Protease (GE Healthcare) were added, and incubation continued

overnight at 4 °C to cleave the GST-fusion and elute the untagged enzyme.

Protein concentrations were determined using Coomassie Plus (Thermo

Scientific).

Purified protein luminescence assays

Luminescence assays were initiated by adding 30 µL of purified luciferase in

enzyme buffer (20 mM Tris [pH 7.4], 0.1 mM EDTA, 1 mM TCEP, and 0.8 mg/mL

BSA) to 30 µL 2x substrate in substrate buffer (20 mM Tris [pH 7.4], 0.1 mM

EDTA, 8 mM $MgSO_4$, and 4 mM ATP) in a black 96-well plate (Costar 3915).

Imaging was performed one minute after enzyme addition using a Xenogen IVIS

100 at a final enzyme concentration of 20 nM and final substrate concentrations

ranging from 0.122 µM to 250 µM. Data acquisition and analysis was performed

with Living Image software. Data are reported as total flux (p/s) for each ROI

corresponding to each well of the 96-well plate.

Cell culture

Chinese hamster ovary (CHO) cells were grown in a CO_2 incubator at 37°C with

5% CO_2 and were cultured in F-12K Nutrient Mixture (GIBCO) and Dulbecco's

Modified Eagle's Medium (DMEM) (GIBCO), respectively. Both media were

supplemented with 10% fetal bovine serum and 100 U/mL penicillin/streptomycin.

Transfections

CHO cells were transfected with codon-optimized firefly luciferase (luc2) as previously described (Mofford et al., 2014). Transient transfections were performed at room temperature using Lipofectamine 2000 on cells plated at 60%–75% confluency in 96-well black tissue culture treated plates (Costar 3916). 0.075 µg DNA/well of pcDNA3.1-luc2 was transfected into CHO cells. Assays were performed in triplicate 24 hrs after transfection.

Western blotting

Media was aspirated from transfected wells in 6-well plates, then PBS added to wash. Ice-cold PBS was used to collect cells with a scraper and transferred to a conical tube. Cells were pelleted, then PBS supernatant removed. Lysis buffer was added and the pellet sonicated. Protein quantity was measured, then lysates were run with SDS-PAGE. Protein was transferred to a nitrocellulose membrane. After blocking the membrane (50:50 mix of Odyssey blocking buffer and TBS), the membrane was rinsed 3X with TBST. The membrane was incubated with primary antibodies for beta actin (Cell Signalling Technology 3700P anti-beta-actin mouse 1:1000) and luciferase (Abcam ab21176 anti-luciferase rabbit, 1:1000 in 1:1 TBST:Odyssey blocking buffer). The membrane was rinsed with TBST 3X. The membrane was incubated with secondary antibodies (LI-COR IRDye 680LT Goat anti-Rabbit 1:20000 and LI-COR IRDye 800CW Goat anti-Mouse in 1:1 TBST:Odyssey blocking buffer), then rinsed 3X with TBST. Imaging was performed with a LI-COR Odyssey.

Live cell imaging

Tissue culture media was removed from CHO cells 24 hrs post-transfection. 60 µl HBSS was added to each well to wash, then removed. 60 µl of substrate was added to each well. Substrate concentrations range from 250 µM to 0.122 µM across the twelve wells of a 96 well-plate, by two-fold dilutions in each successive column. Each substrate concentration was measured in triplicate for each enzyme. After a one minute hold, cells were imaged with an IVIS imaging system. Data acquisition and analysis were done using Living Image software to calculate radiance for each individual well. These values were then analyzed with Graphpad Prism.

Mice

All of the experiments involving mice were conducted in accordance with the Institutional Animal Care and Use Committee of The University of Massachusetts Medical School (docket #A-2474-14). FVB mice were ordered from Jackson Labs. AAV9 vectors containing each chimera and luc2 were prepared in sterile PBS in sufficient quantity to yield 1E11 viral particles in a 50 µl aliquot per mouse. Mice were anesthetized with ketamine/xylazine. Once mice no longer exhibited a toe-pinch response, these vectors were instilled dropwise into anesthetized mice's noses, alternating between the two nostrils. This was achieved by holding the mice upright, with their heads at a 90 degree angle to their body (head parallel with the ground) to allow them to inhale the PBS-vector

solution. As the mice inhaled each drop of the PBS-vector solution, another drop was added to the alternate nostril until the full 50 µl dose was delivered. Once each mouse had inhaled their vector dose, they were kept warm in their cages on a heat mat until recovered.

Mouse Imaging

Prior to mouse imaging, luciferins were prepared in sterile saline at the appropriate concentration (100 mM for D-luciferin sodium salt and 5 mM CycLuc1). Mice were anesthetized using isoflurane, inducing in a chamber outside the IVIS imaging cabinet. Once anesthetized, they were placed into the IVIS imaging cabinet, which has a warmed stage (37 °C) and a manifold with nosecones dispensing isoflurane to maintain anesthesia. Mice were imaged prior to injection of luciferin to establish background signal, then injected intraperitoneally with either 100 mM D-luciferin or 5mM CycLuc1 (4 µl / gram body mass). Mice were subsequently imaged post-injection to measure light emission. The data acquisition and analysis were performed with Living Image software. Identical sized regions of interest were drawn over the lungs of mice to calculate the radiance. The same mice were imaged with both substrates for comparison on separate imaging days.

CHAPTER IX:

Discussion

The glow of bioluminescent organisms has captivated the public's imagination throughout history, illuminating landscapes from the night sky to the depths of the ocean. Bioluminescence is the chemical production of light by a luciferase enzyme oxidizing a small-molecule luciferin. Numerous divergent species have independently evolved the ability to make their own light chemically as selective pressures have fixated the feature for unique ecological benefits (Fallon et al.; 2018.; Petushkov et al., 2014.; Davis et al., 2016.;. Kaskova et al., 2017.; Kaskova et al., 2016.). Many of these unique luciferins and luciferases have been characterized in the last century, while some are the subject of current investigation (Kaskova et al., 2016.). How all of these luciferases and luciferins work on a molecular basis is the subject of active research in an effort to create useful reporters for laboratory use. My thesis aims to expand the bioluminescent toolkit, focusing on two key areas: 1. Improving the in vivo bioluminescent toolkit by characterizing synthetic luciferins capable of producing more robust output than commercially available reporters and pro-luciferins that can report on secondary enzymatic activities in live animals and 2. Characterizing and enhancing the latent luciferase activity in fatty acyl-CoA synthetases that share homology with firefly luciferase as novel platforms for bioluminescent reporter development.

Bioluminescence is frequently used in biological research to illuminate processes *in vitro,* in cells, and in live animals. Because bioluminescence employs chemistry to achieve light output, this circumvents the need for exogenous light sources. Therefore, bioluminescence can capitalize on this lack of extraneous light sources to improve its

signal to background ratio, providing a sensitive imaging modality (Prescher et al., 2010.; Dothager et al., 2009.; Zhao et al., 2010.). This is particularly useful in the context of live animal imaging, permitting measurement of processes within deep tissues (Prescher et al., 2010.; Dothager et al., 2009.; Zhao et al., 2010.).

The chemical nature of bioluminescence also presents limitations. In live animals, luciferins must access the tissues that express luciferase to achieve light emission. For example, the firefly's natural substrate D-luciferin is actively pumped out of the blood-brain barrier by ABCG2 pumps (Zhang et al., 2007.). In addition to the requirement for luciferins to access luciferase, the marine luciferin coelenterazine is prone to auto-oxidation, diminishing the lack of background that makes bioluminescence so attractive (Otto-Duessel et al., 2006.).

My thesis research builds on the growing bioluminescent toolkit for research use, highlighting how synthetic luciferins, mutant luciferases, and specific long-chain fatty acyl-CoA synthetases work on a molecular level and how they can be employed for use in live animal research. In CHAPTER II, we see how the synthetic luciferin, CycLuc1, generates a signal greater than what is possible with D-luciferin in live mouse brain, even when administered at 20-fold lower substrate concentration (Evans et al., 2014.). We used multiple mouse models for complementary *in vivo* experiments to compare CycLuc1 to D-luciferin, including: mice expressing luciferase in brain striatum following adeno-associated viral delivery, mice expressing luciferase in xenografted cells, transgenic mice expressing luciferase ubiquitously, and transgenic mice expressing luciferase in only dopaminergic neurons contained within the substantia nigra. These experiments detail how CycLuc1 can outperform D-luciferin in tissues where substrate

access is a limiting factor. In transgenic mice expressing luciferase under control of the

dopamine transporter promoter, CycLuc1 generated measurable light emission,

demonstrating the ability for this synthetic luciferin to facilitate longitudinal

bioluminescent experiments not previously possible with the natural D-luciferin

substrate.

This is not to say that the synthetic luciferin CycLuc1 is superior to the natural D-

luciferin substrate for all *in vivo* imaging applications. In tissues more easily accessed by

D-luciferin, such as superficial mouse tissues expressing luciferase, D-luciferin can

generate a stronger signal than achievable with CycLuc1 (Evans, et al., 2014.; Mofford

et al., 2015.). Thus, different imaging scenarios can benefit from a broad palette of

bioluminescent reporters optimized for disparate conditions.

In addition to providing more robust light emission than the natural substrate in

some tissues, synthetic luciferins can also be modified to reveal secondary enzymatic

activities (Miska et al., 1987.; Miska et al., 1988.; Geiger et al., 1992., Monsees et al.,

1994.; Wehrman et al., 2006.). We demonstrate this in CHAPTER III, where we created

luciferin amides that serve as luminescent reporters of endogenous fatty-acid amide

hydrolase (FAAH) activity in live mice (Mofford et al., 2015.). The FAAH enzyme is an

important drug target that catalyzes the breakdown of anandamide. Inhibiting this

enzyme has the potential to promote analgesia, but identifying selective inhibitors for *in*

vivo use had historically required sacrificing animals to process tissues for analysis

(Long et al., 2011.). By converting a luciferin's carboxyl group to an amide, they become

pro-luciferins that luciferase is unable to adenylate. We hypothesized such pro-luciferins

would require FAAH's activity for conversion into a luciferin that luciferase could then

adenylate and subsequently oxidize for light emission. In CHAPTER III, we show how these luciferin amides selectively report on FAAH activity and inhibition in live mice in real time (Mofford et al., 2015.). We tested luciferin amides *in* vitro and found that recombinant FAAH enzymes were capable of converting the pro-luciferins to luciferins. Cells that endogenously express FAAH also catalyzed light emission when supplied luciferin amides and responded to FAAH inhibitors via decreased light emission with luciferin amides. Interestingly, these luciferin amides achieved much greater light emission than the parent luciferins in live mouse brain, despite administration at much lower dosages. This reinforces the concept that chemical modification to luciferins can improve their access to some tissues in live animals. The luciferin amides behave like drugs, facilitating the transport of the parent compound into the brain. Considering FAAH's association with membranes for internalizing endocannabinoids (Day et al., 2001.), this presents a powerful paradigm for improved bioluminescent reporter design. The theme of chemical modification of synthetic luciferins to create prodrugs is not novel (Miska et al., 1987.; Miska et al., 1988.; Geiger et al., 1992., Monsees et al., 1994.; Wehrman et al., 2006.) and I expect that exploring more modifications holds promise for creating more selective reporters of endogenous enzymatic activities in cells and live animals. It would be helpful to test if pro-luciferins are impacting the native function of the protein they are interacting with, to avoid confounding variables with experiments. For example, measuring for analgesic phenotypes in mice following exposure to an amide prodrug would be helpful.

In CHAPTERS IV and V (Sharma et al., 2017.; Sharma et al., 2019.), I detail a large panel of novel luciferin analogs that greatly expands the structure space we can explore with complementary luciferases and live animal models. These novel luciferins

help us to greater appreciate what constitutes a luciferin, a theme that depends on the corresponding luciferase we are testing with these compounds. Many of the luciferin analogs exhibit weak light emission, but what constituted a bright luciferin was not always intuitive. The approach of increasingly larger and varied functional groups attached to the core luciferin scaffold allows us to directly assay a luciferase, luciferase mutant, or latent luciferase for activity. A greater diversity of synthetic luciferins increases the capacity for identifying robust and selective reporters with complementary luciferase enzymes. Additionally, some of these luciferins behaved as inhibitors (Sharma et al., 2017.). As more enzymes with latent luciferase activity come to light, these luciferins can serve as tools for interrogating the biochemical intricacies of substrate preference.

Previous work in the lab had identified multiple mutants of firefly luciferase that selectively utililize synthetic luciferin analogs (Harwood et al., 2011.). The firefly luciferase mutants Arginine 218 to Lysine (R218K), Leucine 342 to Alanine (L342A), and the double mutant combining these two mutations had demonstrated selectivity for synthetic luciferins in experiments *in* vitro and in live cells (Harwood et al., 2011.). However, it was not clear how this selectivity would translate to use in live animal models. In CHAPTER IV, we tested these luciferase-luciferin pairs' performance *in vivo* (Adams Jr. et al., 2016.). We used AAV delivery of these enzymes to mouse striatum and compared their relative performance with CycLuc1 and CycLuc2, as well as their amide derivatives to the natural D-luciferin substrate and with wild-type firefly luciferase. Despite emitting no measurable light output with D-luciferin, we found that the L342A mutant catalyzed light emission comparable to or greater than WT luciferase with 400 μmol/kg D-luciferin when we administered 0.4 μmol/kg CycLuc2-amide (1000-fold lower

dose of luciferin amide) (Adams Jr. et al, 2016.). Alternatively, L342A emits virtually no light output with D-luciferin in live mouse brain. This highlights how *in vivo* conditions in mouse brain can enhance the selectivity observed with luciferase-luciferin pairs when translated from *in vitro* or live cell experiments, due to the threshold of light needed for measurable signal. Though selectivity was achieved by our reporters, they are still not orthogonal. Due to the shared evolutionary origins of Fluc and some insect long-chain fatty acyl-CoA synthetases (Oba et al., 2003.; Oba et al., 2004.), combined with their newfound latent luciferase activity only when provided synthetic luciferins (Mofford et al., 2014.), we next considered them as a novel platform for selective luciferase-luciferin development.

Enzymes homologous to firefly luciferase from other insects can selectively catalyze light emission with synthetic luciferins (Mofford et al., 2014.; Mofford et al., 2017.). One of the best characterized of these enzymes is the fruit fly long-chain fatty acyl-CoA synthetase CG6178, whose latent luciferase activity was revealed when our lab screened for activity with some of our synthetic luciferins (Oba et al., 2004.; Mofford et al., 2014.). CG6178 is unable to catalyze light emission with D-luciferin, but emits modest light output with the synthetic luciferin CycLuc2 (Mofford et al., 2014.). To interrogate CG6178's discrimination between D-luciferin and CycLuc2, I determined the structure of the enzyme. In CHAPTER VII, I report the first structure of CG6178. Efforts to co-crystallize CG6178 with CycLuc2 were not successful, but our CG6178 structure highlighted differences in the fatty-acid-binding tunnel that formed the basis of mutagenesis experiments. Initially, we performed mutagenesis to residues that surrounded the active site and found that one region spanning residues 342-347 provided the greatest improvement of CG6178's luciferase activity. When we compared

this region of CG6178's active site with Fluc, we noticed CG6178 has a unique

protrusion in its active site that we hypothesize prevents suitable alignment of D-luciferin

with ATP for the adenylating step. This misalignment of the luciferin relative to ATP,

should it prevent adenylation, would preclude its subsequent oxidation and light

emission. Experiments had already established that CG6178 can oxidize pre-adenylated

D-luciferin and emit light without the adenylation chemistry as a catalytic barrier, lending

credence to this hypothesis (Mofford et al., 2014.). Why CG6178 is able to adenylate

CycLuc2 is not clear, but I hypothesize that the rigid extra cyclic group acts as a handle

to place the appropriate carboxyl group in proximity to the alpha phosphate of ATP for

productive adenylation or that the CycLuc2 substrate may alter the N-terminal and C-

terminal domain interface, allowing CycLuc2 to align for adenylation undeterred by the

bump.

To test the hypothesis that the bump I observe in the active site of CG6178 is

preventing adenylation of D-luciferin, I mutated the residues that contribute to the bump.

Fortuitously, one of the residues that contribute to this bump had already been mutated

by Oba et al. to be the same residue as that in firefly luciferase, based on sequence

alignment (Oba et al., 2009.). This mutation was made in an attempt to functionally

convert CG6178 into a luciferase capable of emitting light with D-luciferin. This point

mutation alone was not sufficient for light emission with D-luciferin. But with the structure

of CG6178 now available, I surmised that extending mutagenesis to include more

residues that comprise the bump in the active site would enhance CG6178's luciferase

activity with synthetic luciferins and permit the enzyme to also adenylate D-luciferin.

Mutating just two residues in this bump region transformed CG6178 from a weak luciferase incapable of emitting light with D-luciferin, to an enzyme capable of not only emitting significant light with D-luciferin, but measurable light output in live mouse brain with CycLuc2-amide. I dub this double-mutant of CG6178 "FruitFire" luciferase. It would still be illuminating to have co-crystal structures of CG6178 with CycLuc2 and D-luciferin, as well as Fruitfire with those substrates, to better understand CG6178's substrate discrimination. Additionally, more mutagenesis experiments to further improve CG6178's activity and selectivity for synthetic luciferins holds the potential for beetle-luciferase based orthogonal reporters. Considering the impact of mutating two residues on CG6178's activity, saturating mutagenesis to these residues akin to the experiments performed by Harwood et al. (Harwood et al., 2011.) would be warranted to optimize CG6178 as a luciferase. Other ACSLs sharing homology with Fluc may also benefit from the same types of mutagenesis experiments. Determining the structures of other ACSLs, such as AbLL and PaLL could inform us in similar ways to enhance them as bioluminescent reporters as we have done with CG6178.

Another example of characterizing selective luciferase reporters is detailed in CHAPTER VIII. Here, we report how generating chimeras that combine the N-terminal domain of firefly luciferase with the C-terminal domains of homologous insect ACSLs create novel luciferases, all capable of emitting light with D-luciferin and the synthetic luciferin CycLuc1. However, the chimeras prefer CycLuc1, emitting more light with this substrate. In live mouse lung, one of the chimeras (Fluc/PaLL) is only capable of emitting measurable light with CycLuc1. Unexpectedly, the Fluc/CG6178 chimera emits more robust light emission with CycLuc1 than even wild-type firefly luciferase with D-luciferin in live mouse lung. This is not consistent with the *in vitro* performance of

Fluc/CG6178, where it does not rival WT Fluc with D-luciferin in light emission. The nature of the discrepancy between how these chimeras' performance *in vivo* versus *in vitro* is not completely understood, but may be related to improved stability or expression of the Fluc/CG6178 chimera *in vivo*. We performed a western blot that supports this hypothesis. Testing the thermal stability and other measures of expression for these enzymes *in vivo* could help to determine the discrepancy between these conditions. Another interesting route to pursue in the pursuit of novel bioluminescencent reporters could improve AbLL and PaLL similar to Fruitfire using directed evolution. Select residues could be targeted based on structures and homology models for saturating mutagenesis and screened for selectivity and improved activity.

The large assortment of synthetic luciferins, mutant luciferases, mutated latent luciferases homologous to firefly luciferase (such as our FruitFire luciferase), and chimeric luciferases have expanded our knowledge of both how bioluminescence works, improves the bioluminescent toolkit, and informs us on how to engineer future bioluminescent reporters. The synthetic luciferin CycLuc1 is useful for generating a robust signal in live mouse brain, an environment whose interrogation of such medically relevant processes as neurodegenerative and other brain processes can greatly benefit from such real-time, longitudinal reporting. The luciferin-amide CycLuc2-amide further improves on the strength of light emission in live mouse brain, even at exceedingly low imaging doses. CycLuc2-amide is also a selective reporter of FAAH activity. Using a pro-drug approach, CycLuc2 is a useful reporter for this important drug target. Mutant firefly luciferase enzymes can selectively emit light with synthetic luciferins in mouse brain, providing an avenue for orthogonal reporters, as we demonstrate in CHAPTER IV. Expanding the luciferase enzyme repertoire was our goal in chapter VII, where we

transformed a fruit fly enzyme into a luciferase capable of use in live mouse brain imaging by just substituting two amino acids. Our structure-driven mutagenesis highlights how important structures are to unlocking the mysteries of enzyme engineering. We generated chimeras mixing ACSLs with Fluc in CHAPTER VIII, where we show how they are selective for synthetic luciferins and perform better than would be expected *in vivo.* In CHAPTERS V and VI, we detail a large panel of novel synthetic luciferins that enabled us to interrogate what constitutes a luciferin and provides a library of novel functionalities ripe for experimentation with different luciferases as they are engineered. The work embodied by this thesis has expanded our knowledge of how bioluminescence works and provided useful reporters already in use by other labs, results that I am humbled to have been a part of.

BIBLIOGRAPHY

Adams Jr., S.T. and Miller, S.C. (2014). Beyond D-luciferin: expanding the scope of bioluminescence imaging in vivo. Curr. Opin. Chem. Biol. 21, 112-120.

Adams Jr., S.T., Mofford, D.M., Reddy, G.S.K.K., and Miller, S.C. (2016). Firefly luciferase mutants allow substrate-selective bioluminescence imaging in the mouse brain. Angew. Chem. Int. Ed. Engl. 55(16), 4943-4946.

Adams Jr., S.T. and Miller, S.C. (2019). Enzymatic promiscuity and the evolution of bioluminescence. FEBS. Early View. Doi: https://doi.org/10.1111/febs.15176.

Ahn, K., Johnson, D.S., Mileni, M., Beidler, D., Long, J.Z., McKinney, M.K., Weerapana, E., Sadagopan, N., Liimatta, M., Smith, S.E., Lazerwith, S., Stiff, C., Kamtekar, S., Bhattacharya, K., Zhang, Y., Swaney, S., Van Becelaere, K., Stevens, R.C., and Cravatt, B.F. (2009). Discovery and characterization of a highly selective FAAH inhibitor that reduces inflammatory pain. Chem. Biol. 16(4), 411-420.

Amaral, D.T., Bonatelli, I.A.S., Cerri, R., and Viviani, V.R. (2019). Phylogenetic analyses and divergence time estimation of Elateroidea (Coleoptera) based on RNA-seq data. Comp. Biochem. Physiol. Part D Genomics Proteomics. 30, 283-289.

Bäckman, C.M., Malik, N., Zhang, Y., Shan, L., Grinberg, A., Hoffer, B.J., Westphal, H., and Tomac, A.C. (2006). Characterization of a mouse strain expressing Cre recombinase from the 3' untranslated region of the dopamine transporter locus. Genesis. *44*(*8*), 383-390.

Bandiera, T., Ponzano, S., and Piomelli, D. (2014). Advances in the discovery of N-acetylcholamine acid amidase inhibitors. Pharmacol. Res. 86, 11-17.

Barr, B.K. and Holewinski, R.J. (2002). 4-Methyl-7-thioumbelliferyl-ß-D-cellobioside: a fluorescent, nonhydrolyzable substrate analogue for cellulases. Biochemistry. 41(13), 4447-4452.

Belshaw, P.J., Schoepfer, J.G., Liu, K-Q., Morrison, K.L., and Schreiber, S.L. (1995). Rational design of orthogonal receptor-ligand combinations. Angew. Chemie. Int. Ed. 34(19), 2129-2132.

Berger, F., Paulmurugan, R., Bhaumik, S., and Gambhir, S.S. (2014). Uptake kinetics and biodistribution of ^{14}C-D-luciferin – a radiolabeled substrate for the firefly luciferase catalyzed bioluminescence reaction: impact on bioluminescence based reporter gene imaging. Eur. J. Nucl. Mol. Imaging. *35*(*12*), 2275-2285.

Blankman, J.L. and Cravatt, B.F. (2013). Chemical probes of endocannabinoid metabolism. Pharmacol. Rev. 65(2), 849-71.

Boger, D.L., Fecik, R.A., Patterson, J.E., Miyauchi, H., Patricelli, M.P., and Cravatt, B.F. (2000). Fatty acid amide hydrolase substrate specificity. Bioorg. Med. Chem. Lett. 10(23), 2613-2616.

Branchini, B.R., Southworth, T.L., Murtiashaw, M.H., Boije, H., and Fleet, S.E. (2003). A mutagenesis study of the putative luciferin binding site residues of firefly luciferase. Biochemistry. 42(35), 10429-10436.

Branchini, B.R., Ablamsky, D.M., Davis, A.L., Southworth, T.L., Butler, B., Fan, F., Jathoul, A.P., and Pule, M.A. (2010). Red-emitting luciferases for bioluminescence reporter and imaging applications. Anal. Biochem. 396, 290-297.

Branchini, B.R., Behney, C.E., Southworth, T.L., Fontaine, D.M., Gulick, A.M., Vinyard, D.J., and Brudvig, G.W. (2015). Experimental support for a single electron-transfer oxidation mechanism in firefly bioluminescence. J. Am. Chem. Soc. 137, 7592-7595.

Cao, Y., Wagers, A.J., Beilhack, A., Dusich, J., Bachmann, M.H., Negrin, R.S., Weismann, I.L., and Contag, C.H. (2004). Shifting foci of hematopoiesis during reconstruction from single stem cells. Proc. Natl. Acad. Sci. U.S.A. *101*(*1*). 221-226.

Carl, P.L., Chakravarty, P.K., and Katzenellenbogen, J.A. (1981). A novel connector linkage applicable in prodrug design. J. Med. Chem. 24(5), 479-480.

Cearley, C.N. and Wolfe, J.H. (2006). Transduction characteristics of adeno-associated virus vectors expressing cap serotypes 7, 8, 9, and Rh10 in the mouse brain. Mol. Ther. 13(3), 528-537.

Chai, X., Cui, X., Wang, B., Yang, F., Cai, Y., Wu, Q., and Wang, T. (2015). Near-infrared phosphorus-substituted rhodamine with emission wavelength above 700 Nm for bioimaging. Chem. Eur. J. 21(47), 16754-16758.

Chen, C-T., Chiang, C-L., Lin, Y-C., Chan, L-H., Huang, Tsai, Z-W., and Chen, C-T. (2003). Ortho-substituent effect on fluorescence and electroluminescence of arylamino-substituted coumarin and stilbene. Org. Lett. 5(8), 1261-1264.

Choi, A. and Miller, S. C. (2018). Silicon substitution in oxazine dyes yields near-infrared azasiline fluorophores that absorb and emit beyond 700 nm. Org. Lett. 20(15), 4482-4485.

Chojnaki, S., Cowley, A., Lee, J., Foix, A., and Lopez, R. (2017). Programmatic access to bioinformatics tools from EMBL-EBI update: 2017. Nucleic Acids Res. 45, W550-W553.

Clapper, J.R., Morenoi-Sanz, G., Russo, R., Guijarro, A., Vacondio, F., Duranti, A., Tontini, A., Sanchini, S., Sciolino, N.R., Spradley, J.M., Hohmann, A.G., Calignano, A., More, M., Tarzia, G., and Piomelli, D. (2010). Anandamide suppresses pain initiation through a peripheral endocannabinoid mechanism. Nat. Neurosci. 13(10), 1265-1270.

Close, D.M., Xu, T., Sayler, G.S., and Ripp, S. (2011). *In vivo* bioluminescence imaging (BLI): noninvasive visualization and interrogation of biological processes in living animals. Sensors (Basel). 11(1): 180-206.

Conley, N.R., Dragulescu-Andrasi, A., Rao, J., and Moerner, W.E. (2013). A selenium analogue of firefly D-luciferin with red-shifted bioluminescence emission. Angew. Chem. Int. Ed. Engl. 51(14), 3350-3353.

Contag, C.H. and Bachmann, M.H. (2002). Advances in in vivo bioluminescence imaging of gene expression. Annu. Rev. Biomed. Eng. *4*, 235-60.

Conti, E., Franks, N.P., and Brick, P. (1996). Crystal structure of firefly luciferase throws light on a superfamily of adenylate-forming enzymes. Structure. 4, 287-298.

Craig, F.F., Simmonds, A.C., Watermore, D., McCapra, F., and White, M.R. (1991). Membrane-permeable luciferin esters for assay of firefly luciferase in live intact cells. Biochem. J. 276(3), 637-641.

Cravatt, B.F., Giang, D.K., Mayfield, S.P., Boger, D.L., Lerner, R.A., and Gilula, N.B. (1996). Molecular characterization of an enzyme that degrades neuromodulatory fatty-acid amides. Nature. 384(6604), 83-87.

Dakanali, M., Roussakis, E., Kay, A. R., and Katerinopoulos, H. E. (2005). Synthesis and Photophysical Properties of a Fluorescent TREN-Type Ligand Incorporating the Coumarin Chromophore and Its Zinc Complex. Tetrahedron Lett. 46(24), 4193-4196.

Davis, M.P., Sparks, J.S., and Smith, W.L. (2016). Repeated and widespread evolution of bioluminescence in marine fishes. PLoS ONE. 11, e0155154.

Day, T.A., Rakhshan, F., Deutsch, D.G., and Barker, E.L. (2001). Role of fatty acid amide hydrolase in the transport of the endogenous cannabinoid anandamide. Mol. Pharmacol. 59(6), 1369-1375.

Dickason-Chesterfield, A.K., Kidd, S.R., Moore, S.A., Schaus, J.M., Liu, B. Nomikos, G.G., and Felder, C.C. (2006). Pharmacological characterizationof endocannabinoid transport and fatty acid amide hydrolase inhibitors. Cell. And Mol. Neuro. 26(4-6), 405-421.

Dothager, R.S., Flentie, K., Moss, B., Pan, M., Kesarwala, A., and Piwnica-Worms, D. (2009). Advances in bioluminescence imaging of live animal models. Curr. Opin. Biotechnol. 20(1), 45-53.

Ettinger, A. and Wittmann, T. (2014). Fluorescence live cell imaging. Methods Cell. Biol. 123, 77-94.

Evans, M.S., Chaurette, J.P., Adams Jr., S.T., Reddy, G.R., Paley, M.A., Aronin, N., Prescher, J.A., and Miller, S.C. A synthetic luciferin improves bioluminescence imaging in live mice. Nat. Methods. 11(4), 393-395.

Fallon, T.R., Lower, S.E., Chang, C-H., Bessho-Uehara, M., Martin, G.J., Bewick, A.J., Behringer, M. Debat, H.J., Wong, I., Day, J.C., Suvorov, A., Silva, C.J., Stanger-Hall, K.F., Hall, D.W., Schmitz, R.J., Nelson, D.R., Lewis, S.M., Shigenobu, S., Bybee, S.M., Larracuente, A.M., Oba, Y., and Weng, J-K. (2018). Firefly genomes illuminate parallel origins of bioluminescence in beetles. eLIFE. 7:e36495.

Fraga, H., Fernandes, D., Fontes, R., and Esteves da Silva, J.C.G. (2005). Coenzyme A affects firefly luciferase luminescence because it acts as a substrate and not as an allosteric effector. FEBS J. 272, 5206-5216.

Fraga, H. (2008). Firefly bioluminescence: a historical perspective and recent developments. Photochem. Photobiol. Sci. 7, 146-158.

Gao, G., Vandenberghe, L.H., Alvira,M.R., Lu, Y., Calcedo, R., Zhou, X., and Wilson, J.M. (2004). Clades of adeno-associated viruses are widely disseminated in human tissues. J. Virol. 78(12), 6381-6388.

Geiger, R., Schneider, E., Wallenfels, K., and Miska, W. A new ultrasensitive bioluminogenic enzyme substrate for beta-galactosidase. Biol. Chem. Hoppe-Seyler. 373, 1187-1191.

Gil, J.S., Machado, H.B., and Herschman, H.R. (2012). A method to rapidly and accurately compare the relative efficacies of non-invasive imaging reporter genes in a mouse model and its application to luciferase reporters. Mol. Imaging. 5, 57-64.

Godinat, A., Park, H.M., Miller, S.C., Cheng, K., Hanahan, D., Sanman, L., Bogyo, M., Yu, A., Kikitin, G.F., Stahl, A., and Dubikovskaya, E.A. (2013). A

biocompatible in vivo ligation reaction and its application for noninvasive bioluminescent imaging of protease activity in living mice. ACS Chem. Biol. 8(5), 987-999.

Granzhan, A., Ihmels, H., and Viola, G. (2007). 9-donor-substituted acridizinium salts: versatile environment-sensitive fluorophores for the detection of biomacromolecules. J. Am. Chem. Soc. 129(5), 1254-1267.

Grimm, J.B. and Lavis, L.D. (2011). Synthesis of rhodamines from fluoresceins using Pd-catalyzed C-N cross-coupling. Org. Lett. 13(24), 6354-6357.

Grimm, J.B., English, B.P., Chen, J., Slaughter, J.P., Zhang, Z., Revyakin, A., Patel, R., Macklikn, J.J., Normanno, D., Singer, R.H., Lionnet, T., and Lavis, L.D. (2015). A general method to improve fluorophores for live-cell and single-molecule microscopy. Nat. Methods. 12(3), 244-250.

Grimm, J. B., Brown, T. A., Tkachuk, A. N., and Lavis, L. D. (2017). General synthetic method for Si-fluoresceins and Si-rhodamines. ACS. Cent. Sci. 3(9), 975-985.

Grzybowski, M., Taki, M., Senda, K., Sato, Y., Ariyoshi, T., Okada, Y., Kawakami, R., Imamura, T., and Yamaguchi, S. (2018). A highly photostable near-infrared labeling agent based on a phospha-rhodamine for long-term and deep imaging. Angew. Chem. Int. Ed. 57(32), 10137-10141.

Haddock, S.H.D., Moline, M.A., and Case, J.F. (2010). Bioluminescence in the sea. Annual review of marine science. 2, 443-493.

Hall, M.P., Unch, J., Binkowski, B.F., Valley, M.P., Butler, B.L., Wood, M.G., Otto, P., Zimmerman, K., Vidugiris, G., Machleidt, T., Robers, M.B., Benink, H.A., Eggers, C.T., Slater, M.R., Meisenheimer, P.L., Kaubert, D.H., Fan, F., Encell, L.P., and Wood, K.V. (2012). Engineered luciferase reporter from a deep sea shrimp utilizing a novel imidazopyrazinone substrate. ACS Chem. Biol. 7(11), 1848-1857.

Hall, M. P., Woodroofe, C. C., Wood, M. G., Que, I., Van't Root, M., Ridwan, Y., Shi, C., Kirkland, T. A., Encell, L. P., and Wood, K. V. (2018). Click beetle luciferase mutant and near infrared naphthyl-luciferins for improved bioluminescence imaging. Nat. Comm. 9(1), 132.

Harwood, K.R., Mofford, D.M., Reddy, G.R., and Miller, S.C. (2011). Identification of mutant firefly luciferases that efficiently utilize aminoluciferins. Chem. Biol. 18(12), 1649-1657.

Hauser, J.R., Beard, H.A., Bayana, M.E., Jolley, K.E., Warriner, S.L., and Bon, R.S. (2016). Economical and scalable synthesis of 6-amino-cyanobenzothiazole. Beilstein J. Org. Chem. 12, 2019-2025.

Heffern, M.C., Park, H.M., Au-Yueng, H.Y., Van de Bittner, G.C., Ackerman, C.M., Stahl, A., and Chang, C.J. (2016). In vivo bioluminescence imaging reveals copper deficiency in a murine model of nonalcoholic fatty liver disease. Proc. Natl. Acad. Sci. U.S.A. 113(50). 14219-14224.

Inagaki, K., Fuess, S., Storm, T.A., Gibson, G.A., Mctiernan, C.F., Kay, M.A., and Nakai, H. (2006). Robust systemic transduction with AAV9 vectors in mice: efficient global cardiac gene transfer superior to that of AAV8. Mol. Ther. 14(1), 45-53.

Jathoul, A.P., Grounds, H., Anderson, J.C., and Pule, M.A. (2014). A dual-color far-red to near-infrared firefly luciferin analogue designed for multiparametric bioluminescence imaging. Angew. Chem. Int. Ed. 53(48), 13059-13063.

Jia, S., Ramos-Torres, K. M., Kolemen, S., Ackerman, C. M., and Chang, C. J. (2018). Tuning the Color Palette of Fluorescent Copper Sensors through Systematic Heteroatom Substitution at Rhodol Cores. ACS Chem. Biol. 13(7), 1844-1852.

Jones, K.A., Porterfield, W.B., Rathbun, C.M., McCutcheon, D.C., Paley, M.A., and Prescher, J.A. (2017). Orthogonal luciferase-luciferin pairs for bioluminescence imaging. J. Am. Chem. Soc. 139(6), 2351-2358.

Kakiuchi, M., Ito, S., Kiyama, M., Goto, F., Matsuhashi, T., Yamaji, M., Maki, S., and Hirano, T. (2017). Electronic and steric effects of cyclic amino substituents of luciferin analogues on a firefly-luciferin-luciferase reaction. Chem. Lett. 46(8), 1090-1092.

Kaskova, Z.M., Tsarkova, A.S., and Yampolsky, I.V. (2016). 1001 lights: luciferins, luciferases, their mechanisms of action and applications in chemical analysis, biology and medicine. Chem. Soc.Rev. 45, 6048-6077.

Kaskova, Z.M., Dorr, F.A., Petushkov, V.N., Purtov, K.V., Tsarkova, A.S., Todionova, N.S., Mineev, K.S., Guglya, E.B., Kotlobay, A., Baleeva, N.S., Baranov, M.S., Arseniev, A.S., Gitelson, J.I., Lukyanov, S., Suzuki, Y., Kanie, S., Pinto, E., Mascio, P.D., Waldenmaier, H.E., Pereira, T.A., Carvalho, R.P., Oliveira, A.G., Oba, Y., Bastos, E.L., Stevani, C.V., and Yampolsky, I.V. (2017). Mechanism and color modulation of fungal bioluminescence. Science Adv. 3(4), e1602847. Kim, J., Urban, K., Cochran, E., Lee, S., Ang, A., Rice, B., Bata, A., Campbell, K., Coffee, R., Gorodinsky, A., Lu, Z., Zhou, H., Kishimoto, T.K., and

Lassota, P. (2010). Non-invasive detection of a small number of bioluminescent cancer cells in vivo. PLoS One. *5*(*2*), 9364.

Kitamura, N., Fukagawa, T., Kohtani, S., Kitoh, S-i., Kunimoto, K-K., and Nakagaki, R. (2007). Synthesis, absorption, and fluorescence properties and crystal structures of 7-aminocoumarin derivatives. J. of Photochem. And Photobiol. A: Chem. 188(2-3), 378-386.

Kojima, R., Takakura, H., Ozawa, T., Tada, Y., Nagano, T., and Urano, Y. (2013). Rational design and development of near-infrared-emitting firefly luciferins available in vivo. Angew. Chem. Int. Ed. Engl. 21;52(4), 1175-1179.

Kosower, E.M. (1982). Intramolecular donor-acceptor systems. 9. Photophysics of (phenylamino)naphthalenesulfonates: a paradigm for excited-state intramolecular charge transfer. Acc. Chem. Res. 15(8), 259-266.

Kranenburg, M., van der Burgt, Y.E.M., Kamer, P.C.J., van Leeuwen, P.W.N.M., Goubitz, K. and Fraanje, J. (1995). New diphosphine ligands based on heterocyclic aromatics inducing very high regioselectivity in rhodium-catalyzed hydroformylation: effect of the bite angle. Organometallics. 14(6), 3081-3089.

Kuchimaru, T., Iwano, S., Kiyama, M., Mitsumata, S., Kadonosono, T., Niwa, H., Maki, S., and Kizaka-kondo, S. (2016). A luciferin analogue generating near-infrared bioluminescence achieves highly sensitive deep-tissue imaging. Nat. Comm. 7, 11856.

Limberis, M.P., and Wilson, J.M. (2006). Adeno-associated virus serotype 90 vectors transduce murine alveolar and nasal epithelia and can be readministered. Proc. Natl. Acad. Sci. U.S.A. 103(35), 12993-12998.

Li, J., Chen, L., Wu, W., Zhang, W., Ma, Z., Chen, Y., Du, L., and Li, M. (2014). Discovery of bioluminogenic probes for aminopeptidase N imaging. Anal. Chem. 86, 2747-2751.

Liang, Y., Walczak, P., and Bulte, J.W.M. (2012). Comparison of red-shifted firefly luciferase Ppy RE9 and conventional Luc2 as bioluminescence imaging reporter genes for in vivo imaging of stem cells. J. Biomed. Opt. 17, 016004.

Liu, J., Sun, Y-Q., Zhang, H., Shi, H., Shi, Y., and Guo, W. (2016). Sulfone-rhodamines: a new class of near-infrared fluorescent dyes for bioimaging. ACS Appl. Mater. Interfaces. 8(35), 22953-22962.

Long, J.Z., Lacava, M., Jin, X., and Cravatt, B.F. (2011). An anatomical and temporal portrait of physiological substrates for fatty acid amide hydrolase. J. Lipid. Res. 52(2), 337-344.

Long, J.Z., and Cravatt, B.F. (2011). The metabolic serine hydrolases and their functions in mammalian physiology and disease. Chem. Rev. 111(10), 6022-6063.

Madisen, L., Zwingman, T.A., Sunkin, S.M., Oh, S.W., Zariwala, H.A., Gu, H., Ng, L.L., Palmiter, R.D., Hawrylycz, M.J., Jones, A.R., Lein, E.S., and Zeng, H. (2010). A robust and high-throughput Cre reporting and characterization system for the whole mouse brain. Nat. Neurosci. *13*(*1*), 133-140.

McCutcheon, D.C., Paley, M.A., Steinhardt, R.C., and Prescher, J.A. (2013). Expedient synthesis of electronically modified luciferins for bioluminescence imaging. J. Am. Chem. Soc. *134*(*18*), 7604-7607.

McElroy, W.D., DeLuca, M., and Travis, J. (1967). Molecular uniformity in biological catalyses: the enzymes concerned with firefly luciferin, amino acid, and fatty acid utilization are compared. Science. 157, 150-160.

McElroy, W.D., Seliger, H.H., and White, E.H. (1969). Mechanism of bioluminescence and enzyme function in the oxidation of firefly luciferin. Photochem. Photobiol. 10, 153-170.

Mezzanotte, L., Fazzina, R., Michelini, E., Tonelli, R., Pession, A., Branchini, B, and Rhoda, A. (2010). In vivo bioluminescence imaging of murine xenograft cancer models with a red-shifted thermostable luciferase. Mol. Imaging Biol. *12*(*4*), 406-414.

Mezzanotte, L., Aswendt, M., Tennstaedt, A., Hoeben, R., Hoehn, M., and Lowik, C. (2013). Evaluating reporter genes of different luciferases for optimized in vivo bioluminescence imaging of transplanted neural stem cells in the brain. Contrast Media Mol. Imaging. 8, 505-513.

Mileni, M., Johnson, D.S., Wang, Z., Everdeen, D.S., Liimatta, M., Pabst, B., Bhattacharya, K., Nugent, R.A., Kamtekar, S., Cravatt, B.F., Ahn, K., and Stevens, R.C. (2008). Structure-guided inhibitor design for human FAAH by interspecies active site conversion. Proc. Nat. Acad. Sci. 105(35), 12820-12824.

Miller, S. C., Mofford, D. M., and Adams Jr., S. T. 2018. Lessons learned from luminous luciferins and latent luciferases. ACS Chem. Biol. 13(7), 1734–1740.

Min, C., Ren, A., Li, X., Guo, J., Zou, L., Sun, Y., Goddard, J.D., and Sun, C. (2011). The formation and decomposition of firefly dioxetanone. Chem. Phys. Lett. 506, 269-275.

Miska, W. and Geiger, R. Synthesis and characterization of luciferin derivatives for use in bioluminescence enhanced enzyme immunoassays. (1987). New

ultrasensitive detection systems for enzyme immunoassays. I. J. Clin. Chem. Clin. Biochem. 25, 23-30.

Miska, W. and Geiger R. (1992). A new type of ultrasensitive bioluminogenic enzyme substrates. I. Enzyme substrates with D-luciferin as leaving group. Biol. Chem. Hoppe-Seyler. 369, 407-411.

Mofford, D.M., Reddy, G.R., and Miller, S.C. (2014). Latent luciferase activity in the fruit fly revealed by a synthetic luciferin. Proc. Natl. Acad. Sci. U.S.A. 111(12), 4443-4448.

Mofford, D.M., Reddy, G.R., and Miller, S.C. (2014). Aminoluciferins extend firefly luciferase bioluminescence into the near-infrared and can be preferred substrates over D-luciferin. J. Am. Chem. Soc. 136(38), 13277-13282.

Mofford, D.M., Adams Jr., S.T., Reddy, G.S.K.K., Reddy, G.R., and Miller, S.C. (2015). Luciferin amides enable in vivo bioluminescence detection of endogenous fatty acid amide hydrolase activity. J. Am. Chem. Soc. 137(27), 8684-8687.

Mofford, D.M., and Miller, S.C. (2015). Luciferins behave like drugs. ACS Chem. Neurosci. 6(8), 1273-1275.

Mofford, D. M., Liebmann, K. L., Sankaran, G. S., Reddy, G. S. K. K., Reddy, G. R., and Miller, S. C. (2017). Luciferase activity of insect fatty acyl-CoA synthetases with synthetic luciferins. ACS Chem. Biol. 12(12), 2946-2951.

Monsees, T., Miska, W., and Geiger, R. (1994). Synthesis and characterization of a bioluminogenic substrate for chymotrypsin. Anal. Biochem.

Morton, R. A., Hopkins, T. A., and Seliger, H. H. (1969). The spectroscopic properties of firefly luciferin and related compounds. An approach to product emission. Biochemistry. 8(4), 1598-1607.

Nakamura, M., Maki, S., Amano, Y., Ohkita, Y., Niwa, K., Hirano, T., Ohmiya, Y., and Niwa, H. (2005). Firefly luciferase exhibits bimodal action depending on the luciferin chirality. Biochem. Biophys. Res. Common. 331, 471-475.

Nakatsu, T., Ichiyama, S., Hiratake, J., Saldanha, A., Kobashi, N., Sakata, K., and Kato, H. (2006). Structural basis for the spectral difference in luciferase bioluminescence. Nature. 440, 372-376.

Oba, Y. Ojika, M., and Inouye, S. (2003). Firefly luciferase is a bifunctional enzyme: ATP-dependent monooxygenase and a long chain fatty acyl-CoA synthetase. FEBS Lett. 540(1-3), 251-254.

Oba, Y., Tanaka, K., and Inouye, S. (2006). Catalytic properties of domain-exchanged chimeric proteins between firefly luciferase and Drosophila fatty acyl-CoA synthetase CG6178. Biosci. Biotechnol. Biochem. 70, 2739-2744.

Oba, Y., Iida, K., and Inouye, S. (2009). Functional conversion of fatty acyl-CoA synthetase to firefly luciferase by site-directed mutagenesis: a key substitution responsible for luminescence activity. FEBS Lett. 583, 2004-2008.

Oba, Y., Kumazaki, M., and Inouye, S. (2010). Characterization of luciferases and its paralogue in the Panamanian luminous click beetle Pyrophorus angustus: a click beetle luciferase lacks the fatty acyl-CoA synthetic acitivity. Gene. 452, 1-6.

O'Brien, P.J. and Herschlag, D. (1999). Catalytic promiscuity and the evolutionof new enzymatic activities. Chem. Biol. 6, R91-R105.

Okamoto, Y., Morishita, J., Wang, J., Schmid, P.C., Krebsbach, R.J., Schmid, H.H.O., and Ueda, N. (2005). Mammalian cells stably overexpressing N-acylphosphatidylethanolamine-hydrolysing phospholipase D exhibit significantly decreased levels of N-acylphosphatidylethanolamines. Biochem. J. 389(1), 241-247.

Orabi, A.I., Sah, S., Javed, T.A., Lemon, K.L., Good, M.L., Guo, P., Xiao, X., Prasadan, K., Gittes, G.K., Jin, S., and Husain, S.Z. (2015). Dynamic imaging of pancreatic nuclear factor kB (NF-kB) activation in live mice using adeno-associated virus (AAV) infusion and bioluminescence. J. Biol. Chem. 290(18), 11309-11320.

Otto-Duessel, M., Khankaldyyan, V., Gonzalez-Gomez, I., Jensen, M.C., Laug, W.E., and Rosol, M. (2006). In vivo testing of Renilla luciferase substrate analogs in an orthotopic murine model of human glioblastoma. Mol. Imaging. 5, 57-64.

Patricelli, M.P. and Cravatt, B.F. (1999). Fatty acid amide hydrolase competitively degrades bioactive amides and esters through a nonconventional catalytic mechanism. Biochemistry. 38(43), 14125-14130.

Pauff, S. M. and Miller, S. C. (2011). Synthesis of near-IR fluorescent oxazine dyes with esterase-labile sulfonate esters. Org. Lett. 13(23), 6196-6199.

Peng, T. and Yang, D. (2010). Construction of a library of rhodol fluorophores for developing new fluorescent probes. Org. Lett. 12(3), 496-499.

Peng, T., Chen, X., Gao, L., Zhang, T., Wang, W., Shen, J., and Yang, D. (2016). A rationally designed rhodamine-based fluorescent probe for molecular imaging of peroxynitrite in live cells and tissues. Chem. Sci. 7(8), 5407-5413.

Petushkov, V.N., Dubinnyi, M.A., Tsarkova, A.S., Rodionova, N.S., Baranov, M.S., Kublitski, V.S., Shimomura, O., and Yampolsky, I.V. (2014). A novel type of luciferin from the Siberian luminous earthworm Fridericia heliota: structure elucidation by spectral studies and total synthesis. Angew. Chem. Int. Ed. 53, 5566-5568.

Pirrung, M.C., Dorsey, A., Howitt, N.D., and Liao J. (2017). ß-deuterium isotope effects on firefly luciferase bioluminescence. ChemistryOpen. 6, 697-700.

Prescher, J.A. and Contag, C.H. (2010). Guided by the light: visualizing biomolecular processes in living animals with bioluminescence. Curr. Opin. Chem. Biol. *14*(*1*), 80-89.

Porterfield, W.B., Jones, K.A., McCutcheon, D.C., and Prescher, J.A. A "caged" luciferin for imaging cell-cell contacts. J. Am. Chem. Soc. 137(27), 8656-8659.

Rabinovich, B.A., Ye, Y., Etto, T., Chen, J.Q., Levitsky, H.I., Overwijk, W.W., Cooper, L.J.N., Gelovani, J., and Hwu, P. (2008). Visualizing fewer than 10 mouse T cells with an enhanced firefly luciferase in immunocompetent mouse models of cancer. Proc. Natl. Acad. Sci. U.S.A. *105*(*38*), 14342-14346.

Ramarao, M.K., Murphy, E.A., Shen, M.W.H., Wang, Y., Bushell, K.N., Huang, N., Pan, N., Williams, C., and Clark, J.D. (2005). A fluorescence-based assay for fatty acid amide hydrolase compatible with high-throughput screening. Anal. Biochem. 343(1), 143-151.

Ramil, C.P., An, P., Yu, Z., and Lin, Q. (2016). Sequence-specific 2-cyanobenzothiazole ligation. J. Am. Chem. Soc. 138(17), 5499-5502.

Reddy, A. R., Prasad, D. V., and Darbarwar, M. (1986). Absorption and fluorescence spectra of 7-aminocoumarin derivatives. J. Photochem. 32(1), 69-80.

Reddy, G.R., Thompson, W.C., and Miller, S.C. (2010). Robust light emission from cyclic alkylaminoluciferin substrates for firefly luciferase. J. Am. Chem. Soc. 132(39), 13586-13587.

Ren, H., Xiao, F., Zhan, K., Kim, Y-P., Xie, H., Xia, Z., and Rao, J. (2009). A biocompatible condensation reaction for the labeling of terminal cysteine residues on proteins. Angew. Chem. Int. Ed. Engl. 48(51), 9658-9662.

Ren, W., Ji, A., Karmach, O., Carter, D.G., Martins-Green, M.M., and Ai, H-W. (2016). A membrane-activatable near-infrared fluorescent probe with ultra-photostability for mitochondrial membrane potentials. Analyst. 141(12), 3679-3685.

Roncoroni, C., Rizzi, N., Brunialti, E., Cali, J.J., Kaubert, D.H., Maggi, A., and Ciana, P. (2012). Molecular imaging of cytochrome P450 activity in mice. Pharm. Res. 65, 531-536.

Rosen, B. R., Ruble, J. C., Beauchamp, T. J., and Navarro, A. (2011). Mild Pd-catalyzed N-arylation of methanesulfonamide and related nucleophiles: avoiding potentially genotoxic reagents and byproducts. Org. Lett. 13(10), 2564-2567.

Safran, M., Kim, W.Y., Kung, A.L., Horner, J.W., DePinho, R.A., Kaelin, W.G. Jr. (2003). Mouse reporter strain for noninvasive bioluminescent imaging of cells that have undergone Cre-mediated recombination. Mol. Imaging. 2(4), 297-302.

Seliger, H.H. and McElroy, W.D. (1962). Chemiluminescence of firefly luciferin without enzyme. Science. 138, 683-685.

Sellmyer, M.A., Bronsart, L., Imoto, H., Contag, C.H., Wandless, T.J., and Prescher, J.A. (2013). Visualizing cellular interactions with a generalized proximity reporter. Proc. Natl. Acad. Sci. U.S.A. 110, 8567-8572.

Shah, K., Liu, Y., Deirmengian, C., and Shokat, K.M. (1997). Engineering unnatural nucleotide specificity for rous sarcoma virus tyrosine kinase to uniquely label its direct substrates. Proc. Natl. Acad. Sci. U.S.A. 94(8), 3565-3570.

Sharma, D. K., Adams Jr., S. T., Liebmann, K. L., and Miller, S. C. (2017). Rapid access to a broad range of 6′-substituted firefly luciferin analogues reveals surprising emitters and inhibitors. Org. Lett. 19(21), 5836-5839.

Sharma, D.K., Adams Jr., S.T., Liebmann, K.L., Choi, A., and Miller, S.C. (2019). Sulfonamides are an overlooked class of electron donors in luminogenic luciferins and fluorescent dyes. Org. Lett. 21(6), 1641-1644.

Shibata, A., Furukawa, K., Abe, H., Tsuneda, S., and Ito, Y. (2008). Rhodamine-based fluorogenic probe for imaging biological thiol. Bioorg. Med. Chem. Lett. 18(7), 2246-2249.

Shinde, R., Perkins, J. and Contag, C.H. (2006). Luciferin derivatives for enhanced in vitro and in vivo bioluminescence assays. 45(37), 11103-11112.

Shoup, T.M., Bonab, A.A., Wilson, A.A., and Vasdev, N. (2015). Synthesis and preclinical evaluation of [^{18}F]FCHC for neuroimaging of fatty acid amide hydrolase. Mol. Imaging. Biol. 17(2), 257-263.

Stacer, A.C., Nyati, S., Moudgil, P., Iyengar, R., Luker, K.E., Rehemtulla, A., and Luker, G.D. (2013). NanoLuc reporter for dual luciferase imaging in live animals. Mol. Imaging. 12, 1-13.

Steinhardt, R.C., Rathbun, C.M., Krull, B.T., Yu, J.M., Yang, Y., Nguyen, B.D., Kwon, J., McCutcheon, D.C., Jones, K.A., Furche, F., and Prescher, J.A. (2017). Brominated luciferins are versatile bioluminescent probes. Chembiochem. 18(1), 96-100.

Stolz, U., Velez, S., Wood, K.V., Wood, M., and Feder, J.L. (2003). Darwinian natural selection for orange bioluminescent color in a Jamaican click beetle. Proc. Natl. Acad. Sci. 100, 14955-14959.

Sundlov, J.A., Fontaine, D.M., Southworth, T.L., Branchini, B.R., and Gulick, A.M. (2012). Crystal structure of firefly luciferase in a second catalytic conformation supports a domain alternation mechanism. Biochemistry. 51(33), 6493-6495.

Takakura, H., Kojima, R., Kamiya, M., Kobayashi, E., Komatsu, T., Ueno, T., Terai, T., Hanaoka, K., Nagano, T., and Urano, Y. (2015). New class of bioluminogenic enzyme-induced electron transfer: BioLeT. J. Am. Chem. Soc. 137(12), 4010-4013.

Tarantal, A.F. and Lee, C.C.I. (2010). Long-term luciferase expression monitored by bioluminescence imaging after adeno-associated virus-mediated fetal gene delivery in Rhesus monkeys (Macaca mulatta). Hum. Gene Ther. 21(2), 143-148.

Van de Bittner, G.C., Dubikovskaya, E.A., Bertozzi, C.R., and Chang, C.J. (2010). In vivo imaging of hydrogen peroxide production in a murine tumor model with a chemoselective bioluminescent reporter. Proc. Natl. Acad. Sci. U.S.A. 107, 21316-21321.

Van de Bittner, G.C., Bertozzi, C.R., and Chang, C.J. (2013). Strategy for dual analyte luciferin imaging: in vivo bioluminescence detection of hydrogen peroxide and caspase activity in a murine model of acute inflammation. J. Am. Chem. Soc. 135(5), 1783-1795.

Viviani, V.R., Bechara, E.J., and Ohmiya, Y. (1999). Cloning, sequence analysis, and expression of active Phrixothrix railroad-worms luciferases: relationship between bioluminescence spectra and primary structures. Biochemistry. 38, 8271-8279.

Waterhouse, A. Bertoni, M., Bienert, S., Studer, G., Tauriello, G., Gumienny, R. Heer, F.T., de Beer, T.A.P., Rempfer, C., Bordoli, L., Lepore, R., Schwere, T. (2018). SWISS-MODEL: homology modeling of protein structures and complexes. Nucleic Acids Res. 46, W296-W303.

Watkins, P.A. (2008). Very-long-chain acyl-CoA synthetases. J. Biol. Chem. 283, 1773-1777.

Wehrman, T.S., von Degenfeld, G., Krutzik, P.O., Nolan, G.P., and Blau, H.M. (2006). Luminescent imaging of beta-galactosidase activity in living subjects using sequential reporter-enzyme luminescence. Nat. Methods. 3, 295-301.

Weimar, J.D., DiRusso, C.C., Delio, R., and Black, P.N. (2002). Functional role of fatty acyl-coenzyme A synthetase in the transmembrane movement and activation of exogenous long-chain fatty acids. Amino acid residues within the ATP/AMP signature motif of Eschericia coli FadD are required for enzyme activity and fatty acid transport. J. Biol. Chem. 277(33), 29369-29376.

Weissleder, R. and Ntziachristos, V. (2003). Shedding light onto live molecular targets. Nature Med. 9, 123-128.

Weng, J-K. (2014). The evolutionary paths towards complexity: a metabolic perspective. New. Phytol. 201, 1141-1149.

White, E.H., McCapra, F., and Field, G.F. (1963). The structure and synthesis of firefly luciferin. J. Am. Chem. Soc. 85, 337-343.

White, E.H., Worther, H., Field, G.F., and McElroy, W.D. (1965). Analogs of firefly luciferin. J. Org. Chem. 30, 2344-2348.

White, E.H., Worther, H., Seliger, H.H., and McElroy, W.D. (1966). Amino analogs of firefly luciferin and biological activity thereof. J. Am. Chem. Soc. 88(9), 2015-2019.

White, E.H., Rapaport, E., Seliger, H.H., and Hopkins, T.A. (1971). The chemi- and bioluminescence of firefly luciferin: an efficient chemical production of electronically excited states. Bioorg. Chem. 1, 92-122.

Wood, K.V., Lam, Y.A., and McElroy, W.D. (1989). Introduction to beetle luciferases and their applications. J. Biolumin. Chemilumin. 4, 389-301.

Woodroofe, C.C., Shultz, J.W., Wood, M.G., Osterman, J., Cali, J.J., Waily, W.J., Meisenheimer, P.L., and Klaubert, D.H. (2008). N-alkylated 6'-aminoluciferins are bioluminescent substrates for Ultra-Glo and QuantiLum luciferase: new potential scaffolds for bioluminescent assays. Biochemistry. *47*(*39*). 10383-10393.

Yin, J. and Buchwald, S.L. (2002). Pd-catalyzed intermolecular amidation of aryl halides: the discovery that xantphos can be trans-chelating in a palladium complex. J. Am. Chem. Soc. 124(21), 6043-6048.

Zhang, B. S., Jones, K. A., McCutcheon, D. C., and Prescher, J. A. (2018). Pyridone Luciferins and Mutant Luciferases for Bioluminescence Imaging. ChemBioChem. 19(5), 470-477.

Zhang, H., Yang, B., Mu, X., Ahmed, S.S., Su, Q., He, R., Wang, H., Mueller, C., Sena-Esteves, M., Brown, R., Xu, Z., and Gao, G. (2011). Several rAAV vectors efficiently cross the blood-brain barrier and transduce neurons and astrocytes in the neonatal mouse central nervous system. Mol. Ther. *19*(*8*), 1140-1148.

Zhang, J., Shibata, A., Ito, M.; Shuto, S., Ito, Y., Mannervik, B., Abe, H., and Morgenstern, R. (2011). Synthesis and characterization of a series of highly fluorogenic substrates for glutathione transferases, a general strategy. J. Am. Chem. Soc. 133(35), 14109-14119.

Zhang, Y., Bressler, J.P., Neal, J., Lal, B., Bhang, H-E.C., Laterra, J., and Pomper, M.G. (2007). ABCG2/BCRP expression modulates D-Luciferin based bioluminescence imaging. Cancer Res. 67, 9389-9397.

Zhao, H., Doyle, T.C., Coquoz, O., Rice, B.W., and Contag, C.H. (2005). Emission spectra of bioluminescent reporters and interaction with mammalian tissue determine the sensitivity of detection in vivo. J. Biomed. Opt. 10(4), 41210.

Zhou, X., Lai, R., Beck, J. R., Li, H., and Stains, C. I. (2016). Nebraska red: A phosphinate-based near-Infrared fluorophore scaffold for chemical biology applications. Chem. Comm. 52(83), 12290-12293.

Zincarelli, C.A., Soltys, S., Rengo, G., and Rabinowitz, J.E. (2008). Analysis of AAV serotypes 1-9 mediated gene expression and tropism in mice after systemic injection. Mol. Ther. 16(6), 1073-1080.